

Physical Structure of Northern Colorado River Basin Cloud Systems

By
Robert M. Rauber

Department of Atmospheric Science
Colorado State University
Fort Collins, Colorado



**Department of
Atmospheric Science**

Paper No. 390

PHYSICAL STRUCTURE OF NORTHERN COLORADO RIVER BASIN CLOUD SYSTEMS

Robert M. Rauber

This report was prepared with support provided by
National Science Foundation Grants ATM-8109490 and ATM-8407543
Principal Investigator: Lewis O. Grant

Department of Atmospheric Science
Colorado State University
Ft. Collins, Colorado

September, 1985

Atmospheric Science Paper No. 390

ABSTRACT OF DISSERTATION

PHYSICAL STRUCTURE OF NORTHERN COLORADO RIVER BASIN CLOUD SYSTEMS

This paper describes the physical structure and temporal evolution of wintertime cloud systems over the Yampa River Basin, one of the eight major subbasins supplying water to the Colorado River. The primary purpose of this work was to provide a firm foundation for the evaluation of precipitation augmentation potential of these cloud systems. The information presented in this paper is based on data collected during two wintertime field programs conducted near Colorado's Park Range. Data from a wide variety of cloud systems were analyzed to determine the temporal variation, physical distribution, and microphysical structure of supercooled liquid water. Ice phase characteristics were studied including crystal concentrations and habits, nucleation, secondary ice particle production, and growth by deposition, accretion and aggregation. The following are the major conclusions of this analysis:

(1) The shallow orographic cloud system with cloud top temperature warmer than about -20°C was identified as the system with the largest potential for precipitation augmentation. This type of cloud system was found to have persistent and significant liquid water contents in three regions: (1) near cloud top, (2) between cloud base and approximately the -12°C level, and (3) in regions of strong orographic forcing. Nucleation observed near cloud top occurred by the condensation-freezing mechanism upwind of the mountain crest. The primary habits of crystals

produced by these cloud systems were dendritic. Aggregation, fragmentation and accretion were all active processes in these cloud systems.

(2) Deep cloud systems with tops colder than -20°C generally were found to have less potential for precipitation augmentation based on their reduced liquid water contents and frequent larger precipitation rates. Liquid water contents in deep stratiform cloud systems were generally limited to the region near the mountain crest. Exceptions were cloud systems where considerable decoupling between the upper and lower cloud layers occurred. The data suggested that deposition or sorption nucleation may predominate at cold temperatures in deep clouds. In general, most particles arriving at the surface had irregular habits. Accretion was negligible, except in cases where decoupling occurred. Aggregation was generally limited to small combinations of cold temperature particles.

(3) Radiometric data suggested that organized convective regions initially contained significant supercooled water, but in a short time, convert to the ice phase. Particles falling from such clouds were frequently rimed and aggregated. Many crystal habits were observed, suggesting complex growth processes.

Three hypotheses for precipitation augmentation are formulated based on the physical distribution of liquid water and evolution of precipitation processes observed in Park Range clouds. Field experiments to test each of the individual hypotheses are described.

Robert M. Rauber
Atmospheric Science Department
Colorado State University
Fort Collins, Colorado 80523
Fall, 1985

ACKNOWLEDGEMENTS

I wish to express my gratitude to my advisor, Professor Grant, for all he has taught me and the opportunities he has given me. In my years at CSU, I have learned much more than meteorology with his help. I also wish to thank my committee members, Dr. William Cotton, Dr. Thomas McKee and Dr. Paul Mielke for their guidance.

Many organizations and individuals were responsible for making this research a success. Beginning with organizations, I wish to thank the staff of the Office of Water Resources Management at the Bureau of Reclamation (BOR) for providing much of the instrumentation, field expertise, and data reduction assistance to the COSE program. The Wave Propagation Laboratory at ERL/NOAA provided expertise both in the field operations and data reduction associated with the microwave radiometer. The National Center for Atmospheric Research (NCAR) Research Aviation Facility, through the sponsorship of the National Science Foundation, provided the Queen Air research aircraft and allowed our group to use their computer facilities. NCAR also provided CSU with computer time from its main computer facility. Colorado International Corporation (CIC) provided the Cheyenne II aircraft and data reduction capabilities. The Steamboat Ski Association generously provided its facilities to the project. The National Weather Service office in Cheyenne, Wyoming provided the program with satellite data throughout the period for use

in the synoptic analyses. This work was sponsored by the National Science Foundation under National Science Foundation Grants ATM-7819261 and ATM-8109590.

From each of these groups, particular individuals helped me assemble this data and understand it. I wish to particularly thank Mr. Jack Snider, from NOAA/WPL, Mr. Paul Lawson, who coordinated the CIC effort, Mr. John Lease, who coordinated our BOR cooperative effort, and Mrs. Judy Bonds, who managed to process a large volume of data from BOR systems within her hectic schedule.

I have had the special pleasure of working with the staff, students and research associates of Professor Grant. I wish to express my deepest gratitude to Mrs. Marion Haurwitz. Without her programming skills, I would still be on page 1. Mr. Feng DaXiong, our visiting scientist from China, taught me to look at crystals one by one and collected the complete ground microphysics data set single-handed. A special acknowledgement is necessary for the staff at Storm Peak Laboratory, Mr. Paul J. DeMott, Dr. Edward E. Hindman, and Dr. Randolph D. Borys, for their efforts at meticulous data collection in extremely adverse weather conditions. I wish to thank Mr. Robert Rilling, Mr. Don Cobb, and Mr. Randy Horn, with whom I've been through three (or four - Don) field programs, for their help throughout the years. Others who participated in the data collection and/or contributed to the success of this work are Dr. William Finnegan, Ms. Taneil Uttal, Ms. Rochelle Blumenstein, Mr. Tim Stoker, Mr. Robert Lee, Mr. John Medina, and Mr. Kapin Tan and Ms. Patricia Walsh. Mrs. Lucy McCall drafted the

multitude of figures. Mrs. Janis Davis and Mrs Brenda Thompson both graciously allowed me to use their offices and word processors.

A special word of thanks to my wife, Ruta. Ruta not only gave me moral support, she was out there in the snow collecting data. She served as the COSE program secretary in the field and read this volume from cover to cover for mistakes. About half-way through this research, she married me! I'd trade 30 PhD's for her friendship.

TABLE OF CONTENTS

Abstract.....iii
Acknowledgements.....v
Table of contents.....viii
List of tables.....xiii
List of figures.....xiv

CHAPTER I INTRODUCTION1

1. Background.....4
A. Coastal mountain ranges.....7
 (1) Central Sierra Research Experiment.....7
 (2) Cascade Atmospheric Water Resources Program.....8
 (3) Sierra Cooperative Pilot Project.....10
B. Inland mountain ranges.....11
 (1) Climax I and II.....12
 (2) Park Range Atmospheric Water Resources Program.....14
 (3) Utah I and II.....16
 (4) Bridger Range Experiment.....16
 (5) Colorado River Basin Pilot Project.....17
 (6) Elk Mountain Experiments.....18
 (7) Utah Physical Experiments.....19
 (8) Utah Federal-State Cooperative Project.....20
2. Summary.....22

CHAPTER II INSTRUMENTATION AND EXPERIMENTAL PROCEDURES.....23

1. The Colorado Orographic Seeding Experiment.....23
2. Instrumentation.....27
A. Aircraft.....27
B. Dual-channel microwave radiometer.....38
 (1) Surface temperature effects.....42
 (2) Ice phase effects.....47
 (3) Relationship between radiometric measurements and total
 condensate produced in the cloud system.....51
 a. Model vertical velocity.....51
 b. Airflow and condensate production.....52
 c. Model limitations.....53
 d. Model results.....55
C. 1.79 cm radar.....57
D. Precipitation intensity, crystal habit, riming and aggregation..59
E. Storm Peak Laboratory measurements.....60
F. Supporting data sets.....60

CHAPTER III	THE WATER PHASE.....	62
1.	Temporal variations of the supercooled water field.....	62
	A. Case studies.....	63
	(1) Pre-frontal and frontal cloud systems.....	63
	a. Case study: 22 January 82.....	63
	b. Case study: 15 December 81.....	71
	c. Case study: 30 December 81.....	81
	(2) Post-frontal cloud systems.....	88
	a. Case study: 21 December 81.....	88
	b. Case study: 13 December 81.....	95
	c. Case study: 27 January 82.....	101
	(3) Orographic systems.....	107
	a. Case study: 14 December 81.....	107
	b. Case study: 16 December 81.....	112
	c. Case study: 13 January 82.....	115
	B. Discussion.....	122
	(1) Pre-frontal and frontal cloud systems.....	122
	(2) Post-frontal cloud systems.....	125
	(3) Orographic cloud systems.....	128
2.	Physical and microphysical structure of the supercooled water field.....	129
	A. Liquid water distribution.....	130
	(1) Cloud top.....	130
	(2) Cloud base.....	137
	(3) Regions of strong orographic forcing.....	141
	B. Microphysical characteristics.....	143
3.	Comparison with other locations.....	148
CHAPTER IV	THE ICE PHASE.....	157
1.	General characteristics of the ice phase.....	157
	A. Crystal concentrations.....	157
	B. Crystal habits.....	160
	(1) Surface measurements.....	160
	(2) Aircraft measurements.....	167
	a. 15 December 81.....	167
	b. 21 December 81.....	174
	c. 5 January 82.....	174
	d. 23 January 82.....	175
	e. 31 January 82.....	176
	C. Precipitation rates.....	176
2.	Growth by vapor deposition.....	178
	A. Dendritic snowfall events.....	179
	(1) Characteristics of the dendritic growth region in shallow cloud systems.....	180
	(2) Trajectories of dendritic crystals in shallow storms.....	184
	(3) Dendritic snowfall from deep storms.....	186
	B. Cold temperature crystals.....	188
	C. Warm temperature crystals.....	191
3.	Ice nucleation.....	194
	A. Review of DeMott et. al. (1986).....	194
	B. 21 December 81 case study.....	197
	C. Surface measurements.....	201

4. Ice multiplication.....	204
A. Review.....	204
(1) Crystal fragmentation.....	204
(2) Ice splinter production during riming.....	205
(3) Droplet shattering upon freezing.....	206
B. Ice particle fragmentation.....	207
(1) Surface observations.....	207
(2) Aircraft measurements.....	210
a. 5 January 82.....	210
b. 31 January 82.....	213
C. Ice splinter formation during riming.....	218
(1) Physical constraints on the Hallett-Mossop (1974) mechanism.....	219
a. Temperature.....	219
b. Presence of small and large droplets.....	219
c. Presence of large ice particles.....	221
(2) Evidence for the Hallett-Mossop (HM) process.....	221
D. Droplet shattering upon freezing.....	229
5. Accretion.....	230
A. Review.....	231
B. Accretion in upper cloud regions.....	233
(1) Cloud top region in warm clouds.....	233
(2) Riming in upper regions of cold clouds.....	235
C. Frequency of accretion and effects on precipitation distribution.....	240
6. Aggregation.....	244
A. Review.....	244
(1) Particle adhesion.....	244
(2) Physical parameters controlling aggregation.....	247
a. Temperature.....	247
b. Crystal concentration.....	248
c. Crystal size and habit.....	248
(3) Collection efficiency and size spectra evolution.....	249
B. Surface observations of ice particle aggregation.....	249
(1) Surface temperature.....	249
(2) Precipitation rate.....	256
(3) Crystal habit.....	258
a. 13 December 81.....	260
b. 14 December 81.....	260
c. 15 December 81.....	264
d. 16 December 81.....	264
e. 21 December 81.....	265
f. 29 December 81.....	265
g. 30 December 81.....	266
h. 4 January 82.....	266
i. 5 January 82.....	267
j. 13 January 82.....	267
k. 16 January 82.....	268
l. 19 January 82.....	268
m. 21-22 January 82.....	268
n. 23 January 82.....	269
o. 27 January 82.....	269
p. 31 January 82.....	269
C. Physical models of aggregation in cold cloud systems.....	270

- (1) Aggregation in a deep cloud system.....270
- (2) Aggregation in a shallow cloud system.....281

CHAPTER V SUMMARY AND CONCEPTUAL MODELS OF PRECIPITATION FORMATION.290

- 1. Summary of data analysis..... 290
 - A. Supercooled water.....290
 - (1) Temporal variations of the supercooled water field.....290
 - a. Pre-frontal and frontal cloud systems.....291
 - b. Post-frontal cloud systems.....293
 - c. Orographic cloud systems.....293
 - (2) Location of the liquid water in Park Range cloud systems...294
 - (3) Microphysical characteristics of the supercooled droplet population.....296
 - B. The ice phase.....297
 - (1) General characteristics.....297
 - a. Ice particle concentrations.....297
 - b. Crystal habits.....297
 - c. Precipitation rates.....298
 - (2) Growth by vapor deposition.....299
 - (3) Ice nucleation.....300
 - (4) Secondary ice particle production.....301
 - (5) Accretion.....302
 - (6) Aggregation.....304
- 2. Conceptual models of Park Range cloud systems.....305
 - A. The shallow stratiform cloud system with cloud top temperature greater than -20°C305
 - B. Deep stratiform cloud systems with tops colder than -20°C310
 - C. Organized convection.....314

CHAPTER VI PRECIPITATION AUGMENTATION.....316

- 1. Requirements for modification of precipitation processes.....317
 - A. Supercooled liquid water.....317
 - B. Artificial ice nucleants.....320
- 2. Hypotheses for modification of precipitation processes.....323
 - A. Precipitation modification by seeding the -10°C to cloudbase region.....324
 - (1) Nucleation.....324
 - (2) Growth processes.....325
 - (3) Hypothesis.....326
 - B. Precipitation modification by cloud top seeding.....327
 - (1) Nucleation.....327
 - (2) Growth processes.....328
 - (3) Hypothesis.....329
 - C. Precipitation modification by seeding the region of strong orographic lift.....330
 - (1) Nucleation.....330
 - (2) Growth processes.....330
 - (3) Hypothesis.....331
- 3. Hypothesis testing.....332
 - A. Instrumentation.....332
 - B. Physical experiments.....334
 - (1) Seeding the low level region.....335

LIST OF TABLES

Number		Page
1.	Cloud physics instrumentation network for COSE, December 1981-January 1982.....	26
2.	Instrumentation list, Colorado Orographic Seeding Experiment, Queen Air N306D.....	29
3.	CIC Cheyenne data acquisition system sensor specification.....	32
4.	JW-FSSP comparison statistics.....	35
5.	Comparison of model predicted integrated condensate and observed radiometric integrated water content.....	56
6.	Droplet spectra characteristics.....	145
7.	Linear regression statistics: droplet concentration vs. liquid water content.....	146
8.	Shadow photograph crystal habit summary.....	163
9.	Shadow photograph general crystal habit summary.....	165
10.	Surface observations of crystal fragmentation.....	209
11.	Surface observations at RAD on 16 Jan 82 during the flight period.....	283

LIST OF FIGURES

Number	Page
1.	The upper Colorado River basin and primary watersheds.....2
2.	1981 COSE field instrumentation network.....24
3.	Topographic profile of COSE study area.....25
4.	N306D flight track for 26 November 1979.....28
5.	Generalized flight track of N83TW.....30
6.	JW vs. FSSP liquid water contents for 5 January 82 flight.....34
7.	2D-c probe artifacts and problem images.....39
8.	Integrated liquid water content observations observed on 20 December 1981.....43
9.	Maximum integrated liquid water contents observed during 360° azimuth scans as a function of surface temperature for nine storm periods.....45
10.	Liquid water content (LWC) and ice crystal concentrations observed during a descent sounding of the Cheyenne II cloud physics aircraft over the radiometer site on 5 January 1981.....49
11.	Surface and remote sensing measurements at the radiometer site (RAD) and Storm Peak Laboratory (SPL)) on 5 Jan 82.....50
12.	Model predicted total condensate (gm^{-3}) and parcel streamlines for the 15 December 1981, 1500 GMT simulation.....54
13.	85 kPa chart for 22 January 82 at 0000 GMT.....64
14.	70 kPa chart for 22 January 82 at 0000 GMT.....66
15.	Time cross section of rawinsonde data for the 22 January 82 storm.....67
16.	Surface and remote sensing measurements at the radiometer site (RAD) and Storm Peak Laboratory (SPL)) on 22 Jan 82 (0030-0330 GMT).....69

17.	85 kPa chart for the 15 December 81 storm at 1200 GMT.....	73
18.	70 kPa chart for the 15 December 81 storm at 1200 GMT.....	74
19.	Time cross section of rawinsonde data for the 15 December 81 storm.....	75
20.	Surface and remote sensing measurements at the radiometer site (RAD) and Storm Peak Laboratory (SPL)) on 15 Dec 81 (1320-1600 GMT).....	77
21.	Surface and remote sensing measurements at the radiometer site (RAD) and Storm Peak Laboratory (SPL)) on 15 Dec 81 (1640-1920 GMT).....	78
22.	Synoptic scale weather features for the 30-31 December 1981 storm system.....	82
23.	Vertical profiles of Equivalent Potential Temperature at 2100 GMT, 30 December 1981 and 0000 GMT, 31 December 1981.....	84
24.	Surface and remote sensing measurements at the radiometer site (RAD) and Storm Peak Laboratory (SPL)) on 30-31 Dec 81....	86
25.	85 kPa chart for the 21 December 81 storm at 1200 GMT.....	89
26.	70 kPa chart for the 21 December 81 storm at 1200 GMT.....	90
27.	Cross section of rawinsonde data for the 21 December 81 storm system.....	91
28.	Surface and remote sensing measurements at the radiometer site (RAD) and Storm Peak Laboratory (SPL)) on 21 Dec 81.....	93
29.	Synoptic scale weather features for the 13 Dec 1981 storm system.....	96
30.	Vertical profiles of Equivalent Potential Temperature at 1500 GMT and 1800 GMT for the 13 December 1981 storm system....	99
31.	Surface and remote sensing measurements at the radiometer site (RAD) and Storm Peak Laboratory (SPL)) on 13 Dec 81.....	100
32.	Synoptic scale weather features for the 27 January 1982 storm system.....	102
33.	Vertical profile of Equivalent Potential Temperature at 1600 GMT on 27 January 1982.....	104
34.	Surface and remote sensing measurements at the radiometer site (RAD) and Storm Peak Laboratory (SPL)) on 27 Jan 82.....	106
35.	Synoptic scale weather features for the 14 December 1981 storm system.....	108

36.	Vertical profile of Equivalent Potential Temperature at 1800 GMT on 14 December 1981.....	110
37.	Surface and remote sensing measurements at the radiometer site (RAD) and Storm Peak Laboratory (SPL) on 14 Dec 81.....	111
38.	Synoptic scale weather features for the 16 December 1981 storm system.....	113
39.	Surface and remote sensing measurements at the radiometer site (RAD) and Storm Peak Laboratory (SPL) on 16 Dec 81.....	116
40.	70 kPa chart for the 14 Jan 82 storm at 0000 GMT.....	118
41.	2100 GMT sounding for 13 January 82.....	119
42.	Surface and remote sensing measurements at the radiometer site (RAD) and Storm Peak Laboratory (SPL) on 13 Jan 82.....	121
43.	Flight cross-section and liquid water content (LWC) measured in a shallow storm system on 16 January 1982.....	131
44.	Condensate production rates (dashed) and ice crystal growth rates as a function of vertical velocity in a water saturated atmosphere at typical atmospheric temperatures and pressures.....	134
45.	Crystal habit climatology for seven shallow storm periods (cloud top > -22°C).....	139
46.	Number flux of crystals at RAD as a function of cloud top temperature.....	142
47.	Droplet concentration vs. liquid water content for N83TW flight on 23 January 1982.....	144
48.	Mean droplet spectra as a function of liquid water content for four flights during the COSE programs.....	149
49.	Ice crystal concentration climatology as a function of temperature at the observation point.....	158
50.	Magono and Lee (1966) ice crystal classification (part 1)....	161
51.	Magono and Lee (1966) ice crystal classification (part 2)....	162
52.	Format for data displayed on Figs. 52-56.....	168
53.	Crystal habits determined from decellerator slide analysis for the 15 Dec 81 flight.....	169
54.	Crystal habits determined from decellerator slide analysis for the 21 Dec 81 flight.....	170

55.	Crystal habits determined from decelerator slide analysis for the 5 Jan 82 flight.....	171
56.	Crystal habits determined from decelerator slide analysis for the 23 Jan 82 flight.....	172
57.	Crystal habits determined from decelerator slide analysis for the 31 Jan 82 flight.....	173
58.	Cumulative frequency diagram showing (A) the percent of observations where the precipitation rate (R) was less than R and (B) the percent of total precipitation which fell at precipitation rates less than R.....	177
59.	Photographs of decelerator slides from the 5 Jan 82 flight when the shallow storm system was present.....	181
60.	Photographs of decelerator slides from the 23 Jan 82 flight near cloud top.....	182
61.	2D-c probe images showing the growth of dendritic crystals in the 5 Jan 82 shallow storm system.....	183
62.	Calculated trajectories of ice particles arriving at RAD and SPL for various mean fall speeds.....	185
63.	Crystals observed at RAD on 13 Dec 81 and 14 Dec 81.....	187
64.	Percent of irregular crystals appearing on shadow photographs as a function of echo top temperature.....	190
65.	Percent of columnar crystals appearing on shadow photographs as a function of echo top temperature.....	192
66.	Percent of needles appearing on shadow photographs as a function of echo top temperature.....	193
67.	Flight track and ice crystal concentrations for the west to east track at -16°C on 21 Dec 81.....	198
68.	Ice crystal size spectra for points on the -16°C west to east flight track displayed on Fig. 65.....	199
69.	Number flux vs. precipitation rate for the 1981-82 data set..	202
70.	Number flux vs echo top temperature for the 1981-82 data set	203
71.	Ice crystal concentrations (l^{-1}) as a function of height and temperature for the 1539-1546 GMT sounding over RAD on 5 Jan 82.....	211

72.	Ice crystal size spectra for selected points on the 5 Jan 82 1539-1546 GMT sounding over RAD.....	212
73.	Ice crystal concentrations as a function of height and temperature for the 2303-2310 GMT sounding 10 km west of RAD on 31 Jan 82.....	215
74.	Ice crystal size spectra for selected points (A-D) on the 31 Jan 82 2303-2310 GMT sounding.....	216
75.	Ice crystal size spectra for selected points (E-G) on the 31 Jan 82 2303-2310 GMT sounding.....	217
76.	19 year climatology of the 70 KPa temperature for the months of November through March at Grand Junction, Co.....	220
77.	Shadow photographs of the 15 Dec 81 storm showing a large number of needles.....	223
78.	Vertical temperature structure of the atmosphere at 1500 and 1800 GMT during the 15 Dec 81 storm system.....	224
79.	Ice crystal concentrations (l^{-1}) as a function of height and temperature for the 1654-1707 GMT, 15 Dec 81 sounding over RAD.....	225
80.	Ice crystal size spectra in the -10°C region of the 1654-1707 GMT, 15 Dec 81 sounding over RAD.....	227
81.	Vertical temperature structure of the atmosphere at 1500 and 1800 GMT during the 21 Dec 81 storm system.....	228
82.	Aircraft flight track for the 21 Dec 81 storm.....	236
83.	Ice crystal concentration (l^{-1}) as a function of height and temperature for the 1632 to 1636 GMT, 21 Dec 81 sounding over RAD.....	237
84.	Ice crystal size spectra at selected points on the 21 Dec 81 1632 to 1636 GMT sounding over RAD.....	238
85.	Largest 2D-c images observed during 1032-1036 GMT, 21 Dec 81 sounding over RAD.....	239
86.	Climatology of rime observations at RAD and SPL.....	241
87.	Shadow photographs showing mixtures of rimed and unrimed particles.....	243
88.	Aggregate flux as a function of surface temperature at RAD...	251
89.	Number of crystals in aggregates as a function of surface temperature.....	252

90.	Climatology of observations of aggregation at RAD and SPL when simultaneous measurements were available	254
91.	Aggregate flux as a function of precipitation rate at RAD....	257
92.	Number of crystals in aggregates as a function of precipitation rate.....	259
93.	Shadow photographs of aggregates in the 15 Dec 81 (a,b) and 29 Dec 81 (c,d) storms.....	261
94.	Shadow photographs of aggregates in the 29 Dec 81 (a), the 30 Dec 81 (b,c) and the 4 Jan 82 (d) storms.....	262
95.	Shadow photographs of aggregates in the 13 Jan 82 (a,b), the 21 Jan 82 (c), and the 27 Jan 82 storms.....	263
96.	Satellite images of the 5 Jan 82 storm at 1315, 1415, and 1515 GMT.....	271
97.	1500 GMT sounding at CG on 5 Jan 82.....	272
98.	Ground based and remote sensing measurements for the 5 Jan 82 storm from 1200-1530 GMT.....	274
99.	Ground based and remote sensing measurements for the 5 Jan 82 storm from 1530-1800 GMT.....	275
100.	5 Jan 82 flight track of Cheyenne II.....	277
101.	Physical model of the aggregation process in the 5 Jan 82 cloud system.....	279
102.	Largest 2D-c images on the 5 Jan 82 sounding.....	280
103.	Vertical profile of the 16 Jan 82 cloud system.....	282
104.	Crystal concentrations, liquid water contents and state parameters from aircraft measurements near the top of the 16 Jan 82 cloud system.....	285
105.	2D-c images from the 16 Jan 82 flight near cloud top.....	286
106.	Droplet spectra from the 16 Jan 82 flight near cloud top.....	287
107.	Conceptual models of the liquid water and ice phase interactions in Park Range cloud systems.....	306

- 108. Radar cloud top climatology for 412.6 hr of significant cloud cover over the Park Range.....307
- 109. Effectiveness (yield) of various nucleants tested and/or developed at the CSU Cloud Simulation and Aerosol Laboratory.322
- 110. Instrumentation network to conduct hypothesis testing field experimentation.....333

CHAPTER I INTRODUCTION

The primary source of water in the southwest United States is the Colorado River. During the recent past, this area has experienced substantial increases in population, agricultural development and energy usage, yet the supply of water to the region has remained unchanged. As demands on the water supply increase, fluctuations in the flow of the Colorado River due to drought will seriously impact the economy of the region as well as the nation. The water dilemma is at hand; the demand on the Colorado River already exceeds the average supply of water available. Fortunately, the water crisis in the Colorado River Basin has been alleviated by a recent series of abnormally wet years. Climatologically, such conditions will not persist.

The Colorado River drains an area of 635,000 km², one-twelfth the area of the United States excluding Alaska. However, 77% of the total runoff to the basin is supplied from 13% of the basin area (Klazura, 1984). Nearly all of this runoff results from winter precipitation. The small area supplying the bulk of the water to the basin consists of eight mountainous regions in Colorado, Utah and Wyoming. Figure 1, from Klazura (1984), shows the locations of these mountain ranges.

Few methods exist to alleviate the impact of a major drought in the Colorado River basin. The best method, conservation, has been utilized extensively throughout the basin through construction of reservoirs and enforcement of regulations concerning water usage and water rights. Snow management techniques have been proposed to limit evaporation of

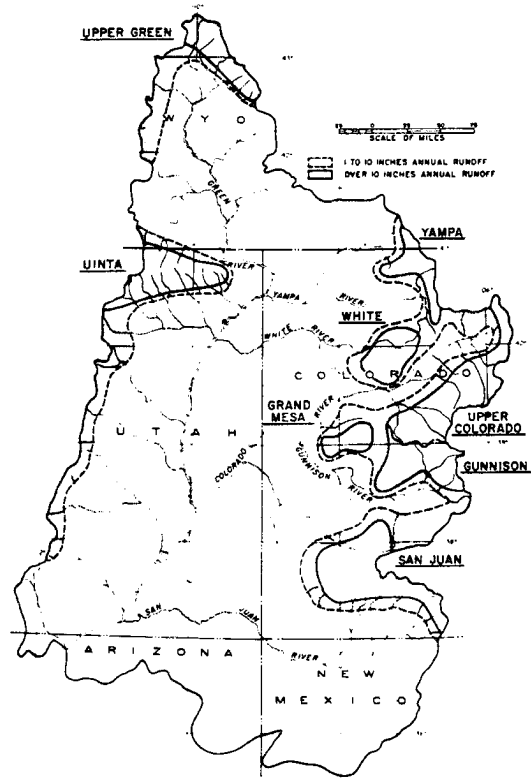


Fig. 1. The upper Colorado River Basin and primary watersheds (from Klazura, 1984).

the snowpack at high elevations. Other methods, such as importation and ocean water desalinization, are too costly to implement. One method to increase natural supplies is through application of weather modification technology.

Weather modification research and operation programs have been active in the western United States since the 1950's. Progress in research has been slow. Conflicting evidence has resulted, partially due to the variability of the storm systems affecting the western United States and partially due to the lack of adequate instrumentation to conduct the investigations. Since the mid-1970's, advances in instrumentation have been substantial. With these new measurement techniques, it is now possible to examine more quantitatively the cloud properties and weather modification potential of these important cloud systems. This dissertation is one contribution toward the re-evaluation of the role of weather modification in the development of the future water resources of this region.

In 1979, Colorado State University began a cloud physics research program to determine the physical structure and weather modification potential of wintertime cloud systems occurring over the Park Range, one of the eight major subbasins supplying the Colorado River. The major thrust of the cloud physics research occurred during two field programs, the first during November and December of 1979 and the second during December and January of the 1981-82 winter. The emphasis of these experiments was to determine the natural physical structure of these cloud systems so that a strong foundation for a weather modification hypothesis could be established.

The purpose of this dissertation is to describe the physical structure and temporal evolution of the wintertime cloud systems which occur over the Northern Colorado River Basin. The specific objectives of this research are to: (1) relate the physical structure of the cloud systems over the region to the large scale environment in which they form; (2) determine the physical distribution, temporal variation, microphysical structure and climatological frequency of supercooled water; (3) examine the physical processes associated with the development of the ice phase, specifically, primary nucleation, ice multiplication, vapor deposition, accretion and aggregation; (4) develop a coherent physical model of the natural precipitation process in these clouds and (5) assess, qualitatively, the potential of weather modification to augment precipitation in this region.

This document is of considerable length. Chapter II contains a discussion of instrumentation. Chapters III and IV contain analyses of liquid and ice phase processes respectively. Chapter V presents a summary of the material in the previous two chapters. For those readers not wishing to examine the detailed analyses, Chapter V is a concise synopsis of this material in this thesis. Chapter VI contains a discussion of precipitation augmentation hypotheses and experiments and Chapter VII summarizes the major conclusions.

1. Background

Weather modification research programs utilize three methods to evaluate the results of experiments. The first method, statistical analysis, uses randomization procedures over a sufficient data sample to insure that a change in precipitation, if it exists, can be recognized as a statistically significant effect. The precipitation data are then

evaluated using statistical techniques to determine the probability that a seeding effect occurred during the experiment. The data are normally stratified according to meteorological partitions which hopefully relate to some physical process associated with cloud system structure. Control stations and covariates are often utilized to strengthen the statistical analyses. Examples of statistical experiments which have been conducted in the western United States include the Climax experiments (Mielke et al., 1971, 1981), the Colorado River Basin Pilot Project (Elliott et al., 1978), and the Bridger Range experiment (Super and Heimbach, 1983).

The second method of analysis is through direct measurement of physical parameters. This method is logistically very difficult, especially in mountainous regions, particularly if one attempts to follow the complete process from nucleation to precipitation. In this method, case studies are developed and eventually generalized into a conceptual model of the chain of events which lead to the change in precipitation. Examples of such programs include the Park Range Atmospheric Water Resources Program (Rhea et al., 1969), the Cascade Atmospheric Water Resources Program (Hobbs, 1975b), and the Sierra Cooperative Pilot Project (Reynolds, 1984).

The third method of analysis and interpretation is to utilize numerical models of the cloud system. If properly modeled, this technique can be used to evaluate the relative roles of many of the physical processes leading to the development of natural and artificially induced precipitation. The words "properly modeled" carry heavy weight. Examples of such modelling attempts include the work

of Fraser et al. (1973), Hobbs et al. (1973), Young (1974b,c), and Plooster and Fukuta (1975).

With any method, it is paramount that the natural physical structure and natural variability associated with the cloud system to be modified is understood. Without such background, the tremendous variability of the structure of the atmosphere, the complications of scale interaction, and the certainty of the "bad draw" will ultimately plunge the scientific results into controversy. This has been the fate of many otherwise carefully planned and executed programs (e.g. Braham et al., 1971, Hobbs and Rangno, 1979; Rangno and Hobbs, 1980; Smith and Miller, 1984).

Weather modification research programs have been carried out in the western United States for over 25 years. The immediate emphasis of the majority of these programs has been to determine the effects of cloud seeding on precipitation. Prior to 1977, little emphasis has been placed on studying the natural physical structure of the cloud systems to be modified. Two notable exceptions have been the Cascade Program (Hobbs, 1975a) and the Colorado River Basin Pilot Project (Cooper and Marwitz, 1980). In the latter case, the majority of the measurements of the natural physical structure of the clouds were made at the end of the project. After 1977, the emphasis in weather modification research turned to physical evaluation. A much stronger emphasis was placed on studying natural cloud conditions. Two factors influenced this change. The first was that physical results such as Hobbs (1975a) and Cooper and Marwitz (1980) conflicted with the conceptual models of cloud system structure that formed the basis of the hypothesis of the earlier experiments. The second and major factor was that new instrumentation

became available to acquire the large quantities of data needed to determine the structure of the natural cloud systems. The purpose of this section is to review what has been learned about the physical structure and evolution of natural cloud systems occurring over the mountains of the western United States. These cloud systems can be divided into two broad groups, coastal mountain ranges (Sierras and Cascades) and inland mountain ranges (Wasatch and Rockies).

A. Coastal mountain ranges

Operational and research programs to augment precipitation along the west coast of the United States have had a long history. Yet few research programs until recently have emphasized the study of the natural cloud systems which effect the region. Six significant weather modification research programs have been conducted in the coastal regions since the late 1950's. These include two in Santa Barbara County (Neyman et al., 1960; Elliott et al., 1971), three in the central Sierra (the Pyramid Lake Program (Squires, 1977), the Central Sierra Research Program (CENSARE) (Rowland et al., 1973), and the Sierra Cooperative Pilot Project (SCPP) (Reynolds, 1984)), and a program in the Cascades of Washington (Cascade Atmospheric Water Resources Program (CAWRP) (Hobbs et al., 1975b). Of these programs, three (CENSARE, CAWRP, SCPP) have attempted to characterize some aspects of the natural state of the cloud systems. Two (CAWRP, SCPP) have made this a major component of the program.

(1) CENSARE

The CENSARE program utilized randomization to determine statistically the effects of cloud seeding in the central Sierra. Significant efforts were made to classify storms based on their synoptic

and mesoscale characteristics. The major component of the cloud physics research associated with natural and seeded storms during CENSARE was an empirical assessment of accretion microphysics by Reinking (1973). This work was later summarized by Reinking (1975, 1979). Reinking found that heavy rime and graupel formation were common to all stages of Sierra storms, accounting for at least half the mass of the total precipitation. In cases where deep, cold clouds were present (based on rawinsonde analysis), few crystals observed by Reinking had the bulk of their diffusional growth occur at temperatures colder than -20°C . Reinking determined that clouds must have non-uniform liquid water contents and that the bulk of the supercooled water was located at temperatures warmer than -10°C . In his habit classification, needles and sheaths account for half the total precipitation sample. Concentrations of crystals nucleated at temperatures warmer than -20°C were substantially greater than the natural nuclei spectra would suggest, with crystal concentrations increasing toward warmer temperatures. Crystal concentrations were found to exceed natural nuclei by 3 to 4 orders of magnitude. However, some uncertainty was introduced in the Reinking study concerning the origin of these crystals since 8 of the 9 storms examined by Reinking were seeded. Reinking provided an extensive climatology of the accretion process in Sierra storms. His results are discussed in Chapter 4.

(2) CAWRP

The Cascade Program was the only large weather modification program prior to 1977 that emphasized study of the natural cloud structure prior to any attempts at modification. It was also the only program which had no statistical component. A detailed review of the program is contained

in Hobbs et al. (1975b). More concise reviews are available in several publications which include theoretical studies of airflow, microphysical processes and trajectories of ice crystals in natural and seeded clouds (Fraser et al., 1973; Hobbs et al., 1973), studies of natural cloud system structure and precipitation characteristics (Hobbs, 1975a; Locatelli and Hobbs, 1974; Hobbs et al., 1974), instrumentation and analysis techniques (Weiss and Hobbs, 1975; Hobbs and Radke, 1975; Radke and Hobbs, 1969; Turner and Radke, 1973), and evaluation of seeding effects (Hobbs and Radke, 1975; Hobbs, 1975b).

With regard to natural cloud system structure, observations during the program indicated that in prefrontal conditions, ice particles dominate over water droplets at temperatures colder than -10°C . The ratio of ice to water was lower in post frontal conditions. Hobbs (1975a) found that the passage of an occluded or warm front was accompanied by a sharp lowering of the diffusional growth layers. As a consequence, particles reaching the ground were converted from unrimed to rimed crystals. Hobbs also found that the maximum ice particle concentrations in the clouds were often several orders of magnitude greater than measurements of ice nuclei. Results of the study also indicated that the growth of precipitation particles by riming and aggregation is particularly rapid in the last kilometer of fall and that snow particles reaching the ground originate 10 to 100 km upwind. During the program, particular emphasis was placed on the competing processes of riming and aggregation. Case studies presented by Hobbs (1975b) showed that seeding typically resulted in a marked decrease in riming and an increase in aggregation of particles arriving at the surface. A significant amount of information was compiled concerning

the physical structure of clouds and precipitation including crystal concentrations, habits, sizes, fallspeeds, and characteristics of rime and aggregation. Information relative to this study will be discussed in more detail in Chapter 4.

(3) SCPP

The SCPP is an ongoing weather modification research program conducted by the Bureau of Reclamation since 1976 in the central Sierra. A large number of reports and publications have been generated by the program concerning natural cloud conditions. These include aircraft observations (Marwitz et al., 1978, 1979; Stewart, 1979; Stewart and Marwitz, 1980; Marwitz and Stewart, 1979; Gordon and Marwitz, 1981; Bradford et al., 1981; Heggli et al., 1983), ground observations (Vardiman and Humphries, 1979; Humphries and Moore, 1981) and radar observations (Johnston, 1981; Huggins, 1981). Studies of the microphysical effects of seeding and dispersion of seeding material have also been reported (Marwitz and Stewart, 1981; Stewart and Marwitz, 1982a,b; Rodi, 1984; Huggins, 1984; Martner, 1984; Humphries, 1984).

Cloud systems affecting the central Sierra in winter are extremely complex at all scales. Marwitz and Stewart (1979) classified the cloud systems into three distinct groups which included stable orographic, bands and unstable orographic. Huggins (1981) expanded this description to seven groups based on precipitation echo types. Aircraft observations in most cases indicated that ice crystal concentrations were one to several orders of magnitude higher than expected, based on standard ice nuclei spectra. Studies such as Stewart (1979), and Vardiman and Humphries (1979) have indicated that the ice multiplication process described by Hallett and Mossop (1974) is frequently active in

the clouds. Ground observations of Humphries and Moore (1981) indicate that irregular crystals account for half of the precipitation, indicating that crystal fracturing (Vardiman, 1978) also occurs. Warm rain processes have also been identified (Stewart, 1979).

Evidence presented by Humphries and Moore (1979) confirm the earlier work of Reinking (1975) at CENSARE that accretion is a dominant growth process in the Sierras and that the liquid water in the cloud is generally in the low cloud levels. Summaries of the SCPP aircraft observations of liquid water and ice crystal distributions by Heggli et al. (1983) for the seven cloud types identified by Huggins (1981) have indicated that, at aircraft altitudes, convective clouds have the highest concentration of supercooled water, particularly 40-90 km upwind of the crest and at temperatures warmer than -10°C . The liquid water/ice crystal concentration ratio was largest 7-10 hours after 700 mb trough passage. Largest liquid water contents were generally between 0°C and -5°C . Wide-area and banded cloud systems were found to contain high ice crystal concentrations and low liquid water contents.

B. Inland mountain ranges

During the last 30 years, wintertime cloud physics and weather modification research programs have been conducted in nine regions of the intermountain west. These include the Park Range area of Northern Colorado (Rhea et al., 1969 and present study), the Climax region of central Colorado (Mielke et al., 1971, 1981), the San Juan mountains of southern Colorado (Grant and Elliott, 1974; Elliott et al., 1978), the Bridger Range of Montana (Super and Heimbach, 1983), Elk Mountain of Wyoming (Politovich and Vali, 1983), the Jemez mountains of New Mexico (Keyes et al., 1973), the Wasatch of northern Utah (Hill, 1979), the

Wasatch of southern Utah (Long, 1984) and the mountains near Elko County, Nevada (Grant and Elliott, 1974).

Of the thirteen previously reported programs, three (Elko, Jemez, Wolf Creek Pass Experiments) had only a statistical component and will not be reviewed here. Of the remaining ten, six reported limited measurements of natural cloud physical structure and four had more comprehensive measurements. These programs are reviewed below.

(1) Climax I and II

The Climax experiments (Mielke et al., 1981) were primarily statistical experiments. However, extensive physical observations of surface ice nuclei (Grant and Mielke, 1967) and limited studies of ice crystal concentrations (Hindman, 1967; Chappell, 1967), precipitation characteristics (Grant, 1965; Hindman, 1967; Chappell, 1970), and radar echo characteristics (Furman, 1967) were collected during certain seasons of the experiment. Additional work was carried out by Chappell (1970) to establish the conditions where the rate of condensate supply balanced the rate of diffusional growth in clouds, but physical data to support the theoretical work was unavailable at the time.

Grant and Mielke (1967) reported the results of extensive nuclei measurements during the five years of the Climax I experiment. The data base consisted of surface ice nuclei measurements over a broad temperature range. The measurements were repeated twice a day on most days of the experiment from two sites. With the exception of one anomalous year, they found that ice nuclei concentrations seldom exceeded 10 l^{-1} at -20°C and were generally less than 1 l^{-1} on unseeded days. On seeded days, substantially higher concentrations were recorded.

Surface observations of ice nuclei concentrations at Climax were also reported by Hindman (1967). Hindman investigated the relationship between ice nuclei concentrations at the Climax High Altitude Observatory and ice crystal concentrations in snowfall during two seeded and two non-seeded storm events. After making several assumptions concerning the large scale and microstructure of the storms analyzed, he concluded that concentrations of ice nuclei and ice crystals were similar in the non-seeded cases but differed by an order of magnitude in the seeded cases (ice nuclei higher). Hindman also presented limited data on the crystal types and accretion characteristics of precipitation during these two storm events. More detailed summaries of crystal habits, sizes and accretion characteristics as well as ice nuclei observations during the Climax experiments were presented by Grant (1965), Chappell (1967), and Chappell (1970) and Vardiman (1972). Vardiman (1972, 1978) also discussed fragmentation as a possible means of crystal concentration enhancement in Climax cloud systems.

Radar observations of cloud systems during the Climax experiment were reported by Furman (1967). Furman examined the echo characteristics of four spring storms with horizontally and vertically scanning 3 cm radars. He determined that mean cloud tops over the Climax region during these storms varied from 450-550 mb, although cloud tops occasionally reached the 350 mb level. Furman's analysis implied that the most intense precipitation (strongest echoes) were consistently located in the vicinity of ridgetop and that propagation of the echo pattern closely followed the 500 mb velocity vector. His work primarily emphasized convective periods which could be most readily observed with the available radar.

Additional work emphasizing the transport and dispersion of silver iodide in the Climax region was conducted by Reid (1976) and Orgill (1971). Reid studied the dispersion of silver iodide with aircraft and surface measurements. Orgill (1971) simulated the transport of seeding material using a physical model of the Climax region in a wind tunnel.

(2) Park Range Atmospheric Water Resources Program (PRP)

The PRP was the first major wintertime weather modification field effort to conduct an extensive physical evaluation of the effects of cloud seeding to augment precipitation (Rhea et al., 1969). Analysis of the physical data was supported by the use of a steady-state numerical model of orographic precipitation developed at EGG Inc. (Willis, 1970). A significant number of transport and dispersion studies were also conducted. The majority of the physical results of the experiment were based on data collected during the 1968-69 field season. The analysis of the 1968-69 data set incorporated both the case study approach as well as statistical analyses of the precipitation data. Unfortunately, only limited data were presented concerning natural cloud system structure. The majority of the data were associated with identification of seeding signatures. This was primarily through analysis of ice crystal replicas, measurements of ice nuclei and silver in snow during pulsed seeding events.

The major results of the PRP based on five winter seasons of operation are summarized by Rhea et al. (1969). During the program, significant amounts of seeding material were found in target area precipitation, in timing and location with calculated occurrence of seeding effects. In several case studies, a positive seeding effect was clearly evident. During the seeding period, small hexagonal plates were

frequently observed in replica samples, although ice nuclei identification indicated that some material had reached the dendritic growth region.

Regarding natural cloud system structure, Rhea et al. made three important observations regarding mesoscale cloud system structure which have been confirmed in the present study (Chapter 3). These are:

- a. "The highest precipitation rates (frequently exceeding 0.1 in hr^{-1}) usually occur in the first 3 to 6 hours following the surface passage of maritime polar fronts. This time period frequently coincides with the existence of 240° to 270° flow above 12000 ft M.S.L. but 280° to 310° flow at lower levels."
- b. "Longer periods of lighter (0.003 to 0.050 in hr^{-1}), mainly orographic precipitation usually continue after passage of the frontal convergence area with cloud tops lowering to between 15000 ft M.S.L. and 11500 ft M.S.L."
- c. "There is usually a convective precipitation component, which is reflected in the unsteady precipitation rates observed. Convective band passages at 2.5 to 4 hour intervals are quite commonly observed."

Rhea (1967) concluded that the first two components mentioned above account for about 80% of the Park Range winter precipitation.

The PRP also made extensive measurements of ice crystal habit. They found that dendritic crystals accounted for 50% of the snowfall. Less than 6% were of columnar or needle habit. This is one very significant difference between the Park Range region and coastal regions discussed in the previous section.

(3) Utah I and II

The two Utah weather modification programs reported by Hill (1979) were statistical experiments. They are mentioned briefly here because of the novel use of aircraft icing reports in the statistical analyses as an indicator of supercooled cloud liquid water content. Hill (1982a) expanded this idea in a second paper. Based on icing observations during 243 events, he concluded that the magnitude of the supercooled liquid water content is primarily related to the cross-barrier wind speed. The critical cloud top temperature below which liquid water would be insignificant was also related to the cross-barrier wind speed. Although this type of analysis is extremely subjective, it does provide a means of developing a cloud climatology with data available from standard pilot reports.

(4) Bridger Range Experiments

The Bridger Range experiments had two strong components, a statistical program (Super and Heimbach, 1983) and a program to determine the transport and dispersion of seeding material. However, limited physical measurements of cloud characteristics were collected on some days.

Radar characteristics of cloud systems over Montana's Bridger Range in both natural and seeded situations were reported by Super et al., (1972). They found that rapid temporal and spatial variations in precipitation intensity were common in all cloud systems, suggesting that wintertime orographic precipitation, even in simple airflow situations, is not a quasi-steady process. These rapid variations also made detection of seeding effects difficult with radar. However, in

some experiments, particularly with aircraft seeding, high reflectivity regions associated with AgI plumes were identified.

Super et al. (1972) also provided a radar derived cloud top climatology for the region based on one winter season which indicated that mean precipitation tops were at 14400 ft M.S.L. Precipitation tops exceeded 16000 ft M.S.L. in only 7% of the cases. Tracking radar studies of airflow over the Bridger Range based on pibal releases indicated that air approaching the barrier accelerated significantly near the crest, particularly at low levels.

During the 1971-72 season, several days were set aside for physical experiments designed to directly detect the effects of cloud seeding. Twelve case studies developed from these experiments were reported by Super et al., (1972). In many cases, changes in the precipitation characteristics observed were attributed to seeding. However, these studies provided little information concerning natural cloud system structure since all were seeded events.

(5) The Colorado River Basin Pilot Project

The Colorado River Basin Pilot Project was conducted in the San Juan Mountains of southwest Colorado during the five winter seasons ending in 1974-75 (Elliott et al., 1978). Physical studies of cloud systems occurring over the San Juan Massif during this period were conducted by the University of Wyoming (Marwitz (1980); Cooper and Saunders (1980); Cooper and Marwitz (1980)) and the University of Washington (Hobbs et al., 1975a). Results of these studies indicate that most storms in the San Juans evolve through four stages related to thermodynamic instability. These were a stable stage, followed by neutral, unstable and dissipation stages.

The stable stage was characterized by blocked flow. During the stable stage, precipitation developed primarily by diffusional growth and liquid water was rarely observed. The neutral stage typically was characterized by deep cloud systems. Liquid water was observed primarily over the barrier during this stage. During the late storm stage, convection was frequently observed. Liquid water was found in three regions: (1) slightly upwind of the barrier; (2) 15-20 km upwind of the barrier associated with the release of convective instability; and (3) 60-70 km upwind of the range associated with an initial rise in the topography. Cooper and Marwitz (1980) stressed the importance of the zone of convergence 15-20 km upwind as a mechanism to transport seeding material to cold cloud levels.

During storm events, ice crystal concentrations far exceeded natural ice nuclei concentrations. According to Cooper and Saunders (1980), no known ice multiplication mechanism could be attributed to these high ice crystal concentrations. Hobbs et al. (1975a) also found high ice crystal concentrations but attributed them to ice multiplication. No mechanism was proposed.

Cooper and Saunders discussed microphysical aspects of the liquid water and ice crystal distributions during San Juan storms. These observations will be discussed more fully later.

(6) Elk Mountain Experiments

Elk Mountain, an isolated peak in south-central Wyoming, has been the site of a cloud physics observatory operated by the University of Wyoming for over 15 years. Numerous reports and publications have resulted from studies of orographic clouds which occur over this peak. Two summary papers concerning Elk Mountain cap clouds have been

presented recently by Cooper and Vali (1981) and Politovich and Vali (1983).

Cooper and Vali discuss the origin of ice in mountain cap clouds. Their study indicated that ice particles originate in association with the initial condensation process at the upwind edge of the cloud and that ice particle production is limited to this region. They determined that contact nucleation or the condensation freezing process must be the mechanism of nucleation of these crystals. No evidence of secondary multiplication processes was observed and nucleation was observed to exhibit a clear temperature trend. Their study indicated that cloud top was composed almost entirely of supercooled water.

Politovich and Vali (1983) discussed the structure and evolution of the supercooled water in these cloud systems. They found that droplet concentrations were typically $250\text{--}300\text{ cm}^{-3}$, and that droplet spectra were consistently very narrow. CCN concentrations were also found to be low. This was attributed to the lack of anthropogenic sources and wintertime snow cover inhibiting mechanical interaction with the surface. Liquid water contents in the cloud were generally in the range of $0.16 \pm 0.15\text{ gm}^{-3}$. Cloud droplet concentrations were found to stabilize near cloud edge and were not a function of liquid water content indicating smooth airflow and continuous condensate production throughout the cloud. Increases in liquid water content were generally associated with a shift in the droplet spectra as the cloud advected across the mountain peak.

(7) Utah physical experiments

Measurements of supercooled cloud water, precipitation, vertical air motion and cloud top temperature were made by Utah State University

(Hill, 1980) in the northern Wasatch Mountains of Utah during the late 1970's. Hill found that the presence of supercooled liquid water in cloud systems over the northern Wasatch was primarily related to the vertical velocity generated by flow deflection over the barrier. This vertical velocity was found to be proportional to the cross-barrier wind speed. The magnitude of the liquid water in the cloud was also modified by the crystal concentrations present in the cloud, as indicated by the precipitation rate. Higher precipitation rates were associated with colder cloud top temperatures. Data presented by Hill also showed that aircraft icing was approximately proportional to cross-barrier wind speed. Using these results, Hill suggested a seeding hypothesis based on cross-barrier wind speed and cloud top temperature criteria.

Marwitz and Stewart (1978) reported the results of four aircraft flights over the northern Wasatch and Uinta Ranges during the spring of 1978. They found that concentrations of supercooled water at flight levels exceeded 0.2 gm^{-3} only in convective elements and that regions of high liquid water concentrations contained few ice crystals. Clouds over the Uinta Range during the study were found to be devoid of liquid water. These clouds had significant amounts of ice crystals, mostly unrimed.

(8) Utah Federal-State Cooperative Project

The Utah Federal-State Program is an ongoing program of research "piggy-backed" on an operational program in the southern Wasatch Mountains of Utah. Preliminary results of this program are contained in project reports by Hill (1982b) and Long (1984). The emphasis of these programs has been the study of ice nuclei dispersion and supercooled liquid water distributions. Studies in this program are not

specifically focused on natural cloud systems, since seeding operations associated with the operational program are routinely performed.

Hill (1982b) found that low level inversions were frequently present over the valley west of the southern Wasatch, even during storm periods. These inversions severely complicated the nuclei dispersion characteristics. The distribution of supercooled water was found to be closely associated with the topography. Liquid water contents were maximum over the range and minimum over the valley. Few events occurred where liquid water was observed during the two month study. However, according to Hill, the period of observation was generally uncharacteristic of storms which affect the area based on climatology. Cloudsonde data reported by Hill indicated that the maximum liquid water contents were at the elevation of the barrier crest. Observations of rime on crystals at the radiometer site during the program generally supported the radiometric measurements of liquid water described above. Aircraft observations of ice particles during the experiment indicated that ice particles grew rapidly in regions of high liquid water content, that riming substantially steepened ice particle trajectories, and that the maximum precipitation rate lags the maximum liquid water content from 0-20 minutes.

Long (1984) confirmed the findings of Hill (1982b) concerning nuclei entrapment by inversions. Long's study of liquid water structure using radiometric data also confirmed that liquid water contents were greatest over higher topography. Long presented climatological values of integrated liquid water content based on radiometric data. These were categorized according to precipitation echo type based on C-band radar operations. Rauber and Grant (1985) reported that shallow

blanket-type clouds contributed 50% of the total precipitation at high altitudes for southern Utah storms during the 1983 program.

2. Summary

Despite the fact that a significant amount of information has been assembled concerning the natural structure of cloud systems over the mountains of the western United States, our knowledge of natural cloud system processes is still fundamentally weak. This is particularly true for clouds which develop over the Colorado River Basin. It is important that the results of past, ongoing and future programs be incorporated into a comprehensive model of natural precipitation formation and development. With this background, the true potential of weather modification to supplement the water resources of the Colorado River Basin can be assessed. This work is one contribution toward that end.

CHAPTER II INSTRUMENTATION AND EXPERIMENTAL PROCEDURES

1. The Colorado Orographic Seeding Experiment

The Colorado Orographic Seeding Experiment (COSE) was organized in 1979 by CSU to study the structure of cloud systems occurring in winter over the Northern Colorado River Basin and to assess their potential for modification to enhance mountain snowpack. During the 1981-82 field phase of the experiment, a comprehensive network of aircraft, remote sensors and ground based observation stations was assembled to investigate the physical and microphysical characteristics of these storms. Because the 1981-82 instrumentation network was specifically designed to study the natural conditions occurring in these storm systems, no seeding operations were conducted during major storm events throughout the experiment. Figure 2, a map of the experimental area, shows the local topography, the location of the major instrumentation, and the location of the experimental area in the state of Colorado. Figure 3 shows a vertical west-east cross-section of the topography over the region. A complete list of all cloud physics instrumentation used during the experiment and the organizations that supplied the instruments is included in Table 1. The 1979 program was similar to the 1981-82 program, but operated with a much smaller instrumentation base. The instrumentation network and data collection procedures associated with the 1979 program have been described by Rauber (1981). Data obtained during the 1979 program with the Queen Air aircraft (N306D) provided by the National Center for Atmospheric Research are used in

COSE FIELD PROGRAM INSTRUMENTATION DEC 81-JAN 82

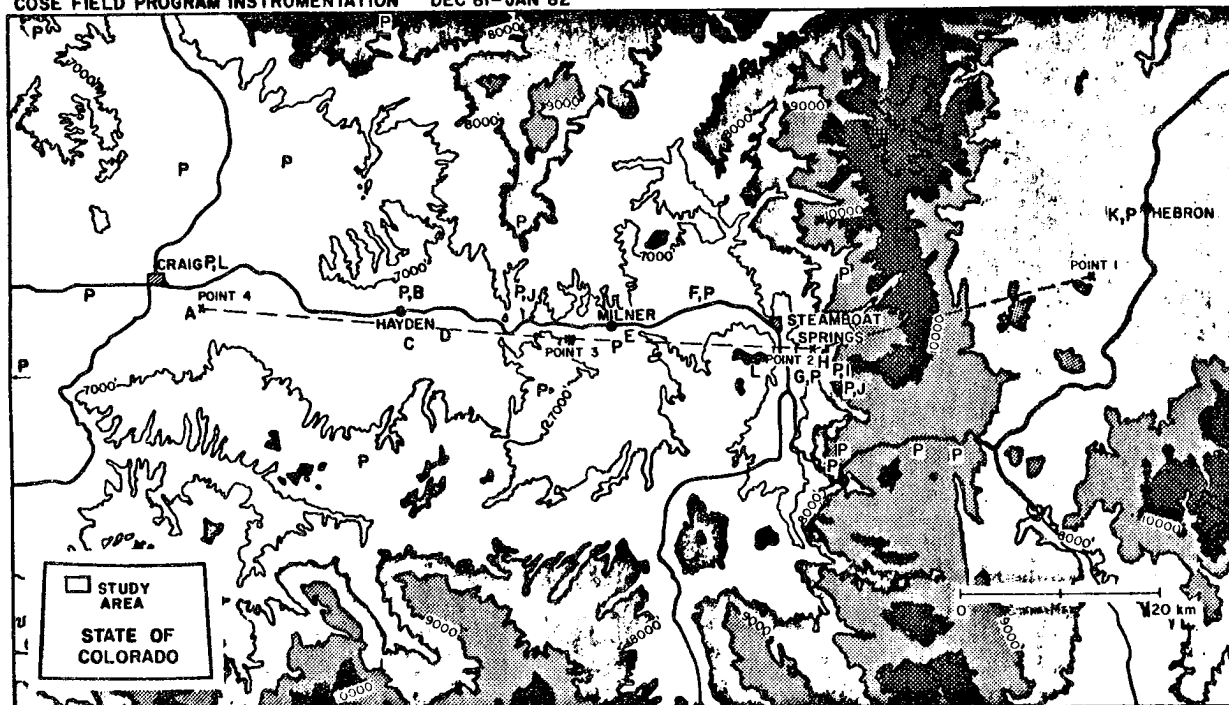


Fig. 2. COSE field program instrumentation network. The insert shows the location of the study area in the state of Colorado. The letters show the position of the major project instrumentation. A: rawinsonde, aerosol sampler; B: AgI, IN_2O_2 generators; C: AgI generator; D: acoustic sounder; E: 0.8 cm radar; F: 3.0 cm radar, acoustic sounder, aerosol sampler; G: 1.79 cm radar, dual-channel radiometer, lidar, ice crystal observations; H: aerosol sampler; I: aerosol sampler, SO_2 monitor; J: Storm Peak Laboratory; K: rawinsonde, aerosol sampler, lidar; L: Dy_2O_3 generator; P: Probe remote weather stations. The dashed line shows the standard flight track. Four points where aircraft soundings occurred are labeled along this line.

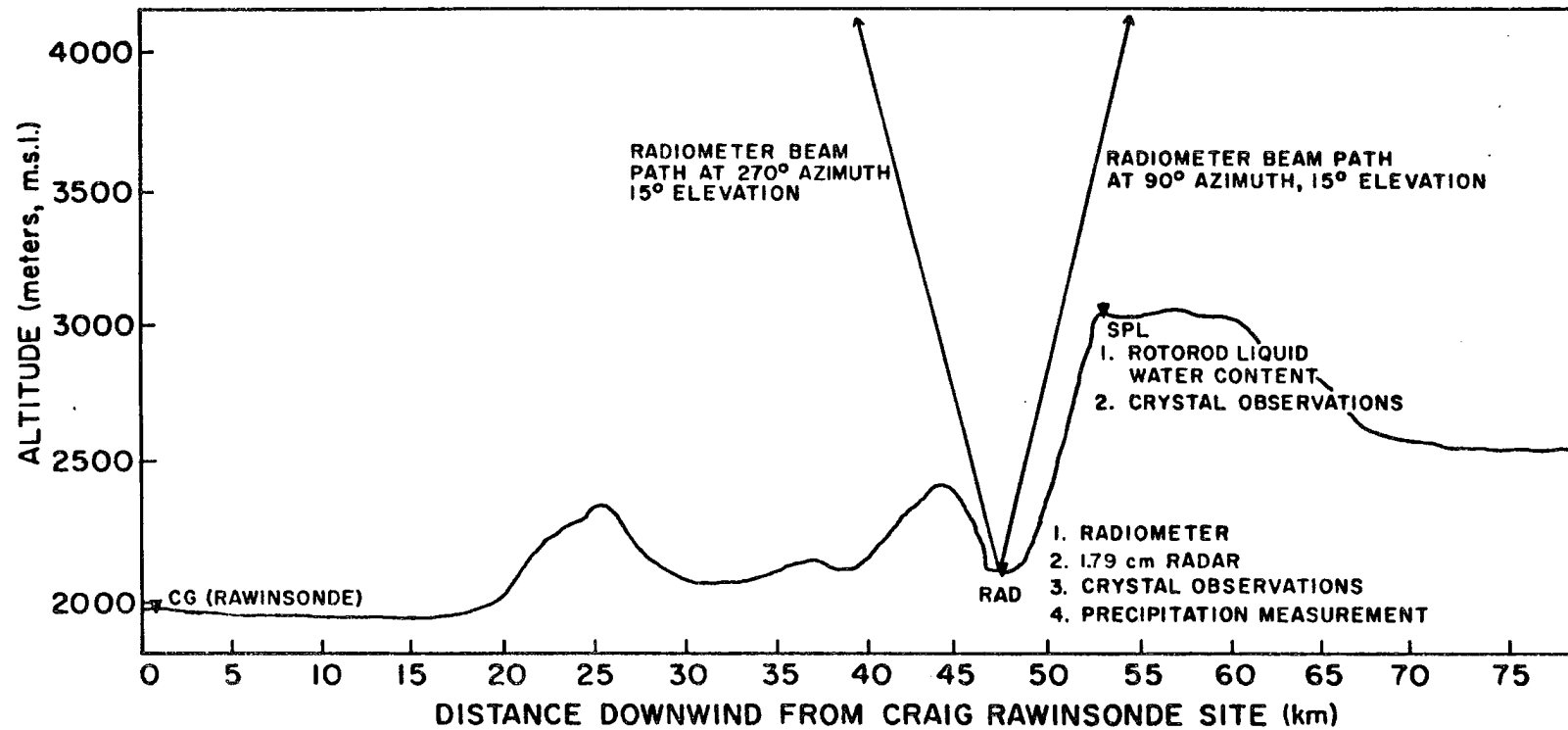


Fig. 3. Topographic profile of the COSE study area showing the location of instrumentation used in the study.

Table 1

Cloud physics instrumentation network for COSE, December 1981-January 1982

<u>Instrumentation</u>	<u>Supplier</u>
<u>Aircraft:</u>	
Cheyenne II	Colorado International Corporation
WP-3D	National Oceanic and Atmospheric Administration
<u>Remote Sensors:</u>	
0.8 cm radar	National Oceanic and Atmospheric Administration
1.8 cm radar	Colorado State University
5.0 cm radar	Bureau of Reclamation
Dual-wavelength Radiometer	National Oceanic and Atmospheric Administration
Lidar	University of Utah
<u>Rawinsonde sites:</u>	
Craig, Colorado	Bureau of Reclamation and Colorado State Univ.
Hebron, Colorado	
<u>Storm Peak Laboratory:</u>	Colorado State University
<u>Probe Micromet Stations:</u>	Bureau of Reclamation

this dissertation. For this reason, a brief review of the instruments available on this aircraft will be presented in this chapter. Unless stated otherwise, all heights reported in this paper are with respect to mean sea level and all times are Greenwich Mean Time (GMT).

2. Instrumentation

A. Aircraft

Aircraft measurements used in this work were collected during six storms in the 1981-82 program and three storms in the 1979 program. These data were collected by cloud physics research aircraft provided by the National Center for Atmospheric Research (NCAR) and Colorado International Corporation (CIC). The NCAR Queen Air (N306D) operated during the 1979 program. In general, flight profiles with N306D consisted of two transects of the Park Range near 4200 m, the minimum flight altitude, and a sounding near Hayden, Colorado, located approximately 40 km upwind of the Park Range crest. One transect was normally 10-20 km south of the other in the vicinity of the Park Range. An example of an N306D flight track from 26 Nov 79 is shown on Fig. 4. Table 2 summarizes the instrumentation specifications for N306D.

The CIC Cheyenne II aircraft (N83TW) was used during the 1981-82 field program. This aircraft had higher performance characteristics and could remain in the study area for a much longer time. Flight profiles generally consisted of horizontal transects across the Park Range at 300 m altitude intervals from Craig, Co. to Hebron, Co. and vertical soundings at four points along the flight path. These points coincided with the major ground based instrumentation. An example of the complete flight track specified by the program design plan is shown in Fig. 5. In general, the track was modified to accommodate changing cloud

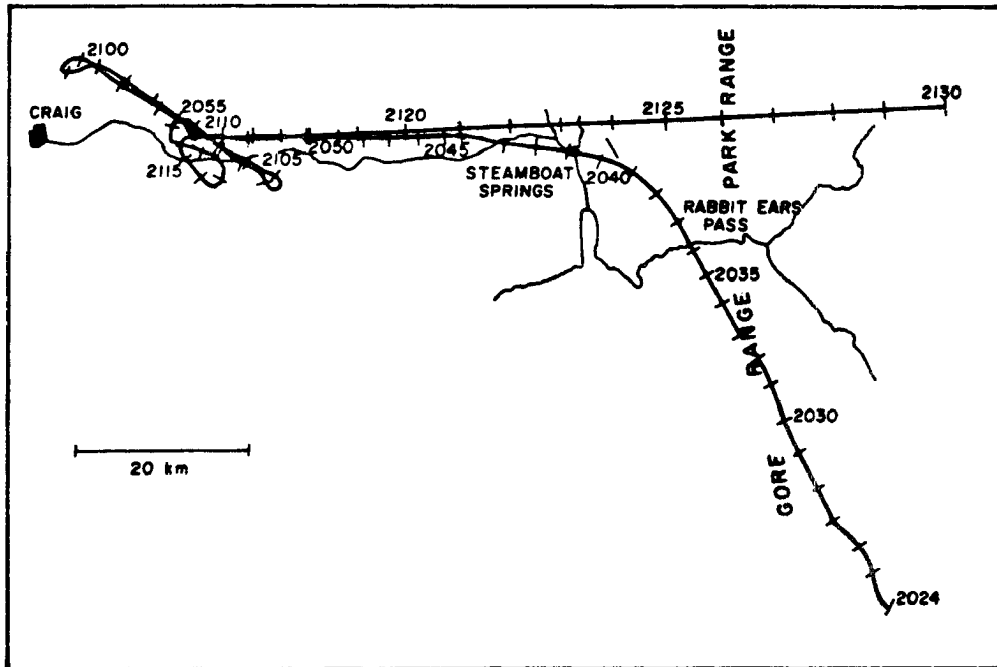


Fig. 4. N306D flight track for 26 November 1979.

Table 2
INSTRUMENTATION LIST
COLORADO OROGRAPHIC SEEDING EXPERIMENT
QUEEN AIR N306D

Instrument	Range	Accuracy	Resolution
Rosemount Temp	-40 C to +40 C	0.5 C	0.02 C
Reverse Flow Temp	-40 C to +40 C	0.5 C	0.02C
E G G Dewpoint	-50 C to +30 C	0.5 C > 0 C 1.0 C < 0 C	0.02 C
Static Pressure	30 to 103.5 Kpa	0.1 KPa	0.01 Kpa
Dynamic Pressure	0 to 6.5 KPa	0.05 KPa	0.002 KPa ₃
J-W liquid water	0 to 2 g/m ³	---	0.005 g/m ³
Wind Speed (WSPD)	---	1+0.5t m/sec t=hours in flight	0.01 m/sec
Wind Direction	0-360 deg	Cot ⁻¹ (WSPD)	
Aircraft Position		1.2 nm/hour	0.1 nm
Pitch, Roll	45 deg	0.05 deg	0.005 deg
Heading	0-360 deg	0.05 deg	0.005 deg
Attack angle	20 deg	0.2 deg	0.01 deg
Sideslip angle	20 deg	0.2 deg	0.01 deg
PMS FSSP	3-45 microns	---	15 channels
Radio altitude	0-2500 ft	5%	10 ft

Photography—One forward looking 16mm color film
time and date encoded, 1 frame per 5 sec.

Colorado State University supplied instrumentation:
PMS 2-D probe with Data Acquisition System
Langer ice nuclei counter

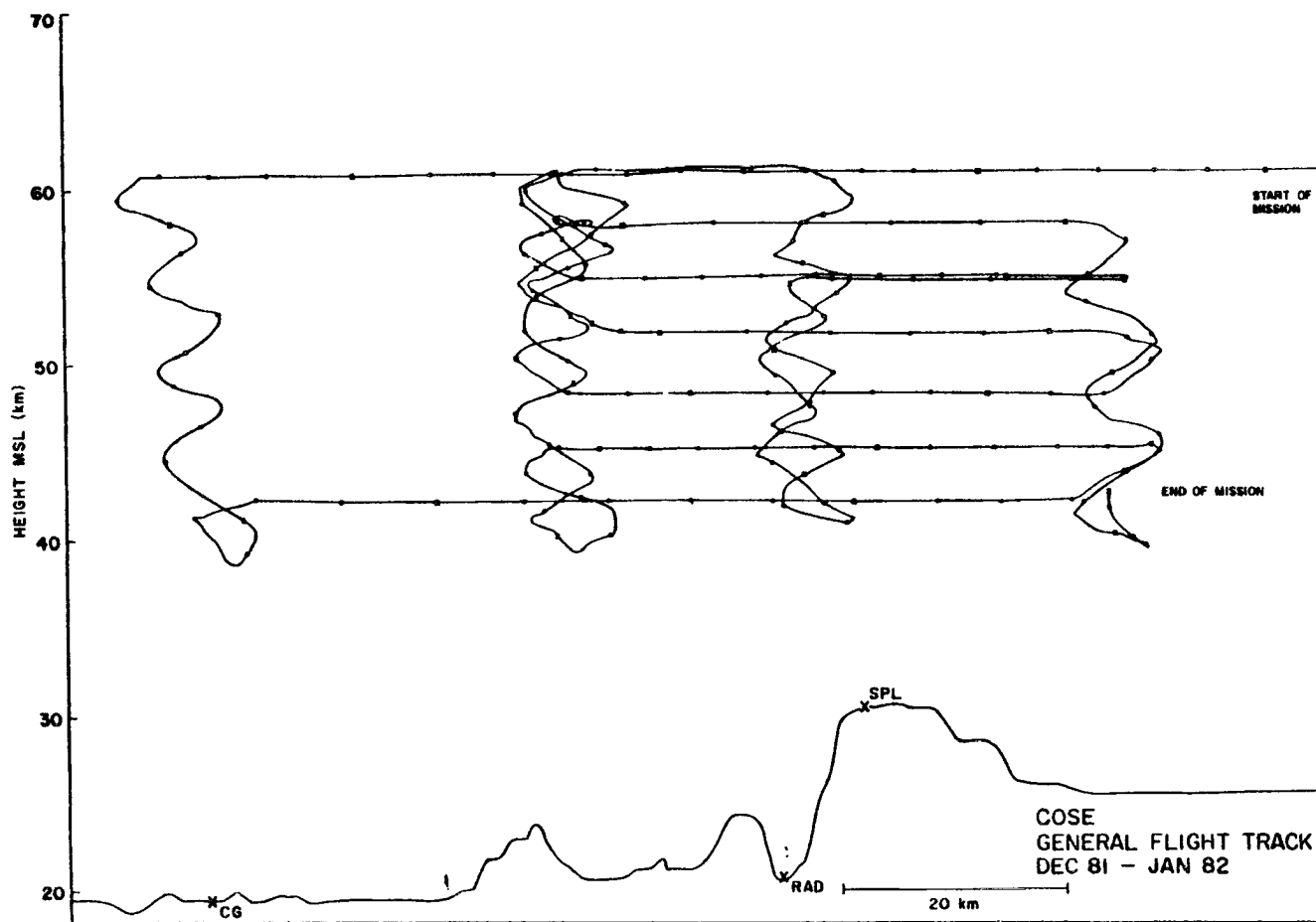


Fig. 5. Generalized flight cross-section used by N83TW aircraft. Track was modified during flights to accommodate changing cloud depth.

conditions, particularly cloud depth. However, the general characteristics were the same for all N83TW flights. The instrument specifications for N83TW are listed in Table 3.

The primary instruments used in this study were the Particle Measuring Systems Forward Scattering Spectrometer Probe (FSSP) and the Two Dimensional Cloud Optical Array Probe (2D-c). Liquid water content was also measured by a Johnson-Williams hot wire device (JW) on both aircraft. Unfortunately, the JW instruments were not calibrated in a wind tunnel prior to the programs as suggested subsequently by Strapp and Schemenauer (1982). Differences between the JW and FSSP measurements were assessed for all flights. The instruments were found to differ generally within a factor of two (JW higher). An example of a JW-FSSP comparison for the 5 Jan 82 flight is shown in Fig. 6. The complete statistics for the comparisons for all flights are summarized in Table 4. The FSSP liquid water contents are reported in this paper.

The characteristics of the FSSP have been studied by Pinnick et al. (1981), Personne et al. (1982), and more recently by Baumgardner (1983), Cerni (1983) and Dye and Baumgardner (1985). Cerni provided a detailed size calibration of the FSSP which included laboratory tests, Mie scattering calculations and airborne measurements. He found that errors as high as 70% in cloud liquid water content could occur due to errors in manufacturer specified bin width sizes and that the size of the bins depended on airspeed. Cerni developed an algorithm to determine the correct bin size and minimize errors associated with the measurement of liquid water content. Cerni's algorithm was incorporated into the processing programs to calculate FSSP bin widths and liquid water contents. Use of his algorithm was justified because the pulse height

Table 3
CIC CHEYENNE DATA ACQUISITION SYSTEM SENSOR SPECIFICATIONS

Parameter Measured	Instrument Type	Manufacturer and Model Number	Combined Performance of Transducer, Signal Conditioning and Conversion				Useable Resolution (s)
			Range	Accuracy	Time Constant (s)	Sample Rate (s)	
Time	Crystal osc	PMS	12 mo	1 s	N/A	0.1s	0.1 s
Temperature	Platinum resistance	Rosemount Eng. Co. 510BF9 Bridge Model 102 Probe	±50°C	0.5°C	1	1 Hz	0.1°C
Dew Point ²	Peltier cooled mirror	Cambridge System Inc. Model 137-C3	±50°C	1°C	1-5 s	1 Hz	0.3°C
Liquid Water ³	Hot Wire	Cloud Technology Model LWH	0-3 gm/m ³	0.3 gm/m ³	0.5	1 Hz	0.01 gm/m ³
Altitude	Static Pressure	Rosemount Eng. Co. Model 830BA	0-15 psia	0.015 psia	0.1	1 Hz	0.007 psia
Altitude	Static Pressure	Setra Systems	0-20 psia	0.015 psia	0.1	1 Hz	0.010 psia
Indicated	Differential pressure	Rosemount Eng. Co. Model 1332B1	±2.5 psid	0.0025 psid	0.1	10 Hz	0.0025 psid
Heading	Gyro	Sperry	0-360°	±2°	0.1	1 Hz	0.1°

Table 3 (Cont.)

Parameter Measured	Instrument Type	Manufacturer and Model Number	Combined Performance of Transducer, Signal Conditioning and Conversion				Useable Resolution (s)
			Range	Accuracy	Time Constant (s)	Sample Rate (s)	
Pitch	Gyro	Sperry	$\pm 85^\circ$	$\pm 2^\circ$	0.1	1 Hz	0.1°
Roll	Gryo	Sperry	$\pm 180^\circ$	$\pm 2^\circ$	0.1	1 Hz	0.1°
Position (azimuth)	VOR	King Radio (HTI Digital Interface)	0-360°	$\pm 2^\circ$	1	1 Hz	0.1°
Position (distance)	DME	ARC Radio Corp.	225 km	0.5 km	1	1 Hz	0.01 km
Vertical Acceleration ⁵	Pendulous Mass	Sundstrand Corp.	± 2 g	0.001 g	0.1	1 Hz	0.0001 g
Cloud Particle Size & Concentration ⁶	Optical Array	PMS 2-D OAP	37.5-1200 μ 0.1-10,000 L^{-1}		Discrete Event	Continuous Continuous	37.5 μ 0.1 L^{-1}
Cloud Droplet Size & Concentration ⁷	Optical Forward Scattering	PMS FSSP	2-45 μ 0.1-10,000 cm^{-3}		Discrete	Continuous	0.5 to 3 μ
Ice Nucleus Concentration ⁹	Optical Scattering	MEE/CSU	30-30,000 L^{-1}		Discrete	Continuous	30 L^{-1}

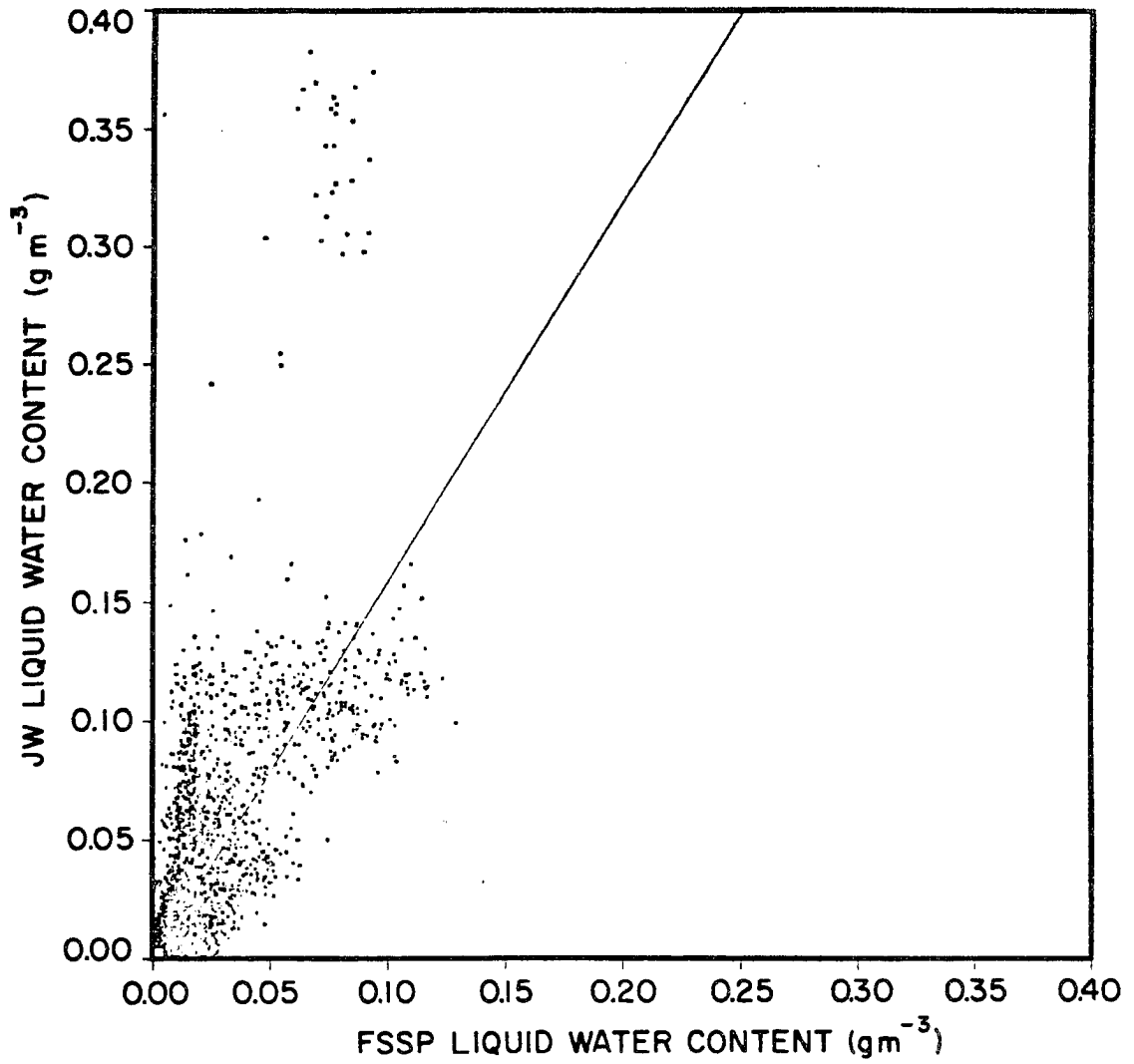


Fig. 6. JW vs. FSSP liquid water contents for 5 January 82 flight.

Table 4

JW-FSSP Comparison Statistics

$$(JW = m(FSSP) + b)$$

Date	Slope	Intercept	Max JW	Max FSSP	Correlation Coefficient
24 Nov 79	1.20	0.00	0.26	0.18	0.77
26 Nov 79	0.52	0.00	0.13	0.15	0.65
22 Dec 79	1.93	0.00	0.54	0.15	0.89
13 Dec 81	FSSP Malfunction				
15 Dec 81	FSSP Malfunction				
21 Dec 81	0.58	0.00	0.08	0.11	0.67
5 Jan 82	1.60	0.00	0.38	0.13	0.74
16 Jan 82	1.37	0.01	0.89	0.22	0.55
23 Jan 82	1.83	0.02	0.80	0.35	0.73
31 Jan 82	JW Malfunction				

analyzer (PHA) levels of the FSSP used in the COSE programs was within 1% of the PHA levels quoted for the instrument calibrated by Cerni. Cerni estimates that with these corrections, errors in the accuracy of liquid water measurements with the FSSP can be reduced to 10-20%. Even with the calibration corrections, the instrument artificially broadens the spectra. No solution to this problem has been reported to date. Cerni also found that cloud droplet concentrations could be seriously underestimated in regions of high concentrations due to finite processing delays associated with the instrument. Cerni's correction algorithm to account for this effect could not be applied because the total strobe rate of the instrument was not recorded. However, this problem is minimal in this study, since cloud droplet concentrations rarely exceeded 300 cm^{-3} . During the COSE programs, the FSSP was operated in the 2-32 μm range.

The two dimensional optical array spectrometer was developed by Particle Measuring Systems as a particle imaging system capable of recording and displaying two dimensional images of atmospheric particles with sizes greater than 25 microns passing through an object plane at typical aircraft speeds. Analytical techniques for transforming raw 2-D data to effective crystal concentration have been primarily developed by Cooper (1977).

Crystal concentrations are calculated from 2-Dc probe data according to various criteria which are related to buffer storage capacity and characteristic shadow pattern. Under conditions when ambient crystal concentrations are 10/liter and crystal sizes in the 0.5-1.0 μm range, the storage buffer loads to capacity in about 0.35 seconds. Under normal experimental conditions, transfer of data to tape

storage at this rate would consume several tapes and leave large data gaps during tape rewind and installation. To eliminate this problem, data were normally transferred once every second to tape, unless a high data rate was required. This meant that approximately 35% of the data passing through the storage buffer was retained for later use.

Two parameters are calculated from the full body of data as it passes through the storage register. These are the number of distinct shadows and the total sample volume. If all of the distinct shadows are assumed to be individual crystals, the average crystal concentration over the one second leg can be calculated by dividing the number of distinct shadows by the sample volume. This number is referred to as the "shadow-or" concentration.

Unfortunately, the shadow-or determination of crystal concentration can be inaccurate due to artifacts produced by liquid water, particles smaller than the resolution of the instrument, and crystals which impact on the probe tips and fracture. Liquid water droplets often produce artifacts which appear as long narrow streaks. These occur when the droplets collide with the probe arm and then streak across the optical path. This problem is not major in cold orographic systems. Less than 0.1% of the images were visually assessed to have streaker characteristics. Counts also occur when no diodes are shadowed due to electronic delays during the passage of particles with sizes near the resolution of the instrument. These particles represent a significant fraction of the images, particularly in ice crystal formation zones. However, if large droplets ($> 25 \mu\text{m}$) are present, they also can contribute to the total count of zero-area images. These zero-area images are subject to interpretation and must be evaluated with other

data, particularly data from the FSSP. Their presence is noted in the text where appropriate. Splash images (broken images) also occur due to crystal fracturing. These images occur more frequently than streakers but still do not contribute significantly to the total image sample. Examples of these artifacts are shown in Fig. 7. In general, shadow-or concentrations are quoted. However, when artifacts or zero-area images significantly affect these concentrations, qualifications will be stated in the text.

B. Dual-channel microwave radiometer

In the late 1970s, the Wave Propagation Laboratory (WPL) of the National Oceanic and Atmospheric Administration (NOAA) developed a passive dual-channel radiometric system to measure integrated liquid water and vapor contents in cloud systems (Guiraud et al., 1979; Hogg et al., 1980). A similar active-passive system was used successfully in the Sierra Cooperative Pilot Project, a weather modification project conducted by the Bureau of Reclamation, to determine integrated liquid water contents along a particular path determined by the position of the radiometer site and the elevation and azimuth angle of the microwave source on a COMSTAR geosynchronous satellite (Snider and Hogg, 1981; Snider and Rottner, 1982). The active-passive system was used to obtain initial verification of the accuracy of liquid measurements by the passive technique (Snider et al., 1980). Recently, WPL has developed an improved system that is steerable and independent of a source of radiation (Hogg et al., 1983). This system was used during the 1981-82 field program.

The dual-channel radiometer simultaneously measures the total amount of liquid water and water vapor contained along the atmospheric

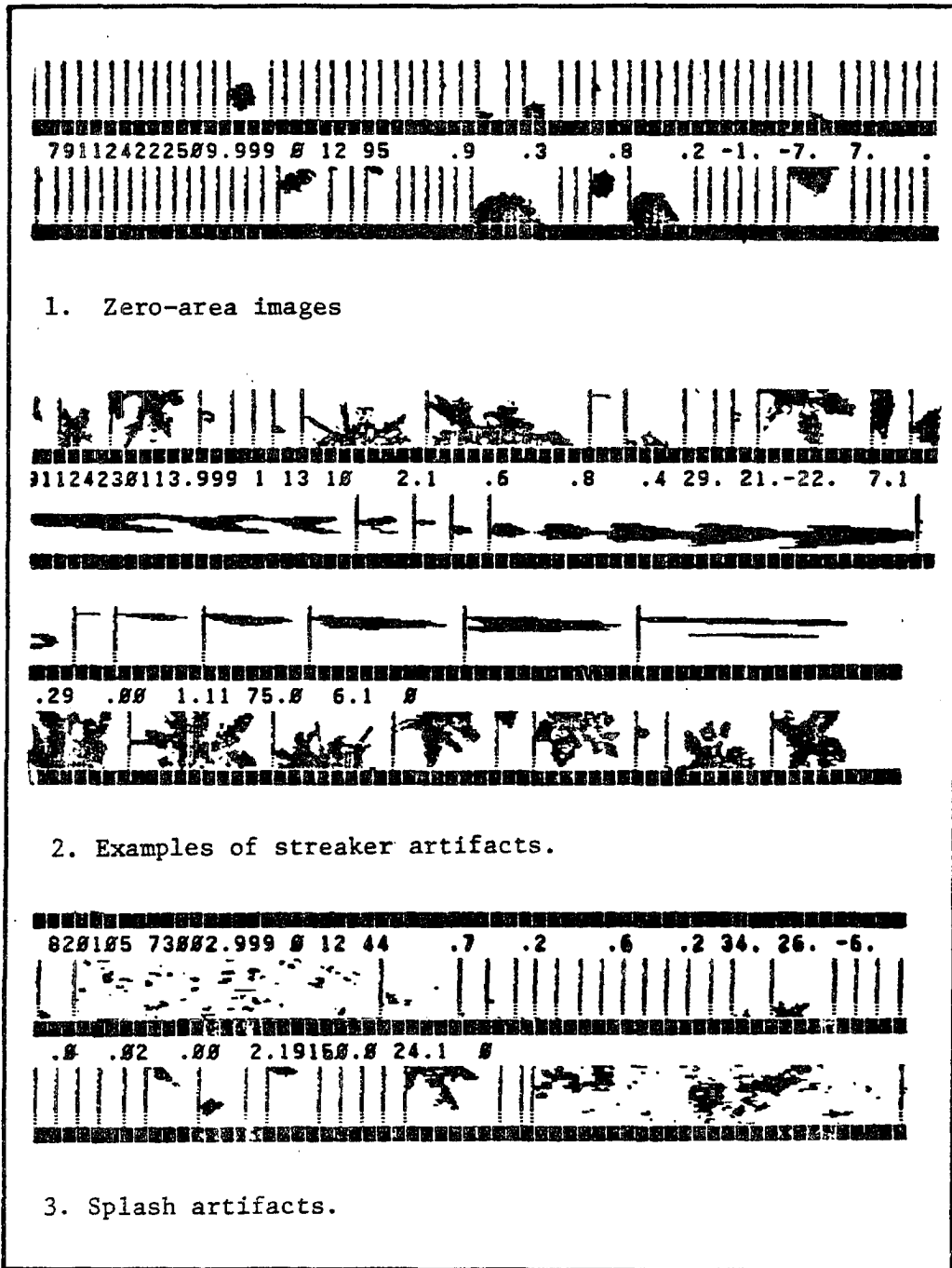


Fig. 7. 2D-c probe artifacts and problem images.

path being observed by the system's antenna. By arranging for the antenna beam to be steered in azimuth and elevation, the system can be used to determine the spatial (two dimensions) and temporal distribution of the water vapor and liquid water throughout the hemisphere surrounding the radiometer. Since the radiometer was not instrumented to provide range information during the 1981-82 season, the distribution of these quantities along the atmospheric path cannot be determined.

Water vapor is determined primarily by measurement of the microwave energy, expressed as a brightness temperature, emitted at 20.6 GHz (wavelength 1.5 cm) by virtue of absorption of microwaves by the water vapor. Similarly, the amount of liquid water contained in clouds along the radiometer beam is determined primarily by measurement of microwave emission by the liquid in a transmission "window" at 31.65 GHz (wavelength 0.95 cm). Since the absorption coefficients for water vapor and liquid water at the two frequencies are known, the observed absorptions (calculated from the observed brightness) may be used in a pair of simultaneous equations to yield independently the integrated water vapor and liquid along the antenna beam. In practice, the simultaneous equations are solved using statistical retrieval methods (Hogg et al., 1983).

Because liquid water at temperatures below freezing absorb microwaves, the radiometer can measure supercooled liquid. However, since the absorption of microwaves by ice is approximately two orders of magnitude less than that by liquid water, ice is assumed to produce essentially zero output from the system.

The radiometer incorporates a steerable antenna so that the spatial and temporal variability of the liquid water and vapor field can be

studied. A standard scanning technique was adopted to observe the evolution of these fields. The antenna was set at a 15° elevation angle and rotated continuously through 360° azimuth sweeps approximately every 15 minutes. By using this technique, it was possible to observe the changes in integrated liquid water content in all directions. The data were then analyzed on azimuth/time diagrams, which allowed for easy interpretation of the lifting mechanisms responsible for the production of cloud water. Radiometric integrated liquid water contents are reported in millimeters. One millimeter of water distributed along a 1 km path is equivalent to a liquid water content of 1 gm^{-3} .

The radiometer was located near Steamboat Springs, Colorado, at an elevation of 2050 m, approximately 6 km west of the crest of the Park Range (3100 m). The Park Range is oriented north-south. An azimuth angle of 0° in the radiometric data presented in the following sections would correspond to the antenna's pointing north, or parallel to the range. At azimuth 90° , the beam points over the range, directly through the region of maximum orographic lift. At 180° , the beam is pointed southward, parallel to the range. At 270° , the beam is directed away from the region of primary lift, over the western valley of the Yampa River.

To date, only a few successful comparisons of radiometric liquid water measurements with simultaneous observations collected by an aircraft flying along the beam have been reported (Snider, 1983). These were all in stratiform cloud systems with very low liquid water contents. Excellent agreement was obtained for these limited comparisons. Unfortunately, many attempts to compare liquid water contents observed with the radiometer with measurements by in-situ

independent instrumentation have been hampered by safety restrictions imposed on aircraft flying over complex terrain. This problem also occurred during the CSU program. Safety limitations did not permit the cloud physics aircraft used in the program to probe the lowest kilometer of the cloud system in the vicinity of the radiometer. To evaluate the ability of the radiometer to measure accurate values of integrated cloud liquid water content, alternate approaches to direct comparison had to be developed.

Three aspects of radiometric liquid water measurements are examined here. The first is the effect of surface temperature on measured liquid water. The second concerns the effects of large ice crystal concentrations present along the radiometer antenna beam. The third aspect considered is the relationship between observed liquid water contents and the magnitude of the total condensate available to the cloud system.

(1) Surface temperature effects

In the 1981-82 experiment, the scanning radiometer was located upwind of the mountain barrier at a low elevation (2050 m) with an unobstructed view both upwind of and toward the mountain. Therefore, it was possible to study the evolution of the cloud water content as air approached and rose over the barrier.

The primary disadvantage of low altitude sites is that the surface temperature can exceed 0°C and precipitation can reach the ground as rain. Unfortunately, the radiometric signal caused by the rain may obscure that caused by supercooled liquid water contained in the clouds. The effect of rain on observed radiometric liquid water contents is illustrated in Fig. 8. During the COSE program, the surface temperature

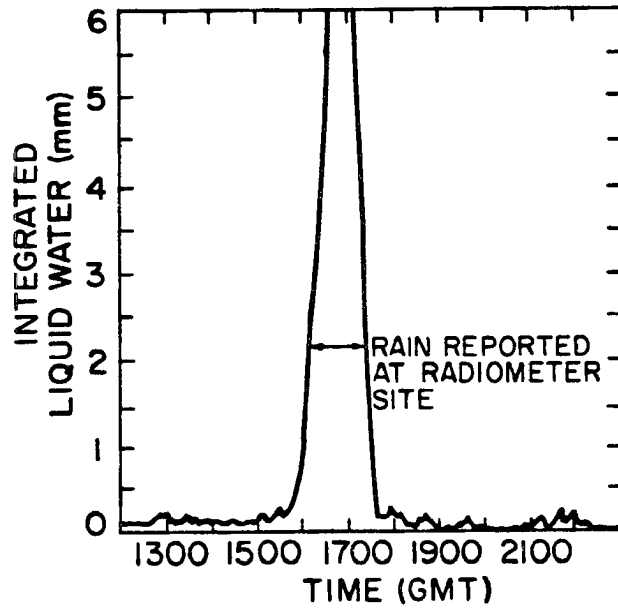


Fig. 8. Integrated liquid water content observations observed on 20 December 1981. The radiometer antenna was pointed vertically during the period. Rain occurred continuously between 1600 and 1730 GMT.

at the radiometer site (RAD) during storm conditions occasionally rose to as high as $+2^{\circ}\text{C}$. However, except for the case shown in Fig. 8, all precipitation occurred as snow.

During most of these storms, the radiometer was rotated through 360° azimuth scans at 15° elevation angle. To examine possible effects of warm, low-level temperatures on observed radiometric liquid water contents, the maximum value of integrated water content observed during each complete scan was plotted as a function of surface temperature for all periods where scanning data were available and snow was falling. The results are displayed in Fig. 9. Although some of the variability in the data is caused by variations in cloud depth and moisture supply, a clear trend toward higher values is observed as the surface temperature increases toward and above 0°C .

Two sources of signal enhancement can occur in these conditions. An apparent, but false, enhancement of liquid water can occur if melting occurs on the exposed reflector. The reflector was cleared of snow regularly during the COSE program, and false signal enhancement due to a wet reflector was not a significant problem. The second and more likely source of the increase is due to the initial melting of the surfaces of the falling crystals after passing through the melting level. Wind tunnel studies by Rasmussen and Pruppacher (1982) have indicated that spherical ice particles near $350\ \mu\text{m}$ radius completely melt in less than 1 minute. These experiments were conducted with warming rates equivalent to lapse rates greater than $1.2^{\circ}\text{C}/100\ \text{m}$. Although these rates are much larger than occur in natural conditions, this study suggests that melting begins rather rapidly once a crystal encounters temperatures above 0°C .

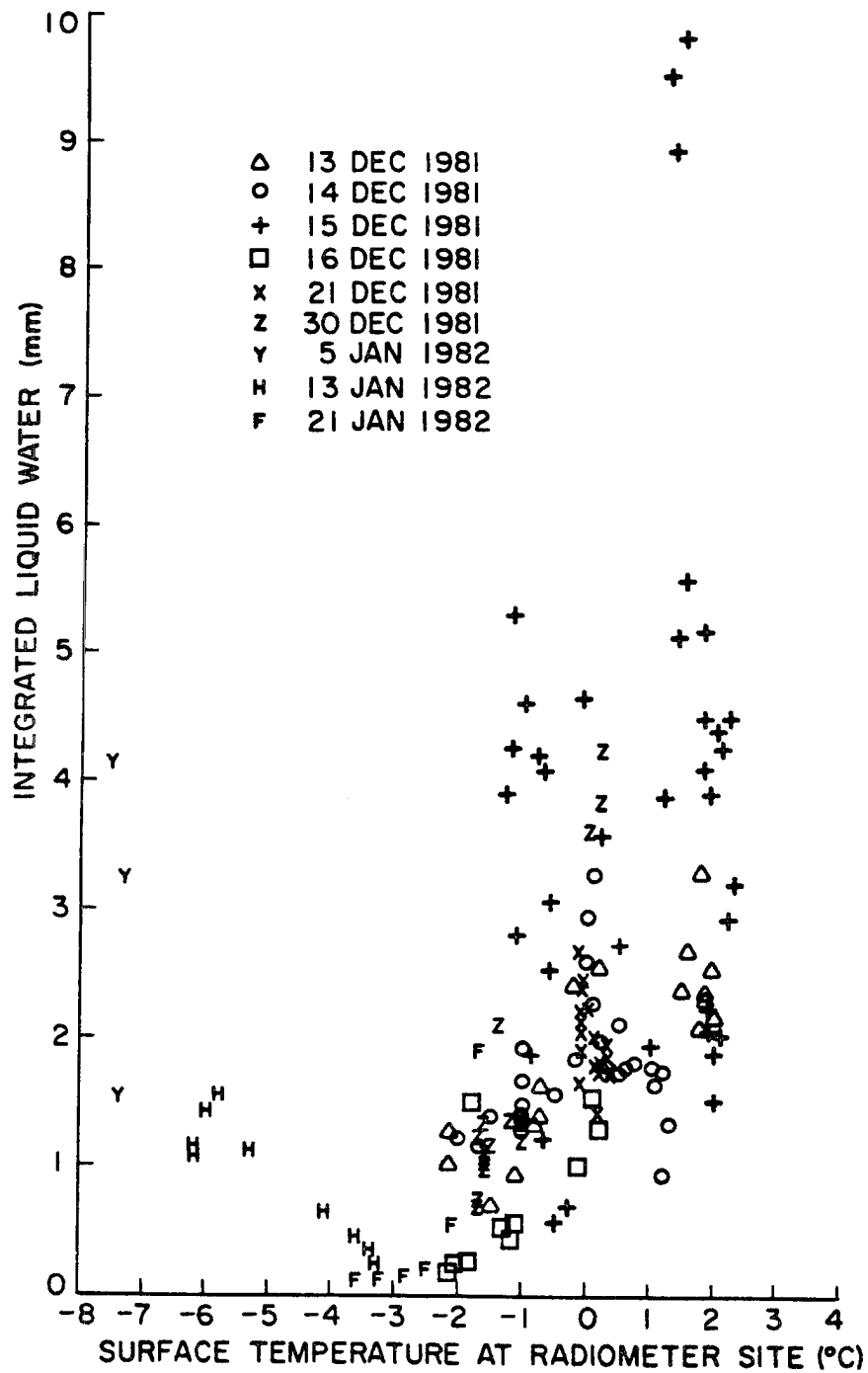


Fig. 9. Maximum integrated liquid water contents observed during 360° azimuth scans as a function of surface temperature for nine storm periods. The elevation angle of the radiometer was 15° .

Observational evidence of Knight (1979) indicates that melting of more complex particles with larger dimensions proceeds in such a way that the distribution of liquid on the ice minimizes the total air surface of the melting crystal. In the case of planar crystals, the liquid surface covers the entire crystal in a smoothly rounded surface, exposing a large liquid surface downward toward the radiometer. Under these circumstances, even minor amounts of melting can result in increases in liquid water contents and potential erroneous interpretation of the supercooled liquid water field. Normally, this situation can be monitored by accurately measuring surface temperature.

A difficult exception may arise when a weak surface inversion is present in the vicinity of the radiometer site. Inversions of this type sometimes occur in mountain valleys in wintertime during storm conditions. The presence of a thin elevated melting layer above the radiometer site may result in enhanced water concentrations. Such a layer may have been responsible for the high values observed on 15 Dec 81 when the surface temperature was between -1.3°C and -0.6°C . The data points were collected between 0620 and 0750 local time. Overcast conditions developed at 0300 local time, so the potential for the development of a radiation inversion in the vicinity of the site prior to the onset of snowfall was strong. Soundings taken upwind of RAD at Craig, Co. indicated that a pool of colder surface air was present in the valley where the radiometer was located. Unfortunately, direct monitoring of a low-level inversion in the vicinity of the radiometer site was not possible. However, it is important to note that a component of the high values observed on 15 Dec 81 was due to supercooled cloud water. Crystal rime observations at RAD and at

mountaintop indicated light to moderate rime on crystals throughout the period. The ratio of supercooled to melted water constituting the total integrated measurement is unknown.

In Fig. 9, two high points occur in the -7°C to -8°C region. These values were observed on 5 Jan 82 during a period when heavily rimed particles fell continuously at RAD. The presence of these heavily rimed particles clearly indicated that large amounts of supercooled liquid water was present. The high radiometric values in this case are representative of actual cloud conditions and not associated with melting processes occurring at the surface or at higher, warmer levels. It is interesting to note that the lowest value (1.53 mm) observed on 5 Jan 82 was measured as the rime accumulation on crystals falling at RAD was rapidly decreasing. This provides additional evidence that the radiometer was responding to the supercooled cloud water field.

(2) Ice phase effects

The radiometer used in the COSE program is designed specifically to monitor microwave energy emitted in the 20.6 GHz (1.5 cm) and 31.65 GHz (0.9 cm) channels. The first corresponds primarily to emissions from the vapor field; the second, from liquid water. Except in cases of heavy rain, the outputs from these channels are independent (Snider, 1983). The values are also assumed to be independent of the ice water content within the beam because of the transparency of ice to microwaves of these frequencies.

An excellent opportunity to verify the small effects of high ice crystal concentrations on the radiometric measurement of cloud liquid water occurred on 5 Jan 82. On this day, an aircraft sounding was performed over the radiometer site while the radiometer was pointing

vertically. The aircraft sounding began at 7000 m and terminated at 4400 m. Simultaneous observations of crystal habit and degree of rime were collected at Storm Peak Laboratory (SPL) at the Park Range crest and at RAD. Liquid water and crystal concentrations determined by the aircraft during the sounding are shown in Fig. 10. In Fig. 11, radiometric liquid water measurements are displayed along with precipitation intensity at RAD and rime characteristics at RAD and SPL.

During the aircraft sounding, the liquid water content rarely exceeded 0.01 gm^{-3} . Ice crystals concentrations increased with depth reaching $60\text{-}100 \text{ l}^{-1}$ in the lowest portion of the sounding. Observations at SPL and at RAD indicated that all the crystals arriving at both sites during the aircraft sounding were unrimed. These surface observations indicate that little liquid water was present over the radiometer site in the levels below the aircraft sounding.

Based on observed high ice crystal concentrations, high precipitation rates, negligible water contents at aircraft levels, and the lack of observable rime on precipitating crystals, this deep cloud system was devoid of liquid water. If the radiometer was sensitive to emissions of radiation from the large population of ice crystals, the radiometer should have indicated a significant signal. The radiometric data displayed on Fig. 11 shows that this was not the case. This study shows that the radiometric response in the 31.65 GHz channel is due to the presence of liquid water in the system and is independent of the concentration of ice crystals. In the following sections, radiometric measurements are compared with model-predicted integrated condensate along the beam path to estimate the representativeness of the liquid water measurements.

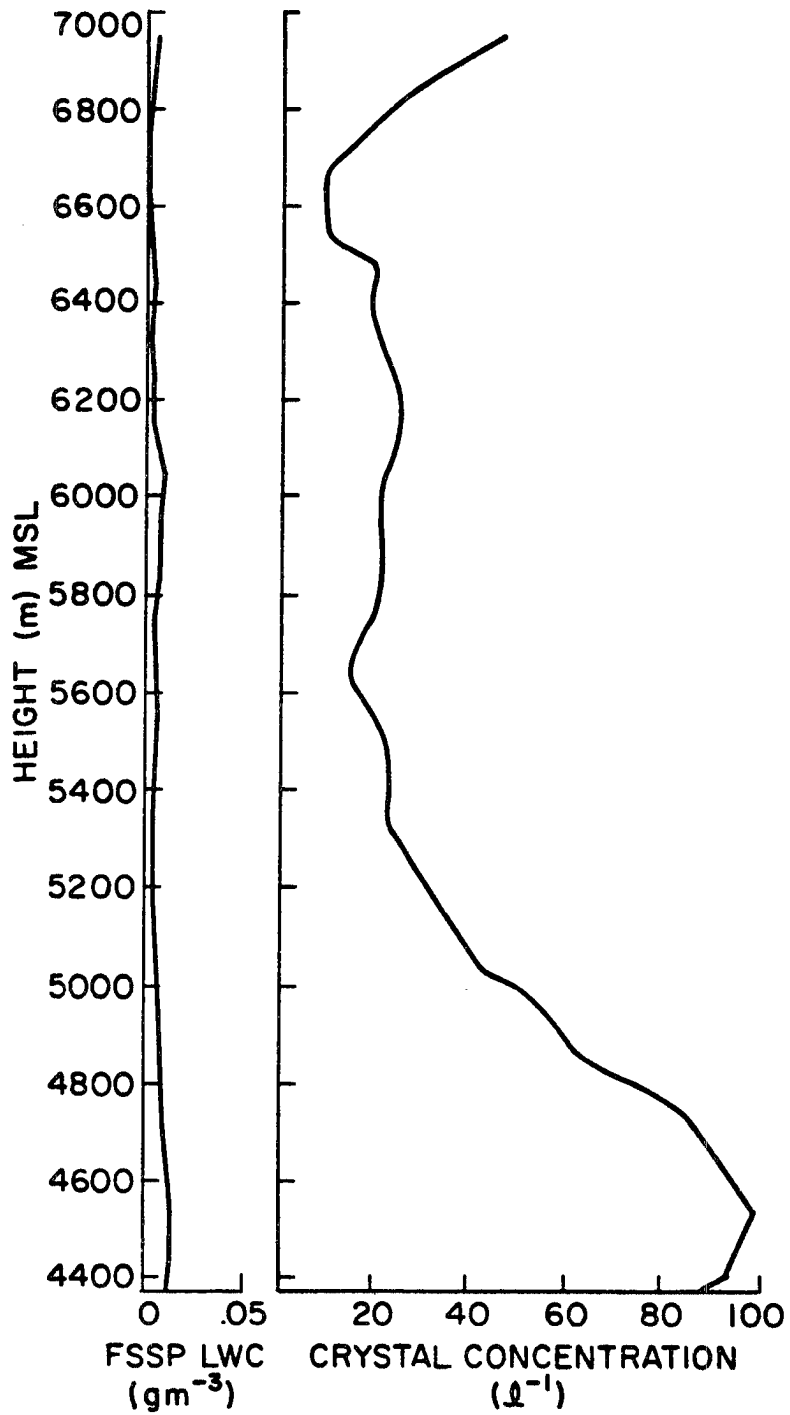


Fig. 10. Liquid water content (LWC) and ice crystal concentrations observed during a descent sounding of the Cheyenne II cloud physics aircraft over the radiometer site on 5 January 1981.

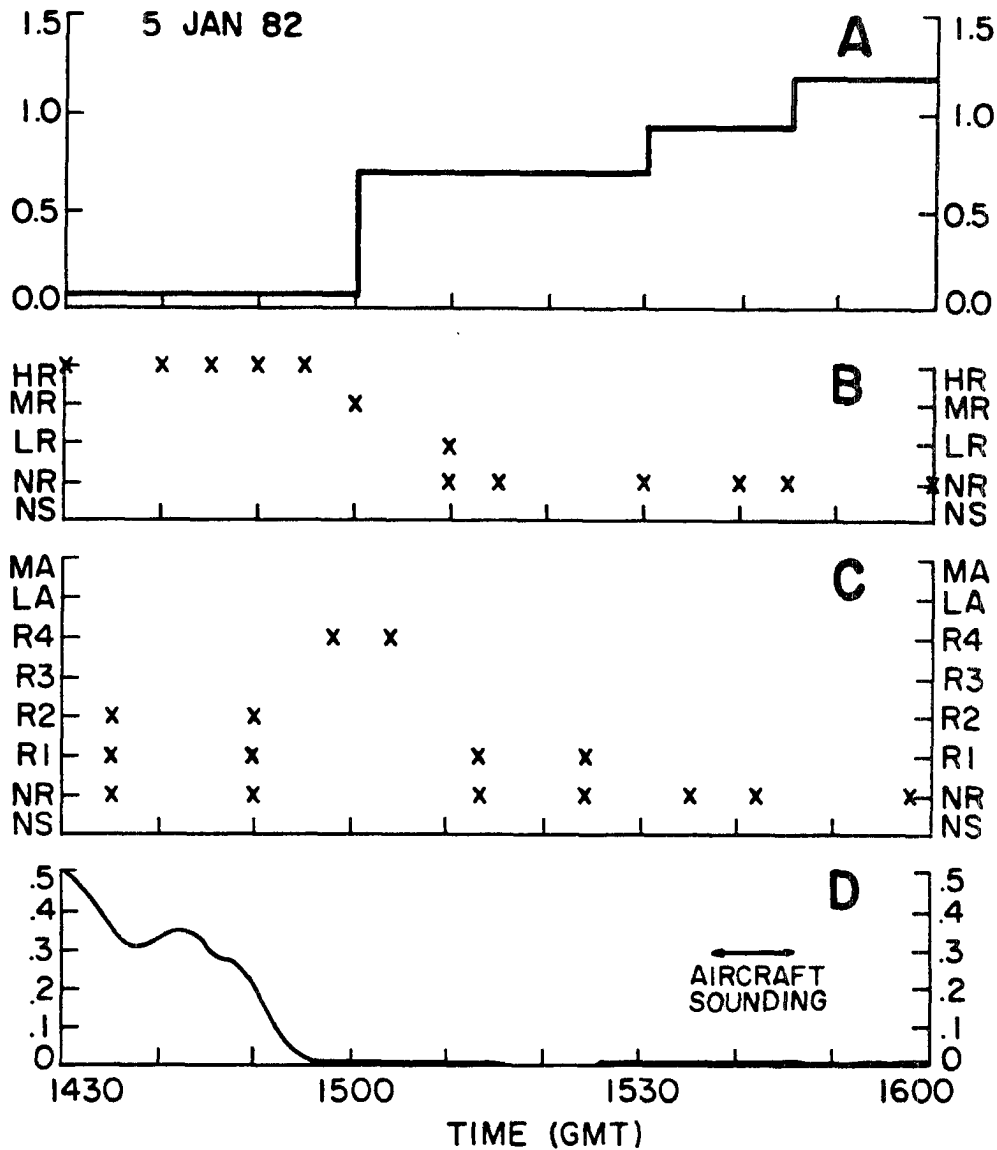


Fig 11. Graph A: precipitation intensity at the radiometer site (mm/h); Graph B: rime characteristics of crystals collected at Storm Peak Laboratory (3100 m). The symbols are HR (heavy rime, crystal habit cannot be distinguished), MR (moderate rime, crystal habit can be distinguished with difficulty), LR (light rime, crystal habit easily distinguished), NR (no rime), NS (no snowfall occurring); Graph C: rime characteristics of crystals collected at the radiometer site (2050 m). The symbols use the Magono and Lee (1966) classification for rimed crystals except for MA (moderately rimed aggregates), LA (lightly rimed aggregates), NR (no rime), and NS (no snowfall occurring). Graph D: integrated liquid water contents from the vertically pointing radiometer (mm).

(3) Relationship between radiometric measurements and total condensate produced in the cloud system

Because of flight restrictions in the complex terrain of the COSE area, no direct comparisons of radiometric liquid measurements with an independent instrument such as the FSSP could be carried out. To estimate the relative magnitude of the radiometer measurements, an alternate approach using an analytical model of airflow and condensate production was developed. Comparisons between model simulations and radiometer results are used here to (1) compare the percentage of the total condensate available to the cloud system to the liquid water content measured by the radiometer and (2) examine how the ratio of these quantities varied as air moved up and over the barrier. The model is described below. The results of the model comparisons are described at the end of this section.

a. Model vertical velocity

The two-dimensional model used in this paper to predict condensate production in stably-stratified orographic cloud systems utilizes an analytical equation for vertical velocity developed in Smith (1979). His review summarized previous work by Queney (1947) and Queney et al. (1960) in their treatment of mountain lee waves. Since a complete derivation of the vertical velocity equation and discussion of its applicability to the mountain airflow problem are given in Smith (1979), only the essential features and assumptions used in the derivation will be repeated here.

The derivation of the vertical velocity equation assumes steady state, hydrostatic conditions, neglects friction and Coriolis accelerations, and utilizes the Boussinesq approximation in density

terms. The governing equations are first linearized, then solved for a second order differential equation in perturbation vertical velocity. A solution to this differential equation is obtained using Fourier methods by choosing a lower boundary condition which assumes an ideal mountain form and an upper boundary condition which requires that phase lines tilt upstream and energy propagates upward. For the broad mountain solution with strong stability, Smith (1979) developed an equation for the vertical displacement of a streamline from which the equation for vertical velocity can easily be derived. This equation is identical to that used by Willis (1970) in previous work in the Park Range region.

b. Airflow and condensate production

Values of vertical velocity were calculated on a 25 X 80 grid (200 m X 1000 m resolution) using input data from special rawinsonde soundings taken 48 km upstream of the radiometer site. Air parcel trajectories over the barrier were calculated by considering the measured horizontal and predicted vertical motion of the air as it passed through the grid. To calculate condensate production and production rates, the equivalent potential temperature of the parcel was calculated from the upwind sounding and conserved from the point of origin throughout the parcel's transit over the barrier. When a parcel was lifted beyond its lifting condensation level, condensation was assumed to occur. All condensate was assumed to remain with the parcel during transit so that the maximum condensate possible could be determined along the radiometer beam. The temperature and saturation mixing ratio of the parcel were calculated as the parcel underwent moist adiabatic ascent and descent. The total condensate in the parcel was then calculated by considering the difference in saturation mixing

ratios at its current location and its lifting condensation level. Integration of the condensate field along the radiometer beam path was performed for two beam positions. Fig. 12 shows the model topography, actual topography, radiometer beam positions for integration, parcel streamlines and the resulting condensate field for the simulation generated from the sounding taken at 1500 on 15 Dec 81.

c. Model limitations

The model described above can only be applied during conditions of stably-stratified flow when significant blocking is not occurring and the winds are predominantly westerly. The model is designed to determine the maximum amount of liquid water which would be present along the radiometer beam if all the condensate remained in the liquid phase and remained with the air parcel as air moved up and over the barrier. For this reason, ice phase processes are not included in the model. Entrainment is neglected. Accumulation regions of liquid water are assumed not to occur. The effects of latent heat release are assumed to be negligible as are radiational cooling effects near cloud top. Because the model terrain is ideal, variations in actual topography may cause deviations in the flow field from that predicted by linear theory. The two-dimensional approximation also artificially simplifies the extreme variations in airflow due to three dimensional variations in topography. When all of these assumptions are considered, the validity of the results becomes an important question. However, as was stated above, the purpose of this study was to determine the maximum amount of condensate likely to be produced as air flows over the mountain. With the exception of latent heat release and radiation, all of the other effects, if active in the cloud system, would tend to

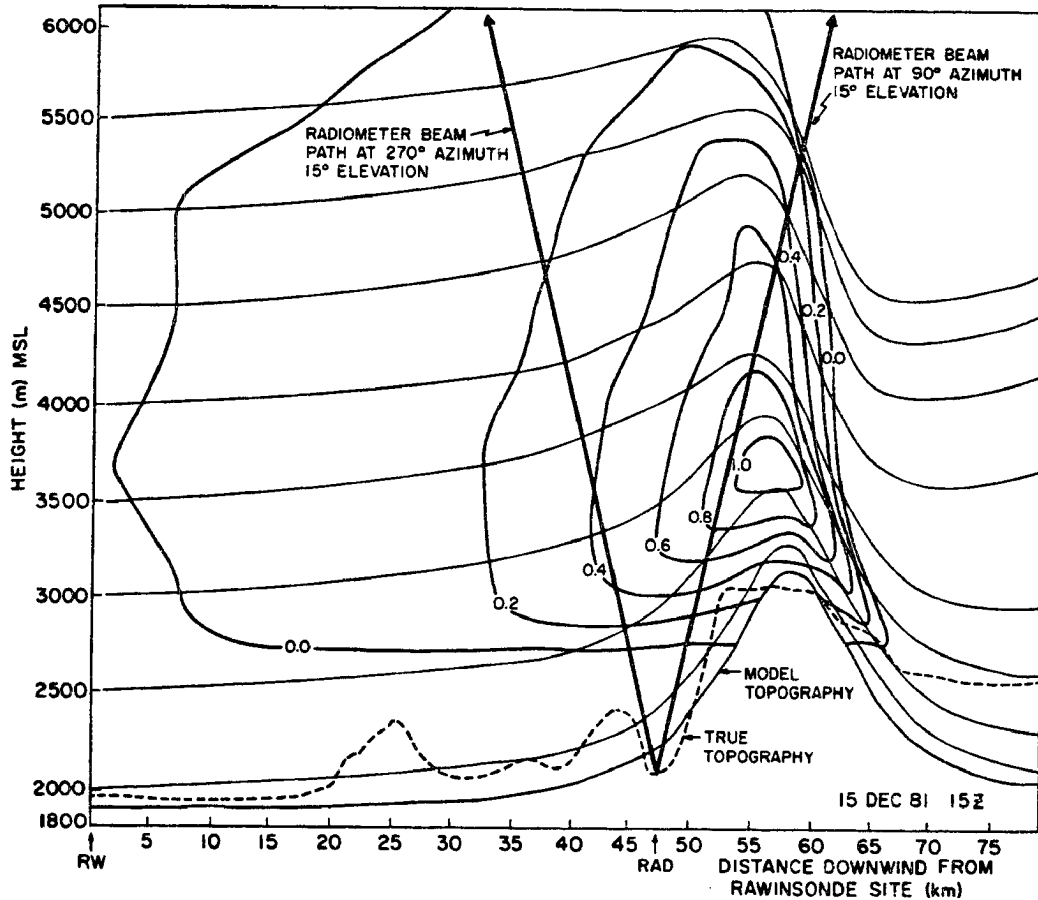


Fig. 12. Model predicted total condensate (gm^{-3}) and parcel streamlines for the 15 December 1981, 1500 GMT simulation. The model topography and the actual topography along a latitude line through the radiometer site (RAD) are indicated. The radiometer beam paths at 270° and 90° azimuth for a 15° elevation angle are also shown. The angle appears much larger because the vertical scale is exaggerated for clarity. The rawinsonde site is indicated as RW.

reduce the total amount of condensate available to the cloud system. In cold orographic systems, buoyancy due to latent heat release should be minor. Radiational effects are confined largely to the cloud top region, where total condensate production is small. For this reason, the model should provide an adequate upper limit to the amount of condensate available to the cloud system. It is this upper limit which was required for the study.

d. Model results

Soundings that met the criteria outlined at the beginning of Sec. c above, that occurred during significant cloud cover events, and that had corresponding scanning radiometer data available were selected for analysis. Six soundings satisfied these requirements. For comparison with the radiometer measurements, a time lag was allowed to account for the time required for air sampled by the sounding to reach the radiometer site. Radiometer data were considered for comparison with the model calculations from the time the air at the 50 KPa level originating at the rawinsonde site first crossed the radiometer beam at the 270° azimuth position to the time the 70 KPa air exited the beam at the 90° azimuth position. This method takes into account both the time lag due to the distance between the sounding launch site and the radiometer site and the tilting of the air column due to the vertical wind shear. Integration of the model-predicted total condensate along the radiometer beam was performed between the radiometer site and the 50 KPa level.

Table 5 summarizes the model results and the radiometric observations. Upwind of the radiometer site (away from the barrier), model-predicted values of the total integrated condensate along the 15°

Table 5

Comparison of Model Predicted Integrated Condensate and Observed Radiometric Integrated Water Content

Sounding	Elevation Angle (Degrees)	Azimuth Angle (Degrees)	Model Predicted Integrated Condensate (cm)	Radiometric Integrated Liquid Water (cm)	Percent of Condensate In Liquid Phase (%)	Surface Temp (°C)	Model 90°/270° Ratio (Mountain /Upwind)	Radiometer 90°/270° Ratio (Mountain /Upwind)
14 Dec 81 (2100 GMT)	15	90	0.256	0.110	42.9	0.1 to 1.4	5.33	4.23
	15	270	0.048	0.026	54.2	0.1 to 1.4		
15 Dec 81 (1500 GMT)	15	90	0.598	0.035	5.9	-1.0 to -0.1	2.05	1.35
	15	270	0.291	0.026	8.9	-1.0 to -0.1		
21 Dec 81 (1200 GMT)	15	90	0.773	0.160	20.7	-0.1 to 0.2	2.47	3.72
	15	270	0.313	0.043	13.7	-0.1 to 0.2		
21 Dec 81 (1500 GMT)	15	90	0.515	0.110	21.4	-0.1 to 0.4	2.96	1.59
	15	270	0.174	0.069	39.7	-0.1 to 0.4		
5 Jan 81 (1200 GMT)	15	90	0.526	0.128	24.3	-8.0	2.21	2.21
	15	270	0.238	0.058	24.4	-8.0		
5 Jan 81 (1800 GMT)	15	90	0.446	0.036	8.1	-3.5 to -2.5	2.13	0.92
	15	270	0.209	0.039	18.7	-3.5 to -2.5		

elevation beam ranged from 0.048 to 0.313 cm for the six periods available. Downwind of the site (over the barrier), precipitable condensate values were significantly higher due to strong orographic lifting. Integrated values in this direction ranged from 0.256 to 0.773 cm. Except for 1800 , 5 Jan 82, radiometric values of liquid water exhibited similar behavior, increasing substantially over the barrier. The last two columns of Table 5 show the magnitude of this increase for both the model calculations and the radiometric observations. The strong agreement between the model and the radiometric observations (correlation coefficient = 0.71) for these cases suggests that the production of the liquid phase in these clouds is strongly related to the condensate supply rate, which is in turn related to the ambient vertical velocity. The values of integrated liquid water were consistently smaller than the predicted total condensate values, reflecting the importance of ice phase processes in these clouds.

If the radiometric water content values are compared with predicted total condensate, an estimate of the percentage of condensate in the liquid phase can be estimated. These percentages appear in Table 5. For the six soundings analyzed, 5-54% of the total condensate available to the cloud system was present in the liquid phase. Caution must be exercised in interpreting this liquid as "supercooled" since three of the six cases have surface temperatures warmer than 0°C. These cases include some of the highest values. In the three cold cases, water contents were still as high as 24%.

C. 1.79 cm radar

The vertically pointing 1.79 cm wavelength radar was specifically designed at CSU for operation during orographic cold cloud storm events.

Built in 1978, the system uses the receiver-transmitter designed for the B-58 aircraft. Coupled to the original duplexer is a double balanced mixer, followed by a radio frequency pre-amplifier and 30 MHz intermediate frequency amplifier. Reflected echoes are digitized by an eight-bit analog-to-digital converter and thereafter loaded into the memory of a minicomputer. Non-averaged data are written onto 9-track magnetic tape once every 30 seconds or multiples thereof. Storage of data in an array of 46 pulses by 200 range bins affords access to individual pulse values for statistical calculations such as signal variance and bias. The computer also produces a real time display of reflected power, calculated in dBZ, based on averages of 46 consecutive pulses. The real-time display is formatted as a horizontal intensity profile with 80 positions, each corresponding to 100 meters vertical distance. The overall effect is to establish a time-height history of the cloud vertical structure from 0.4 to 8.0 km height. Since water droplets are nearly always smaller than precipitation size in the cloud systems observed in winter over the Park Range, the radar return is virtually always due to ice particles in the cloud system. During the COSE program, this radar was colocated with the dual-channel radiometer near Steamboat Springs, Colorado.

On 16 Jan 82, a transmit-receive (TR) tube in the radar failed and had to be replaced. The tube in place prior to the failure had higher general attenuation characteristics than the new tube. As a result, all data prior to 16 Jan 82 has lower reflectivity values than those data collected after this date. Two parameters from the radar, echo top height and cloud maximum reflectivity, are reported in this paper. Radar echo top height was checked during several research flights,

before and after tube replacement, and found to be within 100–200 m of visual cloud top. In this work, cloud top refers to the radar echo cloud top height unless stated otherwise. The maximum reflectivity during storms which occurred after 17 Jan 82 will be higher due to the reduced attenuation.

D. Precipitation intensity, crystal habit, riming and aggregation

Visual observations of snow crystals and special measurements of precipitation were made continuously during storm periods at the radiometer site (RAD). Visual observations of snow crystals were normally conducted at 15–20 min intervals. The crystals were collected on a piece of framed black felt (250 cm²). The length of exposure to snowfall ranged from 3 to 30 seconds depending on the snowfall intensity. In each observation, snow crystal habits were identified and classified according to the scheme of Magono and Lee (1966). The crystals were also examined for accretion and aggregation. The number flux and number of single crystals composing aggregates were determined by counting the number of crystals collected. Shadow photography (Higuchi, 1956) was also used to record the characteristics of the crystals.

Special precipitation intensity measurements were collected at RAD. A plastic receptacle with a 160 cm² opening was used to measure snowfall intensity. Samples 10 to 15 minutes in duration were taken consecutively and weighed manually to determine the average snowfall intensity during the collection period. The Magono and Lee (1966) classification is used throughout this paper.

E. Storm Peak Laboratory measurements

A mountaintop laboratory was operated at the summit of Storm Peak (3100 m) on the Park Range directly east of the radiometer site during the 1981-82 field program. The laboratory was equipped with numerous instruments to measure the characteristics of aerosol and cloud particles in the vicinity of mountaintop. In-cloud liquid water content measurements were made using a Rotorod (registered trademark of Metronics, Inc., Palo Alto, California). This instrument is described in detail by Rogers et al. (1983). Hindman et al. (1983) describe its use in the COSE program. Rime characteristics of crystals at Storm Peak were also recorded approximately every 15 min during most storm periods. Ice crystals were characterized in one of four rime categories. The categories were no rime (NR, no visible accretion of droplets), lightly rimed (LR, accretion of droplets apparent, crystal habit easily identified), moderately rimed (MR, accretion of droplets sufficient to make the crystal habit difficult to distinguish), and heavily rimed (HR, snow pellets or graupel). If no precipitation was falling, the category NS was used. Many other measurements were collected routinely at Storm Peak Laboratory (SPL). The ice crystal rime and Rotorod liquid water content measurements are the primary SPL measurements used in this paper. Also quoted extensively are SPL measurements of crystal habit and aggregation of ice crystals.

F. Supporting data sets

Surface temperature, pressure, wind velocity and precipitation were measured continuously at RAD and at other sites with Portable Remote Observations of the Environment (PROBE) surface weather stations provided by the Bureau of Reclamation. These data were used to monitor

surface temperature at RAD to estimate the effects of melting ice particles and to provide additional information in synoptic and mesoscale analyses of storm evolution.

Special rawinsondes were launched approximately every 3 h near Craig, Colorado (CG), 48 km upwind of RAD. Data obtained were used with the radar data to determine cloud echo top temperature. Synoptic and supporting data were obtained from standard National Weather Service products, from special analyses made available through the Bureau of Reclamation Environmental Data Network and from satellite data provided by the National Weather Service office in Cheyenne, Wyoming.

CHAPTER III THE WATER PHASE

This chapter concerns the physical distribution, temporal variation, microphysical structure and climatological frequency of supercooled cloud water in cloud systems occurring over the Park Range. The chapter is divided into four major sections. The radiometric measurements of the temporal and spatial evolution of the supercooled cloud water field are discussed in Sec. 1. Sec. 2 concerns the physical distribution and microphysical structure of the liquid water field based aircraft and supporting measurements. The results presented in these two sections are used to construct a physical model of the distribution and evolution of liquid water in wintertime cloud systems over the Park Range. This model is discussed in Sec. 3. In Sec. 4, these results are compared with previous work in other mountain regions.

1. Temporal variations of the supercooled water field

During the COSE program, nine storm systems occurred for which scanning radiometer and other supporting data sets were available. These storms occurred in pre-frontal and post-frontal environments and involved cloud systems that included convective bands, embedded cellular convection, widespread stratiform cloud systems and clouds formed by orographic lifting. For presentation as case studies, these storms are divided into three broad categories: storms occurring in the pre-frontal environment or during frontal passage, storms occurring in the post-frontal environment, and orographic storm systems. Section (1) includes the pre-frontal and frontal systems. The first case documents the

passage of a strong convective region. The second case involves a cloud system which developed in the warm sector and involved the passage of two predominantly stable deep cloud regions. The third case occurred during a cold frontal passage. Section (2) includes storms which occurred in a post-frontal environment. In the first case, the storm consisted of widespread clouds with weak mid-level embedded convection. The second case study occurred during the decaying stages of a storm system. During the period a cap cloud with numerous embedded convective cells was present along the Park Range. The third case also involves a cap cloud, but with much greater stability. In Sec. (3), the three case studies presented are clouds formed primarily by orographic lifting. These clouds occurred when a strong cross-barrier pressure gradient was present and middle and low level moist air simultaneously advected into the Park Range region from the west.

A. Case studies

(1) Pre-frontal and frontal cloud systems

a. Case study: 22 January 1982

Synoptic scale and local weather conditions

The evolution of the liquid water field during the passage of a deep convective cloud system on 22 Jan 82 is discussed in this case study. The highest liquid water contents are shown to be associated with the leading edge of this convective system and to decrease substantially following the onset of precipitation. The study concentrates on the period from 0030 to 0330 (all times GMT) at the onset of the storm.

On 22 Jan 82, three distinct airmasses were present over the western United States (Fig. 13). A cold, continental polar airmass

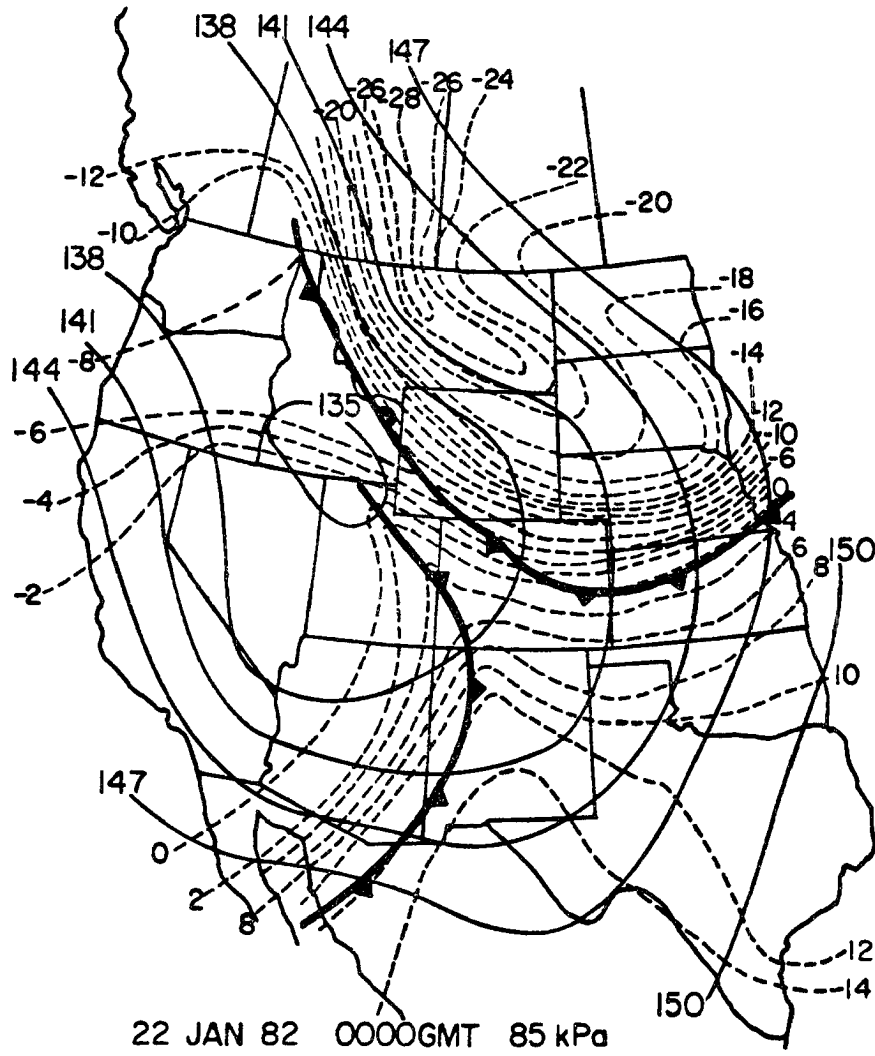


Fig. 13. 85 kPa chart for 22 January 82 at 0000 GMT.

covered most of the northern plain states east of the Continental Divide. The frontal boundary separating this polar air from the warmer airmass to the south had entered eastern Colorado at 0000. To the west, a maritime polar airmass advected eastward associated with a deep trough system. The 85 kPa front associated with this airmass extended southeast from a low pressure center located in northern Utah. At 0000, this front had not yet entered northern Colorado. At mid-levels, a tongue of moisture was evident within the warm air along this front. This moist region is evident on the 70 kPa chart for 0000, shown on Fig. 14. To the west, east of the Sierra Mountains, the airmass was moist. In the vicinity of the front, the moist tongue extended to the 50 kPa level.

The extent of this cloud system was evident on satellite photographs of the storm system. On these photographs, a wide cloud region with cloud top temperatures near -40°C was observed ahead of and over the maritime front. The cloud system extended from New Mexico northward over the polar air in Wyoming, covering the Park Range region. Visual observations at the surface in Steamboat Springs indicated that the leading edge of this cloud system was a shallow mid-level non-precipitating stratus with a base near 4400 m. This stratus deck preceded a region of convective precipitation.

During the period prior to frontal passage (0700), a potentially unstable region was present over an 8 kPa depth centered on the 70 kPa surface (Fig. 15). The equilibrium level for an air parcel originating within this layer was near -40°C , corresponding well to the cloud top observed by the satellite and the radar.

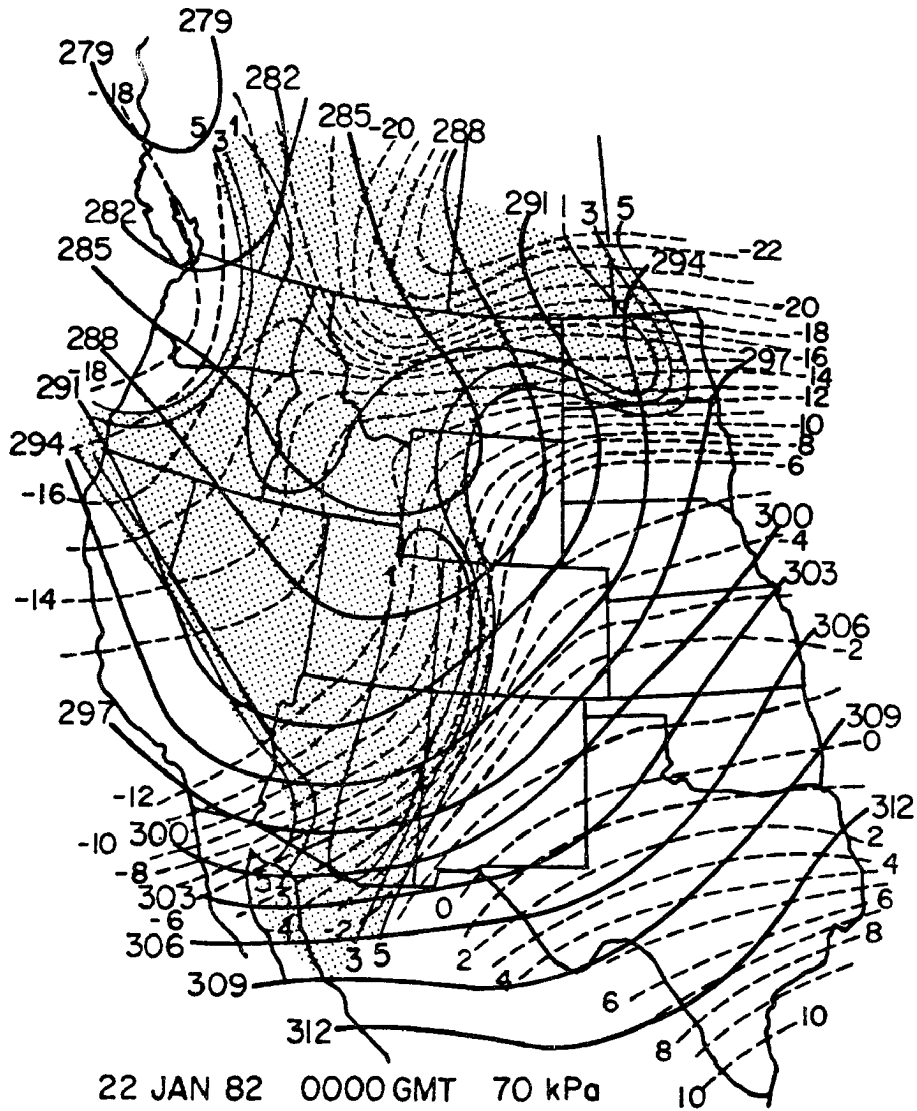


Fig. 14. 70 kPa chart for 22 January 82 at 0000 GMT.

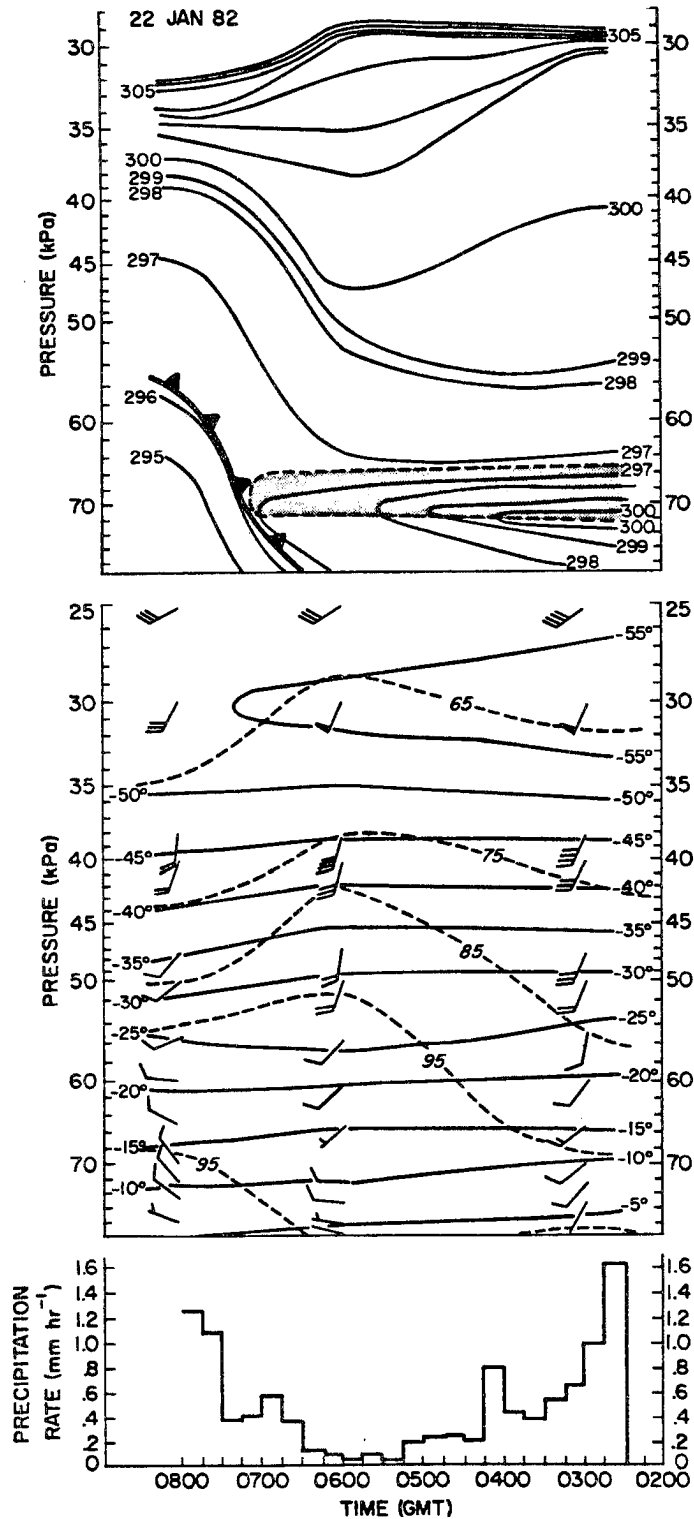


Fig. 15. Time section of equivalent potential temperature (top), and temperature, relative humidity and winds (middle) for the 22 January 82 storm system. Precipitation rates at RAD are shown on the lower part of the figure.

During the pre-frontal period, winds were westerly to southwesterly at low levels, backing to northwesterly after frontal passage. Two periods of heavy (> 1.0 mm/h) precipitation occurred in association with the passage of this cloud system, the first at the leading edge of the deep convection and the second in association with the frontal passage. Scanning radiometric data was available throughout the first heavy precipitation event.

Storm evolution and supercooled water distribution

The time evolution of the supercooled water field, precipitation intensity, and rime characteristics of crystals collected at RAD, rime characteristics of crystals at SPL, radar cloud top and maximum reflectivity, and surface temperature at RAD during the passage of the first convective region are shown in Fig. 16.

Radiometric data collected during the period prior to the passage of the convective band indicated that the mid-level stratiform cloud system preceding the convection contained almost no supercooled cloud water. Weak radar reflectivities during this time indicated that the cloud was composed of ice crystals that were too small to precipitate. No significant orographic enhancement of the cloud water field was evident in the radiometric data, with the possible exception of the period between 0030 and 0045. The lack of orographic enhancement is consistent with observations of boundary layer and mid-level winds, which had weak cross-barrier components in the vicinity of the range.

The approaching convective region was observed initially by the radiometer west of RAD. At this time, the cells within the beam path contained small but significant quantities of supercooled water. As the band approached the barrier, strong orographic enhancement of the

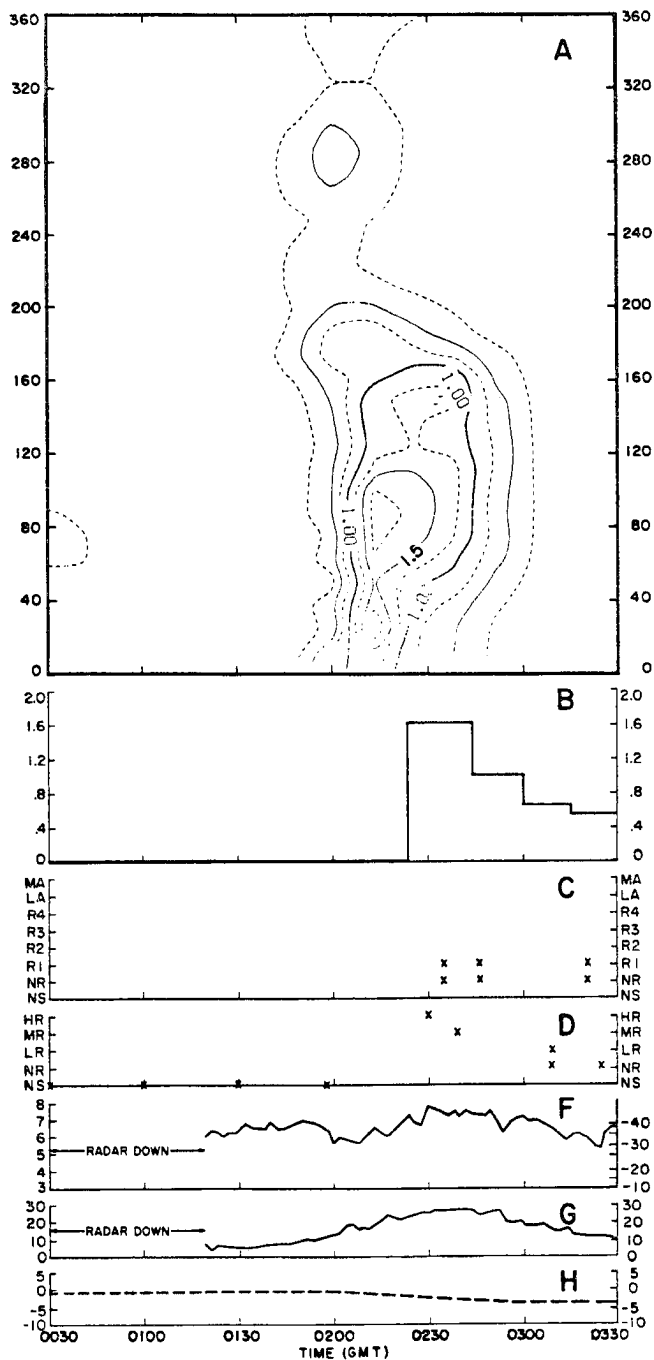


Fig. 16. 22 January 1982 (0030-0330 GMT): (A) Radiometric integrated liquid water content (mm) as a function of azimuth angle from the radiometer; (B) Precipitation intensity at RAD (mm/hr); (C) Rime characteristics of crystals collected at RAD (see Sec. 2C); (D) Rime Characteristics of crystals collected at SPL (see Sec. 2D); (F) Radar determined cloud top height (km) and cloud top temperature ($^{\circ}\text{C}$); (G) Radar observed maximum reflectivity (dBZ); (H) Surface temperature at RAD ($^{\circ}\text{C}$).

vertical motion within the cells resulted in significant increases in observed cloud water contents along and over the barrier. Twenty minutes elapsed between the arrival of the leading edge of the band and the onset of precipitation at SPL and RAD. These observations suggest that the developing convective cells in the vicinity of the ridge were initially composed predominantly of supercooled water.

As cells within the band moved toward the barrier and developed, a continuous conversion of cloud water to the ice phase ensued. This is most evident from the radar reflectivity return, which continually increased between the arrival of the convective region and the onset of precipitation. Once the ice phase was established, rapid depletion of the cloud liquid water occurred, primarily through accretion processes, as shown by the rime characteristics of the ice crystals at SPL and the rapid disappearance of the liquid water throughout the cloud as measured by the radiometer.

Crystals observed at RAD during the passage of the band were unrimed or lightly rimed. Simple trajectory considerations show that these crystals would have originated well upwind of the major concentration of supercooled cloud water indicated by the radiometer. Radiometric observations showed that only small amounts of cloud water were present west of RAD, upwind of the barrier, and that most of the cloud water was present in cells along and over the barrier slopes. For these reasons, crystals arriving at RAD would be expected to interact only minimally in accretion processes.

The radiometric distribution of liquid water during band passage reached a maximum at an azimuth angle of 85° , almost directly over the windward slopes of the range. At 0230 at SPL, heavy precipitation began

to fall consisting of snow pellets and graupel. As the convective cells evolved, the observed radiometric liquid water content in the cloud system decreased substantially in the clouds over the barrier. Corresponding decreases in the amount of rime visible on collected crystals were also observed at SPL, although moderate snowfall continued throughout the period. By 0330, no riming was apparent on the crystals collected at SPL. Radiometric observations at this time indicated that the supercooled cloud water within the cloud system had been largely depleted.

The convective band was very efficient at converting liquid water initially produced in its development stages to the ice phase. Ice particles initially produced in this system rapidly removed the liquid water present through accretion processes and later depleted available condensate by sustained diffusional growth.

b. Case study: 15 December 1981

Synoptic scale and local weather conditions

The cloud system of 15 Dec 81 evolved through several distinct stages, each exhibiting significant variations in the cloud liquid water distribution. The variations were associated with the onset and passage of two deep cloud systems. The passage of these deep clouds was marked by significant increases in precipitation intensity and decreases in liquid water content. The first deep cloud region arrived at RAD at 1450, remaining over the site for approximately 1 hr.

The 15 Dec 81 cloud system occurred while the Park Range region was in the warm sector of a cyclonic storm system located over the western United States. Three airmasses were present, a maritime polar airmass over the west coast, a continental polar airmass over the northern

plains to the east and a modified maritime airmass over the southwest (Fig. 17). The 85 kPa cold front marking the boundary of the maritime airmass was well west of the Park Range region and did not directly effect Park Range precipitation during the case study. The second front, the boundary of the continental polar air, was confined to the plains east of the Continental Divide.

Aloft, a wide region of moisture was present west of the Continental Divide across Colorado, northern Utah and Nevada and north into Idaho. This moist region is evident on Fig. 18, the 70 kPa chart for 1200. This moist region extended to the 50 kPa level. During the six hours between 1200 and 1800, the 50 and 70 kPa temperature at CG changed less than 0.5°C . The storm during this period was confined to the warm airmass.

Unlike the previous study, no low-level instability was present (Fig. 19). Prior to about 1700, regions of potential instability were confined to levels of the atmosphere colder than -25°C (45 kPa). Before about 1700, clouds with tops warmer than -25°C were stable. However, cloud regions reaching the -25°C level, particularly later in the storm near 1500, had the potential to develop into deeper systems through convective motions within the upper levels. After 1700, potentially unstable layers developed in the middle troposphere and the potential for convection increased. Throughout the storm, the low levels of the atmosphere below 50 kPa remained very moist. Winds veered with height up to 55 kPa, having a strong westerly component. Cross-barrier wind speeds throughout the period were near 16 m/s. No significant variations in temperature were observed at any level.

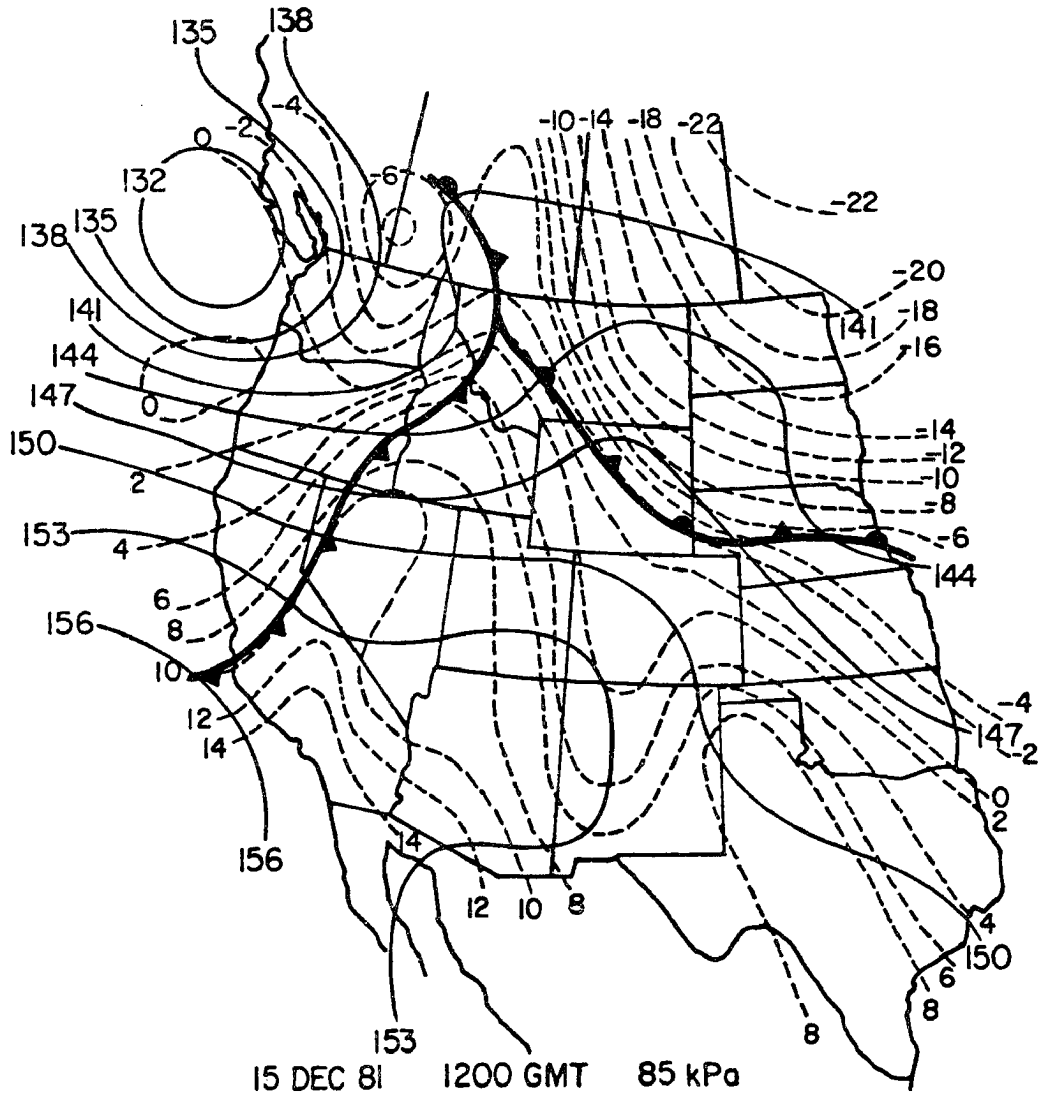


Fig. 17. 85 kPa chart for the 15 December 81 storm at 1200 GMT.

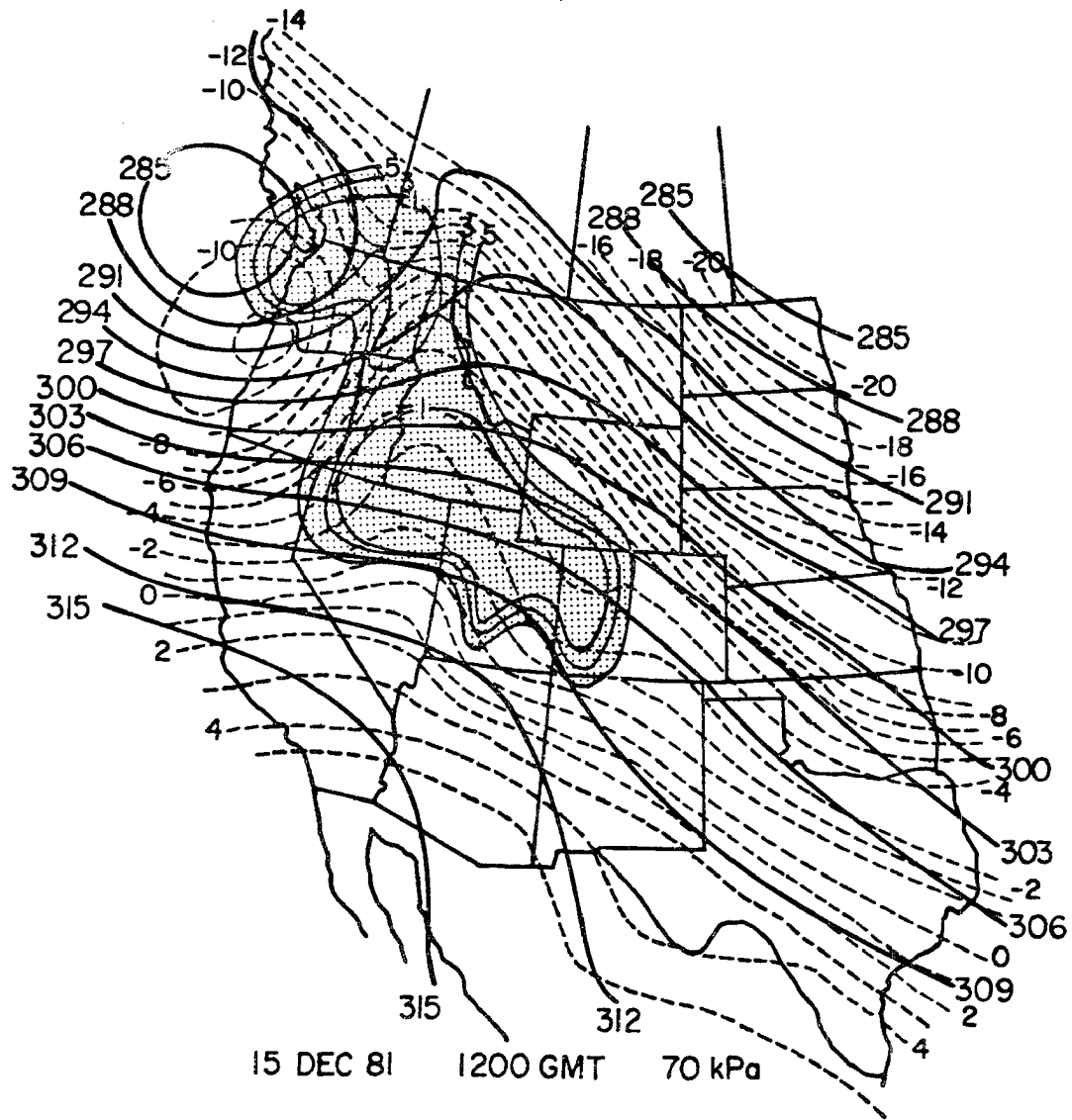


Fig. 18. 70 kPa chart for the 15 December 81 storm at 1200 GMT

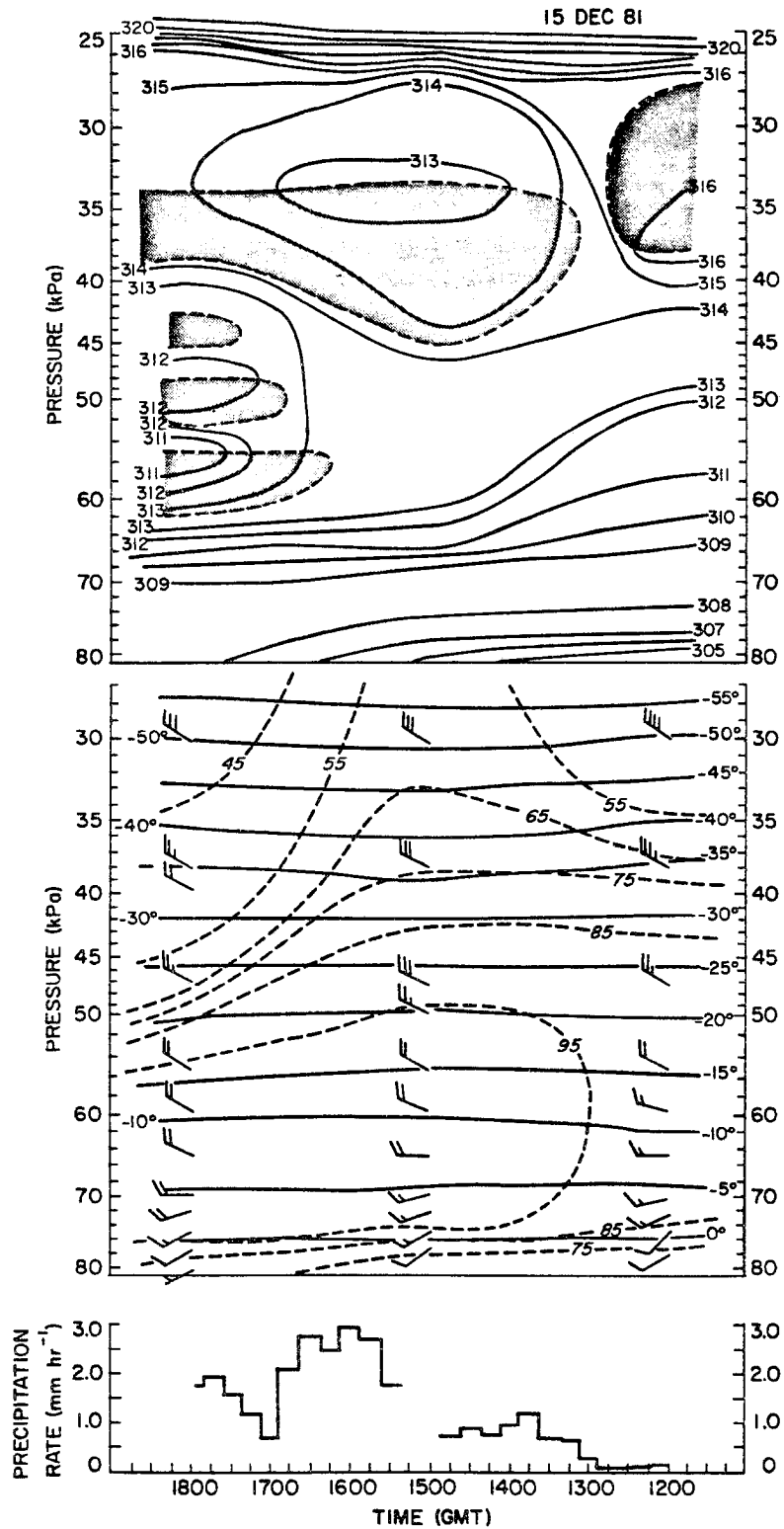


Fig. 19. Time section of equivalent potential temperature (top), and temperature, relative humidity and winds (middle) for the 15 December 81 storm system. Precipitation rates at RAD are shown on the lower part of the figure.

Storm evolution and supercooled water distribution

The time evolution of the supercooled liquid water distribution, precipitation characteristics at SPL and RAD, liquid water contents at SPL, radar characteristics and temperature at RAD are shown on Figs. 20 and 21. During the early stage of this storm, from 1310 to 1450, a stratiform cloud system with tops at 5000 m (-16°C) was present over the Park Range region. Precipitation from this storm fell steadily at a rate of 1 mm/hr at RAD. During this period, radiometric measurements of the cloud water field indicated that cloud liquid water was present throughout the cloud system, but was concentrated over the Park Range, particularly over the mountains southeast of RAD. Simultaneous measurements of rime intensity at SPL and RAD supported the radiometric measurements. At RAD, crystals were observed primarily in the R3, R2, and NR categories, indicating that significant accretion of supercooled cloud droplets occurred in clouds upstream of RAD. Nearly all crystals collected at SPL during the period were moderately rimed. The absence of unrimed crystals at this site provides strong support for the radiometric measurements of increased liquid water content over the Park Range. During the early stage of this storm, mountaintop observations of supercooled water gradually increased from 0.02 gm^{-3} to 0.10 gm^{-3} , paralleling the increases in supercooled water observed by the radiometer in the vicinity of the barrier.

With the onset of the first deep cloud region, cloud tops rapidly increased to 7000-8000 m (-30° to -35°C). Radiometric liquid water content rapidly decreased throughout the cloud system during this stage of the storm. Prior to the onset of the deep cloud system, crystals observed at SPL were all heavily rimed, but as the deep cloud became

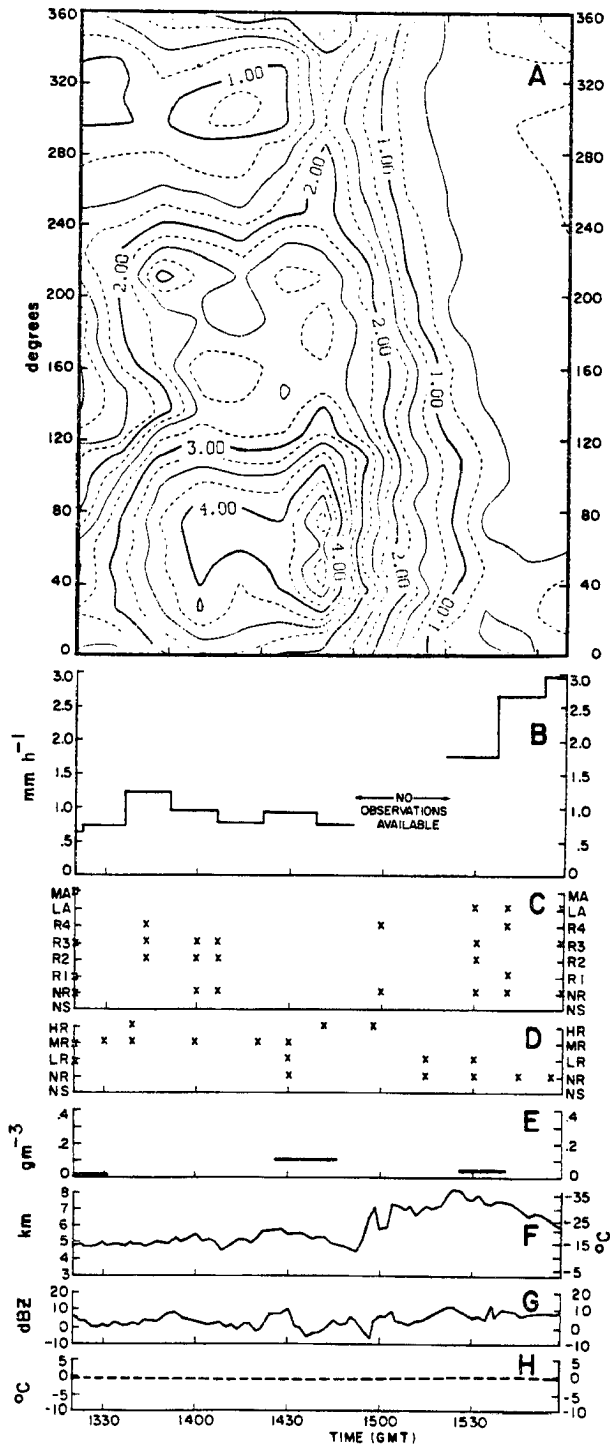


Fig. 20. 15 December 1981 (1320-1600 GMT): (A) Radiometric integrated liquid water content (mm) as a function of azimuth angle from the radiometer; (B) Precipitation intensity at RAD (mm/hr); (C) Rime characteristics of crystals collected at RAD (see Sec. 2C); (D) Rime Characteristics of crystals collected at SPL (see Sec. 2D); (E) Rotorod liquid water content at SPL (gm^{-3}); (F) Radar determined cloud top height (km) and cloud top temperature ($^{\circ}\text{C}$); (G) Radar observed maximum reflectivity (dBZ); (H) Surface temperature at RAD ($^{\circ}\text{C}$).

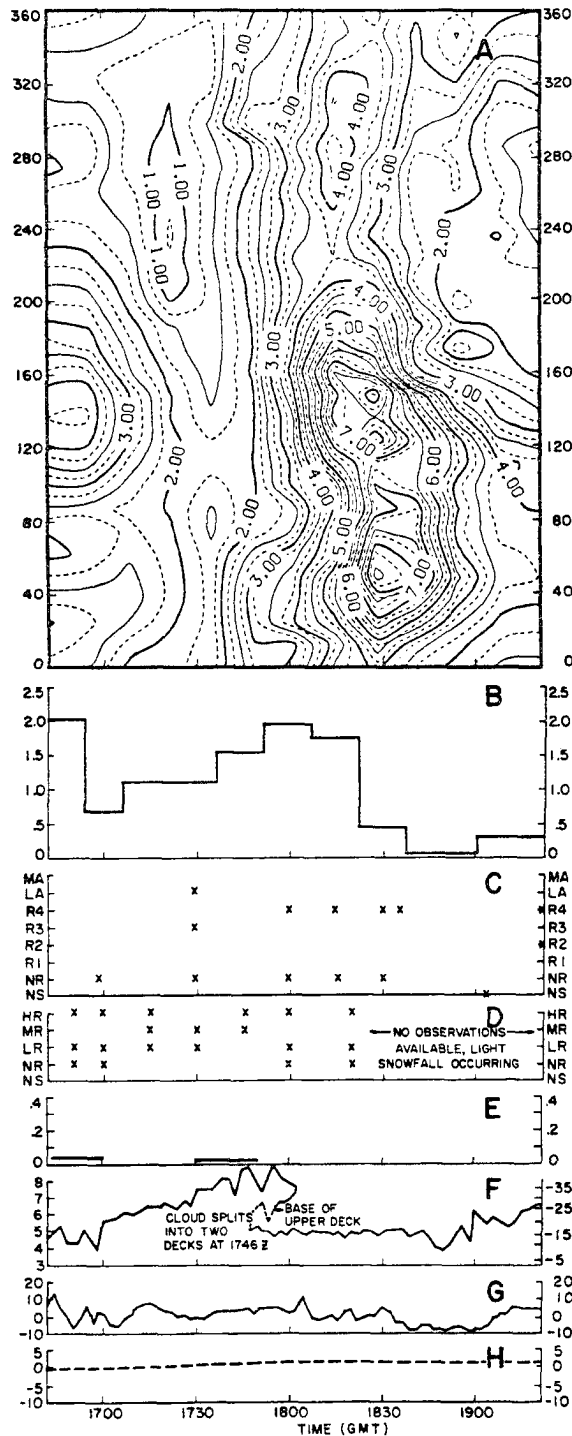


Fig. 21. 15 December 1981 (1640-1920 GMT): (A) Radiometric integrated liquid water content (mm) as a function of azimuth angle from the radiometer; (B) Precipitation intensity at RAD (mm/hr); (C) Rime characteristics of crystals collected at RAD (see Sec. 2C); (D) Rime Characteristics of crystals collected at SPL (see Sec. 2D); (E) Rotorod liquid water content at SPL (gm^{-3}); (F) Radar determined cloud top height (km) and cloud top temperature ($^{\circ}\text{C}$); (G) Radar observed maximum reflectivity (dBZ); (H) Surface temperature at RAD ($^{\circ}\text{C}$).

established in the area, the amount of rime decreased substantially. During this time, precipitation rates increased considerably at RAD and SPL.

Within 40 minutes after the onset of the deep cloud, all crystals observed at SPL were unrimed. Some crystals collected at RAD were aggregated. These particles were mainly small aggregates of cold temperature crystals and a few dendritic aggregates. Many of the aggregates continued to be lightly rimed, although a few crystals continued to be rimed more heavily. Liquid water contents at the surface at SPL during the passage of the band reduced to 0.05 gm^{-3} .

These observations all suggest that the liquid water remaining in the cloud during the deep cloud period was largely confined to the lower levels of the cloud system below SPL and was distributed uniformly in the horizontal throughout the cloud system. The rapid decrease in liquid water throughout the cloud system and the rapid increase in precipitation intensity and depth of the cloud all suggest that additional nucleation of significant numbers of ice crystals and/or ice crystal production through ice multiplication processes was occurring. The significant numbers of ice crystals effectively removed the liquid water remaining in the cloud system by diffusional growth and accretion processes.

Data collection with the radiometer was interrupted at 1558 and resumed at 1633. During this period, cloud tops gradually returned to 5000 m. When the radiometer was reactivated, the liquid water distribution resumed a pattern similar to that observed during the earlier shallow cloud period. The highest liquid water contents were observed over the mountains just northeast of the radiometer. Heavily

rimed crystals were again consistently observed at SPL; unrimed crystals were observed at RAD.

The second deep cloud region moved over the radiometer site at 1700. From this time until 1740, cloud tops gradually increased, reaching 8000 m. At 1746, the cloud deck split, and the portion above 5000 m dissipated. Prior to the split, liquid water contents throughout the cloud system again decreased. Crystals and aggregates at RAD were mostly lightly rimed during this period. At SPL some crystals continued to be heavily rimed, but the intensity of the rime decreased with time. Liquid water contents observed at SPL were quite low during this period. These observations again suggest that enhancement of accretion processes by aggregate and single collectors was significant in the lower regions of the cloud during the onset of the deep cloud region.

When the cloud deck split and the upper deck dissipated, an immediate increase in the liquid water field occurred in all quadrants, particularly over the barrier. Precipitation during this period at RAD consisted of snow pellets and unrimed needles. At SPL, precipitation was similar in character with snow pellets and needles predominating. The liquid water field reached a maximum at 1840, then began to decrease in all directions as a third heavily precipitating cloud system moved into the region.

The radiometric liquid water contents measured during the period after the upper cloud deck dissipated were the highest measured during the field experiment and probably were complicated by melting occurring as the crystals fell through the boundary layer. The surface temperature during this period was between 1°C and 2°C , so at least initial melting of some ice crystal surfaces was likely. However, rime

observations at both sites indicate that a substantial amount of this water existed in the supercooled state.

The evolution of the cloud liquid water in this cloud system was such that the shallow portions of the cloud system with warm cloud top temperatures and low precipitation rates consistently had the highest liquid water contents. The deep cloud regions with cold cloud tops had lower liquid water contents. The decrease in liquid water during passage of the deep clouds was accompanied by an increase in the precipitation rate, indicating that the production of cloud ice particles was significantly enhanced during these periods.

c. Case study: 30 December 81

Synoptic scale and local weather conditions

Major synoptic scale weather features at the surface and 50 kPa for 30 Dec 81 are shown on Fig. 22. The radiometer operated in the scan mode from 2200 on 30 Dec 81 to 0100 on 31 Dec 81.

At 1200 on 30 Dec 81, a low pressure system was centered in eastern Wyoming. From this low, a cold front extended westward into southern Idaho, then southwest into central California. In the warm sector of this storm ahead of the cold front, strong mid-level winds, in association with the moderately moist airmass, produced a widespread stratiform cloud system over the northern Colorado Rockies. 70 kPa wind speeds were 15-18 m/s.

During the early portion of the study period between 1900 and 2210, the study area was in the warm sector of the storm. Light and sporadic precipitation occurred until 2100 in the lower elevations associated with weak embedded convective elements in the cloud system. Light to moderate snow fell at higher elevations. By 2100, all snowfall had

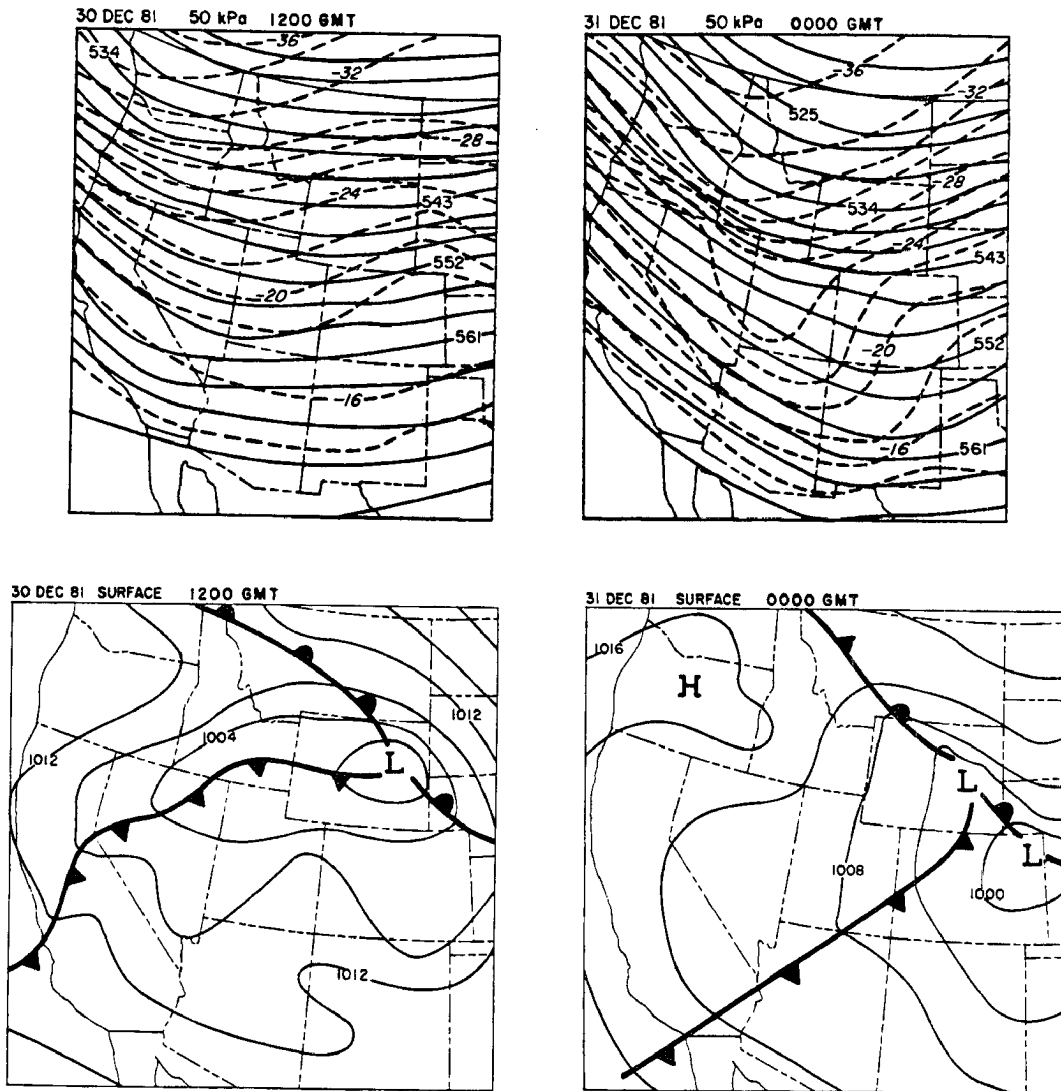


Fig. 22. Synoptic scale weather features for the 30-31 December 1981 storm system.

stopped at both low and high elevation observation stations although cloud cover remained over the region. At and behind the surface frontal boundary, a wide band of convective precipitation developed. Heavy precipitation continued through the remainder of the study period.

Storm evolution and supercooled water distribution

The cloud systems occurring near frontal passage during the 30 Dec 81 storm system were predominantly convective and were characterized by considerably greater cellular structure than in the previous two cases. These cells were emergent from a stratiform layer having a top around 4500 m (-15°C).

For an hour before frontal passage, snow fell in showers at higher elevations from cells that developed upwind of the range near RAD and moved over the ridge. No precipitation was observed at lower elevations during this period. At the time of frontal passage, considerable convective activity developed throughout the region, heavy precipitation began falling at all observation sites, and winds increased substantially at all elevations.

The storm system was organized into two bands of heavy precipitation. Each band took about 1.5 hr to pass through the Park Range region. Between bands, a low level stratiform cloud continued to produce precipitation at significantly lower rates. Vertical profiles of equivalent potential temperature from rawinsondes launched at CG are shown on Fig. 23. These rawinsondes were launched at 2100, just prior to frontal passage, and 0000 (31 Dec), after the front had passed.

Before frontal passage, two potentially unstable layers were present, the first extending from the surface (1886 m) to 2355 m and the second from 4418 m to 6418 m. At 0000, potentially unstable layers were

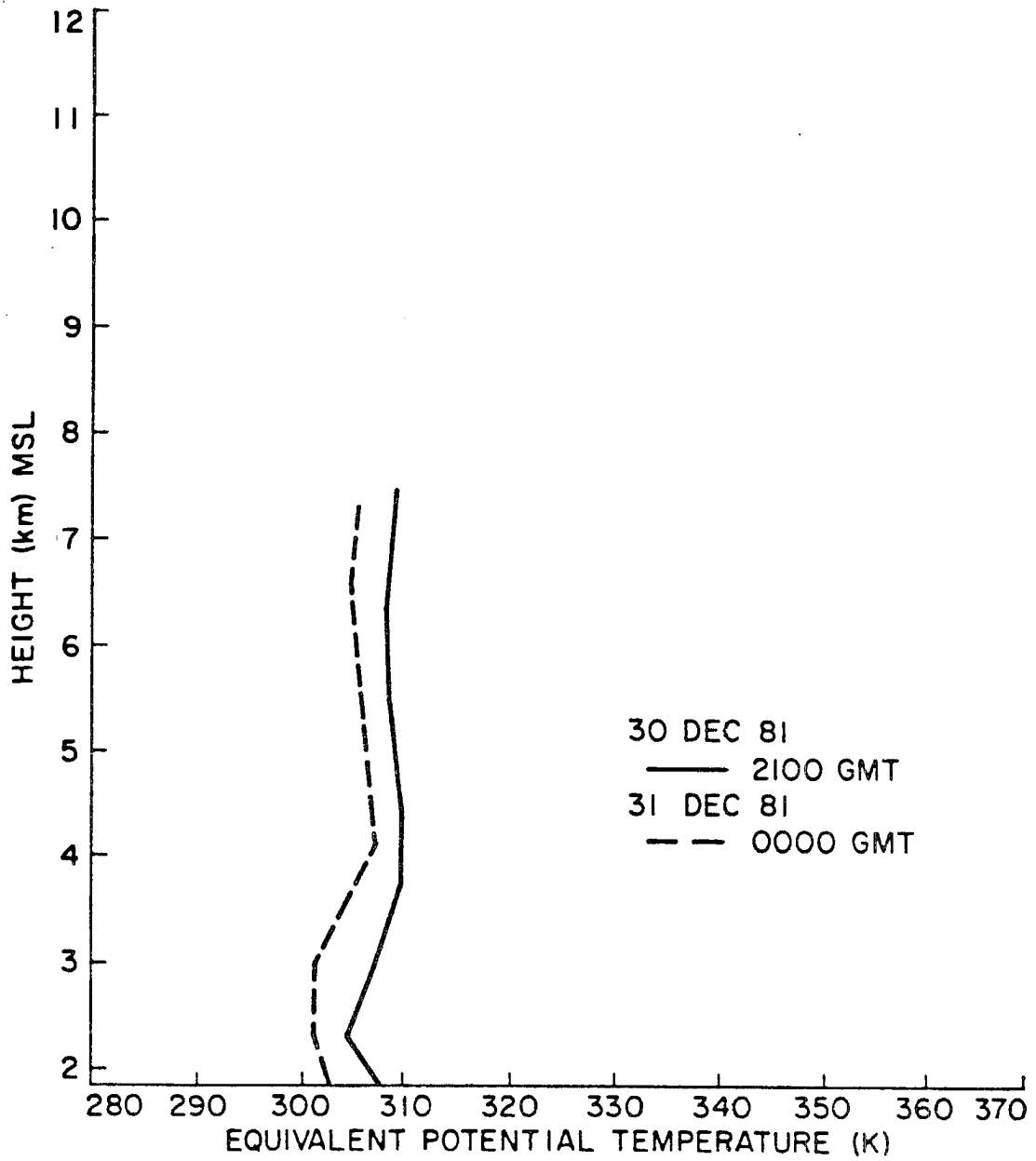


Fig. 23. Vertical profiles of Equivalent Potential Temperature at 2100 GMT, 30 December 1981 and 0000 GMT, 31 December 1981.

present between the surface and 2430 m and between 4127 and 6569 m. The primary difference between these soundings was the presence of the stable layer at 0000 between 3040 and 4127 m associated with the cold frontal surface. The potential instability of the later sounding was also somewhat greater because of cold air advection aloft. The two precipitation bands present after frontal passage developed in response to lifting along the cold frontal surface and subsequent release of the potential instability in the middle troposphere.

The time evolution of the supercooled liquid water field prior to, during and following frontal passage is shown on Fig. 24. Data sets available for the period are included on the figure. SPL did not operate during this storm period. During the time prior to frontal passage, a stratiform cloud deck with considerable cellular convection was present over the area. No precipitation fell in the valley. Occasional snow pellet showers were reported by an observer near SPL. During this time, considerable liquid water was centered primarily over the ridge. The majority of the liquid water was concentrated over the windward slopes with concentrations decreasing to the west away from the primary lift zone. An exception was a strong concentration of water southwest of the site. This localized zone of liquid water to the southwest was probably associated with a region of developing convection. The large concentration of liquid water over the slopes was most likely associated with a stratiform deck over the Park Range that was produced by more uniform lifting as air was forced over the barrier.

The arrival of the frontal zone and the onset of the first period of convective precipitation at about 2300 was marked by a rapid increase in the snowfall rate at RAD and a simultaneous decrease in the liquid

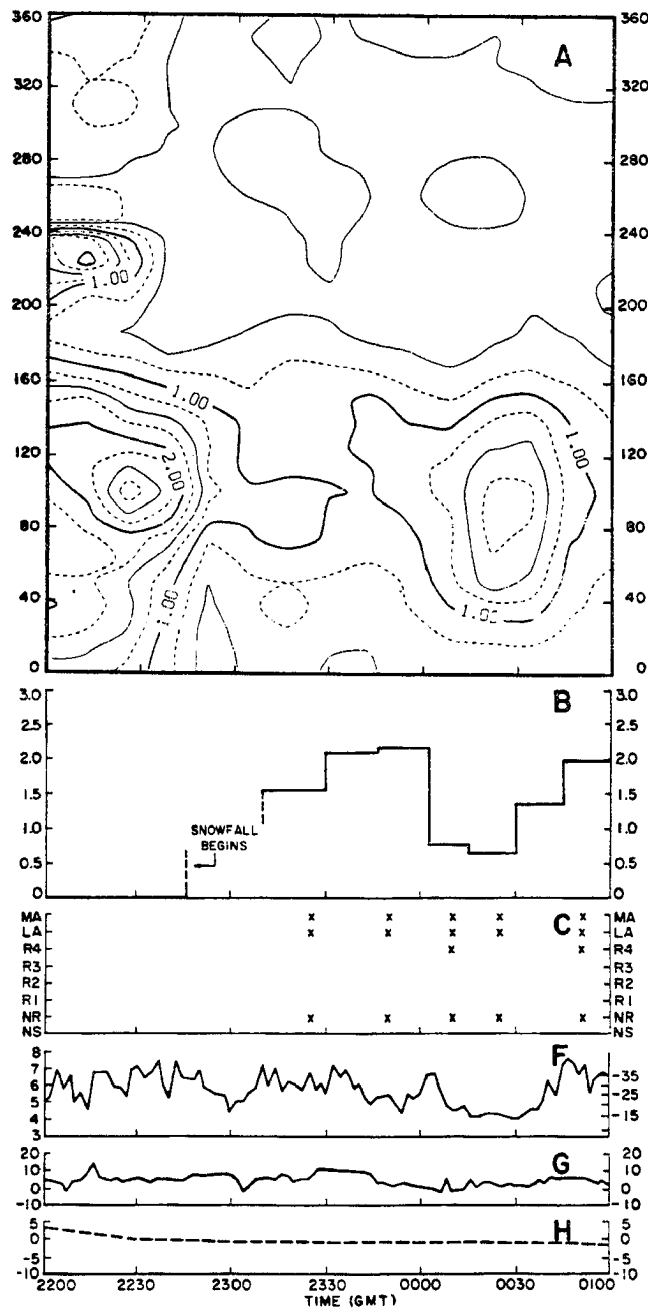


Fig. 24. 30-31 December 1981 (2200-0100 GMT): (A) Radiometric integrated liquid water content (mm) as a function of azimuth angle from the radiometer; (B) Precipitation intensity at RAD (mm/hr); (C) Rime characteristics of crystals collected at RAD (see Sec. 2C); (F) Radar determined cloud top height (km) and cloud top temperature ($^{\circ}\text{C}$); (G) Radar observed maximum reflectivity (dBZ); (H) Surface temperature at RAD ($^{\circ}\text{C}$).

water content of the cloud system, particularly in the vicinity of the barrier. Although substantial decreases were observed, liquid water was present throughout the cloud system during the convective period. Values of integrated liquid water were generally about 0.4 mm upstream of RAD throughout the period. Snowfall during the convective periods consisted primarily of aggregates. These flakes were composed mostly of rimed crystals. Often the rime was of moderate intensity. Some snow pellets were observed. These observations indicate that the passage of the band of convective precipitation resulted in a substantial decrease in the total liquid water present in the system associated with the orographic component of the vertical motion, although some liquid water remained in the system associated with the wide area lifting above the frontal surface and with developing cellular convection. Water removal in this system was primarily through accretion processes.

The passage of the first band occurred at 0000. The cloud system following band passage was largely stratiform with a top around 4200 m (-15°C). During this period, the cloud system returned to a liquid water configuration similar to that observed prior to the arrival of the first band; high liquid water concentrations were centered over the barrier. Liquid water continued to be present in the cloud system upstream of RAD, but in much smaller quantities than were observed over the ridge. Snowfall continued to be aggregated with considerable rime.

The second band arrived at 0030. As precipitation rates increased, a simultaneous decrease in liquid water content over the barrier occurred, similar to what was observed with the first band. Precipitation again consisted largely of aggregates with varying degrees of rime accumulation. Some snow pellets were occasionally observed, but

precipitation was predominantly aggregated crystals. These observations support the earlier conclusion that the ice phase processes associated with a well developed cloud system with embedded convective activity substantially reduce the total liquid water content of the cloud system.

(2) Post-frontal cloud systems

a. Case study: 21 December 1981

Synoptic scale and local weather conditions

The 21 Dec 81 case study concerns the evolution of the liquid water field during a post-frontal cloud system where low-level convective instability was present. This study concentrates on the three hour period from 1320 to 1620, several hours after frontal passage. The front, shown on Fig. 25, marked the boundary between a very warm airmass to the south and modified polar air to the north. Frontal passage occurred at approximately 0600 in the study area. Air in the vicinity and north of the frontal surface was moist at mid-levels (Fig. 26). The moisture extended to the 45 kPa surface.

The frontal surface is evident on Fig. 27, a time-height cross section. After frontal passage, a region of potential instability developed below the frontal surface. Low-level convection may have occurred in the cloud system below the stable frontal layer during this period. The equilibrium level for convective cells originating in this layer was near -12°C , so all convection occurring would have been embedded rather than emergent. During the period, winds were northwesterly at low levels, backing to westerly above the stable layer. The magnitude of the cross-barrier wind speed decreased from 15.5 m/s at 0900 to 8 m/s at 1200 and increased again to 11 m/s at 1500. Cold advection occurred throughout the period.

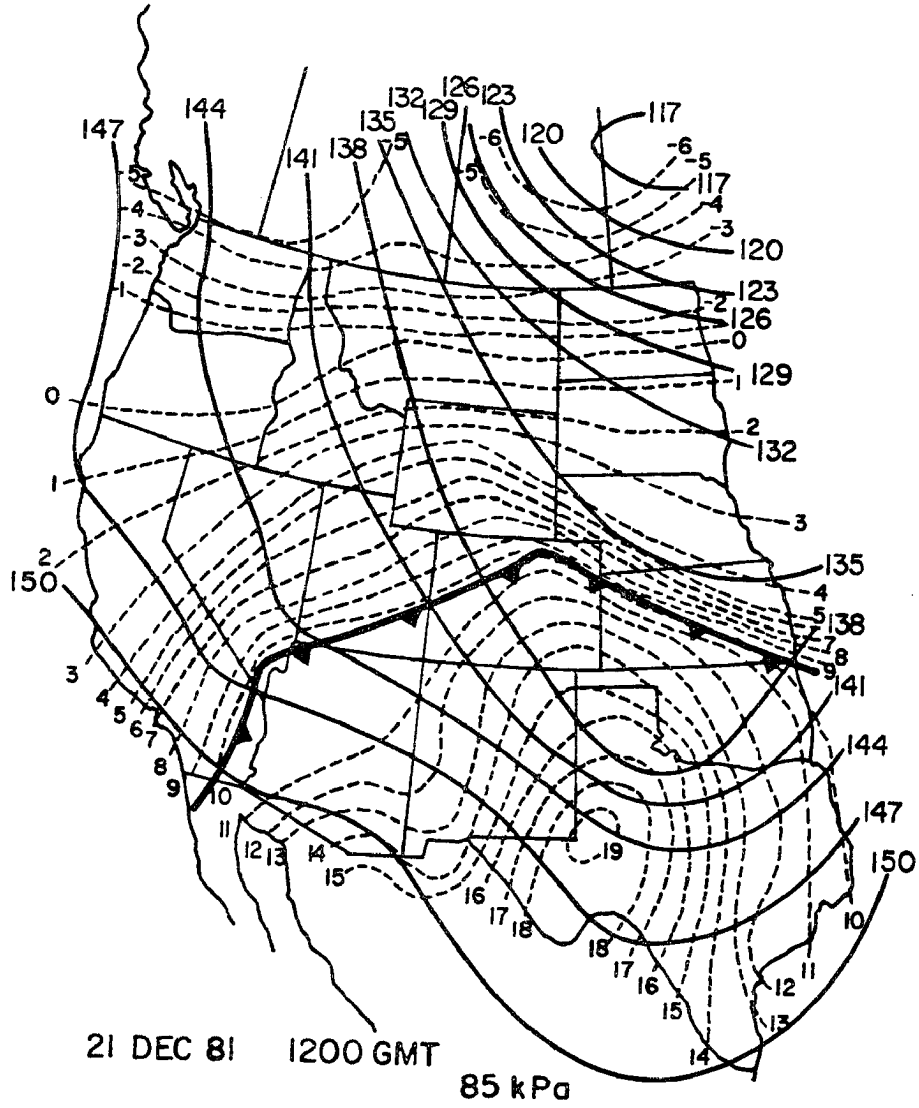


Fig. 25. 85 kPa chart for the 21 December 81 storm at 1200 GMT.

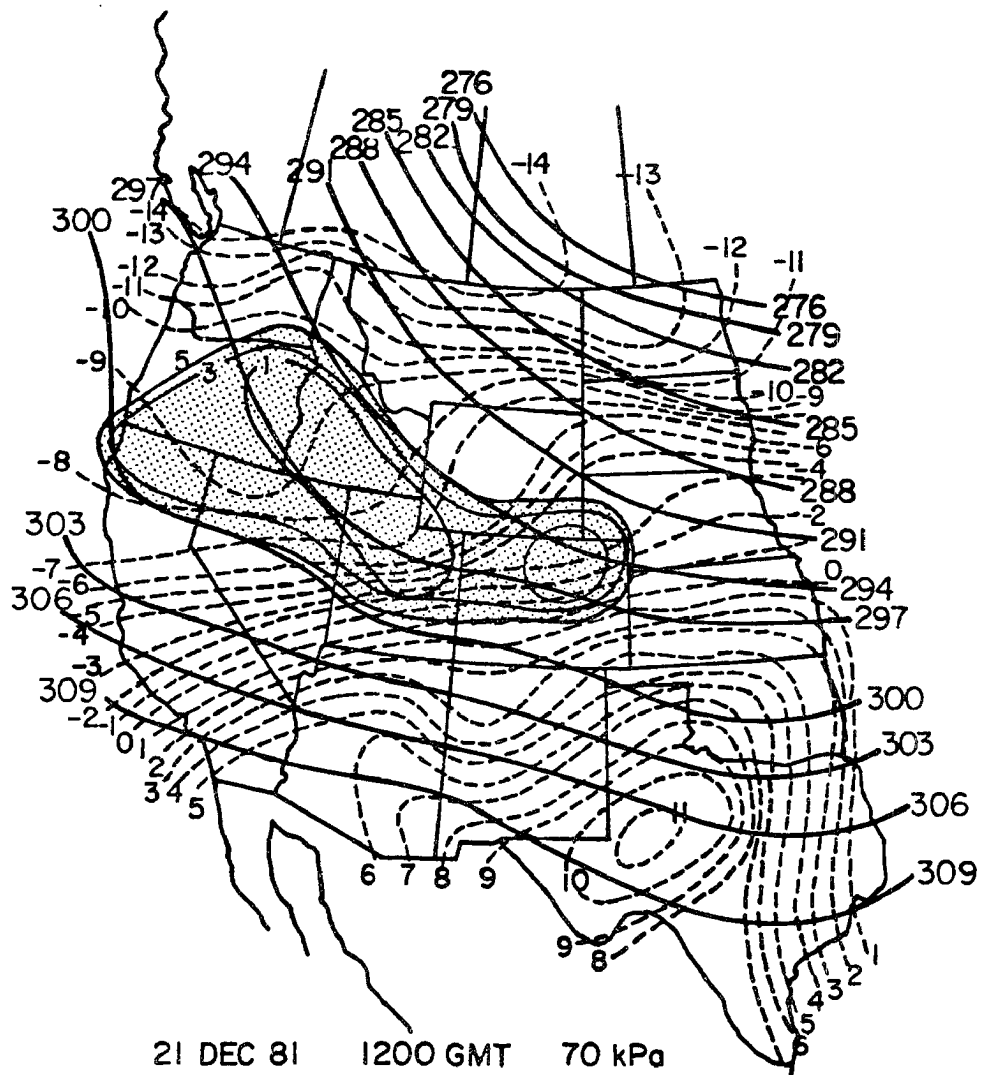


Fig. 26. 70 kPa chart for the 21 December 81 storm at 1200 GMT.

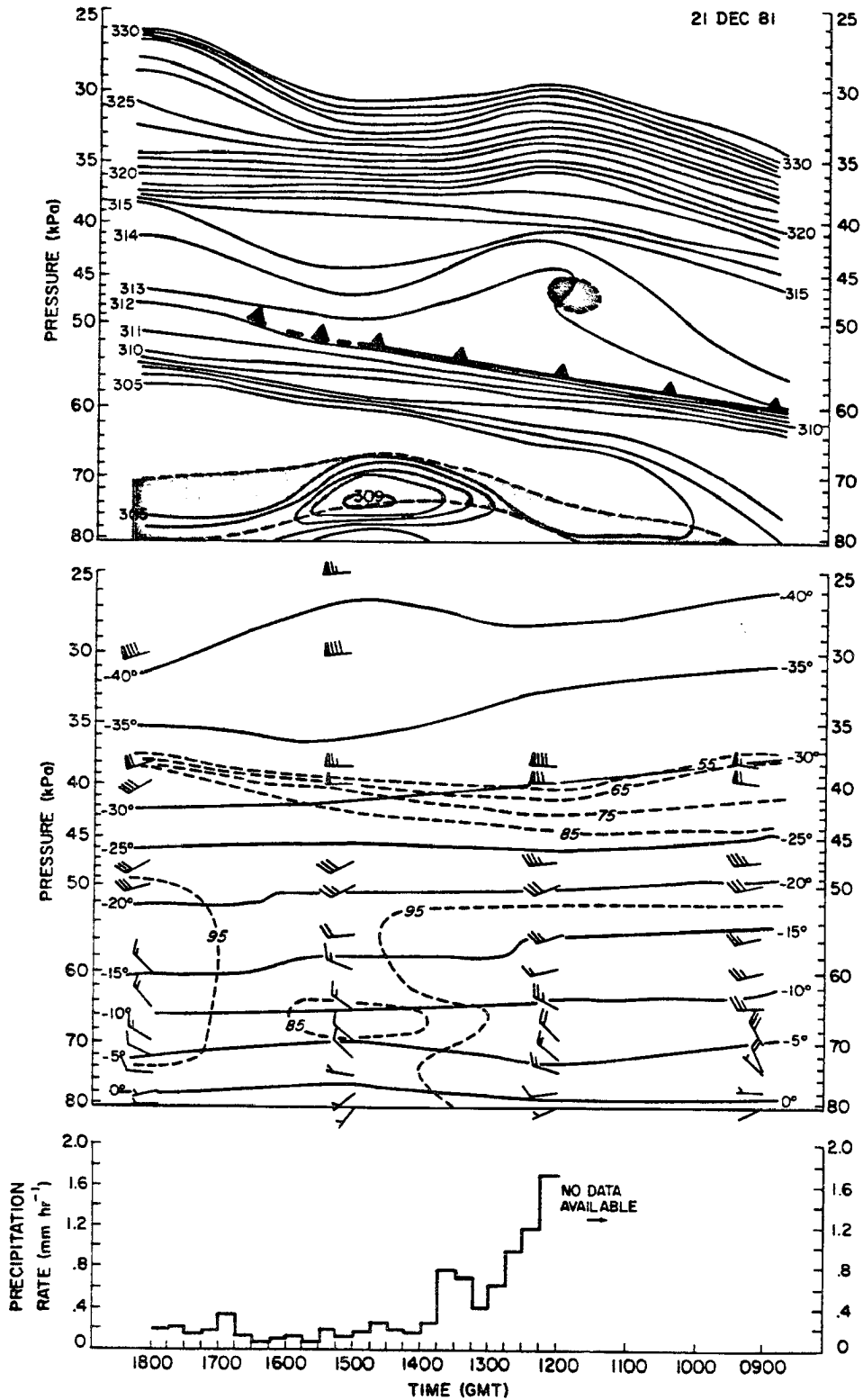


Fig. 27. Time section of equivalent potential temperature (top), and temperature, relative humidity and winds (middle) for the 21 December 81 storm system. Precipitation rates at RAD are shown on the lower part of the figure.

Storm evolution and supercooled liquid water distribution

The time evolution of the supercooled water field and all associated parameters are shown in Fig. 28. During the observation period, liquid water was present throughout the cloud system, but concentrated over the range. Maximum values of liquid water were consistently at an azimuth angle of approximately 90° , directly over the windward slopes. Before the decrease in precipitation rate, crystals were dendritic with many aggregates at RAD. Both single crystals and aggregates generally were lightly rimed. Crystals at SPL were more heavily rimed. These observations support the radiometric measurements of high liquid water contents in the vicinity of the barrier.

After the decrease in precipitation rate at RAD, water contents increased in the vicinity of the mountain. No substantial change occurred upstream of RAD. The increase in liquid water near the mountain was accompanied by an increase in the amount of riming on crystals collected at SPL. During this period, the laboratory was enveloped in a liquid cloud with liquid water content of 0.10 gm^{-3} . At RAD, crystals continued to be lightly rimed.

From 1430 to 1630, the character of the precipitation at SPL and at RAD was similar. Observations at both locations consisted primarily of heavily rimed crystals and unrimed needles. The needles observed may have resulted from secondary ice multiplication production (Hallett and Mossop, 1974) occurring in the cloud just upstream of SPL (see Chap. 4). These needles, forming near SPL, had little time to grow by accretion before impacting on the barrier. For this reason, these crystals were generally unrimed. During the entire period, SPL continued to be

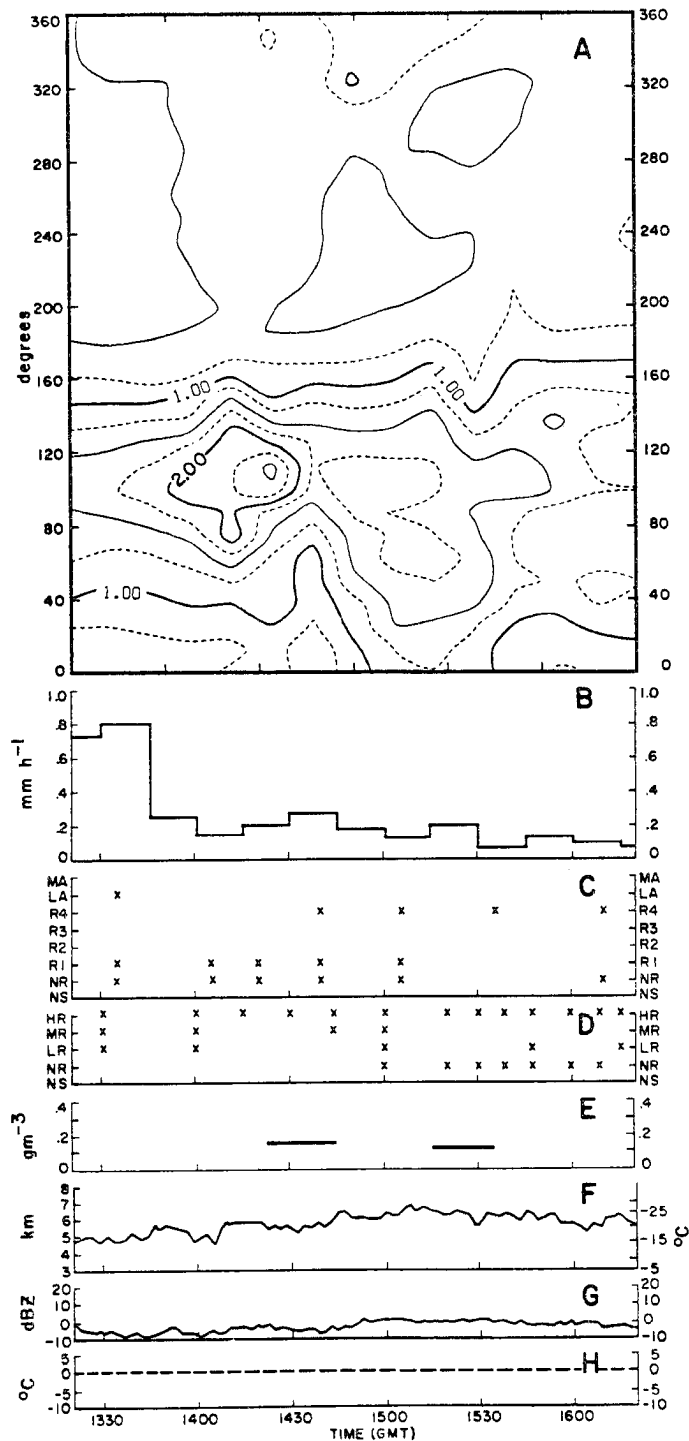


Fig. 28. 21 December 1981 (1320-1620 GMT): (A) Radiometric integrated liquid water content (mm) as a function of azimuth angle from the radiometer; (B) Precipitation intensity at RAD (mm/hr); (C) Rime characteristics of crystals collected at RAD (see Sec. 2C); (D) Rime Characteristics of crystals collected at SPL (see Sec. 2D); (E) Rotorod liquid water content at SPL (gm^{-3}); (F) Radar determined cloud top height (km) and cloud top temperature ($^{\circ}\text{C}$); (G) Radar observed maximum reflectivity (dBZ); (H) Surface temperature at RAD ($^{\circ}\text{C}$).

enveloped in a liquid cloud. The liquid water decreased slowly with time between 1430 and 1630 from a maximum value of 2.50 mm to 1.25 mm.

The production of liquid water in the 21 Dec 81 cloud system may be attributed to two mechanisms. It is clear in this case that a strong orographic effect occurred. Liquid water values were generally 3 to 5 times higher over the ridge than those measured upstream. Convective motions in the low levels may also have contributed to the overall water production. This is particularly true between 1400 and 1600 when the potential instability maxima occurred. If convective motions did contribute to an enhancement of the liquid water field, the enhancement probably occurred near the ridgeline, based on the steady nature of the liquid water field upstream of RAD.

An increase of 0.75 mm in the liquid water over the ridgeline occurred following the reduction in precipitation rate at RAD. No significant change in echo top height occurred in association with this change. At least three mechanisms are possible to explain this observed change: (1) enhanced moisture advection into the radiometric scan volume may have occurred. It is unlikely that the increase in liquid water was due to advection because the increase corresponded to a general decrease in relative humidity measured by the CG rawinsondes and a decrease in the magnitude of the cross-barrier wind speed at 70 kPa. (2) Convective motions in the vicinity of the ridgeline contributed to the liquid water enhancement. The increase in liquid water corresponds closely to the period of maximum potential instability. The correspondence between these two parameters suggests that low level convection was responsible for at least part of the observed increase. (3) Ice particle growth processes were less efficient in the cloud during this period

contributing to an increase in the liquid water production rate. This possibility is supported by the decrease in precipitation rate at RAD. Such a decrease may reflect a decrease in crystal concentration and/or crystal size in the clouds upstream of RAD. If such a change did occur, the effect would be to reduce the rate at which available condensate was converted to the ice phase.

b. Case study: 13 December 1981

Synoptic scale and local weather conditions

Figure 29 shows the evolution of the large scale weather features at the surface and at 50 kPa on 13 Dec 81. The radiometer operated in the scan mode between the hours of 1700 and 2000 during the storm.

At 0000 on 13 Dec 81 a stationary front extended from a low near Laramie, Wyoming, west to northern California where it intersected an approaching Pacific frontal system. By 0600, a low centered in eastern Nevada had developed along the Pacific front. The stationary front extended between this low and the low in eastern Wyoming. As the western front and the associated low progressed southeast across Utah, the stationary front became a cold front and began to move across northwest Colorado. A band of stratiform clouds about 200 km wide developed ahead of this front. Between 1300 and 1500, this band of clouds passed through the study area and produced heavy precipitation. The frontal passage occurred at 1430. Aloft at 1200, a fast-moving short wave with significant cold core temperatures approached the study area from the northwest. As the short wave passed, the temperature at the 50 kPa level dropped 6°C over northern Colorado. This short wave, combined with predominantly westerly, moist mid-level flow behind the front, led to the development of isolated convective cells along the

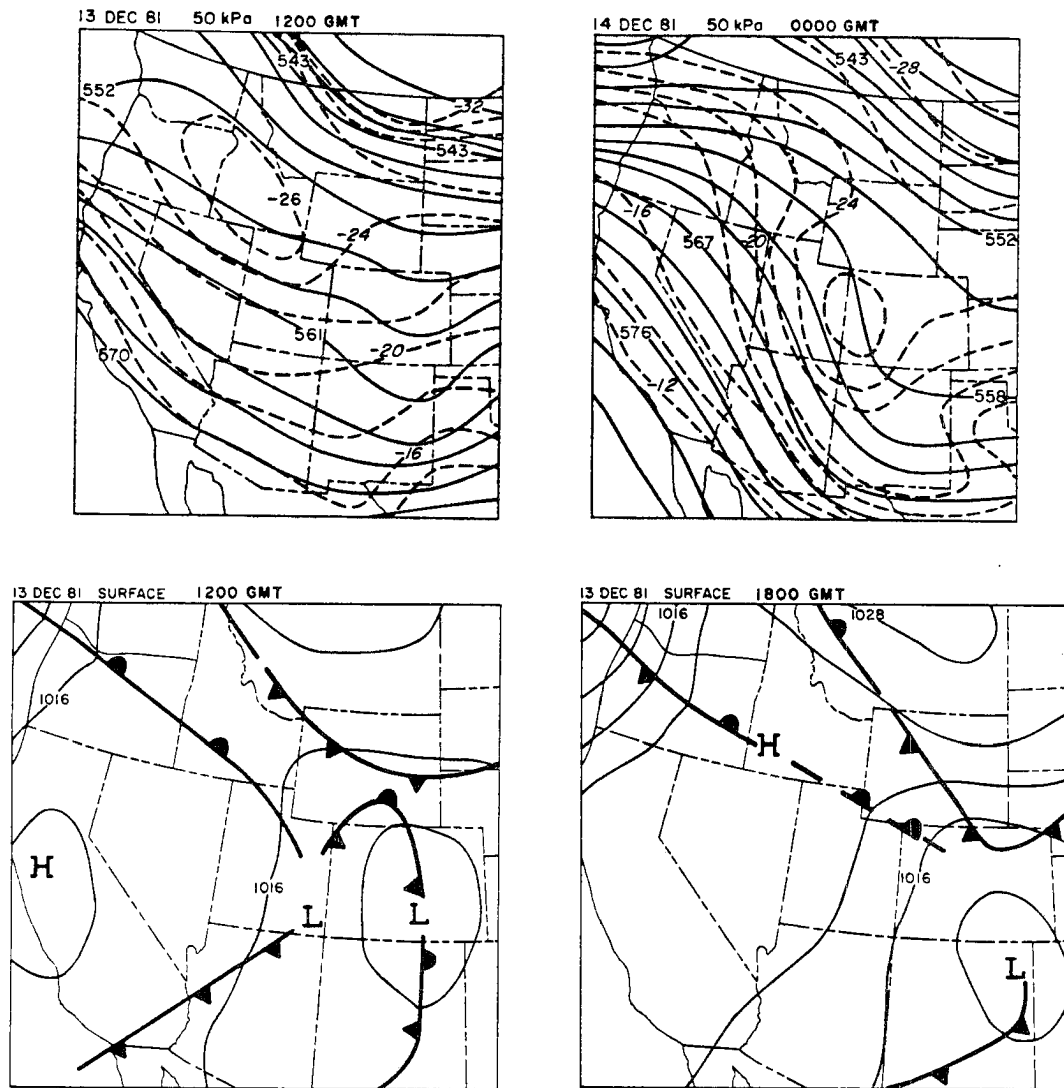


Fig. 29. Synoptic scale weather features for the 13 December 1981 storm system.

ridges. These cells were mostly embedded in a cap cloud which extended west of the ridge about 10-15 km. The average top of this cloud in the vicinity of the vertically pointing radar was 6000 m. The radiometer scans were conducted during the period when the cap cloud was present and initial cellular convection was beginning to develop.

Storm evolution and supercooled water distribution

The storm system of 13 Dec 81 evolved through three distinct stages, each characterized by different regimes of cloud development. During the initial stage, precipitation was produced from a stratiform cloud band which developed ahead of and parallel to the approaching cold front. This cloud system developed in mid-level southwest flow, had a width of about 200 km, and produced steady, moderate to heavy precipitation. Frontal passage marked the transition to the second stage of development. With frontal passage, mid-level winds shifted to westerly and increased in speed. The cloud system from this time onward was maintained primarily by orographic forcing. The clouds during this period were stably stratified. Between 1430 and 1800, the moisture flux from the west steadily decreased; the decrease was accompanied by a decrease in the extent of the cloud system and in the precipitation rate at RAD. Precipitation continued to be heavy at SPL due to strong orographic lifting of the airstream near the ridge. During this period, the atmosphere continually destabilized because of cold air advection aloft. By 1800, convective cells began to develop along the ridges. Precipitation during this latter stage of storm development was primarily produced by orographic forcing, but enhanced in the vicinity of localized convection. The period of radiometric observations covers the latter part of the second stage of storm development and 2 hr during

the convective period. Figure 30, the vertical profile of equivalent potential temperature from rawinsondes launched at 1500 and 1800 at CG, shows the rapid decrease in atmospheric stability associated with the approach of the cold core of the short wave trough. At 1500, no potentially unstable layers were present on the sounding. A neutral layer extended from 5537 m to 6884 m. By 1800, the entire troposphere over the study area had cooled considerably. A potentially unstable layer extended from the surface (1886 m) to 3064 m. Above this layer, a neutral layer extended to 4483 m. Cloud tops were observed to extend to approximately 6000 m.

The time evolution of the supercooled cloud water field and associated parameters are displayed on Fig. 31. Observations of the rime characteristics of crystals at SPL were not made during this storm period. During the latter part of the second stage of this storm, prior to the development of cellular convection, precipitation rates at RAD were approximately 0.4 mm/hr and no rime was observed on any of the crystals. During this period, liquid water was distributed throughout the cloud system with only slight increases in the vicinity of the barrier. With the decline in precipitation intensity, liquid water contents in the vicinity of the Park Range began to increase substantially. At the beginning of this period, Rotorod measurements of liquid water at SPL confirmed the presence of a liquid cloud in the vicinity of the barrier; the liquid water content was about 0.20 gm^{-3} . Within an hour, this value increased to 0.40 gm^{-3} . Simultaneous measurements with the radiometer indicated that these increases were localized over the ridge, but did not extend far upstream. This was also evident from the crystals that fell at RAD. These crystals

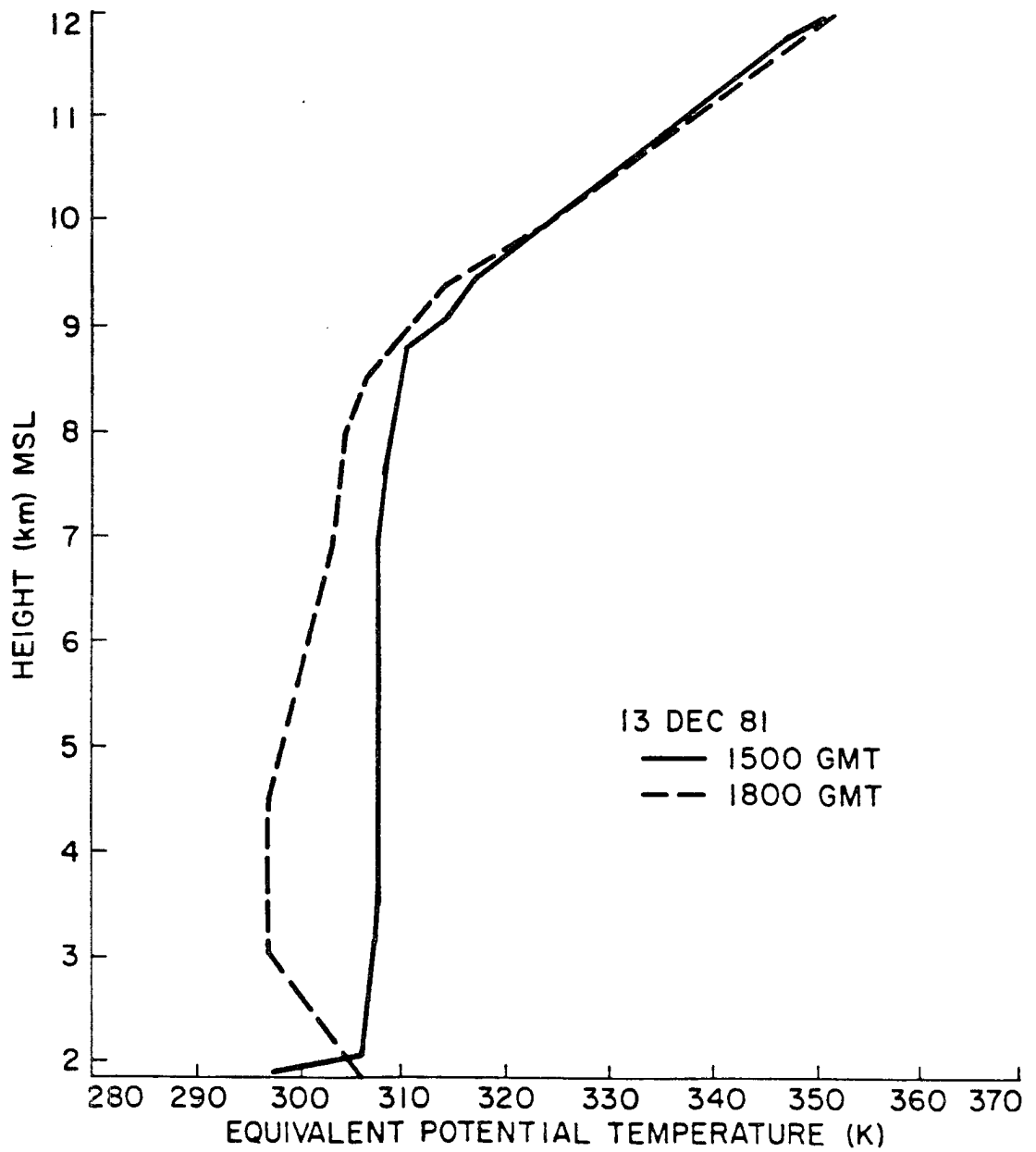


Fig. 30. Vertical profiles of Equivalent Potential Temperature at 1500 GMT and 1800 GMT for the 13 December 1981 storm system.

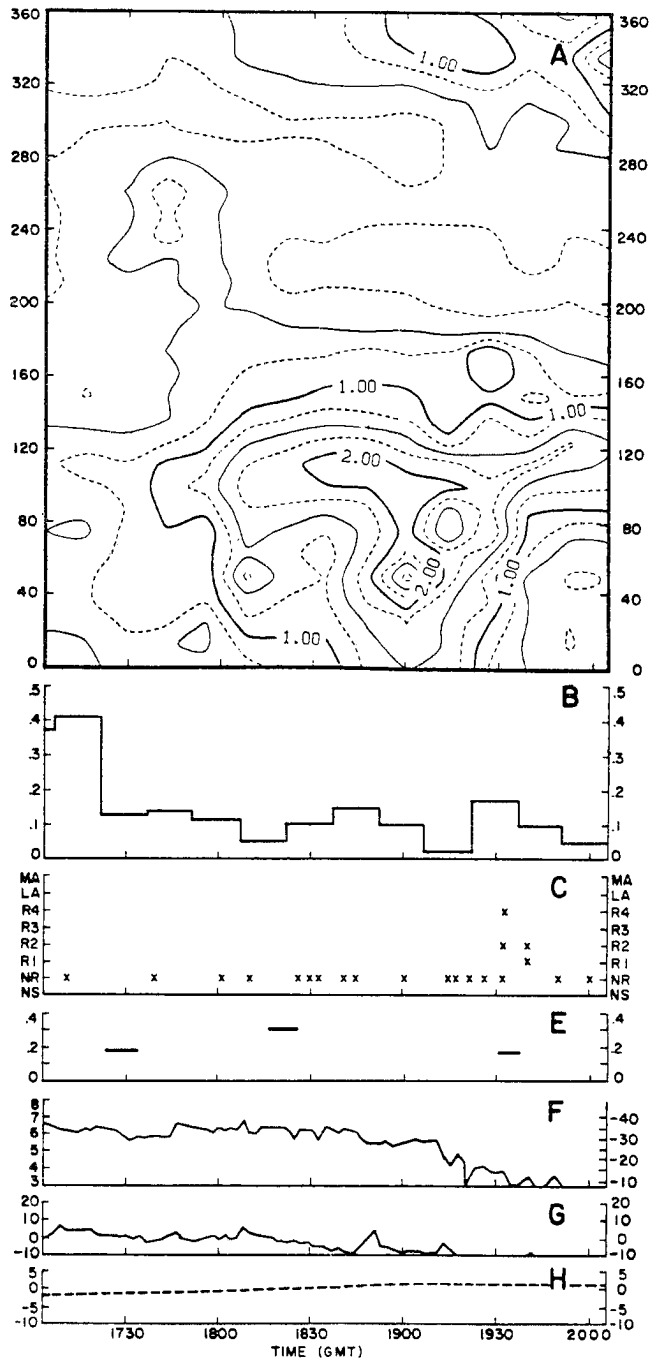


Fig. 31. 13 December 1981 (1700-2003 GMT): (A) Radiometric integrated liquid water content (mm) as a function of azimuth angle from the radiometer; (B) Precipitation intensity at RAD (mm/hr); (C) Rime characteristics of crystals collected at RAD (see Sec. 2C); (E) Rotorod liquid water content at SPL (gm^{-3}); (F) Radar determined cloud top height (km) and cloud top temperature ($^{\circ}\text{C}$); (G) Radar observed maximum reflectivity (dBZ); (H) Surface temperature at RAD ($^{\circ}\text{C}$).

originated well upstream of the mountain and were unrimed throughout the period. It is likely that during the latter stage of storm development, part of the enhanced liquid water field over the barrier was due to liquid water production in convective cells. However, the persistence of the liquid water over the barrier for such a long period suggests that orographic forcing was the dominant mechanism sustaining the liquid water field.

The local effect of convective cells is evident in the crystal observations at 1935 at RAD. Crystals originating in localized convection in the vicinity of RAD fell at the site for 15 min. During this period, precipitation initially contained snow pellets. Unrimed crystals, presumably originating near the upwind locations of the stratiform cap cloud, also fell at RAD during this same period. Although precipitation from the cell fell at RAD, the cell did not move directly over the vertically pointing radar.

The concentration of liquid water in the cloud system reached a maximum just before 1900 and then began dissipating. Rotorod measurements of liquid water also decreased during the period to 0.16 gm^{-3} . During this period, the extent of the cap cloud decreased, mid-level wind speeds declined and the system continued to slowly dissipate. Light snowfall continued until 2125 at RAD, occasionally containing snow pellets associated with cellular convection.

c. Case study: 27 January 1982

Synoptic scale and local weather conditions

Large scale weather features over the western United States at the surface and at the 70 kPa level are shown on Fig. 32. The radiometer performed azimuth scans between 1500 and 1800.

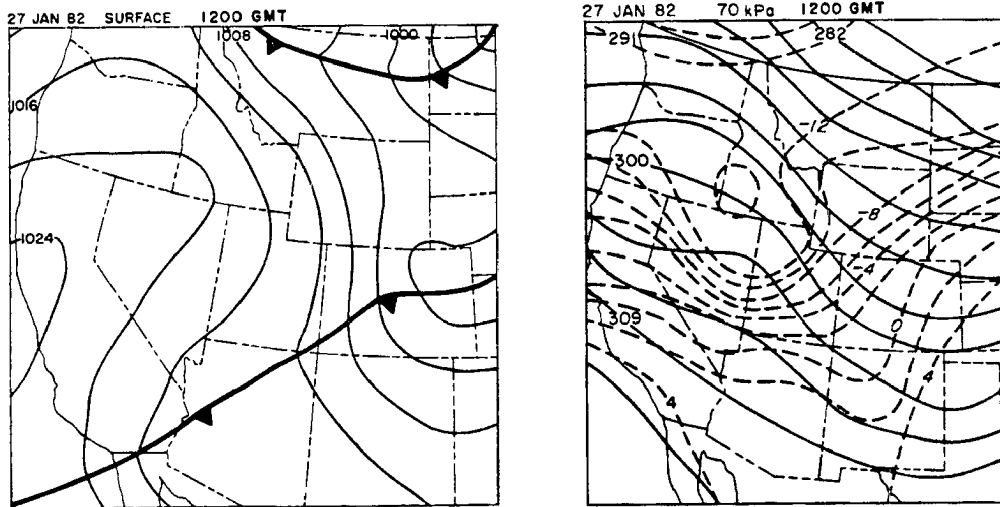


Fig. 32. Synoptic scale weather features for the 27 January 1982 storm system.

AT 1000 on 27 Jan 82, a strong cold front moved through the study area in northwest Colorado. From the time of surface frontal passage until 1530, precipitation fell continuously throughout the Park Range region. This precipitation was associated with an area of cloudiness which extended approximately 300 km northwest of the surface front. At 1530, the western edge of this cloud mass passed over the region and the clouds over the valleys rapidly dissipated. After 1530, strong mid-level winds maintained cap clouds over the higher elevations. The cap clouds persisted until well after 1900 and frequently contained shallow convective elements. The extent of the cap cloud cover decreased during the afternoon and skies were clear by 2100.

Storm evolution and supercooled water distribution

The 27 Jan 82 storm system moved rapidly through the Park Range area, producing about 7 hr of snowfall. Radiometric scans were performed during the latter dissipating stages of this system. During this period, a shallow cap cloud was present over the Park Range. The edge of this cloud extended west of RAD, but the cloud produced no precipitation at RAD or at other valley observation sites. The cap cloud contained embedded shallow convective elements which were primarily along the ridge line.

Figure 33 shows the vertical profile of equivalent potential temperature from a sounding taken at CG at 1600. Two potentially unstable layers were present on the sounding, the lowest between the surface and 2124 m and a second layer between 3208 and 3891 m. The weak convective instability observed within the cap cloud resulted from instability release in the mid-level potentially unstable layer. More important to the production of liquid water in this cloud was the strong

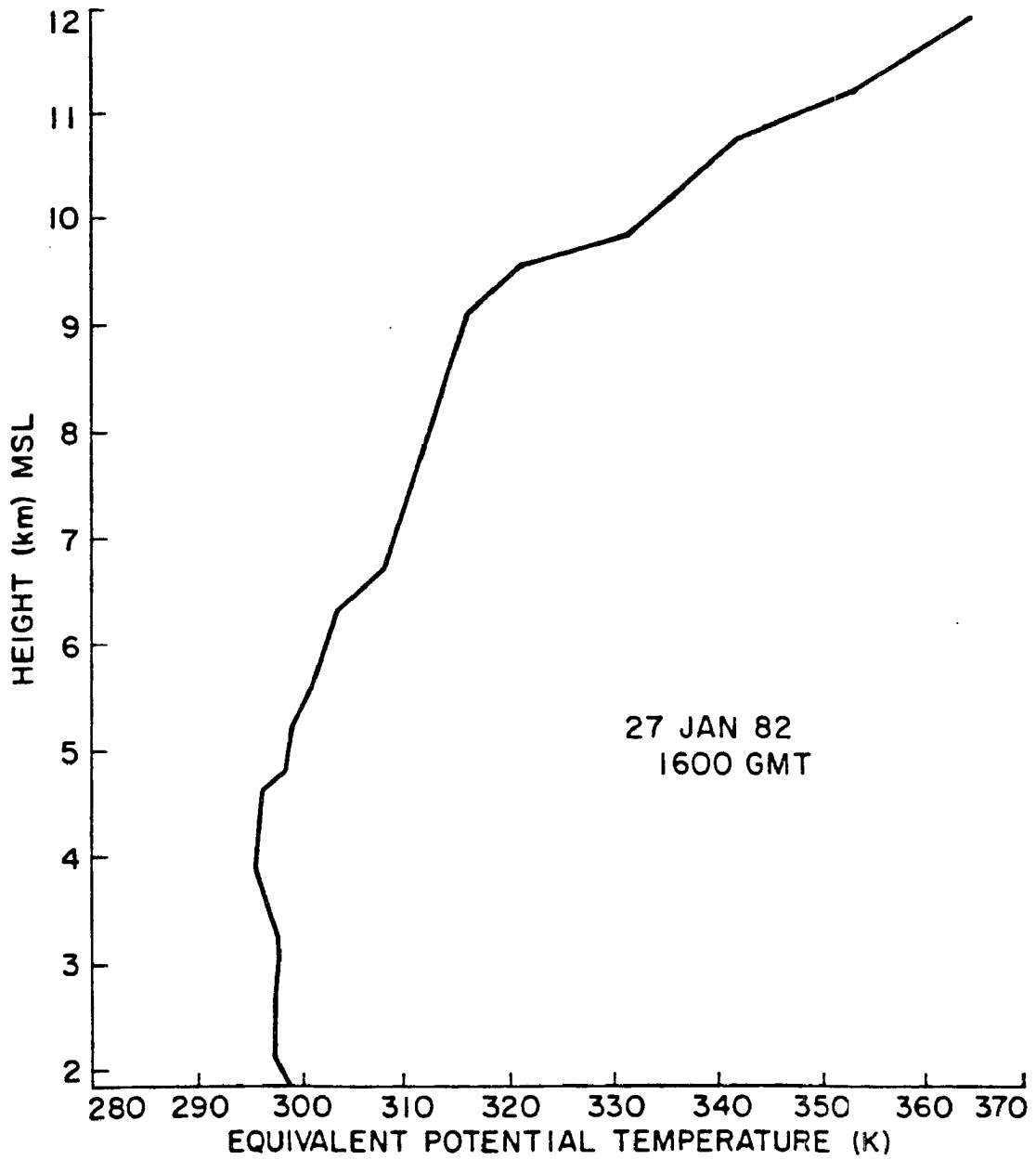


Fig. 33. Vertical profile of Equivalent Potential Temperature at 1600 GMT on 27 January 1982.

orographic forcing of the airflow due to exceptionally strong mid-level winds. The 70 kPa wind speed normal to the barrier from the 1600 CG sounding was 21.7 m/s. Between 1600 and 1900, the 70 kPa normal wind speed reduced substantially to 8.5 m/s. During this period, the extent of the cap cloud over the Park Range decreased. Precipitation at SPL was light in intensity between 1500 and 1800, gradually decreasing as the mid-level wind speed declined.

The time evolution of the supercooled water field is shown in Fig. 34 along with associated parameters. Except for a brief time during the initial part of the scan period, no precipitation occurred at RAD. From the radiometric scans, it is evident that virtually all the liquid water in this cloud system was concentrated over the windward slopes of the barrier. The liquid water content slowly decreased with time, indicating that the production of liquid water was primarily due to the orographic component of the vertical motion. Some contribution to the liquid water field was probably associated with enhanced liquid water production in individual convective elements, but the strong association between the strength of the mid-level winds and the quantity of supercooled water present in the system indicates that the convective component of the liquid water production in the cloud was a secondary effect.

The presence of liquid water in the zone over the windward slopes was confirmed both by observations of crystals at SPL and by the Rotorod measurements. During the observation period, the cloud enveloping Storm Peak had liquid water contents near the surface ranging from 0.25 to 0.32 gm^{-3} . Although only light precipitation fell at SPL, all of the precipitating crystals were rimed. During the first hour of radiometric

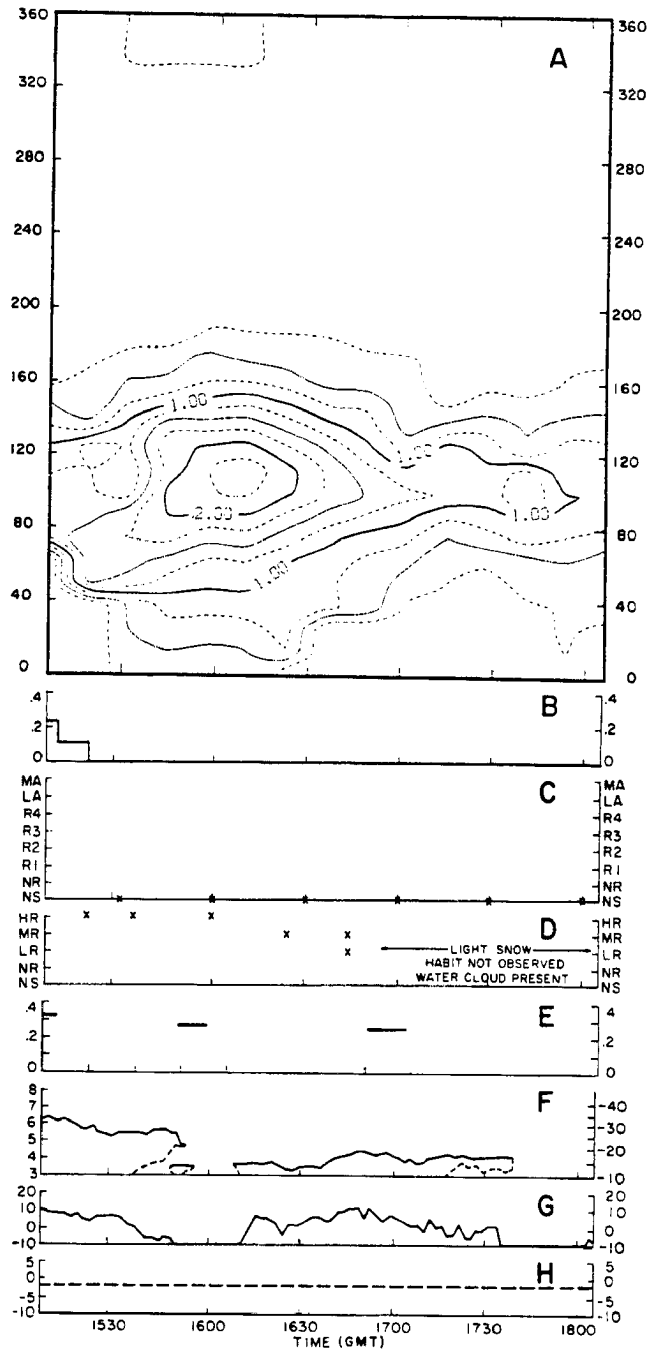


Fig. 34. 27 January 1982 (1500-1805 GMT): (A) Radiometric integrated liquid water content (mm) as a function of azimuth angle from the radiometer; (B) Precipitation intensity at RAD (mm/hr); (C) Rime characteristics of crystals collected at RAD (see Sec. 2C); (D) Rime Characteristics of crystals collected at SPL (see Sec. 2D); (E) Rotorod liquid water content at SPL (gm^{-3}); (F) Radar determined cloud top height (km) and cloud top temperature ($^{\circ}\text{C}$); (G) Radar observed maximum reflectivity (dBZ); (H) Surface temperature at RAD ($^{\circ}\text{C}$).

scans, crystals were heavily rimed. The amount of rime reduced with time as the cloud system slowly dissipated, but the laboratory remained in a liquid cloud throughout the period.

(3) Orographic systems

a. Case study: 14 December 81

Synoptic scale and local weather conditions

The evolution of the large scale weather pattern over the western United States on 14 and 15 Dec 81 at the surface and at 70 kPa is shown on Fig. 35. Radiometric scans were performed during the period 1800-2100.

At 1200, a low pressure center was located in central Montana with a front extending southeast through Salt Lake City, Utah, across Nevada and into central California. This front separated a warm, moist Pacific airmass to the west from colder continental air to the east and south. Well ahead of the front at mid-levels, in a basically anticyclonic upper level flow pattern, an area of moist air and clouds approached the study area. At the same time, a lee side trough was present east of the Continental Divide. During the 12 hr period between 1200 and 0000, the lee side trough deepened significantly in response to the southeasterly movement of the surface low from Montana to western Nebraska, causing an intensification of the pressure gradient across the mountains and an enhancement of the mid-level cross-barrier wind velocity. The storm on 14 Dec 81 developed in response to an intensification of the cross-barrier pressure gradient and a simultaneous influx of mid-level moisture from the west. The presence of a foehn wall visible from the lee side of the Park Range and the shallow nature of the cloud system indicated that the storm during the study period was primarily

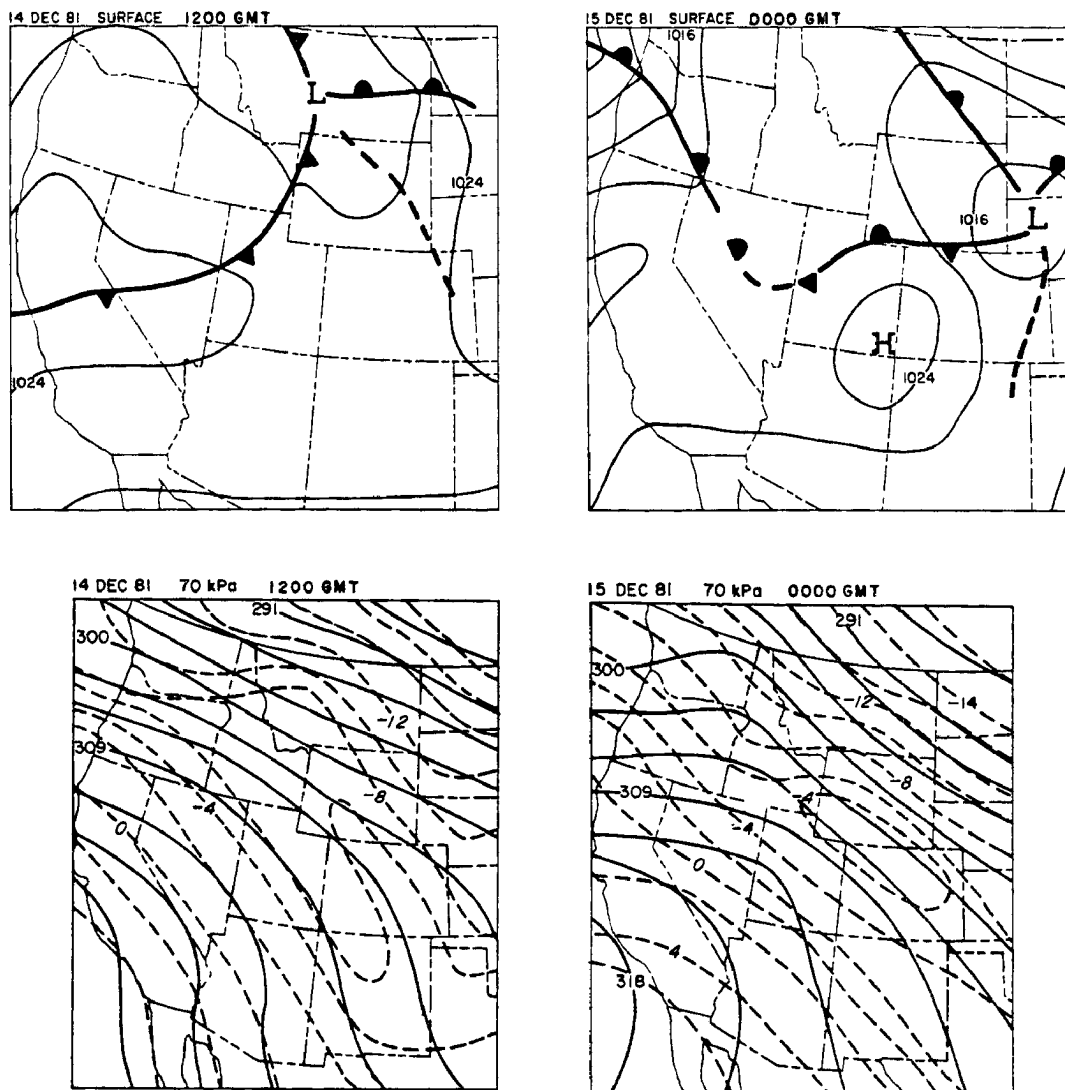


Fig. 35. Synoptic scale weather features for the 14 December 1981 storm system.

orographically forced. Warm air advection occurred during the study period.

Storm evolution and supercooled water distribution

The cloud system occurring on 14 Dec 81 was shallow, with tops around 4000 m (-15°C). Despite these warm temperatures, considerable precipitation fell from the cloud system, predominantly as aggregated crystals. The storm was stably stratified during the observation period. Figure 36, the vertical profile of equivalent potential temperature from an 1800 sounding at CG, indicated that one potentially unstable layer existed between 4097 and 4766 m. For the greater part of this storm, this layer was located above cloud top and did not contribute to cloud destabilization. The intensity of the mid-level winds increased during the period when radiometric scans were conducted. Winds at the 70 kPa level normal to the barrier measured at CG increased from 7.2 m/s at 1800 to 15.7 m/s at 2100. This increase was partly responsible for changes observed in the cloud liquid water distribution.

The time evolution of the supercooled liquid water distribution is shown in Fig. 37, along with associated measurements from SPL and RAD. Between 1800 and 2000, liquid water was present throughout the cloud system, but was concentrated over the mountain crest, particularly to the southeast. Precipitation, primarily aggregates, fell at moderate intensity at RAD. During this time, single crystals collected at RAD had no observable rime accumulation, but some of the crystals clustered in aggregates were lightly rimed. At SPL, the mountain crest was enveloped in cloud with liquid water contents ranging from 0.16 to 0.24 gm^{-3} . Aggregated snowfall was also predominant at this location, but

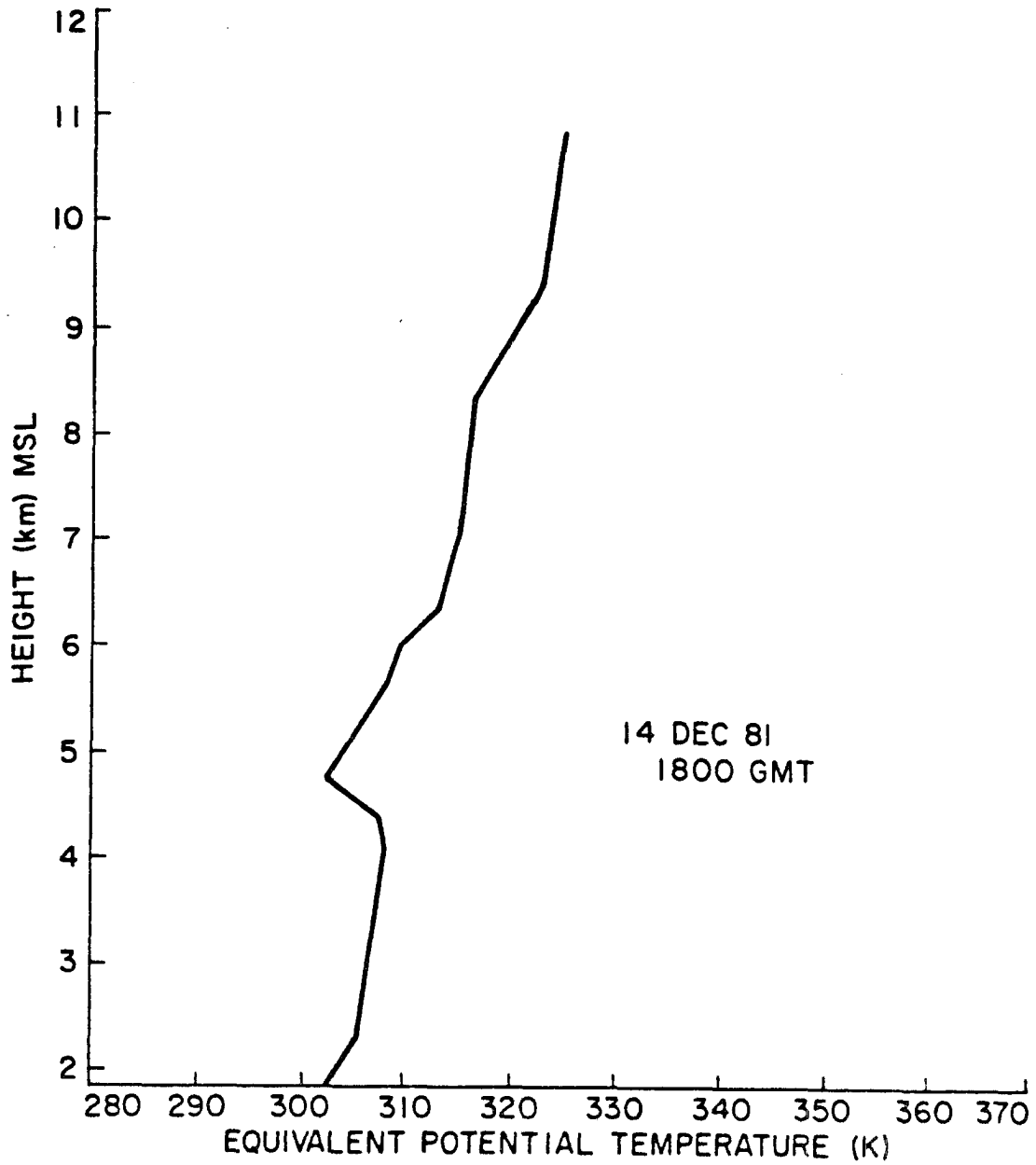


Fig. 36. Vertical profile of Equivalent Potential Temperature at 1800 GMT on 14 December 1981.

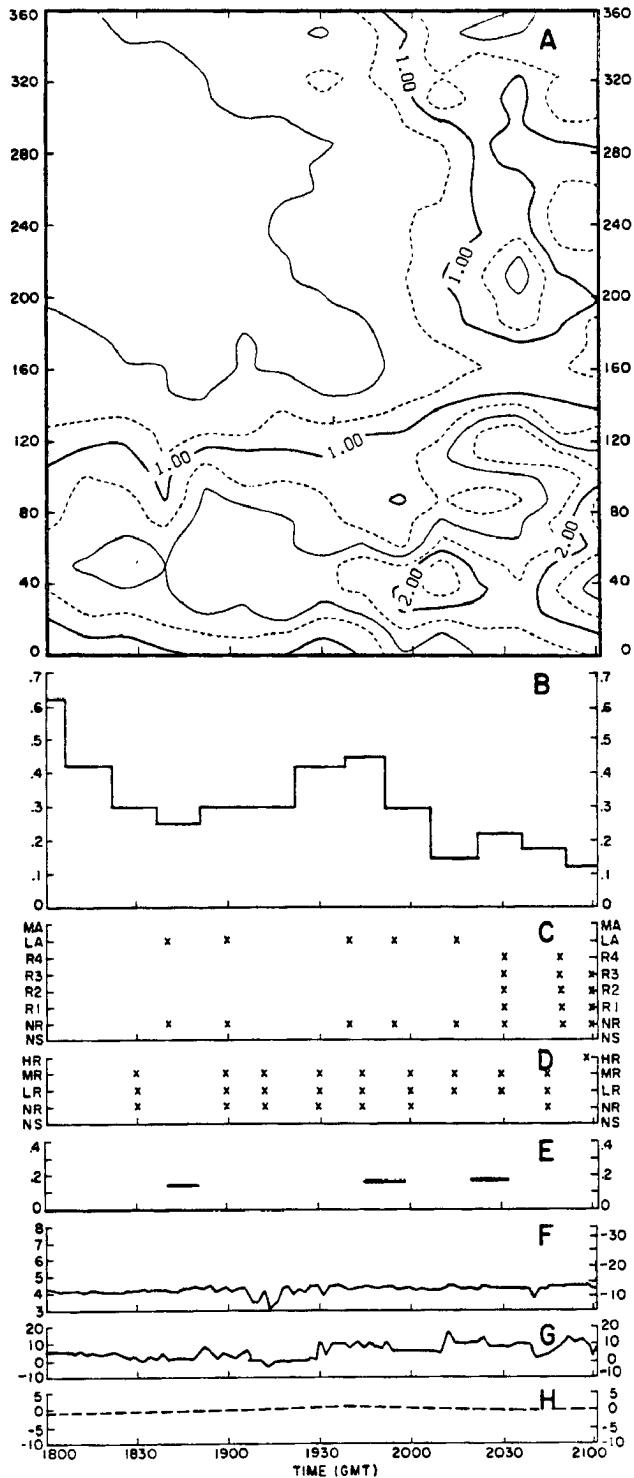


Fig. 37. 14 December 1981 (1800-2100 GMT): (A) Radiometric integrated liquid water content (mm) as a function of azimuth angle from the radiometer; (B) Precipitation intensity at RAD (mm/hr); (C) Rime characteristics of crystals collected at RAD (see Sec. 2C); (D) Rime Characteristics of crystals collected at SPL (see Sec. 2D); (E) Rotorod liquid water content at SPL (gm^{-3}); (F) Radar determined cloud top height (km) and cloud top temperature ($^{\circ}\text{C}$); (G) Radar observed maximum reflectivity (dBZ); (H) Surface temperature at RAD ($^{\circ}\text{C}$).

approximately half of both the single and aggregated crystals observed at this site were lightly to moderately rimed.

A change in the character of the precipitation at RAD occurred at 2030. Just before this time, liquid water contents increased significantly upstream of RAD. This increase in liquid water was accompanied by a decrease in snowfall intensity. By 2030, the predominant precipitation growth mechanism for crystals arriving at RAD had changed from aggregation to accretion, although many of the crystals were only lightly rimed. Liquid water contents also increased in the vicinity of the barrier during this period. Crystals continued to be lightly to moderately rimed and mostly aggregated at SPL until 2100. At 2100, as liquid water contents continued to increase, a reduction in aggregation occurred and all crystals became heavily rimed. No significant change in the character of cloud top occurred during this period. The observed increase in mid-level wind speed during this time may have accounted for the increased liquid water content throughout the cloud. By changing the total growth time available for cloud particles, the increase in wind speed may also have at least partially affected the microphysical growth mechanisms in the cloud; this may partially account for the observed changes in the intensity and character of the precipitation.

b. Case study: 16 December 1981

Synoptic scale and local weather conditions

Major synoptic scale weather features at the surface and at 70 kPa for 16 and 17 Dec 81 are shown in Fig. 38. The radiometer operated in the scan mode from 1200 to 1500 during this storm. At 0600 on 16 Dec 81, a strong low pressure system was centered over the plains of

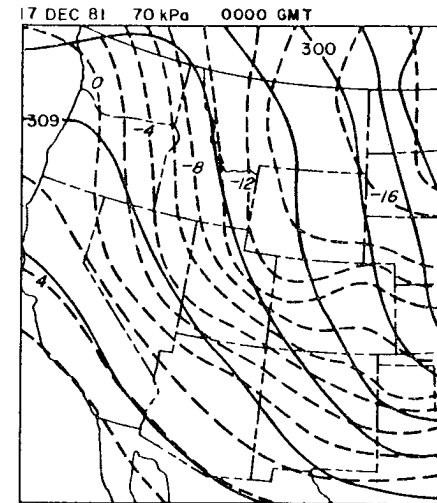
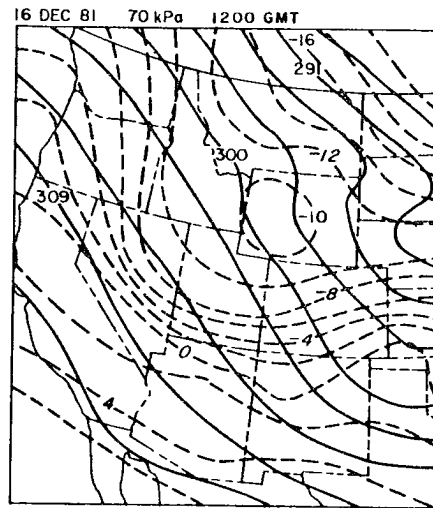
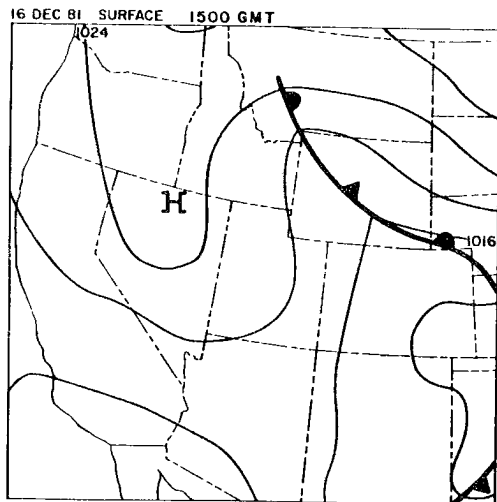


Fig. 38. Synoptic scale weather features for the 16 December 1981 storm system.

northeast Colorado. Extending north and west from this system, a wide area of cloud cover associated with a large occlusion produced widespread precipitation through Wyoming and Montana. As this low pressure system moved southeast during the day, the southern boundary of the moisture associated with the occlusion progressed southward into the Park Range area. Prior to this moisture intrusion, strong mid-level northwesterly winds produced a small orographic cloud system over the Park Range. At 1300, the southern end of the moist occluded airmass entered the area. Until 1400, precipitation from the system fell only on the mountain. From 1400 through 0000 on 17 Dec 81, light to moderate snowfall occurred throughout the Park Range region. The orographic storm system prior to 1400 was forced largely by the strong pressure gradient present across the mountains. After 1400, precipitation processes were significantly enhanced by the advection of deeper clouds and moisture associated with the occluded region into the area. During the study period, winds progressively weakened.

Storm evolution and supercooled water distribution

Before the onset of the deeper clouds associated with the occlusion, the cloud system present over the Park Range region was orographic in nature. Cloud tops during this period were approximately 3800 m (-14°C), and precipitation fell only at higher elevations. After the occluded airmass entered the area, cloud tops increased to 5400 m (-23°C). Within the hour, light precipitation began to fall throughout the valley.

Unfortunately, local soundings were not available during the observation period to assess the potential for instability in these clouds. Qualitative evidence from the vertically pointing radar

indicated that at least the early portion of this storm was stably stratified.

The time evolution of the supercooled water distribution is shown in Fig. 39. Except for one observation near the end of the storm period at SPL, no microphysical observations were available at the SPL or RAD sites. Radar characteristics and RAD surface temperature are included in the figure. During the orographic portion of the storm, liquid water was distributed throughout the cloud, but strongly concentrated over the slopes of the barrier. As the cloud from the occluded region advected into the area, liquid water concentrations throughout the cloud system dropped substantially. This was first evident upstream of RAD and later over the mountain. The reduction in liquid water content throughout the cloud system was most likely associated with more efficient ice crystal production in the cloud system due to nucleation at colder cloud temperatures and subsequent removal of the crystals by diffusional growth and accretion processes. Unfortunately, observations of crystal rime characteristics were not available for this storm.

c. Case study: 13 January 1982

Synoptic scale and local weather conditions

The mechanism of formation of the 13 Jan 82 cloud system was typical of many purely orographic cloud systems occurring over the northern Colorado Rockies. This type of cloud system often occurs when a strong high pressure system develops over the Great Basin, a trough of low pressure is present over the western Great Plains, and the lower atmosphere north and west of the Colorado Rockies is near saturation. The combination of the strong cross-barrier pressure gradient and sufficient low level moisture lead to a quasi-steady state cloud system

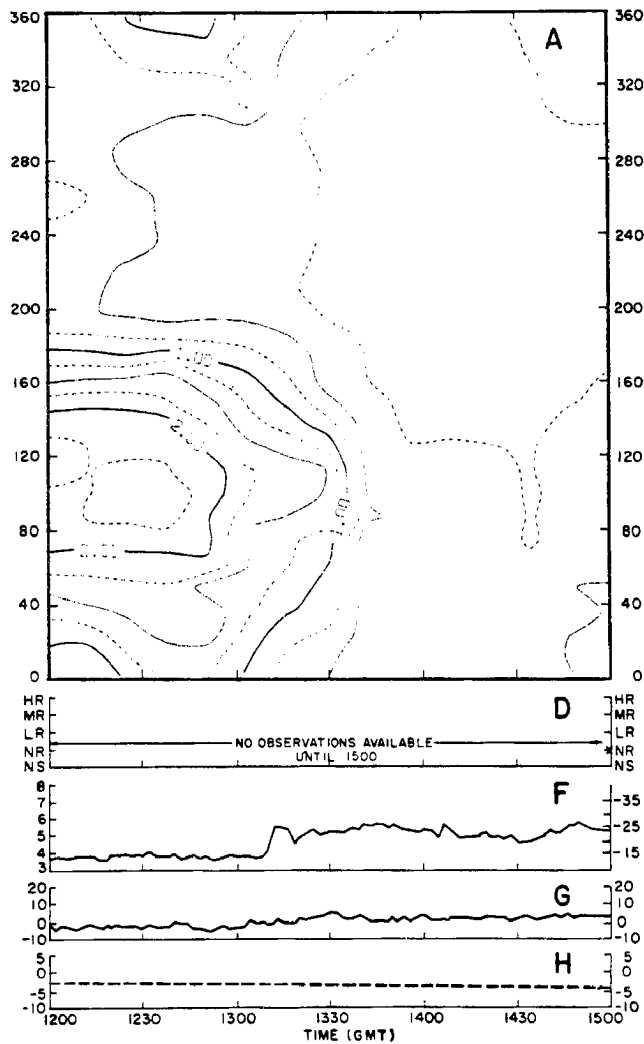


Fig. 39. 16 December 1981 (1200-1500 GMT): (A) Radiometric integrated liquid water content (mm) as a function of azimuth angle from the radio-meter (D) Rime Characteristics of crystals collected at SPL (see Sec.2D); (F) Radar determined cloud top height (km) and cloud top temperature ($^{\circ}\text{C}$); (G) Radar observed maximum reflectivity (dBZ); (H) Surface temperature at RAD ($^{\circ}\text{C}$).

that exists for many hours. Despite the generally low precipitation rates associated with this type of cloud system, the system often produces a substantial amount of precipitation because of its duration.

On 13 Jan 82, a rapidly moving trough system had passed through Colorado and had propagated eastward into Texas. To the west of the trough, shown on Fig. 40, a strong high pressure system and associated upper level ridge continued to build over the western United States. Along the east side of this ridge system, west of the Continental Divide, a shallow mid-level layer of moisture produced shallow orographic cloud systems over the mountains of Utah and northern Colorado. During the period from 1200 to 0000, the ridge system continued to build eastward with warm advection occurring throughout the depth of the troposphere. Moist air continued to advect into the Park Range region from the northwest. During the entire period, a widespread shallow cloud system was present over the western slopes of the mountains. Radar cloud tops seldom exceeded 1 km above ridgetop level, although light to moderate snow fell continuously at both mountain and valley sites throughout the day.

Figure 41 shows a sounding taken at 2100. The atmosphere was stable during the period. The upper cloud region was marked by a near isothermal 5 kPa deep layer. Two moist layers were identified in the rawinsonde data. Cloud top of the upper layer was -21.3°C , very close to that measured with radar and satellite. Despite the shallow nature of this cloud system, it produced precipitation at RAD at rates varying from 0.1 to 0.8 mm/h.

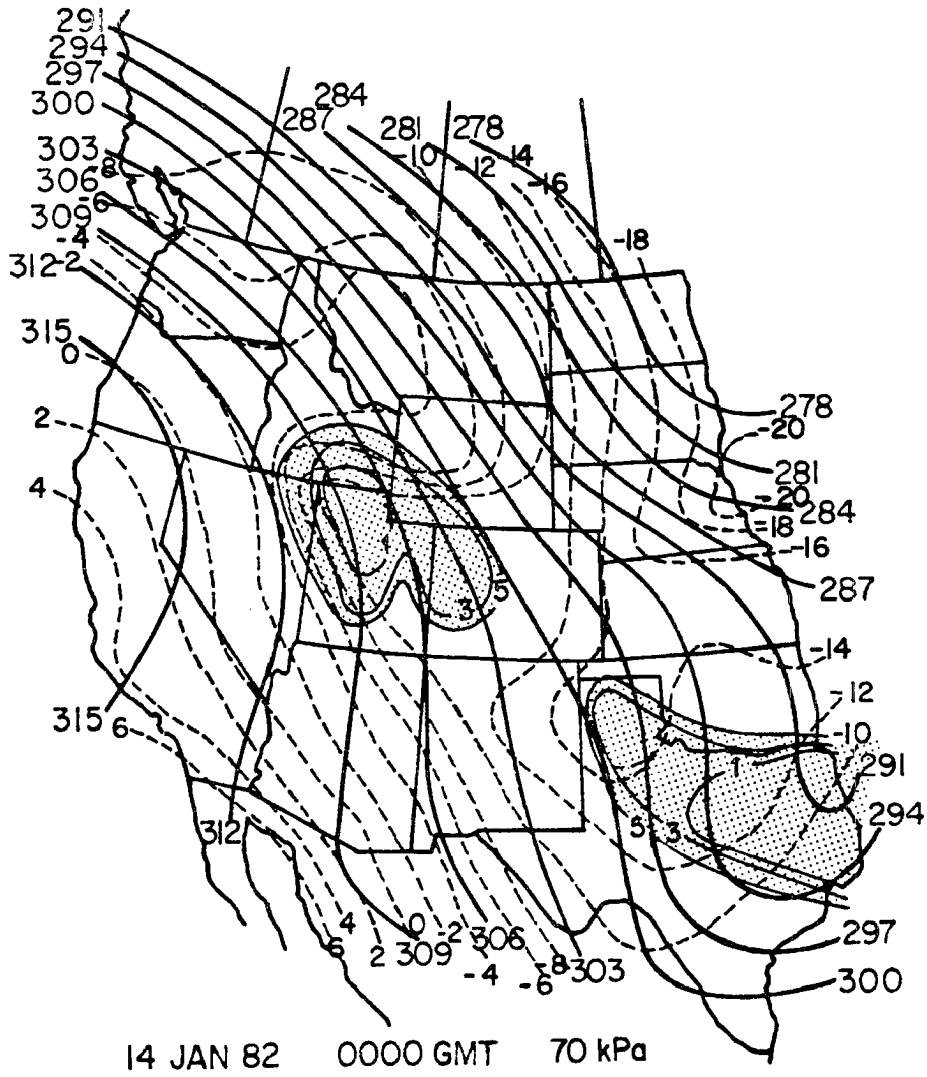


Fig. 40. 70 kPa chart for 14 Jan 82 at 0000 GMT.

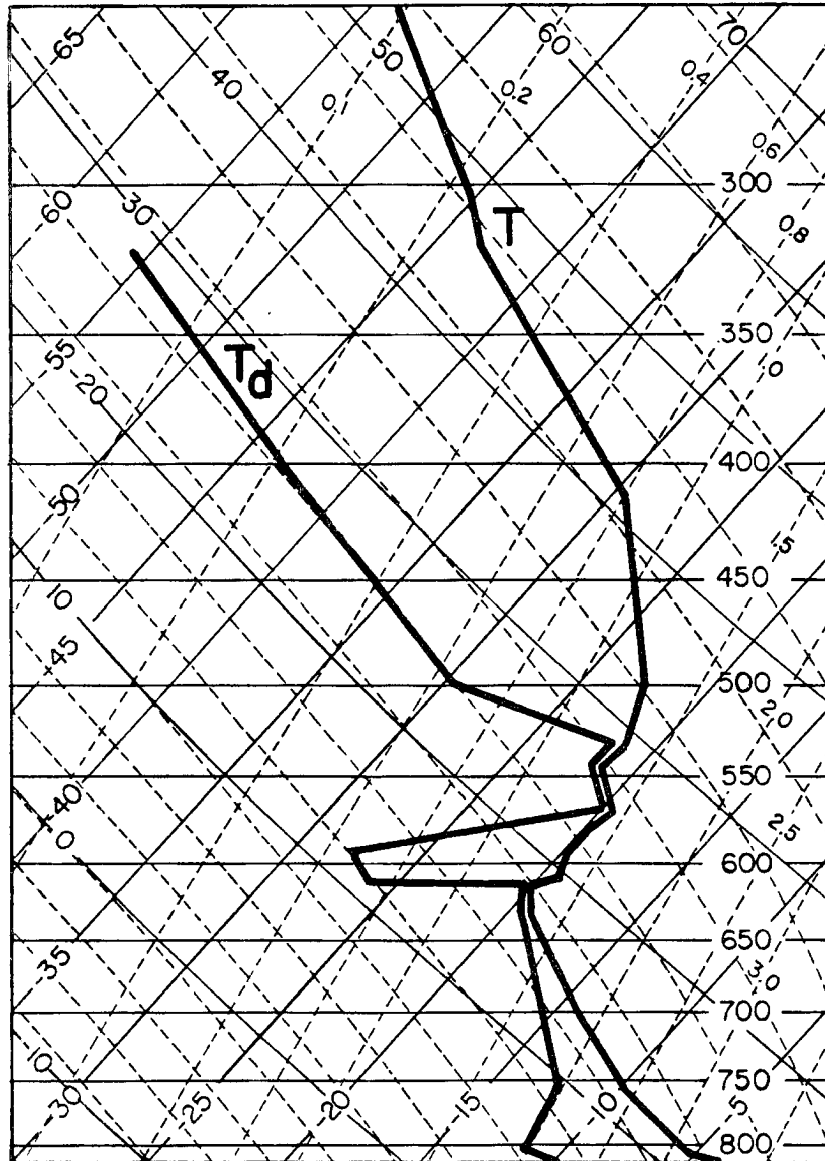


Fig. 41. 2100 GMT sounding for 13 January 82.

Storm evolution and supercooled water distribution

The time evolution of the supercooled liquid water distribution during a three hour period from 2030 to 2330 is shown in Fig. 42. Associated parameters from RAD are also shown. SPL operated on a limited basis during this storm. Only one observation of crystal rime characteristics was available during the scan period. Precipitation rates during the storm varied slowly. Corresponding variations were observed in the liquid water distribution; liquid water contents increased in the cloud from 0.25 mm to 1.25 mm as the precipitation rate decreased from 0.8 to 0.1 mm/h. Precipitation particles were generally dendritic and lightly aggregated. At the beginning of the radiometric scans, nearly all the precipitation was unrimed, although a few R3 crystals were occasionally observed. Extremely light rime was also occasionally observed on crystals collected in aggregates. As precipitation rates decreased and the cloud water content increased, the frequency of rime on the aggregates increased. Many R3 crystals were also observed at RAD after this time. The maximum liquid water contents occurred at 2235, the time of the lowest precipitation rates. From this time onward, precipitation rates started to increase and liquid water contents throughout the cloud system began to decrease slowly. Throughout most of the period, water contents were slightly larger over the slopes of the ridge.

The single observation at SPL at 2240 occurred at the time of the maximum liquid water contents. The observation was taken at a temperature of -10°C . Precipitation at this location was moderate to heavy and consisted of aggregates of unrimed planar crystals. This limited observation, together with the observations of rime at RAD,

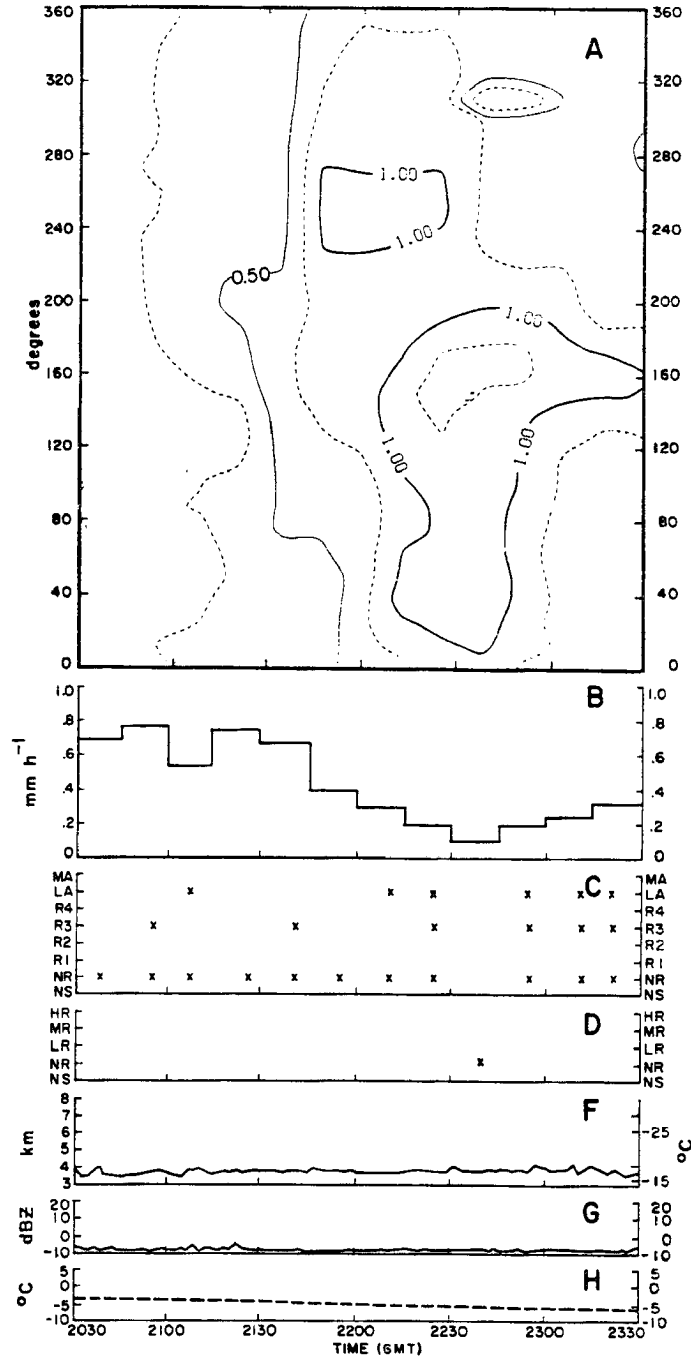


Fig. 42. 13 January 1982 (2030-2330 GMT): (A) Radiometric integrated liquid water content (mm) as a function of azimuth angle from the radiometer; (B) Precipitation intensity at RAD (mm/hr); (C) Rime characteristics of crystals collected at RAD (see Sec. 2C); (D) Rime Characteristics of crystals collected at SPL (see Sec. 2D); (F) Radar determined cloud top height (km) and cloud top temperature (°C); (G) Radar observed maximum reflectivity (dBZ); (H) Surface temperature at RAD (°C).

suggests that the liquid water detected by the radiometer was located in the low levels of the cloud system between cloud base and ridgetop.

The primary characteristic of the liquid water evolution on 13 Jan 82 was the inverse relationship between precipitation rate and cloud water content. No significant change in cloud top temperature occurred. Changes in the cross-barrier wind speed were uncertain because only one sounding was available. The 70 kPa cross-barrier wind speed at that time was 9.7 m/s.

The processes in the cloud system which resulted in the observable changes in liquid water content and precipitation rate are uncertain. One possible mechanism which would result in such observed behavior is a decrease in either ice crystal concentrations or growth rates within the cloud. Such changes could be related to variations in the moisture supply, ice nuclei concentrations or several other factors.

B. Discussion

(1) Pre-frontal and frontal cloud systems

Pre-frontal cloud systems in the northern Colorado Rockies are generally characterized by wide area stratiform cloud regions formed primarily by lifting associated with the Rocky Mountain massif. Regions of deeper clouds and heavier precipitation are frequently superimposed on this stratiform cloud system. Many of these regions are observed to be convective, but some occur in a stably stratified or neutral atmosphere.

The mesoscale characteristics of the stratiform component of the pre-frontal cloud system are strongly controlled by the depth of the moisture in the pre-frontal environment and the strength of the component of the wind normal to the barrier. In the northern Colorado

Rocky Mountain region, these parameters are closely associated. Because the mountains in this region are oriented north-south, winds with a strong southerly component undergo weak orographic forcing. In addition, the source of air is much more continental, generally originating over the southwest desert regions and often crossing several mountain ranges before arriving in the area. Pre-frontal mid-level winds with a strong westerly component undergo stronger orographic forcing and generally have higher moisture content. The predominant direction of the flow is closely associated with the orientation of the approaching front. The southwesterly flow situation applies to the case of 22 Jan 82. The 15 Dec 81 case is an example of more predominant westerly flow. The pre-frontal environment of the 30 Dec 81 case was more similar to 22 Jan 82, but not as extreme. The stratiform clouds in the pre-frontal environment for the three cases discussed had tops around 4000-5000 m and weak reflectivities. With the exception of the 22 Jan 82 case, which had a strong southerly mid-level wind component prior to the passage of the convective band, precipitation rates were low in the valley and moderate at high elevations. On 22 Jan 82, the cloud was non-precipitating prior to band passage.

The convective regions of the pre-frontal environment are sometimes organized into a banded structure. The duration of these convective bands is generally about an hour. Two or three of these convective regions are frequently observed prior to frontal passage. In one case, 30 Dec 81, the convective activity was less organized. The convective components of the pre-frontal cloud systems have higher precipitation rates at all elevations and stronger radar reflectivities.

The distribution of supercooled water in the stratiform regions of cloud systems in the pre-frontal environment is closely related to the strength of the orographic component of the airflow. In the case of 22 Jan 82, where this component was extremely weak, the shallow stratiform cloud system contained virtually no supercooled water. In the more developed cases of 15 Dec 81 and 30 Dec 81, supercooled water was present throughout the cloud system. Highest values were located over the windward slopes of the range in the zone of strong orographically forced vertical motions.

The concentration of liquid water in convective regions in the pre-frontal environment was observed to be much lower than in the stratiform cloud regions. Maximum liquid water contents in the convective regions were observed during the initial stages of development, but the concentration of liquid water was rapidly depleted by extremely efficient precipitation growth processes. In general, within 15-20 minutes after the onset of the convection, liquid water concentrations reached a minimum. Evidence from rime observations at SPL and RAD indicated that any supercooled water present in these cloud systems after the initial period was confined to the lower cloud levels.

The microphysical characteristics of precipitation observed at SPL and RAD during stratiform and convective storm periods provided important information concerning the evolution of the precipitation process during these events. During stratiform periods, cloud particles arriving at RAD were often lightly rimed. At SPL, the concentration of rime on the particles was considerably greater. Precipitation rates were generally low at RAD and moderate at SPL. With the onset of convective activity, the amount of rime observed on crystals sometimes

increased initially, but rapidly reduced in intensity and often was completely eliminated. Precipitation observed during convective periods was heavy at both sites and consisted initially of rimed and aggregated particles followed by a decrease in rime.

These observations imply that mid-level stratiform cloud systems have ice crystal concentrations that are low enough that the condensate supply rate in the cloud frequently exceeds the bulk diffusional growth rate of the ice phase, particularly in the vicinity of the barrier. In general, the production and growth of water droplets in this environment is sufficient that accretion processes become important. In the case of mountaintop precipitation, accretion often becomes the dominant growth process. Significant amounts of liquid water are frequently present at the barrier crest.

With the onset of convection, liquid water production is initially enhanced, particularly in the vicinity of the barrier, but rapid production of ice crystals in the cloud system leads to effective removal of the water initially by accretion and later by diffusional growth processes. Indications that cloud ice crystal concentrations are generally large are the high precipitation rates associated with these bands and the tendency for aggregation of the falling crystals. After convective periods, the liquid water distribution was generally observed to return to a configuration similar to that in the stratiform cloud system prior to band passage.

(2) Post-frontal cloud systems

Post-frontal cloud systems are also characterized by wide area stratiform cloud regions. These stratiform systems generally have a much stronger orographic wind component because of considerably greater

mid-level wind speeds normal to the barrier. Two regions of convective instability were observed in these systems, the first occurring just after frontal passage and the second during trough passage as the storm is decaying. The first region of convection associated with frontal passage was discussed in the 30 Dec 81 case. The discussions concerning convection in the previous section all apply to this region. The second convective period occurred late in the storm. Convective cells during this period were disorganized, shallow, and occurred primarily over higher topography.

In general, the stratiform component of the post-frontal cloud system produced significant amounts of precipitation at high elevations. Three factors contributed to this large amount of precipitation: (1) winds in the post-frontal airmass had a strong orographic component forcing additional condensate production in the vicinity of the mountain; (2) the post-frontal airmass typically has its origins over the northeast Pacific Ocean and often contains considerable middle and low level moisture; (3) probably most important, these cloud systems often exist for long durations. The horizontal extent of the cloud varies with the moisture supply, generally decreasing with time, but a cap cloud extending 15-20 km upstream can often survive for 24-36 hr. This cloud makes little contribution to the total snowfall at low elevations, but can contribute substantially to the snowfall at higher elevations.

The distribution of the supercooled liquid water in the stratiform regions of the post-frontal cloud system is generally well defined and strongly associated with the orographic component of the vertical air motion. High liquid water concentrations were found to develop about

10-15 km upwind of the barrier crest and reach a maximum over the windward slopes. This is expected since condensate supply rates are generally highest in this region. The presence of this zone of high liquid water content was most evident on 27 Jan 82, but also evident on the other post-frontal cases. In these cases, lesser amounts of liquid water were also present upstream.

The initial convective bands associated with frontal passage generally move through the region within an hour or two. These bands produce moderate to heavy precipitation at both valley and mountain sites. Radar evidence from the 30 Dec 81 case indicates that these bands may be less organized, possessing more cellular structure. Precipitation intensity and cloud depth during these periods are similar to the pre-frontal bands described in the previous section. The late post-frontal period is characterized by weak cells extending to about 6000 m. These cells usually occur in the latest part of the storm. Because of their limited duration and spatial extent, they probably make a minor contribution to the total snowpack.

The concentration of the cloud water in the convective bands in the post-frontal regions is complicated somewhat by the interaction of the convective and orographic components of the airflow. The convective activity generally consisted of deep clouds capable of producing effective numbers of ice crystals to accrete any water droplets generated by the convective vertical motions. However, steady orographic production of additional cloud water in the low levels of the cloud may have occurred on some occasions. This may be the explanation for the observed rime collected on aggregates observed at RAD on 30 Dec 81. In

general, however, total cloud water concentrations decreased substantially during periods of organized convection.

The distribution of supercooled water in the late post-frontal convective cells is difficult to ascertain because these cells generally develop over the ridges in regions of strong orographic lift. With radiometric data, it is difficult to separate the contribution of the convective and the orographic components of the motion. In general, the steady nature of the cloud liquid water field in the vicinity of the barrier during these periods indicates that the predominant mechanism producing the liquid water in these clouds is vertical motion due to orographic lifting.

The microphysical characteristics of the precipitation observed at SPL and RAD were consistent with the liquid water measurements. During stratiform events, generally light rime, no rime or no precipitation was observed at RAD, while nearly all precipitation observed at SPL was moderately to heavily rimed. During organized convective activity, high precipitation rates and some aggregation occurred. Some rime was observed at RAD during band passage.

(3) Orographic cloud systems

Orographic systems, as discussed in this paper, are cloud systems that occur over mountainous regions during periods when no major synoptic scale disturbance is directly influencing the region. These cloud systems typically form when a strong cross-barrier pressure gradient is present and sufficiently moist air is simultaneously advected into the region from the west. The clouds are generally shallow, stable, and persist for many hours. Despite their shallow nature, they can produce significant amounts of precipitation at both

low and high elevations because of continuous production of cloud condensate for a long period of time.

The distribution of liquid water in these cloud systems was found to vary considerably from storm to storm. The highest liquid water contents were generally found over the slopes of the barrier. However, liquid water was observed to increase uniformly throughout the cloud system on 13 Jan 82 and 14 Dec 81 without any significant changes in the mesoscale characteristics of the storm systems, except for a reduction in precipitation rate.

These observations indicate that variations in ice crystal concentrations in these clouds strongly affect the liquid water production in the clouds. The causes of these variations are poorly understood. Recent evidence presented by DeMott et al. (1985) indicates that enhanced nucleation of ice particles occurs in localized zones of high supersaturations associated with vertical motions near cloud top. Variations in crystal production may in fact be associated with small scale changes in the characteristics of cloud top. Processes associated with these changes will be discussed in the following chapter.

2. Physical and microphysical structure of the supercooled water field

Five N83TW and three N306D flights occurred during the COSE programs for which FSSP and supporting data were available. The eight flights all occurred in cloud systems which were stable to neutrally stratified, or had only weak low level convective instability. Airborne data during periods of strong convective band passage were not obtained, primarily due to logistics problems associated with forecasting and aircraft base location. Two flights occurred in shallow cloud systems with tops slightly above the minimum allowable aircraft altitude. The

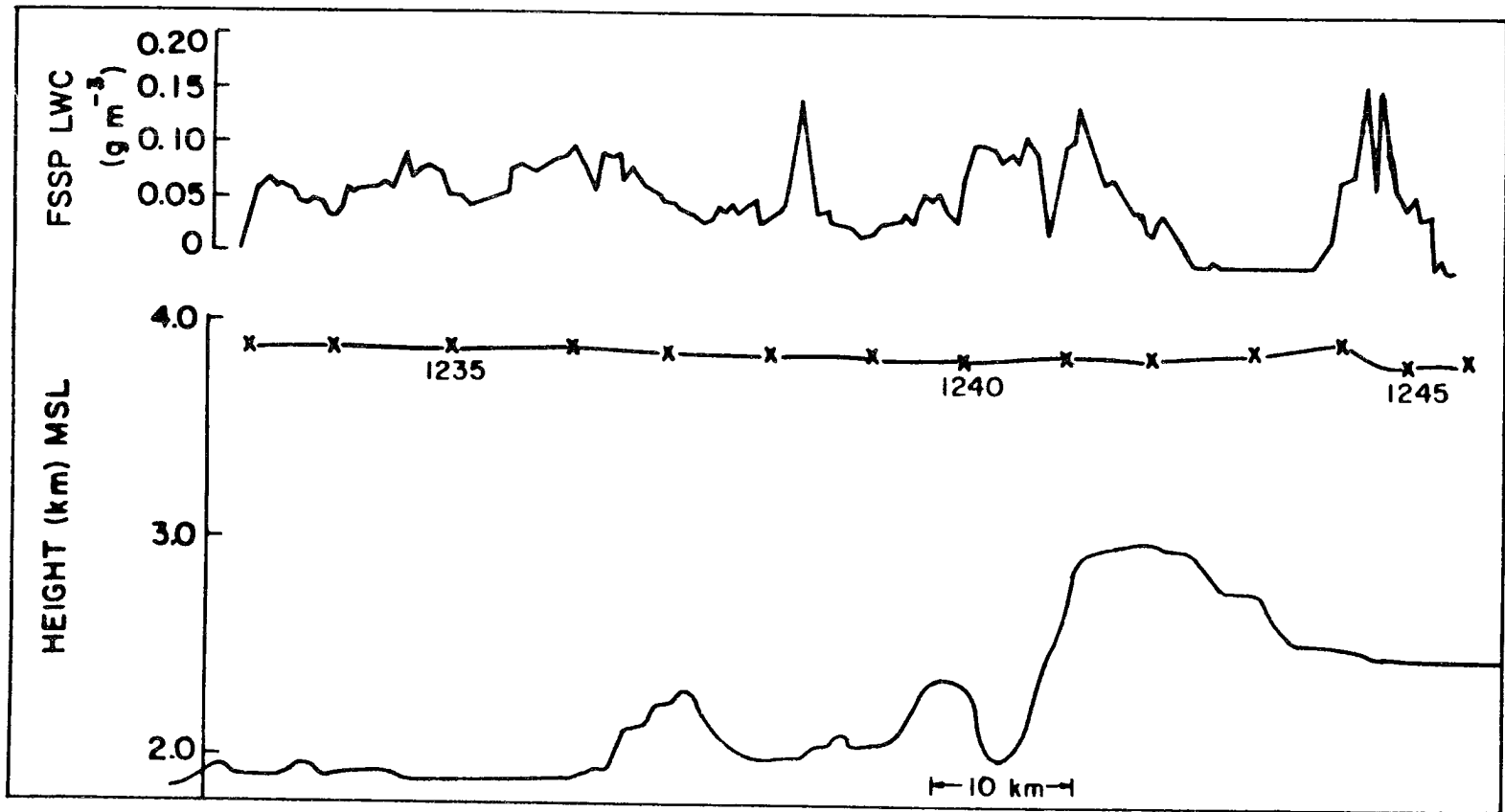
cloud top temperature (CTT) in these systems was between -15° and -20°C . Flight tracks in these systems consisted of the lowest horizontal leg in Fig. 5. Five flights occurred in deep cloud systems (CTT $< -25^{\circ}\text{C}$). One flight occurred during the transition from a shallow cloud to a deep cloud. All N306D flights were in deep cloud systems.

A. Liquid water distribution

Supercooled water can be produced locally in cloud systems in regions where the condensate supply rate exceeds the diffusional growth rate of ice crystals present in the cloud volume. In stratified cloud systems over the Northern Colorado River Basin, three regions of the cloud exist where this condition is frequently met. Two of these regions are directly observable with aircraft in the Park Range area. The third is below the minimum altitude for aircraft flight, but can be inferred from radiometric measurements, observations of crystal habit at the surface, and measurements of ice crystal growth rates reported in the literature. These three regions are discussed below.

(1) Cloud top

Three N83TW flights occurred when shallow cloud systems were present over the Park Range. These clouds extended at least 60 km upwind of the crest of the range, had cloud tops near the 60 kPa level (-15°C to -20°C) and produced precipitation at RAD and SPL. During these flights, supercooled liquid water was consistently observed near cloud top. Liquid water contents generally varied between 0.05 and 0.10 gm^{-3} but occasionally exceeded 0.30 gm^{-3} . An example of liquid water measurements near cloud top on 16 Jan 82 is shown in Fig. 43. Only one penetration of cloud top occurred in a deep cloud system. During this penetration, 0.09 gm^{-3} liquid water was observed at -31°C .



16 JAN 1981

Fig. 43. Flight cross-section and liquid water content (LWC) measured in a shallow storm system on 16 January 1982. The cloud top temperature was -18°C .

The presence of liquid water near cloud top results from an imbalance between the condensate supply rate and ice crystal mass growth rate which is unique to this region of the cloud. Observations of ice crystals near cloud top in the Park Range region have indicated that crystal sizes in this region seldom exceed 100 μm . This is not surprising; ice particles of larger size soon fall deeper into the cloud. Because of the minimal size of the crystals present in the cloud volume near the top of the cloud, the mass deposition rate on the crystals is relatively small.

The water balance near cloud top can be examined quantitatively by considering the instantaneous condensate supply rate as a function of pressure, temperature and vertical velocity and comparing it with the ice crystal mass growth rates for crystal populations of various mean size and concentration. Condensate supply rates were calculated using the pseudoadiabatic thermodynamic energy equation,

$$c_p d \ln T - R_d \ln P + d \left(r_{vs} \frac{L_v}{T} \right) = 0,$$

in the form,

$$\frac{d}{dt} \rho_v = \left(\left(\frac{c_p}{L_v} - \frac{r_{vs}}{T} \right) \Gamma_m - \frac{g}{L_v} \right) \rho_w.$$

Here c_p is the specific heat of dry air at constant pressure, R_d is the gas constant for dry air, L_v is the latent heat of vaporization, r_{vs} is the saturation mixing ratio, P is pressure, T is temperature, ρ_v is vapor density, Γ_m is the moist adiabatic lapse rate, ρ is air density, w is vertical velocity and g is gravity.

Ice crystal growth rates were calculated using the equation presented by Pruppacher and Klett (1978, p.448) with the ventilation factor equal to unity and the capacitance factor either that of a small

plate (for temperatures warmer than -22°C) or that for a columnar crystal.

Figure 44 summarizes the results of these calculations. Four diagrams are shown in the figure. Figure 44a represents conditions characteristic of an extremely warm cloud top in the Park Range region ($T = -10^{\circ}\text{C}$, $P = 65 \text{ kPa}$). Figure 44b shows conditions near cloud top for conditions characteristic of the cases presented in this paper ($T = -15^{\circ}\text{C}$, $P = 600 \text{ kPa}$). Figure 44c illustrates conditions characteristic of the warmest cloud top temperatures where columnar crystals are likely to be produced and Fig. 44d shows the conditions typical at the tops of deep, cold cloud systems over the Park Range. All four figures show instantaneous condensate production rates near cloud top as a function of cloud top temperature, pressure and vertical velocity. Also shown are mass growth rates for several uniform size distributions of ice particles as a function of crystal concentration. In these diagrams, production of the liquid phase will be maintained in regions where the condensate supply rate exceeds the diffusional growth rate of the ice crystals present in the volume.

Figure 44a shows that liquid water can be produced at -10°C by a 0.01 m s^{-1} updraft if the concentration of ice crystals is less than 50 l^{-1} near cloud top and the crystals are no larger than $50 \mu\text{m}$. Liquid water production will occur at this vertical velocity and temperature if the crystals are smaller than $200 \mu\text{m}$ and do not exceed 12.5 l^{-1} . For greater updraft speed, a substantial increase in both crystal concentration and size would be necessary to maintain equilibrium. At -15°C (Fig. 44b), the concentration of ice crystals required to remove the water mass produced by vertical motion near cloud top is somewhat

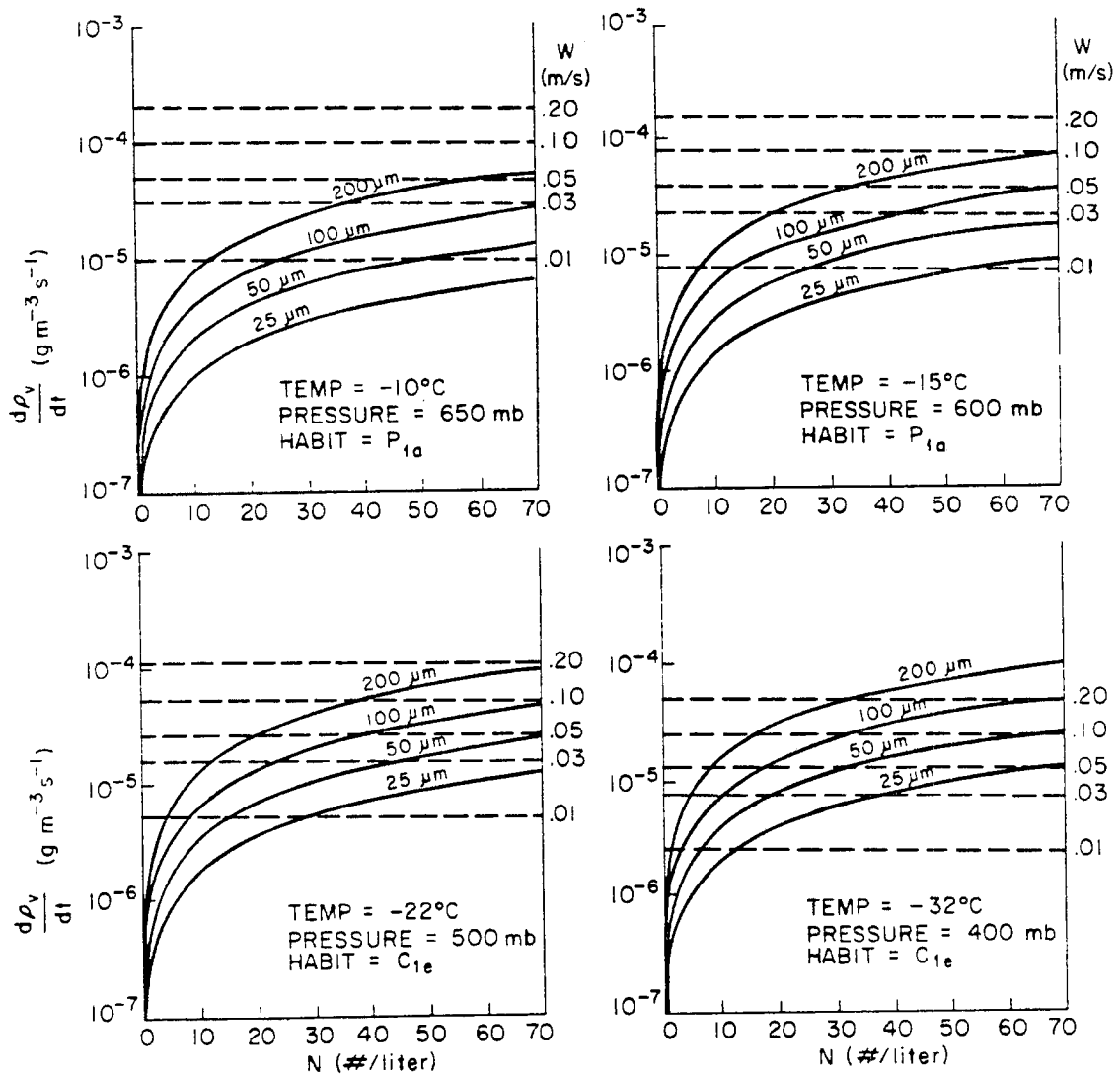


Fig. 44. Condensate production rates (dashed) as a function of vertical velocity in a water saturated atmosphere at typical atmospheric temperatures and pressures. Also shown are ice crystal growth rates (solid) for several uniform size distributions of P_{1a} and C_{1e} crystals as a function of crystal concentration.

reduced. Still, 25 μm ice crystals in concentrations of 50 l^{-1} are required to extract the water mass produced by a 0.01 m s^{-1} updraft. Ice crystals of 200 μm size in a concentration of 6 l^{-1} would have the same effect. For a 0.05 m s^{-1} updraft, 32 crystals of 200 μm size would be required. At colder temperatures (Figs. 44c,d), the requirements for ice crystal concentration and size become less stringent, but the presence of supercooled water can still occur, at least for some cloud conditions.

It is important to note that in complex terrain, updraft velocities frequently exceed 0.01 m s^{-1} due to perturbations in the airflow associated with topographic obstructions. Figure 44 includes calculations for updraft velocities near cloud top as high as 0.20 m s^{-1} . When velocities of this magnitude are considered, liquid water production can occur over a wide range of ice crystal sizes and concentrations. It is because of the characteristic small sizes of crystals populating the cloud top region that these minimal updraft velocities are capable of generating at least small quantities of supercooled water. Evidence from the COSE data set indicates that this supercooled liquid layer can occur even in cold, deep systems. On 21 Dec 81, liquid water was observed at cloud top when the cloud top was at 43.5 kPa and the temperature was -31°C . In this case, the liquid water content was 0.09 g m^{-3} .

Two additional processes operate in the region near cloud top in wintertime mountain cloud systems which were not considered in these calculations, but can significantly affect the production of supercooled water, the evolution of the droplet distribution and the ice nucleation rate. Cloud top entrainment can modify the droplet distribution

substantially by causing droplet evaporation in the entraining regions. Entrainment can also limit the production of liquid water if the mixing processes are significant. In most cloud systems over the Park Range in wintertime, the upper regions of the cloud are stably stratified and often capped by an inversion. In those cases, the mechanism of entrainment is most likely associated with instability induced by vertical shear. In this case, entrainment regions would be localized regions where droplet evaporation would occur.

Radiative cooling also has not been considered in the calculations. This process serves to enhance the production of liquid water near cloud top. The effects of radiative cooling can be examined qualitatively by comparing radiative cooling rates near cloud top with the moist adiabatic cooling rates. Chen (1984) has considered the radiative cooling rates associated with the tops of the marine stratocumulus layer with cloud top temperatures near $+10^{\circ}\text{C}$. Chen found that radiative cooling rates can exceed 200°C/day within a narrow (5 kPa) layer near cloud top. Subsequent unpublished work with Chen's model has indicated that cooling rates of this magnitude also occur at the top of much colder cumulonimbus clouds with top temperatures between -30°C and -40°C (Chen, personal communication). The weak dependence of cloud top temperature on the magnitude of the radiative cooling rates in the Chen studies suggests that the rates found by Chen can be used to estimate the importance of radiative cooling near the tops of Park Range cloud systems.

Consider a cloud system with a cloud top temperature of -20°C at a pressure of 50 kPa. For a moist adiabatic ascent of an air parcel near cloud top, the cooling rate due to adiabatic expansion is given by

$$\frac{\delta T}{\delta t} = 665.3 w \text{ K/day}$$

with w (vertical velocity) in ms^{-1} . If one considers the value of radiative cooling near cloud top to be of the magnitude of 200°C/day , as determined by Chen (1984), cooling by adiabatic expansion would require a 0.3 m/s updraft to equal the radiative cooling rate near cloud top. Although these estimates are crude, they point to the importance of radiative processes in the cloud top region. Clearly, the production of liquid water near cloud top is strongly reinforced by radiative cooling. In fact, in many cases, radiative cooling may be the dominant term in the total cooling rate and hence in the liquid water production.

(2) Cloud base

Mean cloud base, as determined by visual observations during precipitating storms over the Park Range, occurs between 200 and 300 m below ridgetop. Occasionally cloud base can lower to as much as 500 m below ridgetop or rise to about 50-100 m above ridgetop. Cloud base temperature normally varies between -5°C and -10°C , although more extreme values occasionally occur.

The lower part of the cloud was inaccessible to aircraft during the COSE programs. The radiometric measurements of liquid water over the Park Range presented in the previous section have shown that liquid water is frequently present in significant quantities in these cloud systems, particularly when the cloud top temperatures are warm. However, the location of the liquid water could not be specified in the vertical.

Observations of crystal habit and degree of rime at RAD provide evidence that part of the liquid water present in the system is located in the lower cloud layers. Figure 45 summarizes the crystal observations collected at RAD during seven storms where the radar cloud top was warmer than -22°C . This level was chosen to insure that all crystals forming in the upper part of the cloud would have planar habits. Only crystals which nucleated and grew at temperatures warmer than about -9°C would acquire columnar characteristics. It can be seen from Fig. 45 that nearly all the crystals falling as precipitation at RAD during these events originated at temperatures colder than -9°C . Only 1% of the observations had any crystals with distinct columnar shapes. In nearly all samples, rime accumulation was present on some of the crystals. Because most of the rimed crystals were already well developed when the rime accumulation occurred, the crystals had to encounter the liquid water during the lower part of their trajectories through the cloud.

The existence of supercooled water at low cloud levels can be related to the growth rates, habits, and concentrations of ice crystals present in the Park Range cloud systems. Many experiments have been conducted in laboratories to determine the growth rates for ice crystals as a function of temperature (e.g. Ryan et al., 1976). These experiments have consistently shown that crystal axial growth rates exhibit a sharp maximum along the planar, or a-axis at -15°C for planar crystals and a maximum at -6°C along the basal, or c-axis for columnar crystals. However, little information exists concerning the growth rates of well developed planar crystals originating at cloud temperatures between -12°C and -22°C after they fall into the cloud region between

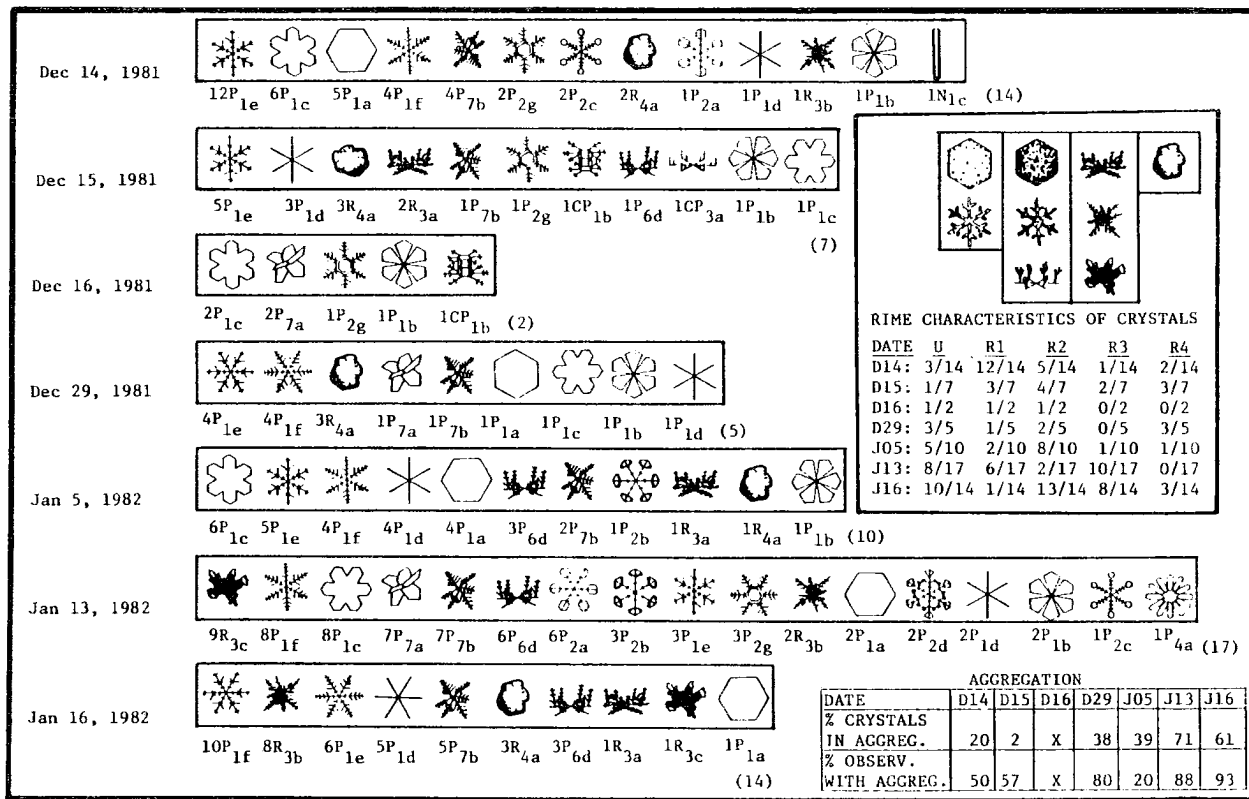


Fig. 45. Crystal habit climatology for seven shallow storm periods (cloud top $> -22^{\circ}\text{C}$). The total number of observations during each storm is given in parenthesis. The crystal habit and number of observations where that crystal habit was observed are listed below each crystal. Riming and aggregation statistics are given in the boxes in a similar manner. The crystal depictions and habit classification are taken from Magono and Lee (1966).

-9°C and -5°C . From Fig. 45, it is clear that virtually all of the crystals precipitating from these systems fall into this category.

Measurements of crystal axis dimensions by several authors (Auer and Veal, 1970; Ono, 1969, 1970; Kajikawa, 1972; Davis, 1974) have shown that the thickness and diameter of planar ice crystals possess characteristic relationships. Since a-axis growth is suppressed between -4°C and -9°C and c-axis development is limited by the crystal structure of well developed a-axis crystals, it is likely that a minimum in the bulk ice crystal diffusional growth rate exists between -9°C and cloud base in Park Range cloud systems. It is important to note that although a-axis growth rates increase with decreasing temperature below -9°C , they do not become significantly larger until about -12°C or -13°C (Ryan et al., 1976). Under some conditions, it may be possible for the low level liquid water region to extend to such temperatures. An additional factor contributing to the production of liquid water in the low levels of the cloud is the larger condensate production rates associated with the warmer temperatures near cloud base.

The most important contributor to the decrease in liquid water content associated with deep cloud systems with cold cloud tops is the frequent large concentration of ice particles associated with these systems. Although direct measurements of ice crystal concentrations in the lowest cloud levels could not be obtained with aircraft, measurements of number flux of ice crystals at RAD were routinely made. Figure 46 shows the relationship between number flux of crystals at RAD and echo top temperature for storms occurring during the 1981-82 experiment. It can be seen from this figure that the presence of deep clouds with tops colder than -22°C often resulted in half to an order of

magnitude increase in the number of crystals arriving at the surface. This large crystal flux has three effects on the liquid water zone near cloud base: (1) the greater flux of crystals eliminates liquid water present in the cloud low levels by accretion; (2) the increase in crystal concentration increases the bulk ice crystal growth rate limiting the production of cloud water; and (3) the presence of columnar crystals originating at higher cloud levels enhances the bulk diffusional growth rate. These three effects combine to reduce or eliminate the low level water zone in deep cloud systems.

(3) Regions of strong orographic forcing

Aircraft observations of liquid water, as well as the radiometric measurements, have generally shown that the highest liquid water contents are located directly upwind of mountain crests. Liquid water contents were found to vary significantly in this region from storm to storm. The maximum liquid water content observed was 0.43 gm^{-3} just upwind of the Park Range crest. The liquid water content in this region were generally between 0.05 and 0.20 gm^{-3} .

The presence of liquid water near the barrier crest results from high condensate production rates associated with the large vertical velocities induced by airflow deflection over the steep topography. However, data presented in the previous section indicate that the magnitude of the liquid water content in this zone is modulated by the net water depletion associated with the accretional and diffusional growth of crystals passing through the zone. The number of ice particles passing through this region is probably small for cloud top temperatures warmer than about -22°C , based on Fig. 46. However, at colder cloud top temperatures, the number flux of particles can

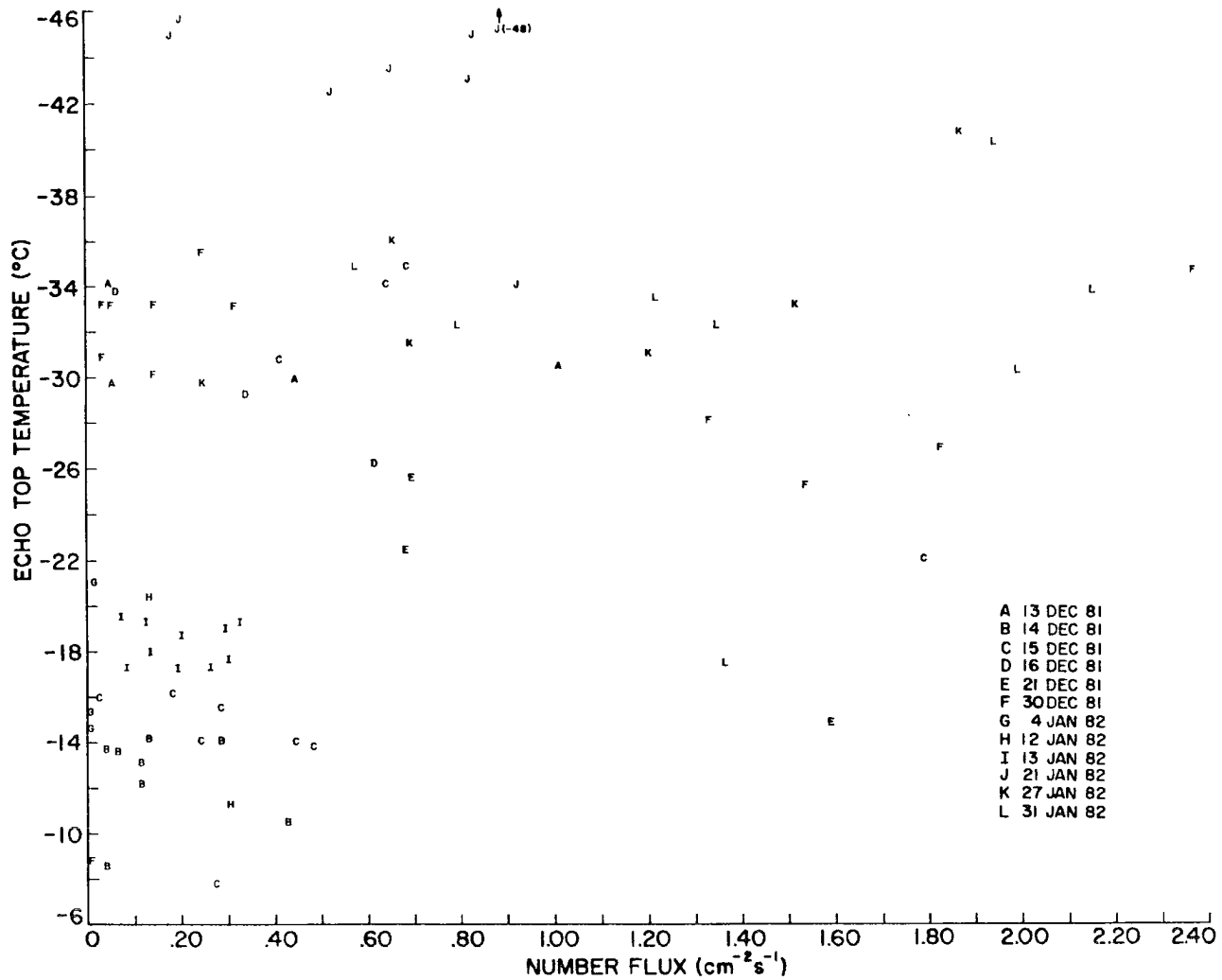


Fig. 46. Number flux of crystals at RAD as a function of echo top temperature.

frequently be large. Under these conditions, removal of liquid by accretion and diffusional growth can be significant.

B. Microphysical characteristics

Droplet concentrations in all cloud systems were very low compared to those expected for continental cloud systems. On one flight, cloud regions where liquid water contents were measured at $0.35\text{--}0.40\text{ gm}^{-3}$ had a mean droplet concentration of only 70.9 cm^{-3} . Table 6a summarizes the measurements of droplet concentration as a function of liquid water content for all flights. The mean concentration of droplets never exceeded 300 cm^{-3} in any liquid water content category during any of the flights. Droplet concentrations varied by as much as an order of magnitude in comparable liquid water content categories. In all cases, the concentration of droplets was found to be a function of liquid water content. Figure 47 shows the relationship between droplet concentration and liquid water content for the 23 Jan 82 flight. The best fit line and correlation coefficient based on a linear regression analysis between liquid water content and droplet concentration for each flight is given in Table 7.

At least four environmental factors contribute to the low droplet concentrations and variations summarized in Table 6a: (1) During the winter in the northern Colorado Rockies, stable layers are frequently present over broad regions. These stable layers limit the mixing which occurs between boundary layer air and the mid-level cloud layers and inhibit the rate at which cloud condensation nuclei (CCN) are resupplied to the cloud system; (2) a large fraction of the land surface in the area is frequently snow covered during winter. Snow cover inhibits mechanical interaction with the surface, reducing the supply of CCN; (3)

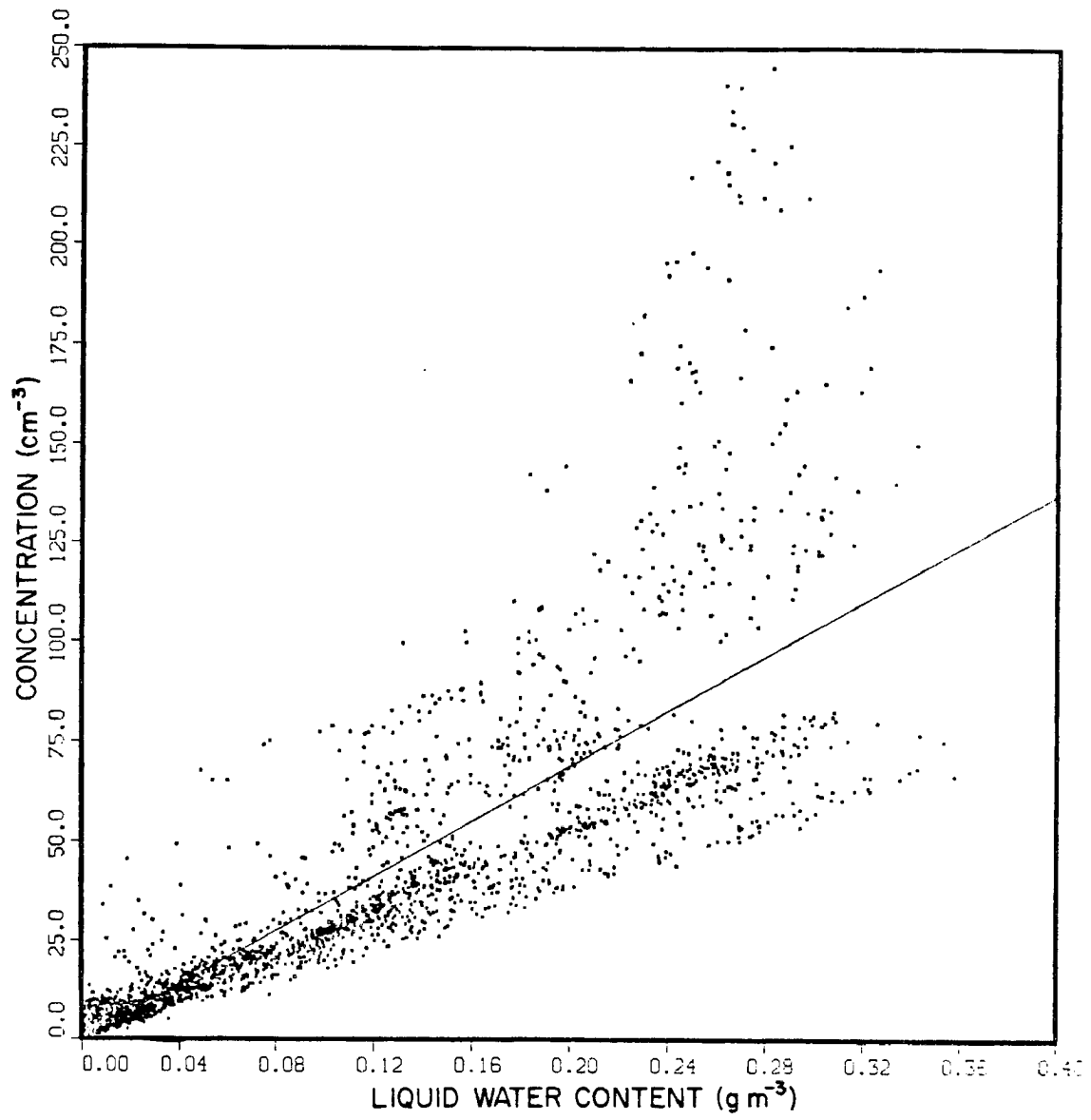


Fig. 47. Droplet concentration vs. liquid water content for N83TW flight on 23 January 1982.

Table 6
Droplet Spectra Characteristics

LWC (gm^{-3})	.01<LWC<.05	.05<LWC<.10	.10<LWC<.15	.15<LWC<.20	.20<LWC<.25	.25<LWC<.30	.30<LWC<.35	.35<LWC<.40
<u>a. Concentration (cm^{-3})</u>								
23 Jan 82	8.6 ± 6.0	22.2 ± 9.1	40.0 ± 14.9	58.0 ± 22.0	77.6 ± 34.1	101.3 ± 51.6	102.1 ± 41.8	70.9 ± 6.1
5 Jan 82	20.7 ± 12.6	32.2 ± 11.0	36.2 ± 4.4	--	--	--	--	--
24 Nov 79	45.6 ± 21.1	52.0 ± 9.8	54.4 ± 7.5	62.7 ± 2.5	--	--	--	--
21 Dec 81	51.8 ± 17.1	62.1 ± 15.1	--	--	--	--	--	--
22 Dec 79	103.8 ± 49.0	243.9 ± 80.9	263.0 ± 48.7	--	--	--	--	--
16 Jan 82	114.5 ± 41.8	131.7 ± 33.7	140.9 ± 40.0	162.2 ± 54.3	242.7 ± 10.1	--	--	--
31 Jan 82	128.0 ± 103.4	244.5 ± 59.4	--	--	--	--	--	--
26 Nov 79	171.9 ± 67.9	--	--	--	--	--	--	--
<u>b. Mean Diameter (μm)</u>								
23 Jan 82	15.7 ± 2.5	16.9 ± 1.8	16.8 ± 2.1	16.4 ± 2.4	16.9 ± 2.0	17.2 ± 2.2	17.9 ± 2.0	20.0 ± 0.9
5 Jan 82	9.8 ± 3.6	13.7 ± 3.0	17.0 ± 1.6	--	--	--	--	--
24 Nov 79	10.5 ± 1.9	12.8 ± 1.1	14.9 ± 0.6	15.8 ± 0.4	--	--	--	--
21 Dec 81	8.7 ± 1.4	11.8 ± 1.0	--	--	--	--	--	--
22 Dec 79	7.7 ± 1.2	8.1 ± 0.7	9.1 ± 0.6	--	--	--	--	--
16 Jan 82	7.8 ± 1.4	9.7 ± 1.1	11.3 ± 1.2	12.3 ± 1.3	11.5 ± 0.3	--	--	--
31 Jan 82	8.6 ± 4.5	7.8 ± 0.5	--	--	--	--	--	--
26 Nov 79	5.7 ± 0.6	--	--	--	--	--	--	--
<u>c. Standard Deviation (μm)</u>								
23 Jan 82	5.7 ± 2.2	6.0 ± 1.9	5.5 ± 1.9	5.8 ± 2.2	4.8 ± 2.0	4.0 ± 1.5	3.9 ± 1.4	5.5 ± 0.3
5 Jan 82	5.0 ± 1.2	6.0 ± 2.3	3.4 ± 2.5	--	--	--	--	--
24 Nov 79	2.3 ± 0.8	3.2 ± 0.6	4.3 ± 0.7	4.5 ± 0.3	--	--	--	--
21 Dec 81	2.7 ± 0.8	3.1 ± 0.8	--	--	--	--	--	--
22 Dec 79	1.8 ± 0.4	1.8 ± 0.3	2.1 ± 0.3	--	--	--	--	--
16 Jan 82	1.9 ± 0.7	2.3 ± 0.7	2.7 ± 0.6	2.6 ± 0.4	2.4 ± 0.1	--	--	--
31 Jan 82	2.9 ± 1.8	1.8 ± 0.2	--	--	--	--	--	--
26 Nov 79	1.9 ± 0.3	--	--	--	--	--	--	--

Table 7

Linear Regression Statistics

Droplet Concentration (C) vs. Liquid Water Content (LWC)

$$C = m(\text{LWC}) + b$$

Date	Slope (m) ($\text{cm}^{-3} \text{g}^{-1} \text{m}^3$)	Intercept(b) (cm^{-3})	Correlation Coefficient
23 Jan 82	344.0	0.0	0.89
5 Jan 82	512.0	3.8	0.69
24 Nov 79	527.6	0.7	0.60
21 Dec 81	1406.0	2.9	0.80
22 Dec 79	2844.6	1.7	0.90
16 Jan 82	1612.9	9.7	0.83
31 Jan 82	4685.1	-6.3	0.80
26 Nov 79	2636.5	-22.0	0.81

the northern Colorado Rocky Mountain region is relatively free of large anthropogenic sources of CCN. Except for isolated power plants and mines, many which do not operate in winter, few significant sources are present; (4) scavenging of CCN can occur in cloud systems developing over upwind barriers such as the Wasatch and Uinta Ranges of Utah. When these factors are considered, it is not surprising that the concentration of droplets measured in the clouds is quite low. Variations in the stability of the airmass, the extent of snow cover and the predominant wind direction can lead to the variations in droplet concentration listed in Table 6a.

Both the ambient concentration of CCN and the highest supersaturation to which those CCN are subjected will limit the maximum concentration of droplets present in the cloud system. If the flow through the cloud system is relatively smooth, the maximum supersaturation will be achieved close to the upwind edge of the cloud and the droplet concentration will be established at that point. An excellent example is the data reported by Politovich and Vali (1983) for the winter cap clouds which form over Elk Mountain, Wyoming. In that case, an increase in liquid water content was reflected primarily as a change in droplet size, with little effect on the ambient droplet concentration. The fact that droplet concentration is a function of liquid water content in Park Range clouds indicates that peak supersaturations are achieved at a number of locations in the cloud at the leading edge of local liquid water production zones. These zones can be associated with gravity waves generated in the flow by topographic variations as well as vertical motions generated by convective or shear instability. In all cloud samples, liquid water

contents were found to vary significantly over short distances in the cloud systems.

The mean droplet diameter and standard deviation of the droplet spectra in Park Range cloud systems were strongly and inversely related to the ambient droplet concentration. Mean droplet spectra for four liquid water content ranges for four flights are shown in Fig. 48. The spectra are arranged in the figure so that the cloud with the highest droplet concentrations is on the left and the lowest on the right. A systematic broadening of the spectra is evident as the concentration of droplets available to the cloud system decreases. Tables 6b and 6c summarize the mean droplet diameter and standard deviation of the droplet spectra as a function of liquid water content for all flights.

In cases where large droplet concentrations were observed, the small mean diameter and narrow dispersion characteristics limit droplet size. Flights with low droplet concentrations had significant numbers of large droplets ($> 20\mu\text{m}$). Based on these observations, accretion will be much more effective during storm systems which are naturally deficient in CCN. During these storms, large droplets with high efficiency for collection by ice crystals will cause the accretion process to accelerate, resulting in a more efficient precipitation process.

3. Comparison with other locations

Previous studies on the variability of liquid water in wintertime cloud systems over the mountains of the western United States have been published by Cooper and Marwitz (1980) for the San Juan Mountains of Colorado, Heggli et al. (1983) for the Sierra of California, and Hobbs (1975a) for Washington's Cascades. Both the physical distribution and temporal variations in the liquid water field were addressed in these

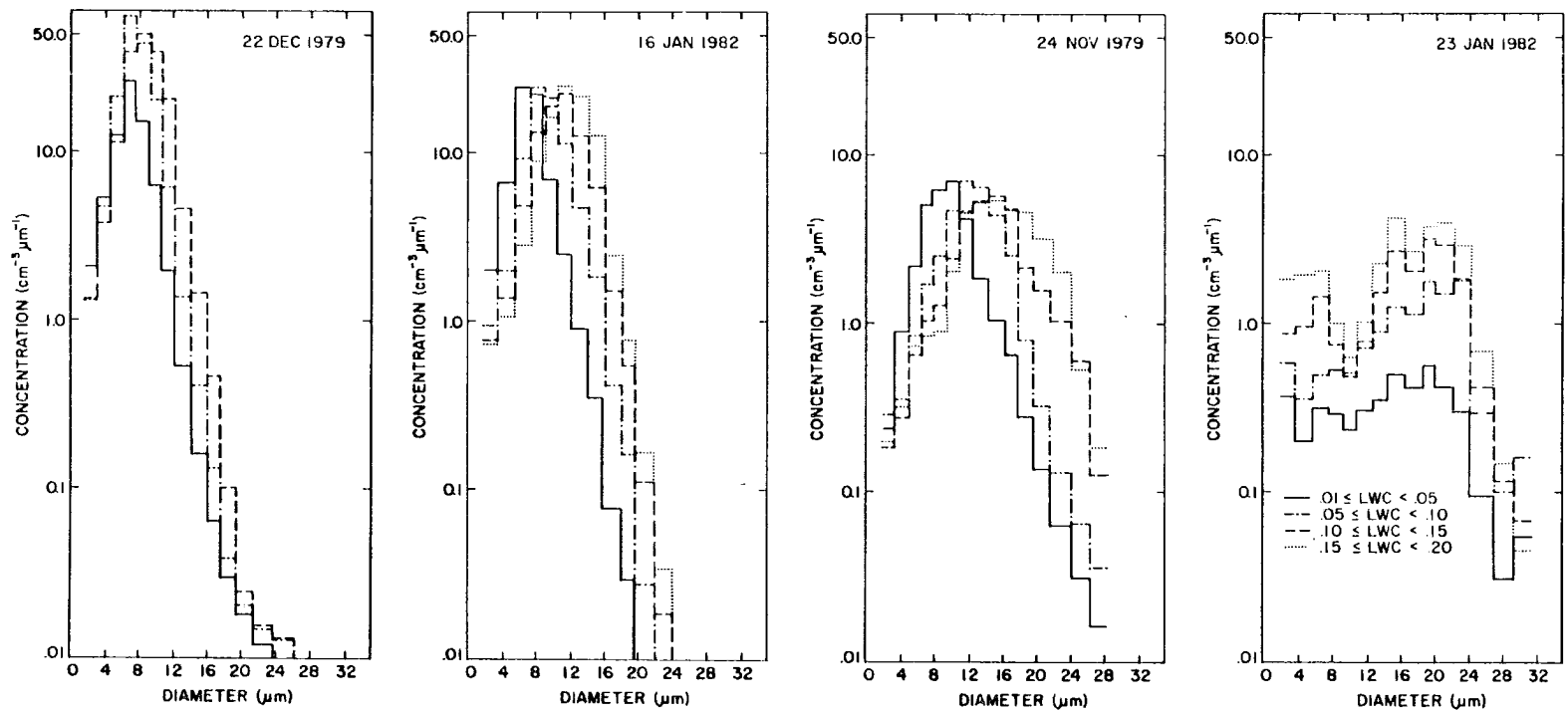


Fig. 48. Mean droplet spectra as a function of liquid water content for four flights during the COSE programs. Spectra statistics for all COSE flights are given in Table 6.

studies. However, because of the difference in observation technique, temporal variations were generally addressed on time scales associated with the passage of synoptic disturbances. This thesis is the first effort at documenting liquid water variations on short (10 min) time scales. Comparisons concerning the temporal nature of the liquid water field are addressed here only for synoptic time scales.

Although the San Juan Mountains and the Park Range are both in Colorado, the storms which affect these two mountain ranges have quite different synoptic origin. Thus, Cooper and Marwitz (1980) found that storms in the San Juan region progress through four stages, a stable stage followed by neutral, unstable and dissipative stages. In general, liquid water contents were found to increase in the cloud from near zero values in the stable stage to values between 0.5 to 1.0 gm⁻³ in the unstable stage. The increase in liquid water through these stages was attributed to increased convective instability and a reduction in blocked flow upwind of the mountains. In general, the highest and most persistent liquid water contents were found in the vicinity of the mountain slopes.

The pre-frontal storms in this thesis differed from the initial stage of the San Juan studies both in the degree of instability, the importance of blocked flow and in the magnitude of the liquid water. Clouds in the pre-frontal environment in the Park Range region were observed to undergo considerable variations in cloud depth, cloud top temperature, precipitation rate and liquid water content. In two cases, deep convective motions were possible due to the presence of low-level potentially unstable layers. In the storms studied, winds below barrier height at CG had westerly components. The 15 Dec 81 storm had some

characteristics of the neutral stage in the San Juans. The most similar aspect was that the middle troposphere was near neutral throughout a large depth. However, the 15 Dec 81 storm was observed to undergo considerable variation in cloud depth during its evolution, a feature not observed in the San Juans.

The unstable storm stage in the San Juan studies and the post-frontal storms discussed in this paper exhibited many similar characteristics. Both storm types were characterized by low level potential instability. Convection was generally confined to the lower cloud levels and was embedded rather than emergent. Cloud tops were relatively uniform. Liquid water contents were highest in the vicinity of the mountain slopes. The production of liquid water was associated with both orographic and convective vertical motions.

One major difference between the San Juan studies and the present study was that shallow orographic storms were not observed in the San Juans. This may be due to a limited sample, or may be a significant difference in the characteristics of the cloud systems between the two mountain ranges. The existence or frequency of occurrence of such storms in the San Juan region has not been clearly established.

Coastal storm systems, such as those described by Heggli et al. (1983) and Hobbs (1975a), exhibit greater amounts of convection and synoptic scale organization than do storms over the interior mountains of Colorado. In addition, the storms are warmer, with source air for the clouds originating over the warm Pacific Ocean at temperatures well above 0°C . As a result, the evolution of the storms, magnitudes of the liquid water contents and temporal variations of the liquid water fields

can be expected to differ significantly. Some general comparisons are noted here.

Heggli et al. (1983) categorized storms of the Sierra Cooperative Pilot Project (SCPP) using radar classifications and summarized the variations in liquid water content as a function of those classifications. Based on two years of aircraft data collected during the various precipitation echo types (PET), these authors concluded that cellular convective regions had the highest liquid water contents. High liquid water contents were also associated with the post 70 kPa trough environment, with the maximum tending to occur between 6-10 h after trough passage.

Comparisons between this study and the present one are complicated by differences in approach. The Sierra study used a statistical approach while the approach here has been the case study approach. In both cases, it is clear that significant variations in the liquid water content occurred in association with the passage of mesoscale features. The enhancement of liquid water contents in the vicinity of the mountain in the unstable post-trough period of the Sierran storms corresponds generally to the post-frontal period of the Park Range storms.

Hobbs (1975a) found liquid water present in all stages of Cascade storm systems, but water contents were higher during the transitional and post-frontal periods. He found that the distribution of liquid was generally the same in orographic storms in the pre-frontal and post-frontal periods, suggesting some similarity between the orographic storms of the Cascades and the Park Range region. In the Cascades as well as in all of the other study areas, the post-frontal stage was more unstable and had strong cross-barrier wind components. As a result,

liquid water production occurred steadily in the vicinity of the mountain slopes.

Studies of the distribution of liquid water in cloud systems over western mountain ranges have been reported by Hill (1980), Cooper and Saunders (1980), Cooper and Vali (1981), Politovitch and Vali (1983), Hobbs (1975a) and Heggli et al. (1983). Hill (1980) emphasized the importance of the liquid water zone generated by vertical motion near the barrier crest. His studies, which were conducted in the Wasatch Mountain region of northern Utah, led to the conclusion that the quantity of supercooled water present in the cloud systems over the Wasatch was related to the cross-barrier wind speed and inversely related to the precipitation rate. He found that the precipitation rate was inversely related to cloud top temperature. These results are in general agreement with his observations.

Cooper and Vali (1981) discussed the structure of cap cloud systems over Elk Mountain, Wyoming and storm systems over the San Juan Mountains of southwest Colorado. Their study indicated that the tops of cap clouds over Elk Mountain were composed primarily of liquid water. They also identified a liquid water zone near the cloud leading edge. Insufficient data were available from the Park Range data set to confirm the presence of liquid water at the cloud inflow boundary; the clouds normally extended far upwind of the main study area. However, the arguments presented in this paper for cloud top hold equally well at the cloud leading edge. For this reason, it is likely that the leading edge of Park Range clouds also contained liquid water.

Cooper and Saunders (1980) discussed the distribution of liquid water in clouds over the San Juan Mountains in more detail. Three

regions of liquid water were found: (1) 15-20 km upwind of the mountain associated with convection; (2) directly over the mountain crest and (3) 60-70 km upwind associated with a rise in the topography. The storms were categorized in four stages, as discussed in Part I. The stable and neutral stage of the San Juan storms had characteristics very similar to the deep precipitating stratiform clouds studied during COSE. In this study, liquid water was found only in the vicinity of the mountain in values $< 0.2 \text{ gm}^{-3}$. Liquid water contents were similar for the San Juans, $< 0.1 \text{ gm}^{-3}$ in the stable stage and $< 0.3 \text{ gm}^{-3}$ in the neutral stage. The San Juan cloud systems were generally deep during these stages with cloud tops above the 40 kPa level. The general structure of the unstable stage of San Juan storms was similar to the post-frontal storms studied in the Park Range region (see Part I). However, penetrations of the low level convective regions were not possible with aircraft to determine the magnitude of the liquid water contents. The values of 0.5 to 1.0 gm^{-3} reported over the ridge in the upper levels of the San Juan storms were not observed over the Park Range. This may have been due to a greater depth of the embedded convection in the San Juans. In the Park Range storms, the equilibrium level was generally below the minimum flight altitude. Shallow orographic storms, such as those described here and in Part I, were not among the eight storms studied in the San Juan project.

Liquid water contents measured in cloud systems over coastal mountains are generally higher in all storm stages. Thus, Hobbs (1975a) found liquid water contents ranging between 0.0 and 0.5 gm^{-3} in pre-frontal storms and as high as 0.5 to 2.0 gm^{-3} in transitional storms. Post-frontal storms in his study had liquid water contents between 0.1

and 1.0 gm^{-3} . One interesting aspect of Hobb's study was the presence of water at temperatures warmer than -10°C . Hobbs found that the liquid water content at temperatures warmer than -10°C increased with increasing wind speed in pre-frontal clouds. Riming frequently occurred at these levels. In shallower post-frontal clouds, Hobbs found that (1) low temperature crystals became less common; (2) water droplets became increasingly common, even at temperatures as cold as -15°C ; (3) the ratio of ice to water decreased; and (4) at temperatures below -8°C , the clouds frequently contained only supercooled water. Riming was common in the low levels of these clouds. The observations of Hobbs support the arguments made here for Park Range clouds.

Liquid water contents reported for Sierra clouds by Heggli et al. (1983) were also higher than those observed in the Park Range region. Heggli et al. found the maximum liquid water content to occur near the freezing level in all storms and the highest liquid water contents to occur in association with strong convection. The magnitude and frequency of convection in winter in the Sierras is much greater than the Park Range due to the warmer structure of the California storms. In addition, the freezing level in the Sierras is frequently within the cloud while in the Park Range region, the atmosphere is generally below 0°C .

The microphysical characteristics of the liquid water regions in San Juan storms were also discussed by Cooper and Saunders. They observed two characteristic droplet spectra in their study. Narrow droplet spectra were generally found in the upwind water zone and near cloud base. Wide spectra with large drops were found near the mountain, particularly during the unstable storm stage. They frequently observed

bimodality in the spectra in this region. These results are generally similar to that found in the Park Range during storms which had relatively large droplet concentrations but differed from our observations in clouds with characteristically low concentrations. In these storms, which included the most stable storms, bimodality was frequently observed.

Microphysical measurements made in the Park Range studies differed from those reported by Politovitch and Vali (1983) for Elk Mountain cap clouds. In their study, droplet concentrations were established near the cloud edge and were generally independent of liquid water content. Droplet concentrations were generally higher than those reported in the Park Range clouds by a factor of 2-4 and droplet spectral dispersion (standard deviation/mean diameter) were lower by a factor of 2. The differences between our observations and those of Politovich and Vali are probably due to the mechanism of cloud formation. According to their study, Elk Mountain cap clouds typically occur during periods when surface winds are 10-20 m/s. Under these conditions, significant transport of boundary layer air to cloud levels occurs. This would introduce larger CCN concentrations into the cloud, accounting for the larger droplet concentrations and narrow droplet spectra characteristics. In addition, the flow over Elk Mountain is relatively laminar. In this situation, independence between droplet concentration and liquid water content would be expected.

CHAPTER IV THE ICE PHASE

The physical processes which lead to precipitation development in Park Range cloud systems are discussed in this chapter. The chapter is divided into six major sections. General characteristics of the ice phase including measured ice crystal concentrations, crystal habits and precipitation characteristics are discussed in Sec. 1. Crystal growth by vapor deposition is discussed in Sec. 2. Section 3 describes nucleation processes in Park Range cloud systems. This section summarizes and extends the work of DeMott et al. (1986). Secondary ice crystal production processes (ice multiplication) are discussed in Sec. 4. Crystal fracturing, ice splinter production during riming, and droplet shattering during freezing are considered. Section 5 considers the role of accretion in precipitation formation. Section 6 considers the aggregation process.

1. General characteristics of the ice phase

A. Crystal concentrations

Figure 49 displays the complete climatology of measured cloud ice particle concentrations for the 1981-82 flights of the Cheyenne II as a function of temperature. The data are displayed as a cumulative distribution, each line specifying the percent of measurements with concentrations less than the value given on the ordinate. Sample sizes for each temperature range are given to the right of the figure. In this figure, ice crystal concentrations were determined by the shadow-or method (see Chap. II,2,a). These values have an error of less than 1%

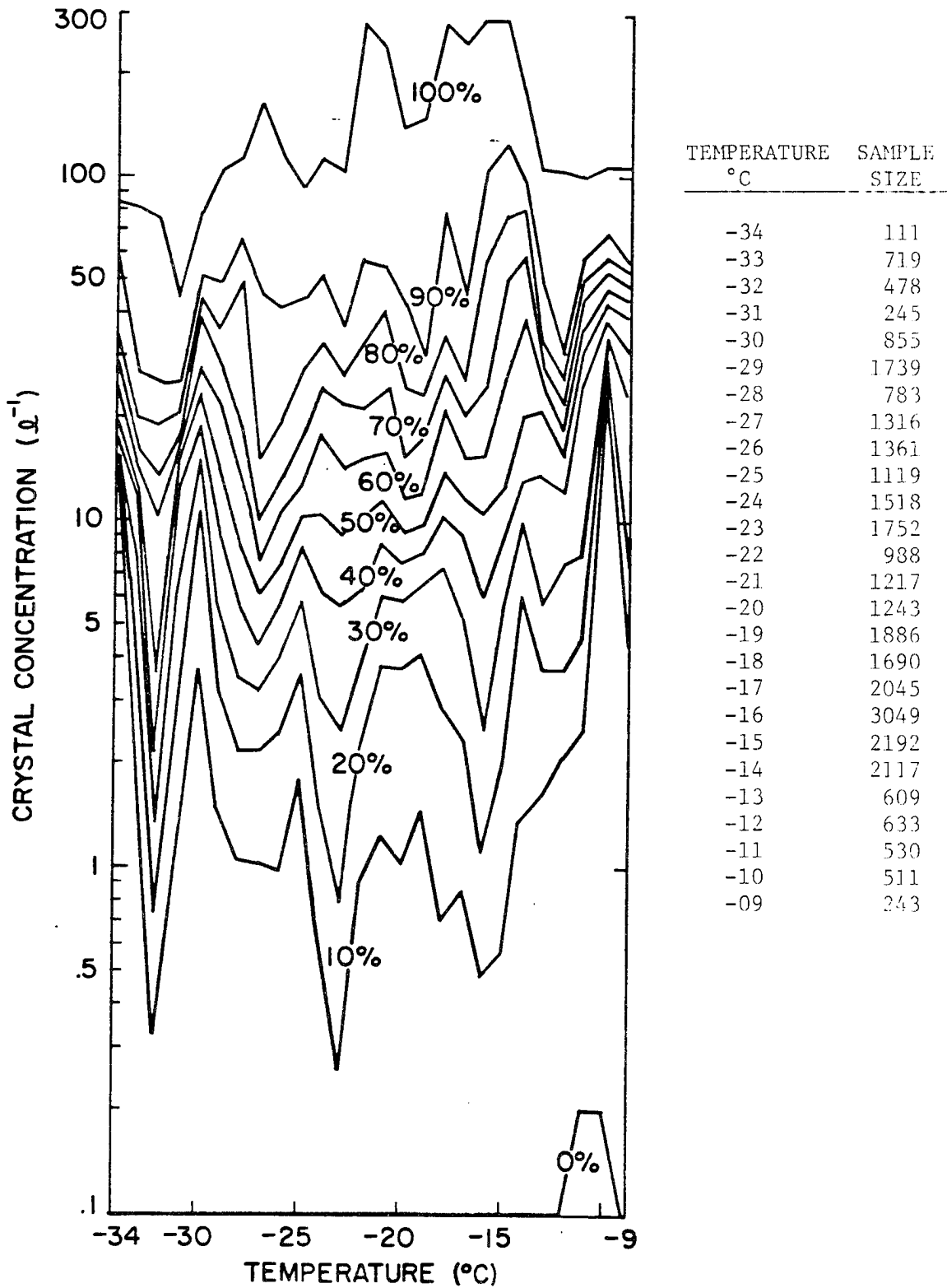


Fig. 49. Ice crystal concentration climatology as a function of temperature at the observation point. Each line specifies the percent of measurements with concentrations less than the value given on the ordinate.

due to artifacts of the 2D-c probe and represent the largest possible values of measured concentration. Temperature refers to the ambient temperature at the point of measurement. The sample time was one second (approximately 100 m of flight path). Data were included in the sample if the aircraft was in a cloud which had a 2D-c ice particle concentration of at least 0.1 l^{-1} or an FSSP droplet concentration of at least 20 cm^{-3} . Data were plotted only for temperatures which had a sample size of at least 100.

A wide range of ice particle concentrations, spanning three orders of magnitude, were measured at all temperatures. The highest concentrations measured were 290 l^{-1} at -15°C to -16°C . 50% of the measured values were less than 20 l^{-1} except at the warmest temperatures. A general trend toward higher crystal concentrations was evident at temperatures warmer than the dendritic growth temperature range ($> -17^{\circ}\text{C}$). This trend was particularly pronounced in certain data sets where dendritic crystals were observed. A possible explanation for ice crystal concentration enhancement at these temperatures will be discussed in Sec. 4. Crystal concentrations at temperatures between -20°C and -30°C displayed no significant trends as a function of temperature. 10% of the observations were less than 1.0 l^{-1} , 50% less than 10 l^{-1} and 90% less than 50 l^{-1} . At colder temperatures ($< -30^{\circ}\text{C}$), concentrations tended to decrease compared to warmer temperature values. This was particularly true for observations between -31°C to -33°C .

The most important feature of this climatology is the extreme variability in ice particle concentration which can occur at any temperature. Mechanisms responsible for these variations in ice particle concentration are discussed in later sections.

B. Crystal habits

This section presents an overview of the crystal habits observed at the ground and in the middle and upper levels of Park Range cloud systems. The information draws from many case studies which will be discussed in more detail in later sections. Crystal habits were recorded directly at RAD with shadow photography and in-situ in the clouds with a particle decelerator on board the Cheyenne II aircraft.

(1) Surface measurements

Table 8 presents a summary tabulation of crystal habits appearing on shadow photographs during the 13 storms when photographs were available. The crystals were categorized according to the scheme of Magono and Lee (1966). For convenience, the Magono and Lee classification is included as Figs. 50 and 51. Two changes to this classification were made. The category R4b was split into two, one for snow pellets and a second for larger graupel. The side plane group, S1, S2 and S3 were combined in the irregular group. Such particles have highly variable configurations of plates, sideplanes, columnar extensions, and irregular planar faces which generally conform to no particular pattern. As such, they are irregular.

A total of 51,193 crystals were examined. A general summary of the habit structure of these crystals is given in Table 9. Irregular single particles dominated most of the sample. 71.07% of all particles examined were irregular. The production of such a large number of irregular particles in these cloud systems can be attributed to three factors:

- (a) A significant number of the particles were combinations of plates, side planes, planar extensions and variously oriented planar












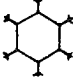











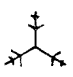









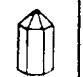



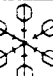

	N1a Elementary needle		C1f Hollow column		P2b Stellar crystal with sectorlike ends
	N1b Bundle of elementary needles		C1g Solid thick plate		P2c Dendritic crystal with plates at ends
	N1c Elementary sheath		C1h Thick plate of skeleton form		P2d Dendritic crystal with sectorlike ends
	N1d Bundle of elementary sheaths		C1i Scroll		P2e Plate with simple extensions
	N1e Long solid column		C2a Combination of bullets		P2f Plate with sectorlike extensions
	N2a Combination of needles		C2b Combination of columns		P2g Plate with dendritic extensions
	N2b Combination of sheaths		F1a Hexagonal plate		P3a Two-branched crystal
	N2c Combination of long solid columns		F1b Crystal with sectorlike branches		P3b Three-branched crystal
	C1a Pyramid		F1c Crystal with broad branches		P3c Four-branched crystal
	C1b Cup		F1d Stellar crystal		P3a Broad branch crystal with 12 branches
	C1c Solid bullet		F1e Ordinary dendritic crystal		P3b Dendritic crystal with 12 branches
	C1d Hollow bullet		F1f Fernlike crystal		P3 Malformed crystal
	C1e Solid column		P2a Stellar crystal with plates at ends		F3a Plate with spiral plates

Fig. 50. Magono and Lee (1966) ice crystal classification (part 1).

	F6a Plate with spatial dendrites		CP3a Plate with scrolls at ends		R3c Graupel-like snow with hoarlike extensions
	F6c Stellar crystal with spatial plates		S1 Side planes		R1a Hexagonal graupel
	F6d Stellar crystal with spatial dendrites		S2 Scalelike side planes		R1b Lump graupel
	F7a Radiating assemblage of plates		S3 Combination of side planes, bullets and columns		R1c Cone-like graupel
	F7b Radiating assemblage of dendrites		R1a Rimed needle crystal		I1 Ice particle
	CP1a Column with plates		R1b Rimed columnar crystal		I2 Rimed particle
	CP1b Column with dendrites		R1c Rimed plate or sector		I3a Broken branch
	CP1c Multiple capped column		R1d Rimed stellar crystal		I3b Rimed broken branch
	CP2a Bullet with plates		R2a Densely rimed plate or sector		I4 Miscellaneous
	CP2b Bullet with dendrites		R2b Densely rimed stellar crystal		G1 Minute column
	CP3a Stellar crystal with needles		R2a Stellar crystal with rimed spatial branches		G2 Germ of skeleton form
	CP3b Stellar crystal with columns		R3a Graupel-like snow of hexagonal type		G3 Minute hexagonal plate
	CP3c Stellar crystal with scrolls at ends		R3b Graupel-like snow of lump type		G4 Minute stellar crystal
					G5 Minute assemblage of plates
					G6 Irregular snow

Fig. 51. Magono and Lee (1966) ice crystal classification (part 2).

TABLE 8
SHADOW PHOTOGRAPH CRYSTAL HABIT SUMMARY
1981-82 STORMS

Dates	<u>13D</u>	<u>14D</u>	<u>15D</u>	<u>16D</u>	<u>21D</u>	<u>29D</u>	<u>30D</u>	<u>04J</u>	<u>12J</u>	<u>13J</u>	<u>21J</u>	<u>27J</u>	<u>31J</u>
Habit	Number of crystals												
<u>NEEDLES</u>													
N1a	11	0	654	0	33	0	1	0	0	0	0	0	0
N2a	0	0	0	0	1	0	0	0	0	0	0	0	0
<u>COLUMNS</u>													
N1c	21	7	24	0	5	2	1	2	2	0	0	0	0
N1e	0	0	0	31	0	0	0	0	0	0	34	105	94
N2c	9	0	0	19	0	0	0	0	0	0	11	11	21
C1c	0	0	0	0	0	0	0	0	1	0	6	7	137
C1e	0	24	4	16	1	0	0	0	73	1	137	119	213
C2a	6	0	0	1	0	0	0	0	0	0	0	2	10
C2b	0	0	0	0	0	0	0	0	0	0	4	4	4
R1b	1	0	0	0	0	0	0	0	0	0	0	0	0
<u>PLATES</u>													
P1a	10	101	39	44	0	14	8	28	99	182	107	73	188
<u>PLANAR DENDRITES</u>													
P1b	0	1	4	1	0	0	0	4	0	20	0	0	27
P1c	3	43	19	30	8	28	1	55	4	71	6	6	18
P1d	0	10	27	0	14	47	27	48	4	118	40	6	33
P1f	2	697	266	2	17	297	154	143	1	419	48	24	146
P2a	0	19	75	0	1	15	3	11	0	28	0	2	41
P2c	0	0	0	0	0	0	0	0	0	3	0	0	0
P2d	0	28	0	1	1	5	2	15	0	14	0	0	0
P2e	0	0	0	0	0	0	0	0	0	3	0	0	0
P2f	0	0	3	0	0	1	0	0	0	79	1	0	70
P2g	0	3	3	17	1	3	0	0	0	53	0	0	6
P3a	0	3	0	0	0	0	0	0	0	1	1	0	1
P3b	0	0	0	0	0	0	0	0	0	1	1	0	0
P3c	0	5	0	0	0	0	0	0	0	2	0	0	0
P4a	0	2	0	0	0	0	0	0	0	4	0	0	0
P4b	0	0	1	0	0	0	0	0	0	3	0	0	0
P5	0	0	1	0	0	0	0	0	0	0	0	0	0
R2b	0	10	10	0	0	0	3	2	0	0	0	0	0

TABLE 8 (continued)
SHADOW PHOTOGRAPH CRYSTAL HABIT SUMMARY
1981-82 STORMS

Dates	<u>13D</u>	<u>14D</u>	<u>15D</u>	<u>16D</u>	<u>21D</u>	<u>29D</u>	<u>30D</u>	<u>04J</u>	<u>12J</u>	<u>13J</u>	<u>21J</u>	<u>27J</u>	<u>31J</u>
Habit	Number of crystals												
<u>COMBINATION OF PLATES</u>													
P7a	0	0	0	0	0	0	0	0	35	18	33	0	293
P6a	0	1	0	0	0	0	0	0	0	0	0	0	0
<u>CAPPED COLUMNS</u>													
CP1a	20	0	5	3	0	0	0	0	0	0	34	9	22
CP1b	0	0	0	0	0	0	0	0	0	0	0	0	1
CP1c	4	0	29	0	0	0	0	0	0	0	4	2	5
<u>SPATIAL DENDRITIC FORMS</u>													
P7b	0	0	3	0	0	8	2	0	0	35	10	13	34
R3b	0	0	58	0	6	71	0	1	0	312	1	0	33
<u>HEAVILY RIMED PARTICLES</u>													
R3c	0	25	227	7	39	0	93	0	0	56	0	38	49
R4a	0	0	1	0	0	0	3	0	0	0	0	0	0
R4b (snow pellet)	0	0	16	0	0	5	502	11	0	0	0	1	4
R4b (graupel)	0	0	0	0	0	0	131	0	0	0	0	0	0
<u>BROKEN DENDRITIC BRANCHES</u>													
I3a,b	1	482	449	0	26	371	656	101	6	1111	92	236	438
<u>IRREGULAR</u>													
I1,2,4	2281	2133	4484	1834	2344	61	6365	209	1212	745	4617	5772	4330
<u>CRYSTALS IN AGGREGATES</u>													
	0	99	0	0	0	227	378	0	0	457	253	493	154
<u>TOTAL</u>													
	2369	3701	6402	2015	2894	1155	8330	630	1438	3827	5443	6934	6420

TABLE 9
SHADOW PHOTOGRAPH CRYSTAL HABIT SUMMARY
1981-82 STORMS

GENERAL SUMMARY OF CRYSTAL HABITS

Habit	Number of Crystals	Percent of total sample
Planar Dendrites	3700	7.23
Spatial dendrites	587	1.15
Dendritic branches	3969	7.75
Plates	893	1.74
Plate assemblies	380	0.74
Needles	700	1.37
Columns	1170	2.29
Capped columns	138	0.27
Heavily rimed crystals	1208	2.36
Crystals in Aggregates	2061	4.03
Irregular	<u>36387</u>	<u>71.07</u>
Total	51193	100.00

faces. These crystals were common when the cloud extended to temperatures well below -20°C . These particle types are characteristic of such cold temperature regions (see, for example, Ono, 1969).

- (b) A large number of irregular particles were sufficiently rimed so that the original habits were obscured, but not enough to be categorized as graupel or snow pellets.
- (c) Many of the particles were fragments. Most of these were associated with dendritic snowfall. Fragments which could clearly be identified as originating from dendrites, such as complete dendritic arms, were classified as dendritic fragments (I3a, I3b). Otherwise, the irregular class was used.

Excluding irregular particles, the majority of the particles (16.13%) were dendritic. If one includes crystals in aggregates, which were primarily composed of dendrites, greater than 20% of the particles had dendritic habits. Of this group, 7.23% were planar dendrites, 7.75% were broken branches, and 1.15% were spatial dendrites.

Plates and plate assemblies comprised 2.48% of the sample. The plates observed were generally small ($< 1000 \mu\text{m}$). 1.37% of the crystals were needles. Nearly all of these were associated with a heavy needle snowfall over a 90 minute period on 15 Dec 81. This case is discussed in detail in Sec. 4. Columns, bullets and capped columns comprised 2.56% of the sample. The lack of columns at the surface is interesting, particularly since columnar habits were one of the most common habits observed by the aircraft.

(2) Aircraft measurements

Replicas of ice crystals captured in formvar with the decelerator were available for five flights of the Cheyenne II. In general, the slides contained considerable clutter due to multiple crystal impacts and fragmentation on impact. This was particularly true of delicate crystals such as dendrites. In this analysis, regions of the slides were ignored where high particle density obscured habit identification. Irregular particles were generally ignored because they could have resulted from fragmentation on impact or have been the result of multiple impacts. This analysis must be treated as qualitative because of this selection bias. However, the slides yielded very important information concerning trajectories of ice particles and diffusional growth of crystals within mountain cloud systems. The decelerator data for each flight are summarized on vertical cross-sections of the Park Range region (Figs. 53-57). Figure 52 explains the format of the data displayed on Figs. 53-57.

a. 15 December 81: The decelerator slide analysis for the 15 Dec 81 flight has been analyzed and discussed extensively by Uttal (1985). The data reduction on Fig. 53 is based on her work. Uttal found that upwind of the Park Range crest, crystal trajectories in the upper region of the 15 Dec 81 cloud were quasi-horizontal leading to considerable habit stratification based on temperature. Despite the pronounced number of columns and bullets at cold temperatures, few of these crystals were ever observed at the surface. In fact, precipitation was dominated by snow pellets, needles and plate assemblies. These observations, and the trajectory analysis of Uttal, suggest that interaction between the upper cloud layers and precipitation during this period of the storm was

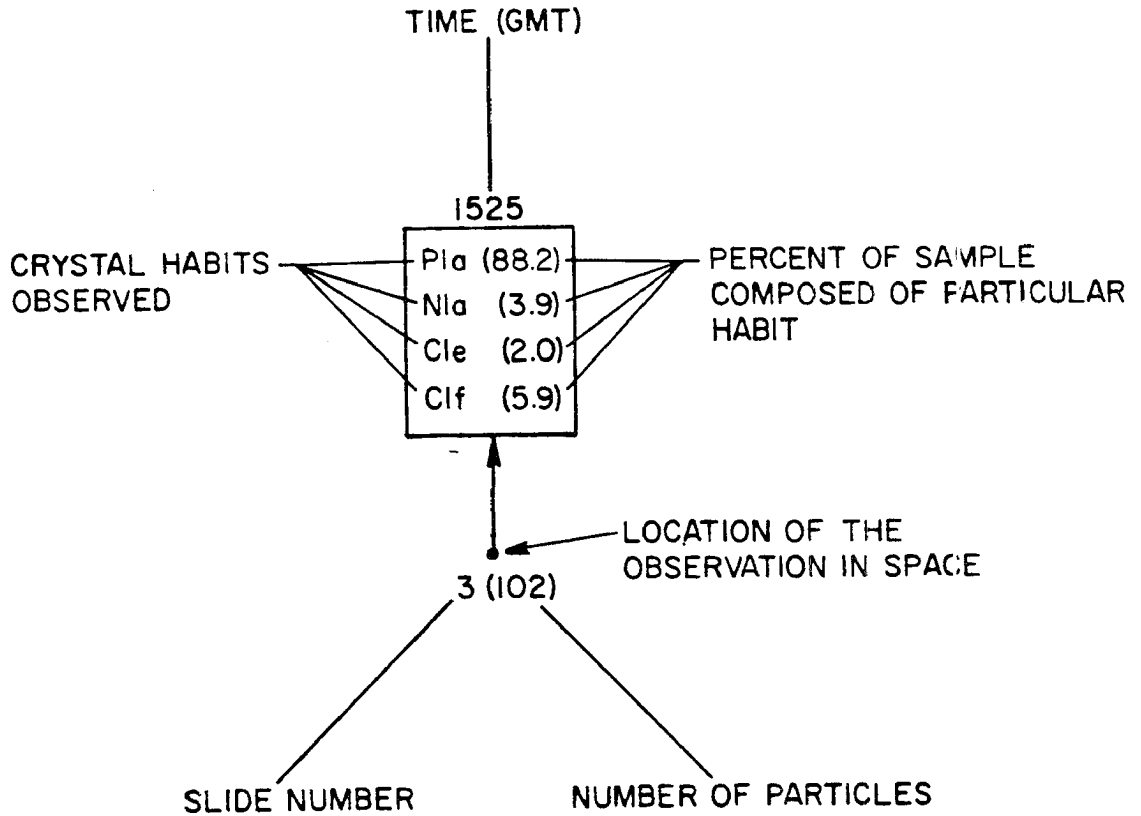


Fig. 52. Format for data displayed on Figs. 52-56.

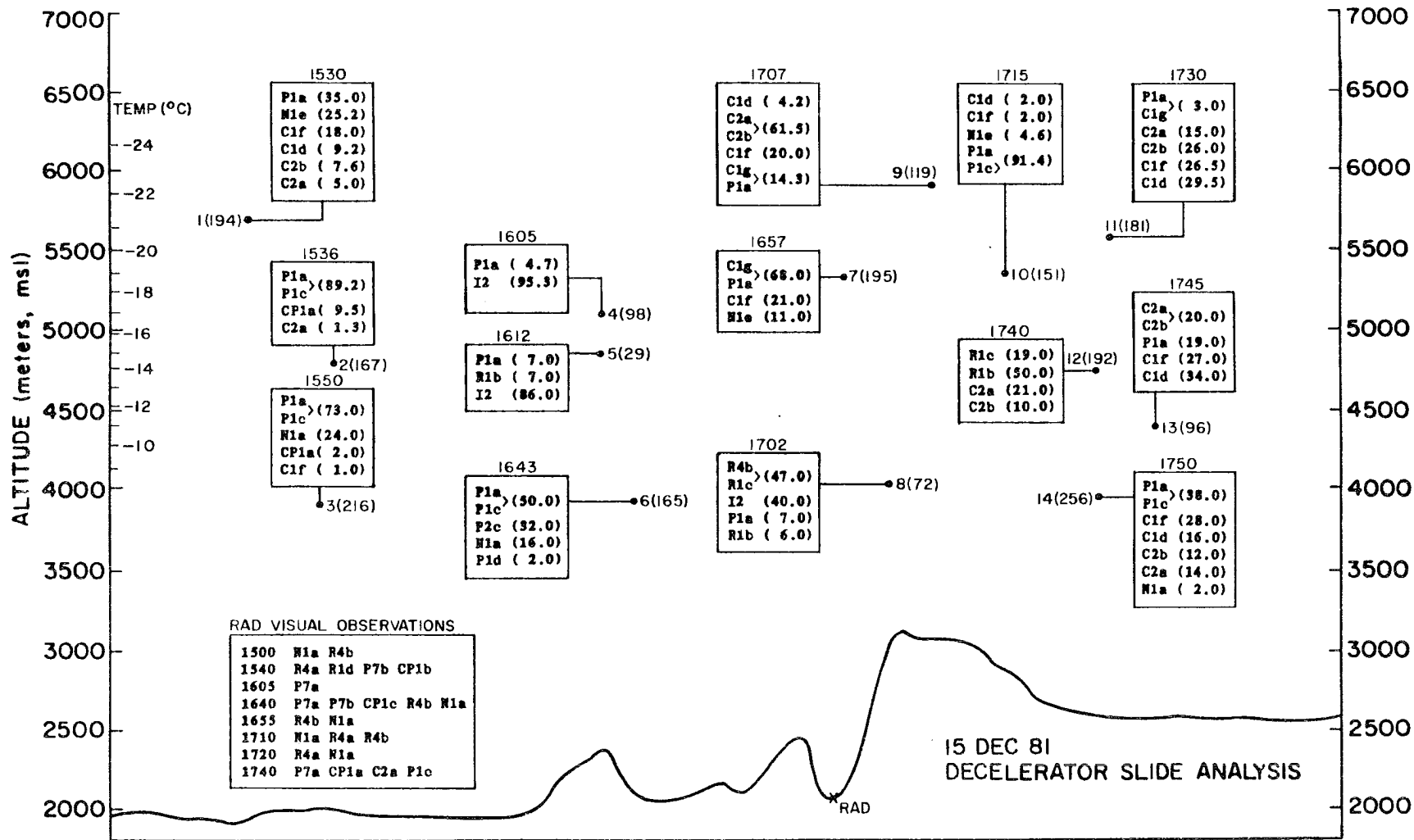


Fig. 53. Crystal habits determined from decelerator slide analysis for the 15 Dec 81 flight (analysis based on Uttal, 1985). See Fig. 52 for data format.

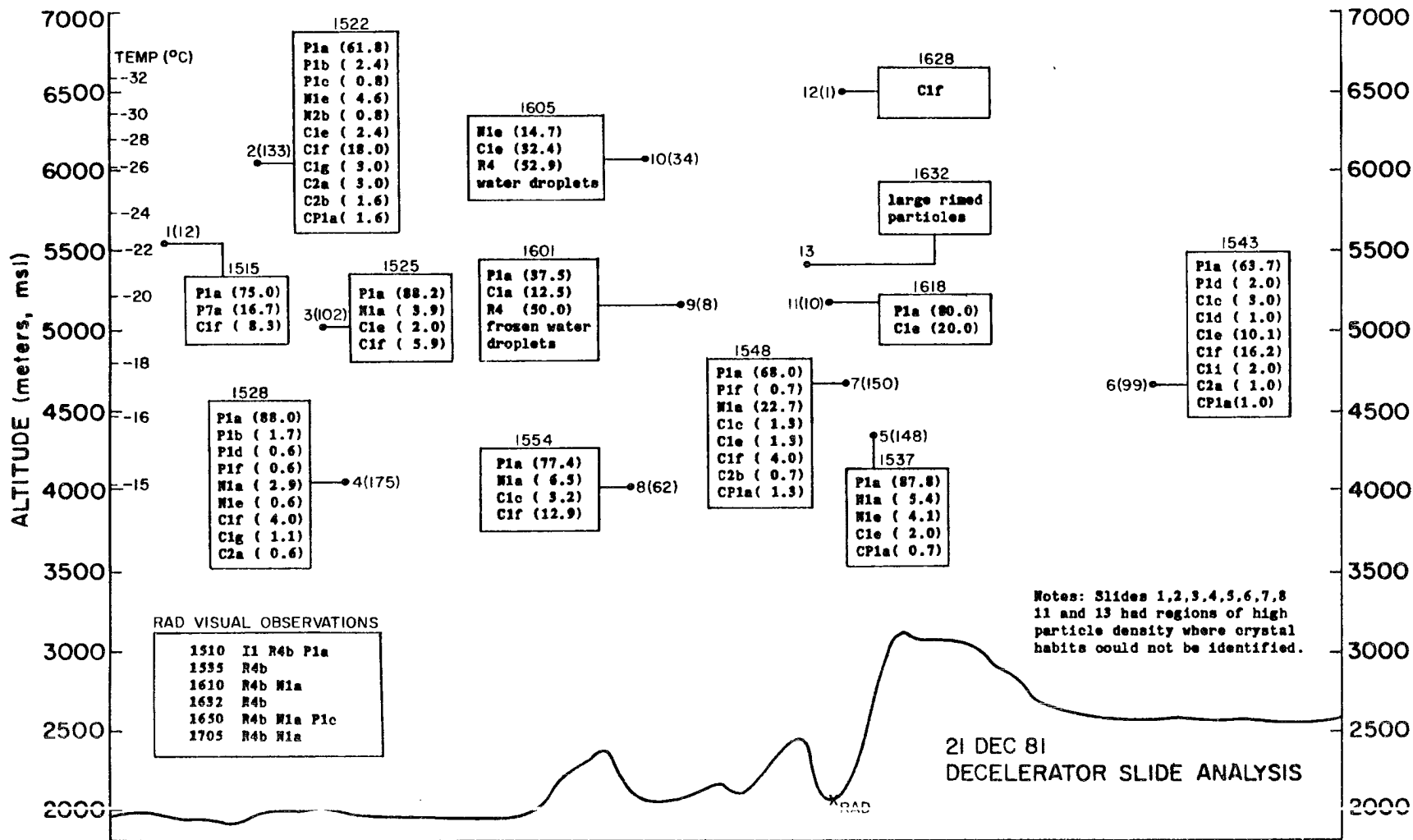


Fig. 54. Crystal habits determined from decelerator slide analysis for the 21 Dec 81 flight. See Fig. 52 for data format.

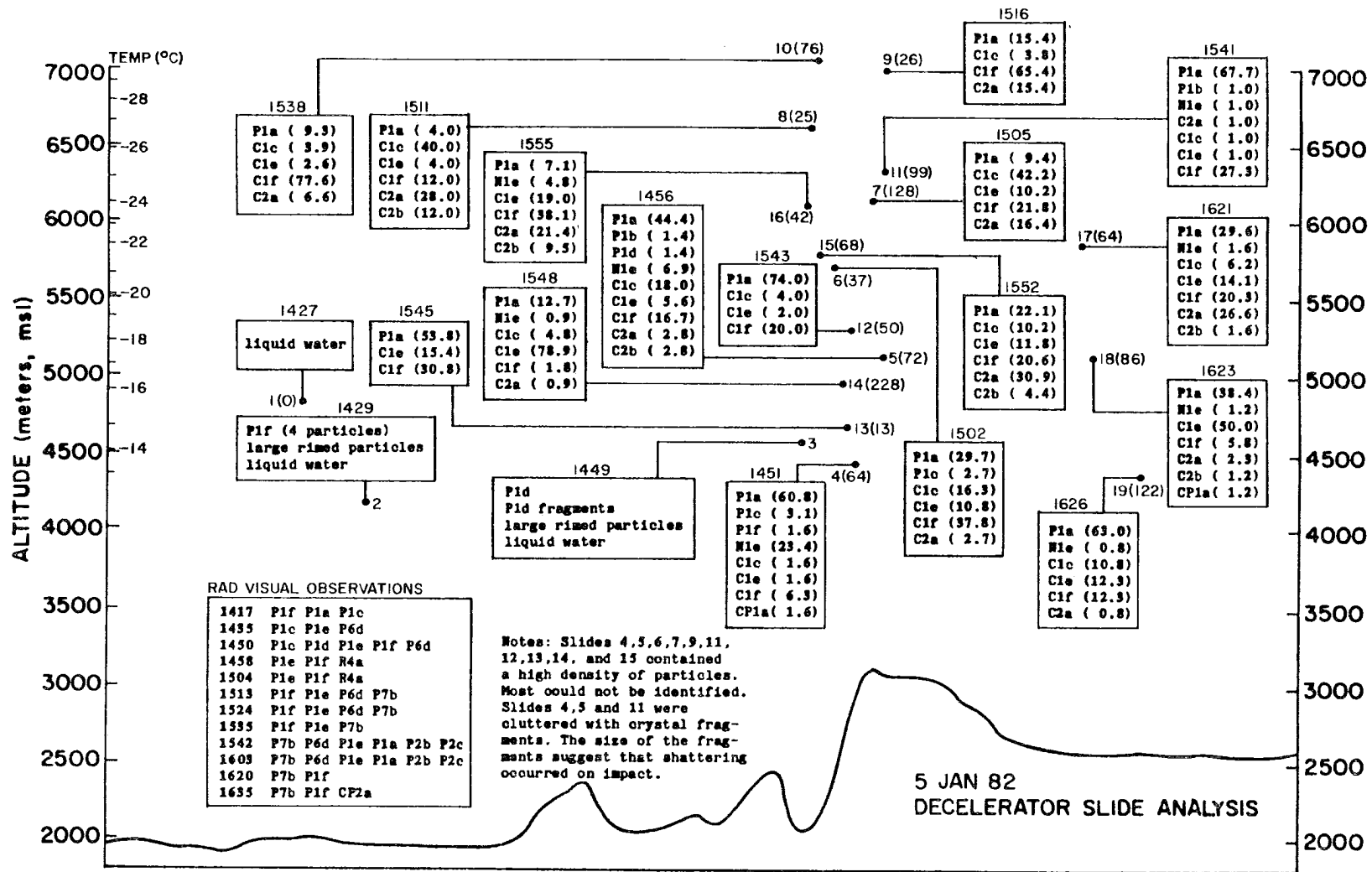


Fig. 55. Crystal habits determined from decelerator slide analysis for the 5 Jan 82 flight. See Fig. 52 for data format.

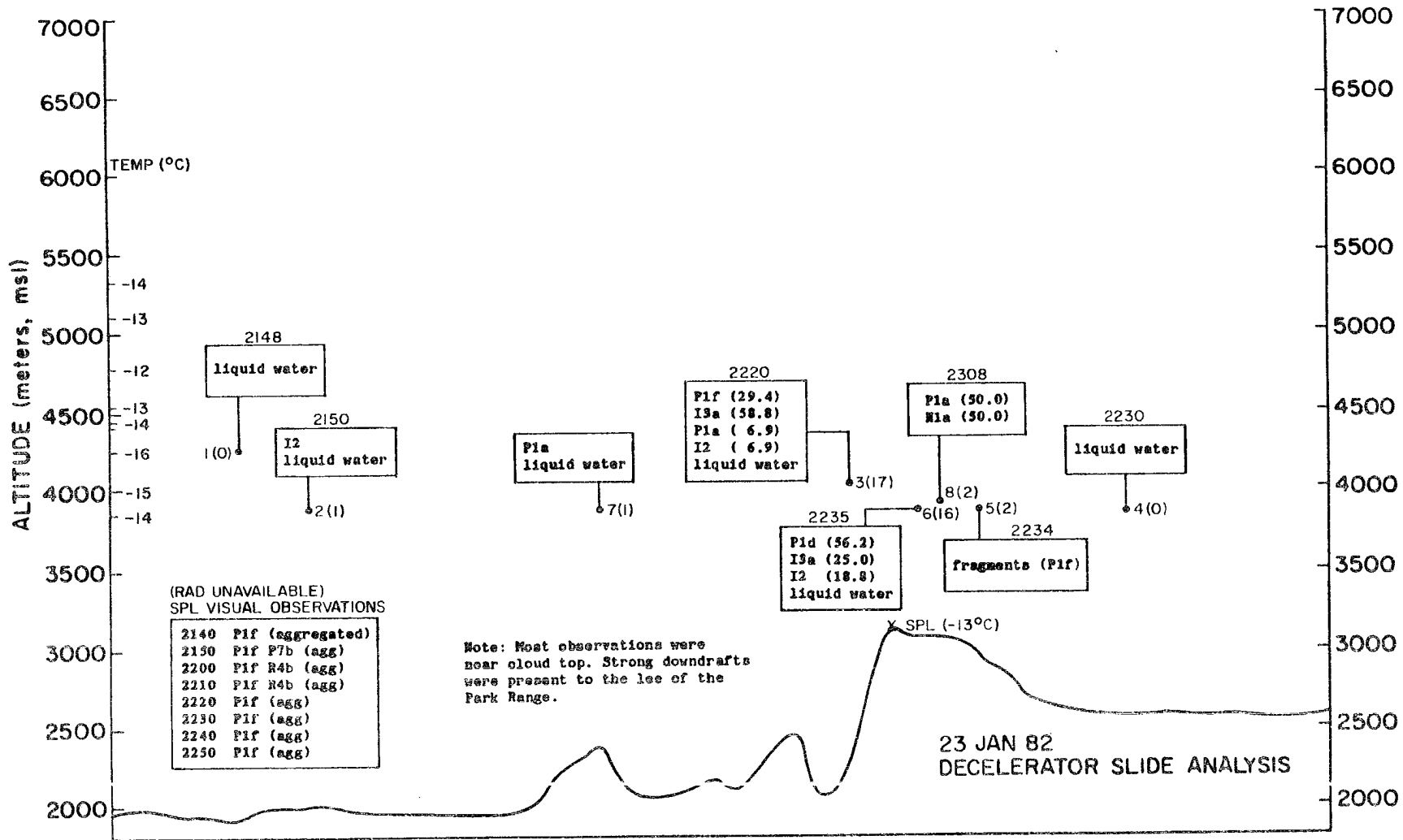


Fig. 56. Crystal habits determined from decelerator slide analysis for the 23 Jan 82 flight. See Fig. 52 for data format.

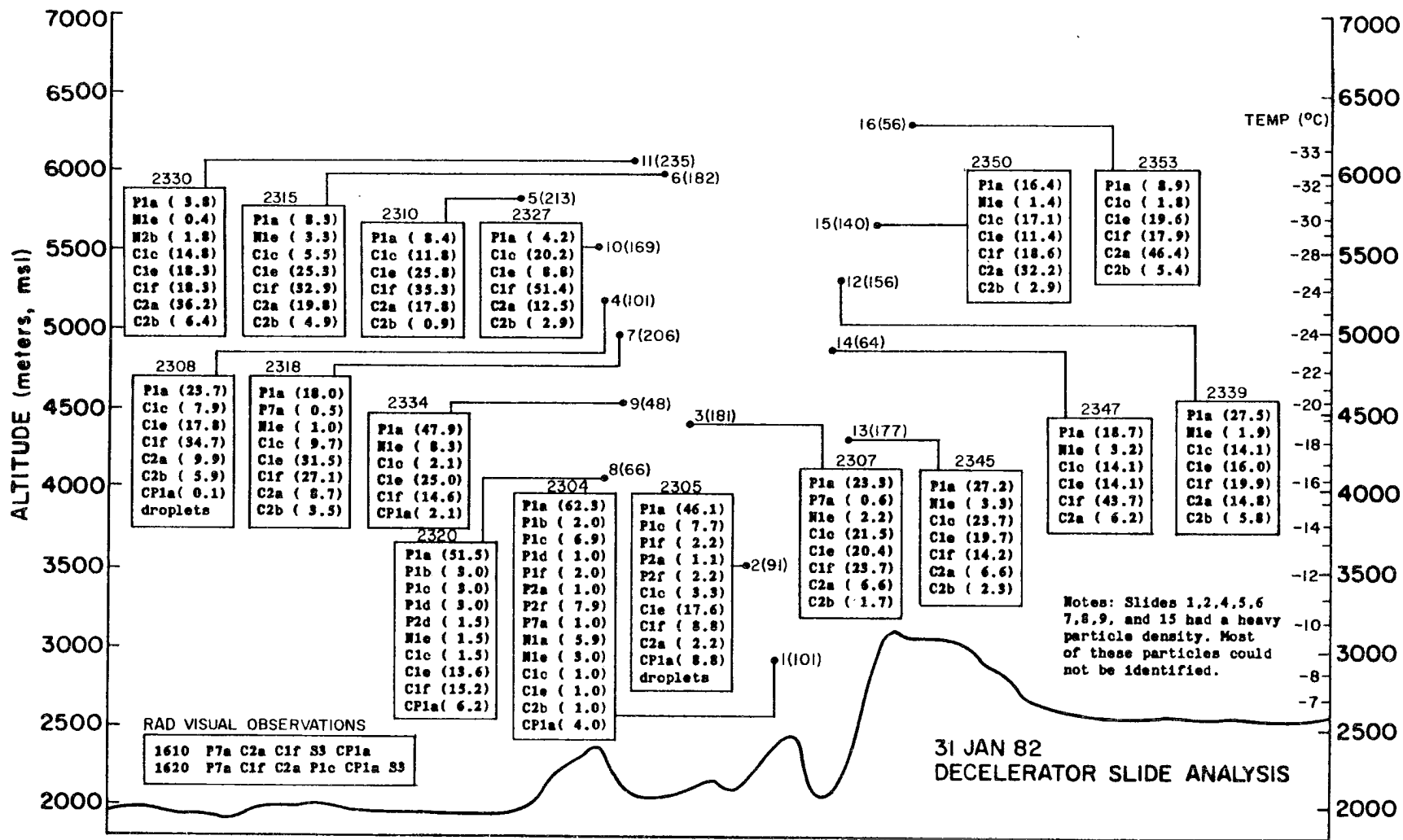


Fig. 57. Crystal habits determined from decelerator slide analysis for the 31 Jan 82 flight. See Fig. 52 for data format.

minimal. It is possible, however, that crystals forming the kernel of the snow pellets may have originated at higher cloud levels. This possibility was not investigated in the trajectory analysis. Additional analysis of the 15 Dec 81 case is presented in Sec. 4.

b. 21 December 81: Data for the 21 Dec 81 flight are displayed on Fig. 54. With the exceptions of slides 10, 12, and 14, the upper regions of the 21 Dec 81 cloud system were dominated by hexagonal plates (P1a). Columns (C1e, C1f), bullets (C1c), long columns (N1e) and cross-column assemblies (C2a, C2b) comprised most of the remaining sample. Frozen water droplets and large rimed particles were observed upwind of the mountain at points 9, 10, and 11 in the upper levels of the cloud system. Supercooled water was observed by the FSSP in this region during the flight. As with the 15 Dec 81 cloud system, crystal habits observed at RAD did not mirror those observed by the aircraft. The dominant particles observed at RAD during the flight were irregular rimed particles, approaching the rime coverage of snow pellets. Needles were also present. Physical processes governing particle growth in this cloud system will be discussed more extensively later in this chapter in sections 3, 4, and 5.

c. 5 January 82: Figure 55 contains the complete decelerator record for the 5 Jan 82 flight. The cloud system of 5 Jan 82 underwent an extreme transition during the course of the flight. The early portion of the flight, prior to 1450, occurred near the top of a shallow orographic cloud system. Slides 1, 2, and 3 were collected in this region. At 1450, a very deep cloud system advected into the area overrunning the shallow orographic system. Slide 4 was collected as the transition was in progress and all slides following were within the deep cloud system.

The nature and evolution of precipitation in the shallow cloud system are discussed in Sec. 2 and 3 of this chapter. Processes in the deep cloud system are discussed in Sec. 4 and 6.

Samples collected near the top of orographic cloud system primarily contained liquid water. However, several well formed dendrites were present on two of the slides as well as a few rimed particles. These slides provide important information concerning dendrite growth in shallow cloud systems. This is discussed more extensively in Sec. 2.

The transition slide, slide 4, was taken over the mountain crest as the cloud transition phase commenced. This slide, at -13°C , primarily contained plates but also contained a mixture of cold temperature columns. This slide also had a very heavy density of particles which could not be identified. These appeared to be fragments. The same was true of slide 5, also taken during the cloud system transition at -17°C . After the transition, the dominant crystal habits were columnar. Plates also made up a significant portion of the slides.

In contrast to the cloud observations by the aircraft, the surface precipitation was dominated by aggregates of planar dendrites. Spatial dendrites were also present. These precipitation characteristics persisted throughout the flight during the deep storm phase. Unfortunately, only one slide was taken in the dendritic zone during this time. This slide had such a high density of particles that only 13 individual particles could be identified. These were split evenly between plates and columns.

d. 23 January 82: During the flight period, the 23 Jan 82 storm was shallow, stable, and capped by an inversion. The decelerator data for this flight are displayed on Fig. 56. All samples were collected near

cloud top and were composed entirely of liquid water, dendrites or rimed particles. Surface precipitation observations at SPL (RAD observations were unavailable) indicated that the snowfall was almost entirely dendritic. This cloud system was similar to the 5 Jan 82 shallow system and will be discussed more completely in Sections 2, 3 and 6.

e. 31 January 82: The decelerator record for the flight of 31 Jan 82 is displayed on Fig. 57. This flight was the only opportunity to obtain low level information near the mountain during the COSE programs. On 31 Jan 82, the aircraft departed from Steamboat Springs airport after the onset of the storm. Samples collected at the low altitude points 1 and 2 contained a mixture of plates, dendrites, columns, capped columns and other particles. At middle and high levels, the dominant crystal habit was columnar. Plates were numerous on several slides and irregular particles were present on all slides. The limited number of visual observations, supplemented by several shadow photographs, indicated that crystal habits observed at the ground were similar to those observed by aircraft. This was in contrast to the deep cloud systems described earlier where a distinct decoupling between the upper cloud region and the low level precipitation processes was evident.

C. Precipitation rates

98.5 hours of precipitation occurred during measurement periods at RAD during the 1981-82 program. 58.04 mm of precipitation (water equivalent) accumulated during those periods. From these data, a climatology of precipitation rates and precipitation accumulation was assembled. The results are shown as cumulative frequency distributions in Fig. 58.

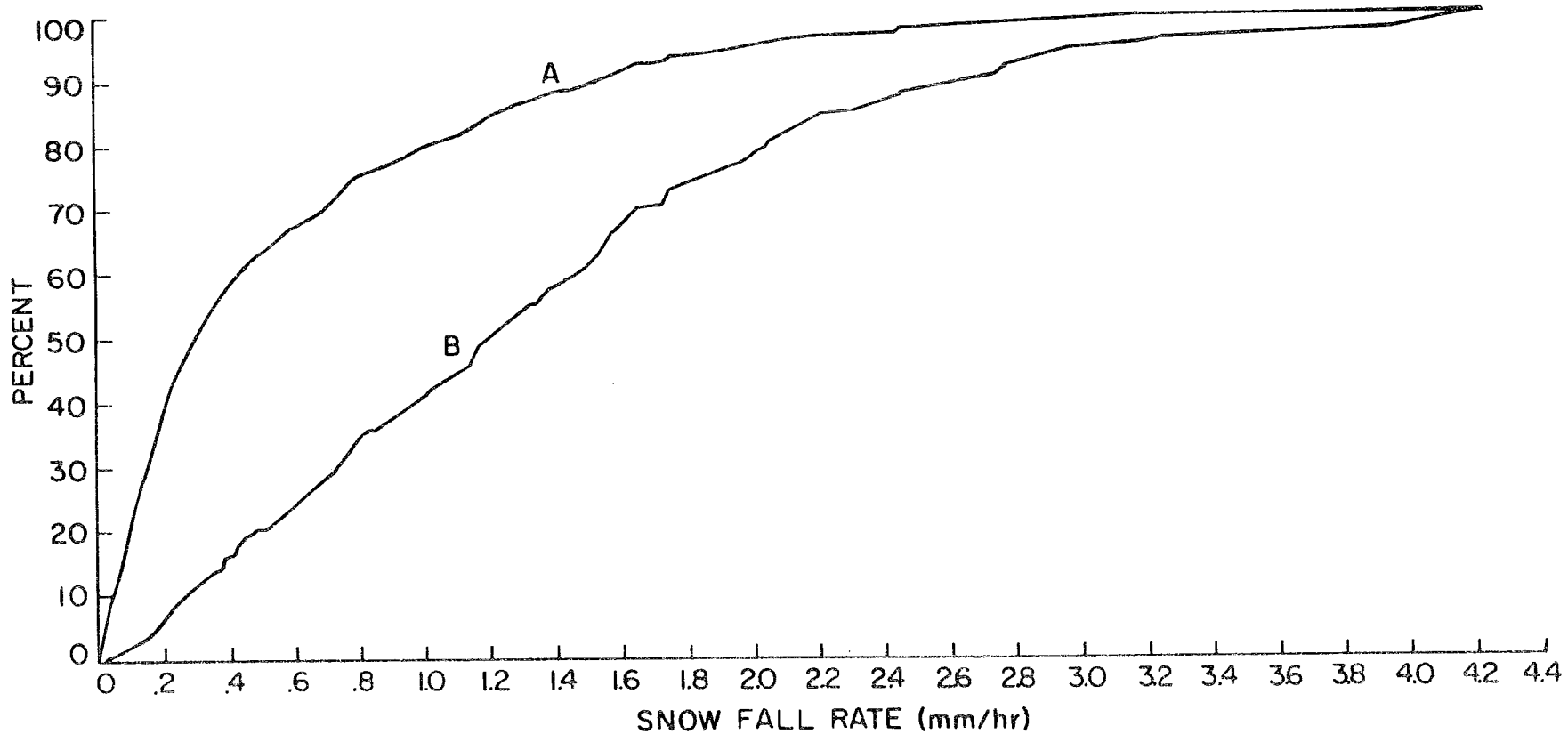


Fig. 58. Cumulative frequency diagram showing (A) the percent of observations where the precipitation rate (R) was less than R and (B) the percent of total precipitation which fell at precipitation rates less than R .

According to these data, low snowfall rates are very common in Park Range systems. The nearly straight line character of line B in Fig. 58 between the 0 and 90% level indicates that equal amounts of precipitation were produced over the field season in each precipitation rate interval. This is due to the disproportionate amount of time at which low snowfall rates occur. Forty percent of the time that measurements were conducted, the snowfall rate at RAD was between 0.0 and 0.2 mm/h. This snowfall accounted for only 6% of the total accumulation. Snowfall rates between 0.2 and 1.0 mm/h accounted for 35% of the total precipitation. Such snowfall rates occurred during 40% of the observation period. Snowfall rates between 1.0 and 2.0 mm/h accounted for 37% of the precipitation. These events occurred during 15% of the observation period. Snowfall rates greater than 2.0 mm/h accounted for 22% of the precipitation, although they only occurred 5% of the time.

2. Growth by vapor deposition

Analysis of growth by vapor deposition with field data is most adequately done in a Lagrangian reference frame, following particles as they move along trajectories through the cloud system. The point of nucleation should be known as well as characteristics of the changing environment. Such analysis is far beyond the capabilities of this data set. The approach taken here was to examine three aspects of the diffusional growth process in Park Range cloud systems. In the first section, characteristics of the cloud environment which lead to the production and growth of dendritic crystals are discussed. The second section considers cold temperature crystals ($<-17^{\circ}\text{C}$) and their influence

on the cloud environment. The last section discusses warm temperature crystals ($> -10^{\circ}\text{C}$) and their contribution to Park Range snowfall.

A. Dendritic snowfall events

Dendritic crystals comprised about 20% of the snowfall during the 1981-82 storm events. A common feature of all but one dendritic snowfall event was the shallow nature of the clouds. Except for part of the 5 Jan 82 storm system, virtually all major dendritic snowfall events had echo tops in or near the dendritic temperature range.

Studies such as Kobayashi (1961) and Rottner and Vali (1974) have shown that laboratory grown dendrites only develop in environments supersaturated with respect to water. Marshall and Langleben's (1954) analysis suggests that effective supersaturations at ice crystal surfaces are increased by the presence of cloud droplets. Together these studies suggest that the ideal environment for dendritic growth in the atmosphere would be a region of supercooled liquid water production between approximately -17°C and -13°C .

As discussed in Chapter 3, cloud top provides a unique environment for liquid water production, particularly in shallow cloud systems with cloud top temperatures warmer than about -20°C . In the Park Range region in wintertime, the tops of shallow cloud systems frequently are near or within the dendritic growth region. This was the case for seven shallow cloud systems occurring during the two month field program. These cases produced light to moderate (0.0 to 0.7 mm/h) snowfall primarily composed of dendrites. Fortunately, five of these cases were studied extensively, three with aircraft in the cloud top region. These data are summarized below.

(1) Characteristics of the dendritic growth region in shallow cloud systems

The 5 Jan 82 storm system underwent considerable evolution during passage through the Park Range region. During the period from 1400 to 1450, the storm system had characteristics discussed above -- the cloud system was shallow, had tops near -17°C , and produced light rimed dendritic snowfall. The tops of this cloud system were penetrated by aircraft and a descent sounding through the dendritic zone was completed upwind of the mountain range near CG. This cloud system was chosen to discuss the characteristics of the dendritic growth region because it was the most complete data set. The other two cloud systems with aircraft data had similar characteristics. Data from these systems will be included in the discussion where appropriate.

Figures 59 and 60 contain photographs of decelerator slides taken in the cloud top region during the 5 Jan 82 and 23 Jan 82 shallow storm events. On these slides, dendritic and stellar crystals were interspersed among liquid water droplets and liquid water accumulations. Some rimed particles were also evident. These slides show that dendritic crystal production can occur quite rapidly near cloud top in these systems due to the presence of water droplets. The presence of dendrites indicates that saturation with respect to water is maintained in this region of the cloud and that water supersaturations probably often occur. Once formed, the growth of these dendritic crystals was rapid. Figure 61 shows a series of 2D-c images taken during a descent through cloud top and the dendritic growth temperature range during the 5 Jan 82 storm. Over the 800 m (4°C) vertical distance, particles nucleated and grew into stellar structures. By the time the particles

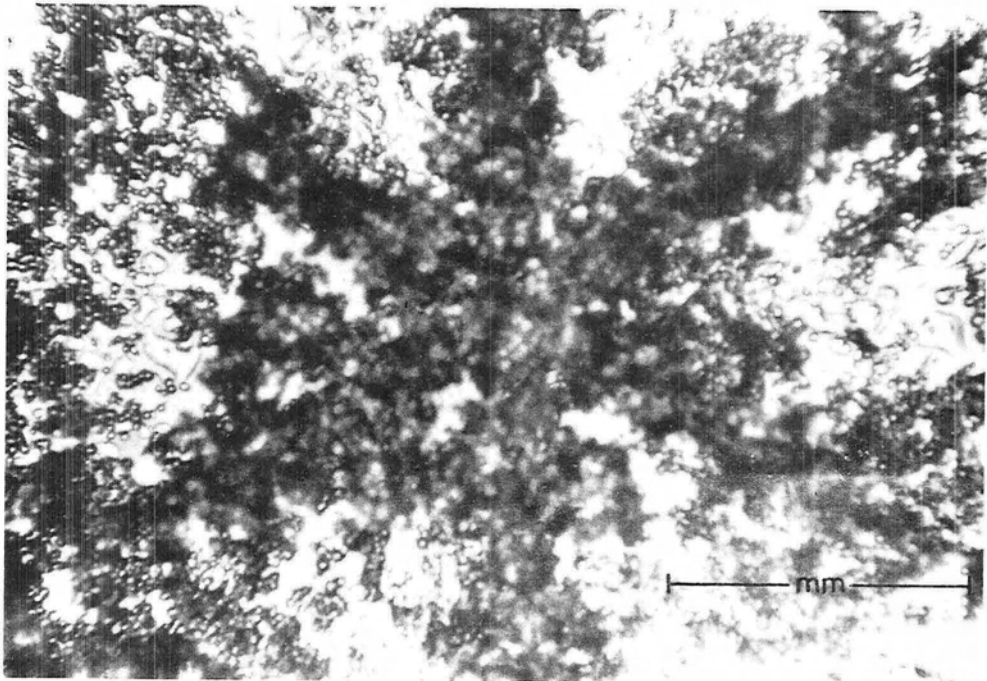
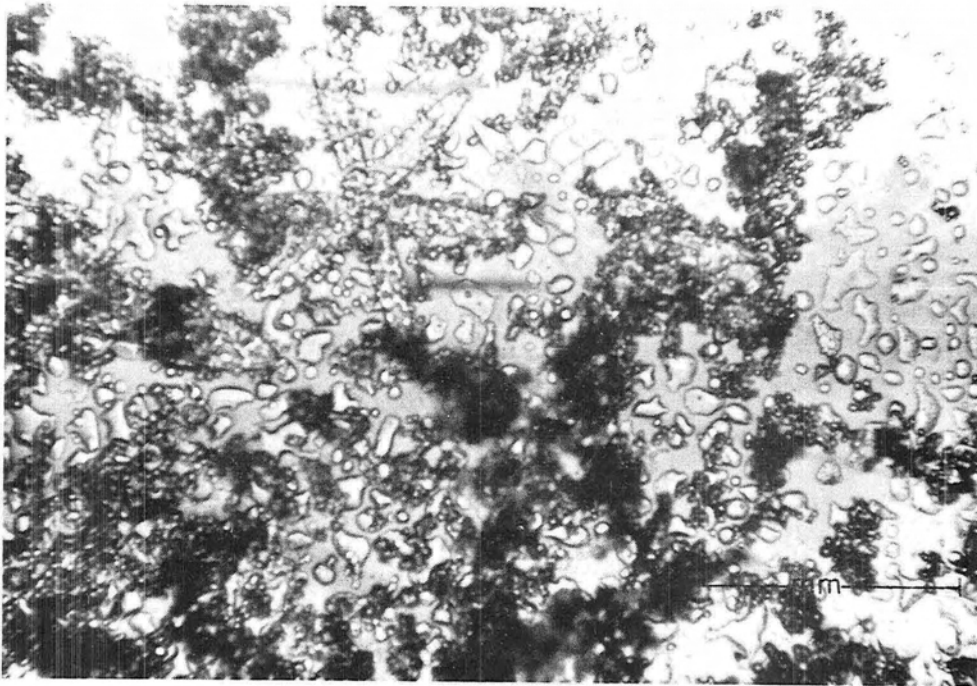


Fig. 59. Photographs of decelerator slides from 5 Jan 82 flight when the shallow storm system was present.

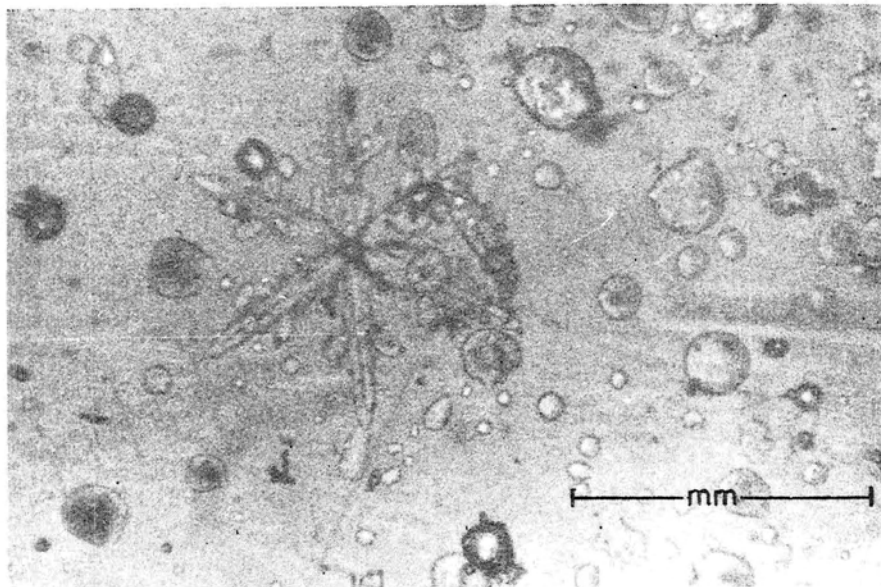
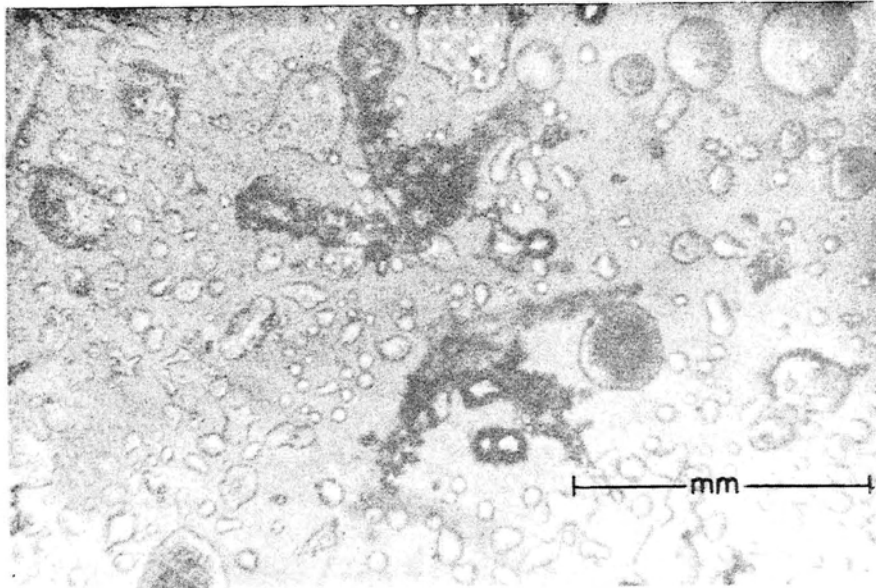


Fig. 60. Photographs of decelerator slides from 23 Jan 82 flight near cloud top.

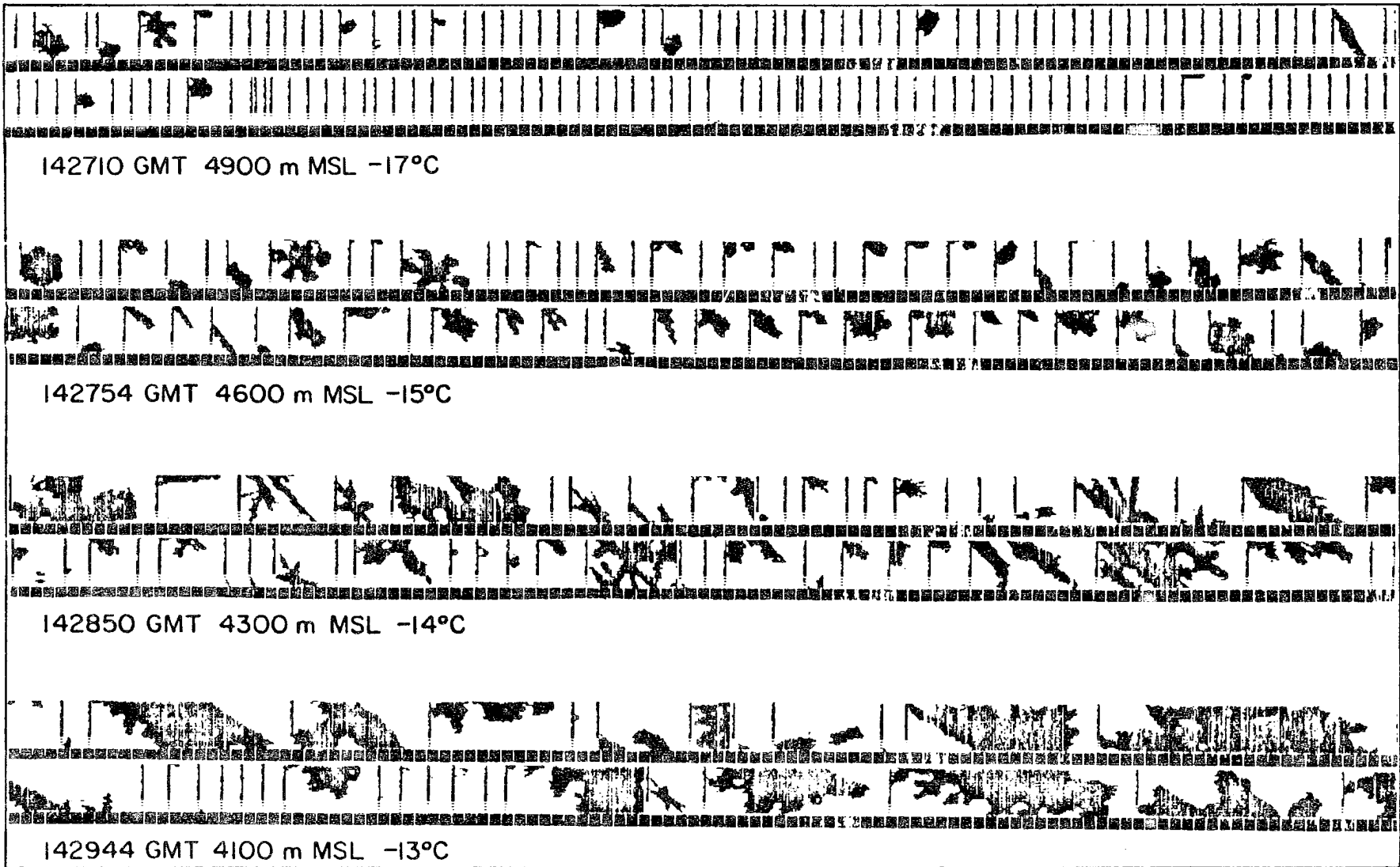


Fig. 61. 2D-c probe images showing the growth of dendritic crystals in the 5 Jan 82 shallow storm system.

had fallen 800 m, they reached proportions (2-3 mm) where aggregation was occurring.

Approximate growth rates for dendritic particles can be estimated in this cloud. Consider a particle which nucleated at 4900 m (-17°C) and fell 800 m to -13°C , growing to a size of 3 mm (largest image) during the fall. If one assumes an average fall velocity of 0.3 m/s over the distance of the fall, the average growth rate would have been 1.1 $\mu\text{m/s}$. This estimate is not far from those carefully measured in the laboratory by Ryan et al. (1976). Ryan et al. found growth rates near 1.0 $\mu\text{m/s}$.

(2) Trajectories of dendritic crystals in shallow storms

The rate at which dendritic crystals formed in the upper cloud region actually reach the surface is a function of the horizontal extent of the cloud system and the wind velocity profile in the cloud. These parameters change considerably from cloud to cloud as well as within storms due to variations in the vapor supply in the upwind airstream. For this reason, generalizations about trajectories and precipitation rates are not warranted.

However, the 16 Jan 82 shallow cloud system provided an opportunity to estimate various trajectories of ice particles arriving at the observation sites RAD and SPL. 16 Jan 82 was chosen because this storm had a well defined upwind cloud edge. Figure 62 shows a profile of the cloud system. Mean particle trajectories are shown for particles arriving at RAD and SPL. Each trajectory was calculated assuming a mean net fall speed. Size thresholds of particles growing at 1 $\mu\text{m/s}$ growth rates from the cloud boundaries are also shown. If one assumes that the mean fall speed of an unrimed dendrite throughout its trajectory was

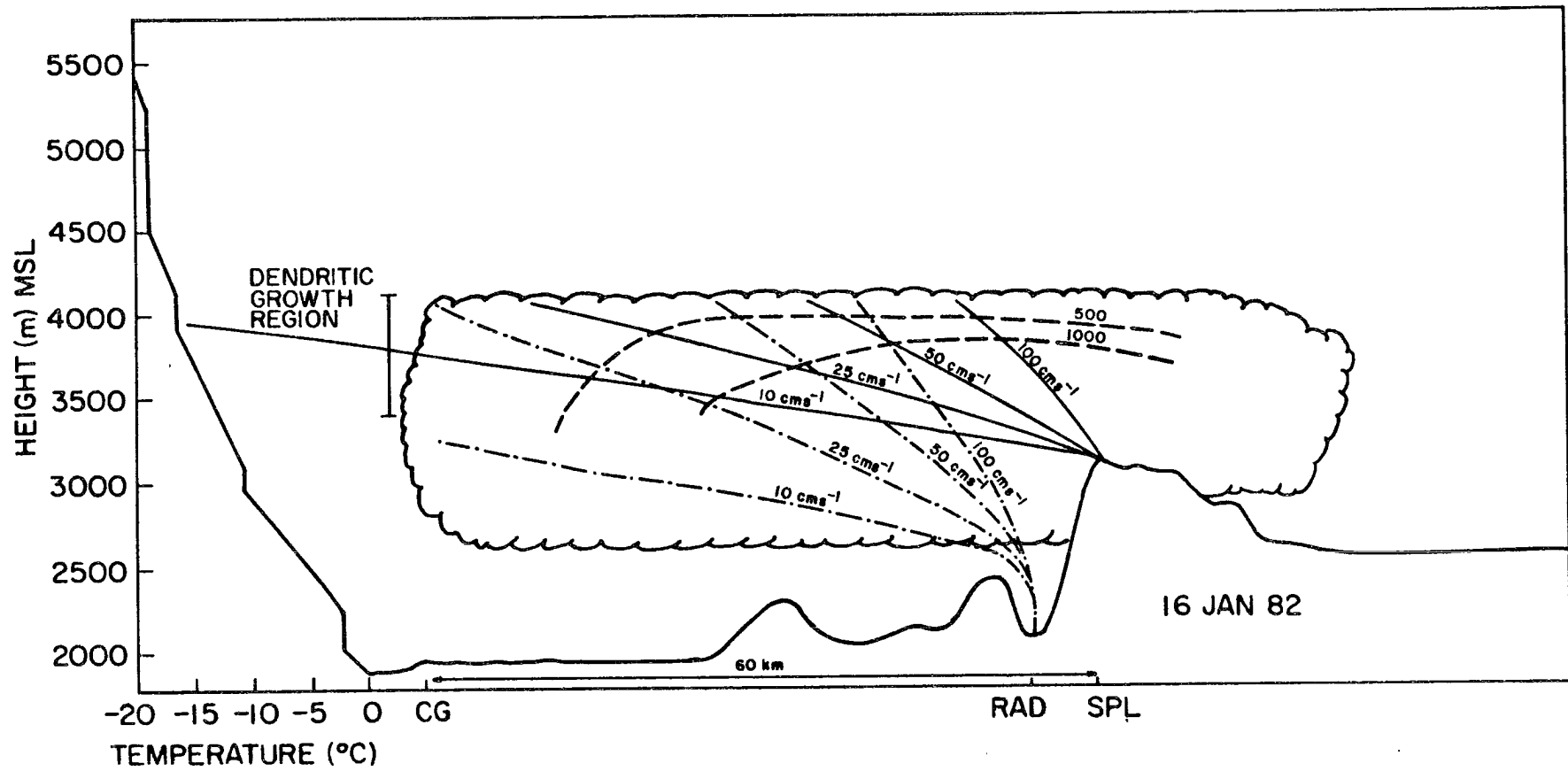
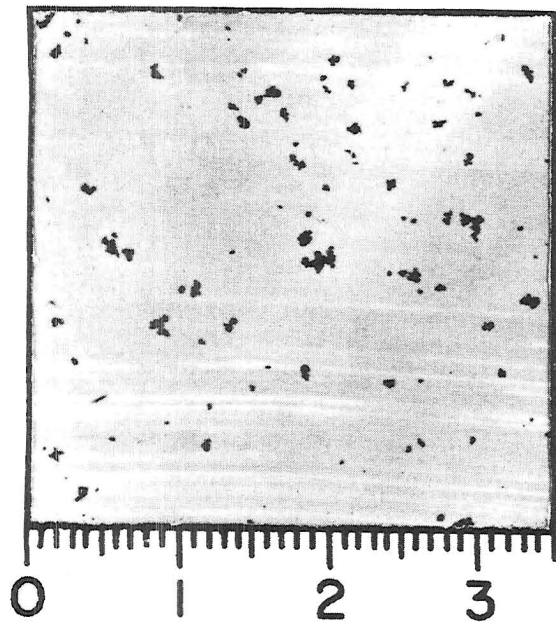


Fig. 62. Calculated trajectories of ice particles arriving at RAD and SPL for various mean fall speeds.

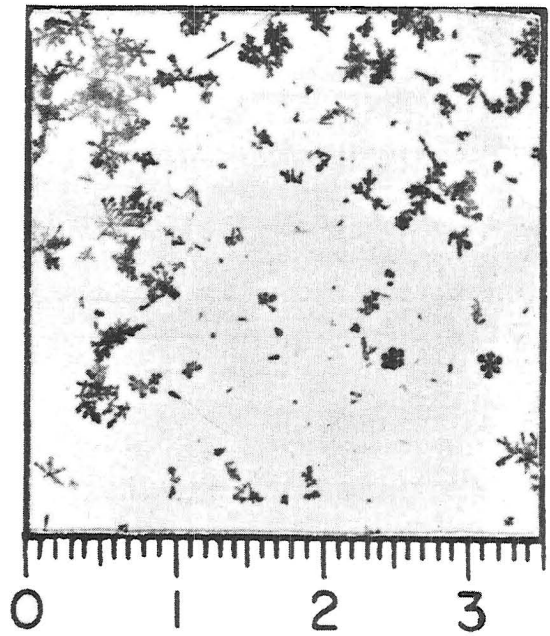
only 0.1-0.25 m/s, crystals originating in the dendritic zone near the upwind edge of the 16 Jan 82 cloud system could still arrive at RAD. Riming in the low levels and near the barrier crest would increase the particle fall velocity and subsequent likelihood of surface impact occurring in the valley. Aggregation would also contribute to higher fall velocities. At higher mountain elevations, the probability of many particles reaching the surface is greater. If one considers the effects of riming on the fall velocities of the particles near the mountain crest, it is clear that many of the dendritic particles formed in the cloud would impact near mountaintop. This is one reason why heavier snowfall rates consistently occur near mountaintop during these shallow storm events. However, cloud systems with much greater horizontal extent have a much greater capacity to produce valley as well as mountain snowfall. The storm of 14 Dec 81 was such an event. Valley snowfall rates were as high as 0.7 mm/h during this storm. Figure 63 b,c,d shows photographs of dendrites collected at RAD during this storm.

(3) Dendritic snowfall from deep storms

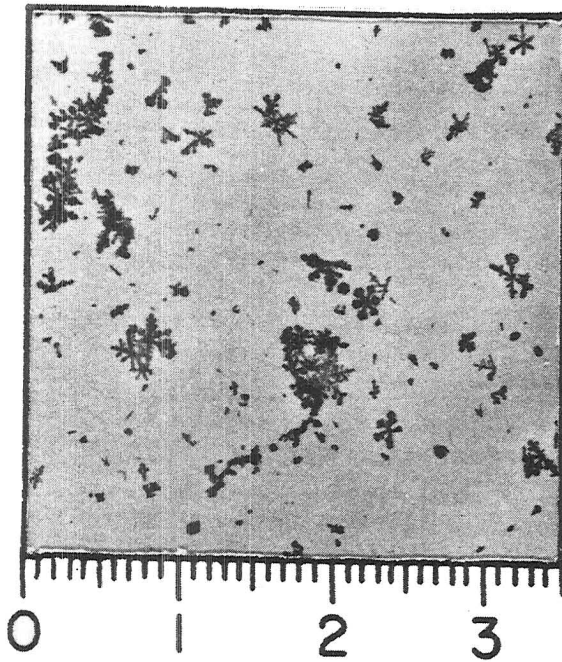
Shallow storm systems dominated dendritic snowfall events during the 1981-82 field season. However, occasional dendrites were observed to fall from deeper cloud systems with cold tops. On only one occasion were dendrites the dominant habit in snowfall from deep clouds. This case also occurred on 5 Jan 82 during the deep storm phase from 1450 to 1700. The complete 5 Jan 82 case is described in detail in Sec. 6 on aggregation processes. Evidence from the 5 Jan 82 aircraft soundings over RAD suggest that dendrites formed in this cloud system in the absence of supercooled water. However, these observations are not conclusive because they were limited to one point very near the mountain



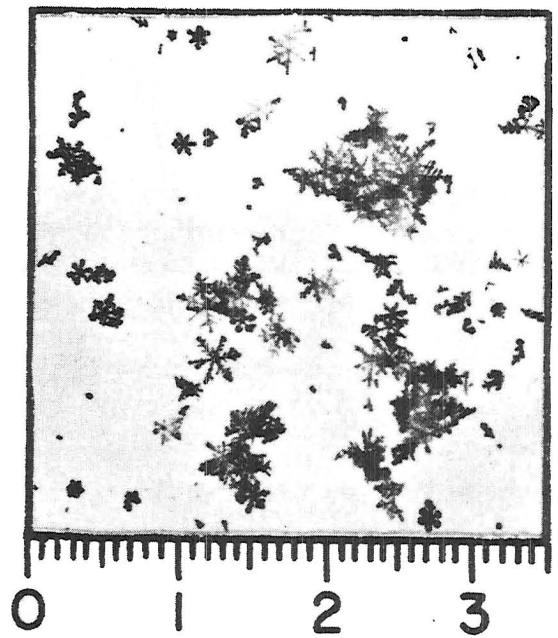
a



b



c



d

Fig. 63. Dendritic crystals observed at RAD on 13 Dec 81 (a) and 14 Dec 81 (b,c,d).

crest. The possibility that supercooled liquid water existed upwind of the mountain cannot be ruled out. Pilot reports from the research aircraft indicated an upper deck prior to the onset of the deep cloud system and virtually no cold temperature crystals were observed at the surface throughout the deep storm event. These observations suggest that a multilayer cloud system may have been present upwind of the sounding location. Without more data, the source of the dendrites observed at the surface during this deep storm event are speculation at best. However, it is important to document that such cases do occur.

B. Cold temperature crystals

The origin and diffusional growth patterns of crystals formed at cold cloud temperatures are particularly difficult to assess with field data. In this section, the complexities which lead to the wide variety of crystal forms originating at cold temperatures ($<-20^{\circ}\text{C}$) are discussed qualitatively. This section is included because the most important component of Park Range cloud system precipitation, irregular crystals, include these cold temperature habits.

Studies of crystal diffusional growth in the literature have concentrated on measurement of the growth rates, dimensions and habits of crystals growing at particular temperatures and vapor density excesses (aufm Kampe, 1951; Nakaya, 1954; Hallett and Mason, 1958; Kobayashi, 1961; Rottner and Vali, 1974; Ryan et al., 1976). These experiments have provided important information about the growth of natural ice crystals in the atmosphere. However, in natural cloud systems, ice crystals are continuously exposed to variations in temperature and vapor density excess, as well as pressure, proximity to supercooled liquid water droplets, ventilation rates and several less

significant factors. The combined effect of all of these variations on the actual diffusional growth of natural ice crystals is unknown. Clearly, a crystal collected at the ground at a temperature of -3°C which originated hundreds of kilometers upwind at a temperature of -29°C can possess characteristics of many growth environments. Since each individual crystal encounters a unique set of environmental conditions during its trajectory, a wide variety of complex crystal shapes can be expected. Indeed, this is the case in Park Range cloud systems, particularly those clouds with tops much colder than -20°C . Figure 64 shows the percent of irregular single crystals appearing on shadow photograph as a function of echo top temperature. Nearly all the photographs taken when the echo top was colder than -20°C contained a high percentage of irregular single particles. The two outlying points colder than -30°C (L and J) occurred during a period of dendritic snowfall and aggregated snowfall respectively. Virtually all other points were above 50% and most above 70%. As discussed earlier, a large class of irregular crystals were composed of variable combinations of sideplanes, plates, columnar and planar extensions and irregular protrusions. These irregular particles, characteristic of cold temperature growth, are clear records of the variable environments in which they grew.

An important aspect of deep wide-area cloud systems is the influence that the crystal flux from colder cloud levels can have on the mid-level dendritic growth layers. In this data set, dendritic crystals seldom appeared in significant numbers during periods of heavy irregular crystal snowfall. In most cases, the two crystal habits seldom appeared together at all. One possible reason for such exclusion is that

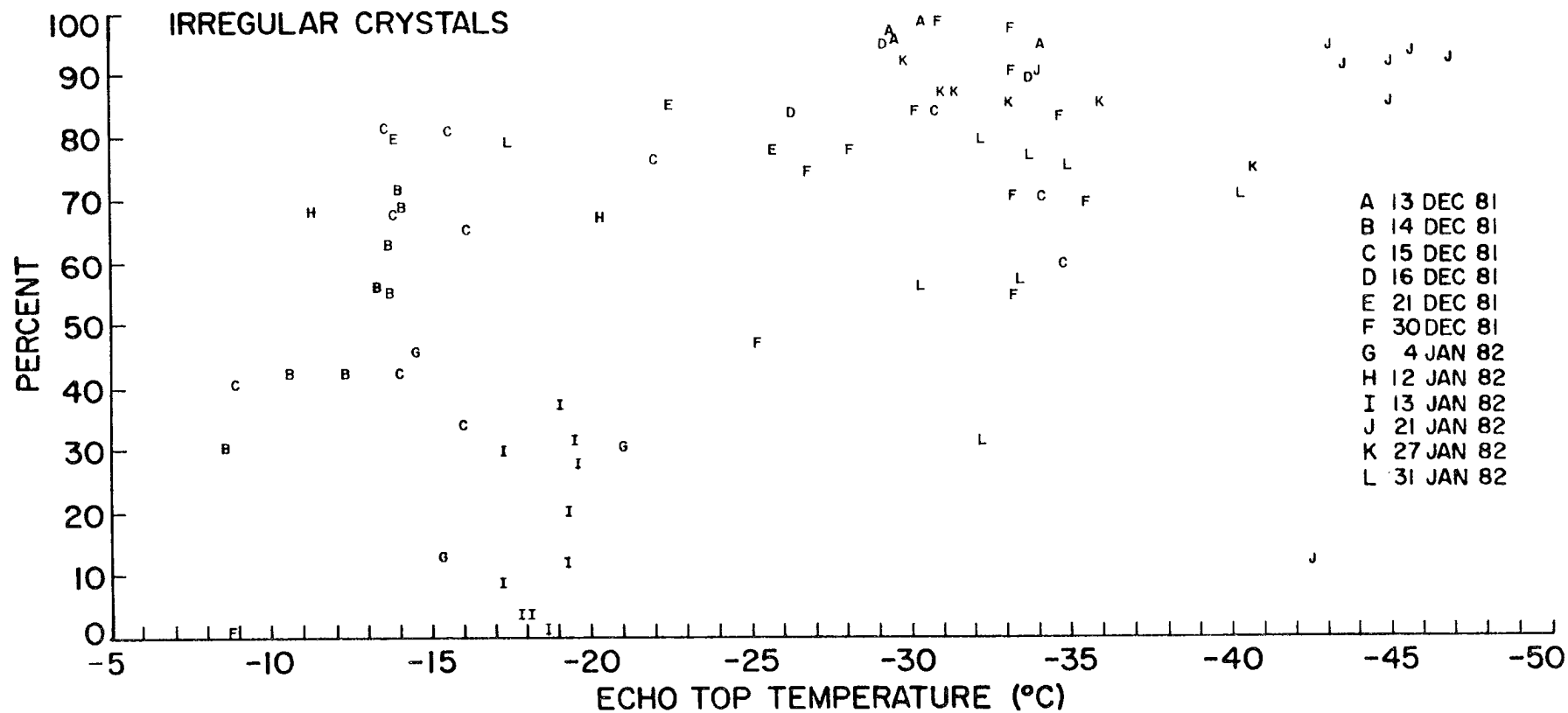


Fig. 64. Percent of irregular crystals appearing on shadow photographs as a function of echo top temperature.

dendritic crystals require water supersaturation to develop. A significant flux of cold temperature crystals through the dendritic zone would reduce the potential for such supersaturations to occur. Thus, to a large degree, the crystal habits would be mutually exclusive. The available data suggests that this often is the case.

C. Warm temperature crystals

Warm temperature ($> -10^{\circ}\text{C}$) crystals are crystals which nucleate and grow in the lowest, warmest levels of Park Range cloud systems. In general, such crystals should not have a structure confounded by multiple growth regimes and should appear in precipitation as columns or needles. In Chapter 3, the presence of supercooled water near cloud base was partially attributed to the scarcity of these crystals in the low levels of many orographic cloud systems. In this section, this assumption is evaluated more quantitatively.

Figure 65 shows the percent of columnar crystals (N1c, N1e, N2c, C1c, C1e, C2a, R1b, CP1a, CP1b, CP1c) appearing on the shadow photographs as a function of echo top temperature. Figure 66 shows a similar plot for needles (N1a, N2a). 60% of the photographs taken when echo tops were warmer than -20°C had no columnar crystals whatsoever. 87% of the photographs contained less than 2% columnar habits. However, 3 photographs did contain 4-7% columns and one photograph on 12 Jan 82 had a large population (16.8%) of columns. Radar echoes on this day were shallow and broken suggesting small isolated cloud cells.

With the exception of 15 Dec 81, needles were quite rare in Park Range cloud systems. Most observations contained no needles at all. Needles exceeded 2% of the crystal population on only one photograph (21 Dec 81) excluding the 15 Dec event. The high percentage of needles

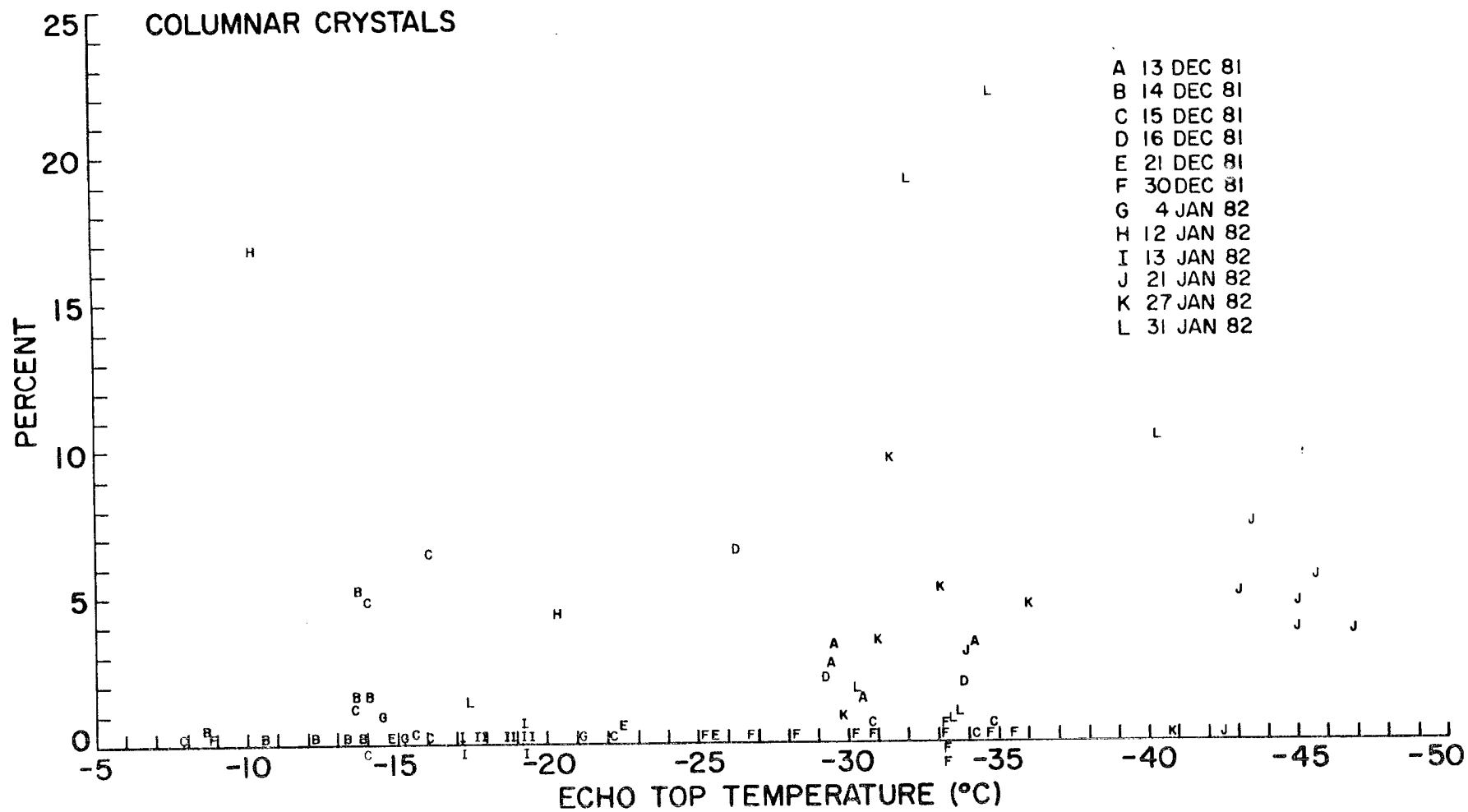


Fig. 65. Percent of columnar crystals appearing on shadow photographs as a function of echo top temperature. Columns include habits N1c, N1e, N2c, C1c, C1e, C2a, R1b, CP1a, CP1b, and CP1c in this analysis.

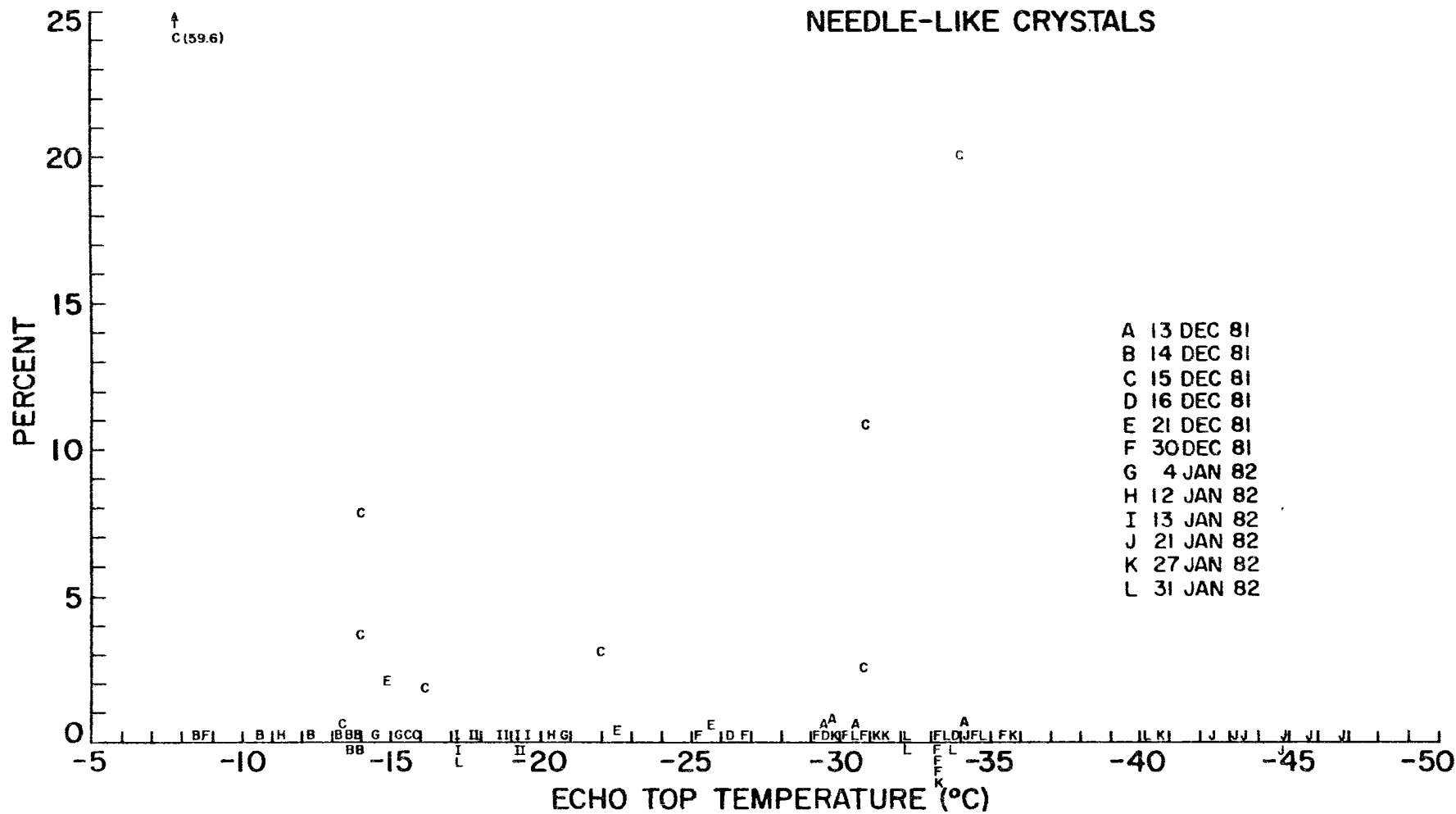


Fig. 66. Percent of needles appearing on shadow photographs as a function of echo top temperature. Needles in this analysis include N1a and N2a habits.

present in snowfall on 15 Dec 81 may have been associated with secondary ice particle production. This case is discussed in detail in Sec. 4.

The large majority of the cloud systems with echo tops warmer than -20°C contained few ice particles nucleated and grown at temperatures warmer than -10°C . Although such particles do exist, they seldom exceeded more than 2% of the total crystal population arriving at the ground as precipitation. The important exception was the 15 Dec 81 case.

The data on Figs. 65 and 66 also extend to the cold temperature ranges. Columnar crystals were more commonly observed during cold cloud events. Although such particles probably originated in the higher cloud levels, the possibility exists that at least some of them originated at warmer cloud temperatures. With the present data, no conclusion could be drawn. However, the columnar crystals were generally a mix of pure columns as well as capped columns and bullets. The latter two are associated with cold temperatures which suggests that the remaining columns indeed fell from the high cold regions of the cloud.

3. Ice nucleation

The primary work on natural ice nucleation processes in Park Range cloud systems will be published shortly by DeMott et al. (1986), hereafter referred to as DM. For completeness of this present work, the article by DM is summarized here. Two additional data sets not included in the DM study are addressed in later sections.

A. Review of DeMott et al. (1986)

Previous work on ice nucleation in orographic cloud systems, reported by Cooper and Vali (1981) and Rogers (1982), described the formation and development of ice crystals in cap clouds over Wyoming's

Elk Mountain. Both of these studies found that ice originated only in association with the initial condensation at the upwind edge of the cap cloud. These investigators concluded that condensation freezing or contact nucleation were functioning.

DM extended the work of these investigators by studying nucleation processes in two larger orographic cloud systems over the Park Range. The cloud systems occurred on 16 Jan 82 and 23 Jan 82. DM used the laboratory developed chemical kinetics methodology described by DeMott et al. (1983) to identify the primary mechanism of ice nucleation operating in these cloud systems. DM showed that rate constants governing the formation of ice crystals in nucleation regions of these clouds were too large to support contact freezing nucleation. DM calculated that ice nuclei would have to have radii $< 0.007 \mu\text{m}$ to account for the rapid nucleation rates observed. Such radii are unrealistically small for atmospheric ice nuclei.

Evidence supporting condensation freezing nucleation as the dominant nucleation mechanism was presented by determining the rate constants for ice crystal formation in nucleation zones and comparing them with supersaturations estimated from droplet spectra changes. Rate constants, estimated supersaturations, and increases in total ice crystal concentration all correlated well, strongly implying that condensation freezing nucleation was the dominant mechanism.

One region of apparent ice crystal enhancement with a behavior anomalous to that observed upwind of the Park Range occurred in the descending air on the lee side of the mountain. In this region, cloud ice crystal concentrations rose sharply in coincidence with rather strong liquid water depletion. The source of the crystals could not be

identified from the data set. DM hypothesized that contact nucleation by thermophoretic collection (Young, 1974a) may have occurred or that the aircraft may have encountered a region of compressed airflow in the descending lee wave which induced a local convergence of ice crystals.

DM used arguments presented in Chapter 3 to show that the cloud top environment is favorable to liquid water formation. Because this region is the coldest region of the cloud and has a favorable water balance for supporting water supersaturations, DM concluded that the cloud top region acted as a primary source region for ice crystals. However, DM noted that cloud top temperature alone will not correlate well with ice crystal concentrations in a set of observations of many orographic cloud systems because supersaturations at cloud top are also a function of vertical velocity as well as ambient droplet and ice crystal size spectra and concentration. DM also pointed out that ice nucleation may well occur in the lower regions of the cloud where liquid water production is occurring. Data were too sparse to address such a problem conclusively.

Summarizing from DeMott et al. (1986):

"In the case studies of winter orographic cloud systems presented, primary ice crystal nucleation was identified to occur mainly in association with liquid condensate production. Condensate production occurred not only at cloud edge, but within the upper cloud region, in regions where orographically induced lifting was occurring. A correlation between the estimated supersaturation and both the numbers and rates of appearance of new ice particles supported condensation freezing as the functioning ice nucleation mode. The dependence of this nucleation mode on both temperature and supersaturation makes it difficult to determine a simple ice nucleus temperature spectra and could easily be a source of a wide variance of ice crystal concentrations at a particular temperature. The quantification of such a process is not possible with the small data set presented in this paper. Laboratory methods, such as those employed by Rogers (1982) are perhaps the best approach to quantifying the condensation freezing process for a range of temperatures and supersaturations.

Theoretical calculations of the water balance in the upper cloud regions of the systems studied explained the frequent existence of liquid water in these cloud regions and confirmed this to be a location favorable for condensation freezing nucleation to occur on natural nuclei. Cloud top is a primary source for natural nucleation because of 1) supersaturations generated in this region, 2) the location near to a continuous nucleus supply (via cloud top entrainment), and 3) the occurrence of the coldest cloud temperatures there."

The study of DM examines the nucleation process at the top of two shallow cloud systems. However, evidence from other cases suggests that nucleation may occur deeper within the cloud, particularly in the region of orographic lift. The 21 Dec 81 case study is an example of a case when nucleation may have occurred interior to the cloud. This case is described in the following section.

B. 21 Dec 81 case study

The 21 Dec 81 storm system was a deep cloud system with tops near -31°C . The data used in this study were collected during a west to east pass toward and over the Park Range at the -16°C level. A data analysis similar to that of DM was not possible because ice crystals at the observation level could have originated above, below or at the observation level. However, this case is important because it does provide evidence of ice nucleation in mid-levels of deep mountain cloud systems. The newly nucleated crystals developed in the primary lift zone of the Park Range.

Ice crystal concentrations along the flight path are displayed on Fig. 67. Crystal concentrations were steady at about 10 l^{-1} until the aircraft was about 10 km upwind of the Park Range crest. Between this point and the east slope of the range, concentrations rose somewhat monotonically to 35 l^{-1} . Shown on Fig. 68 are six ice crystal size spectra taken along the flight path. The spectra are averages over 30

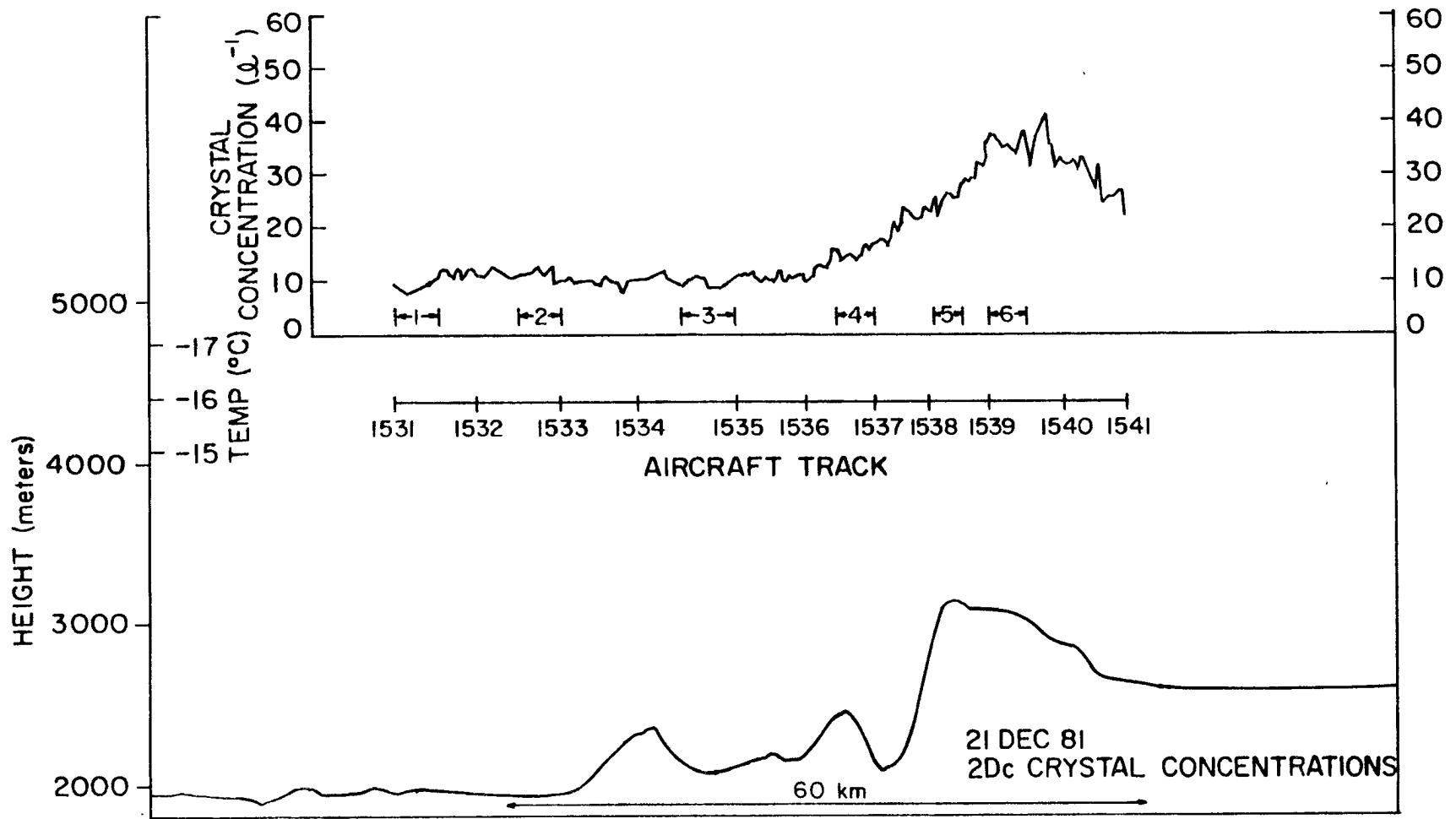


Fig. 67. Flight track and ice crystal concentrations for the west to east track at $-16^{\circ}C$ on 21 Dec 81. Locations of ice crystal size spectra on Fig. 68 are also displayed on this figure.

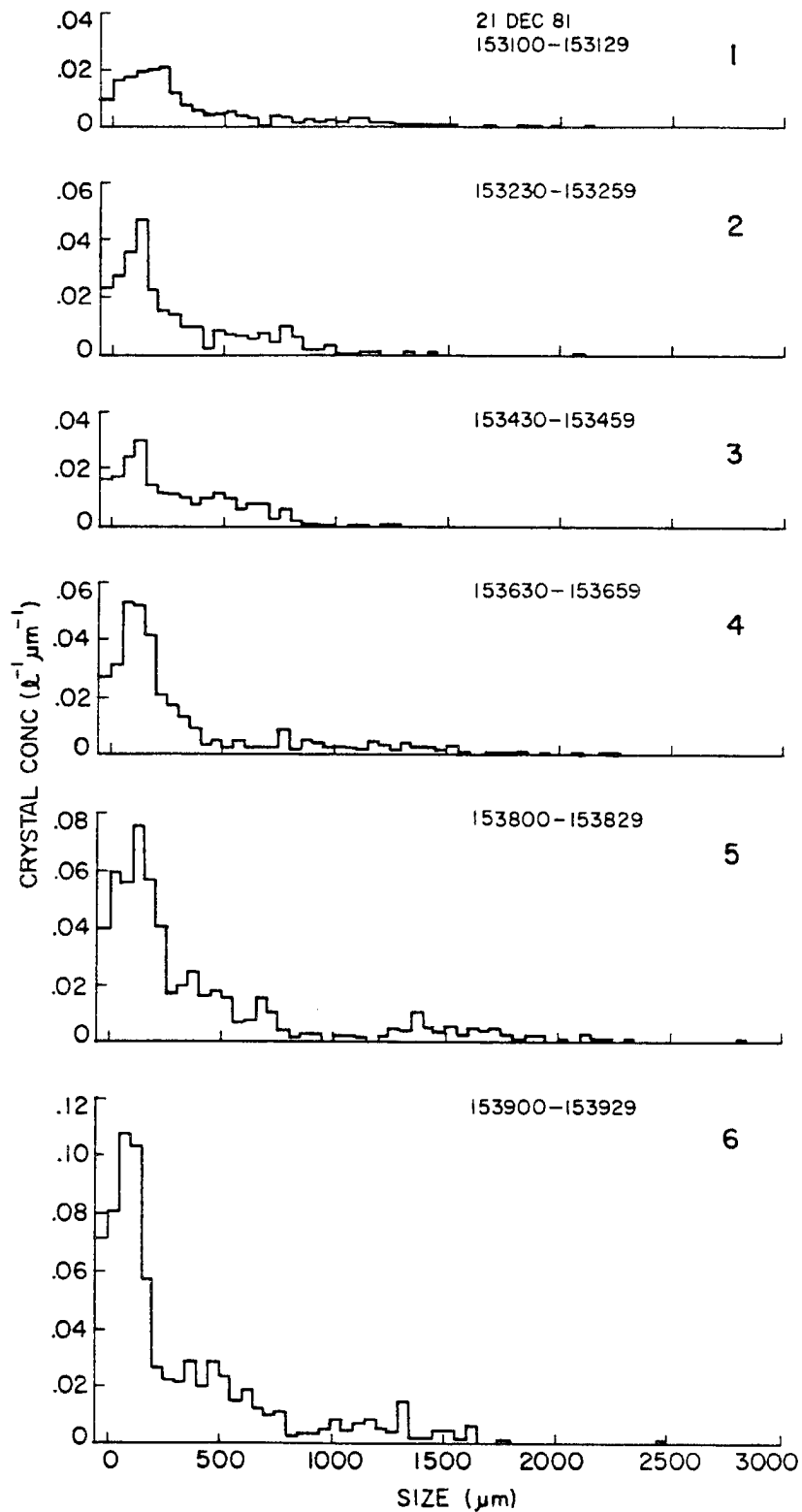


Fig. 68. Ice crystal size spectra for points on the -16°C west to east flight track displayed on Fig. 67. Zero area images are displayed as a separate category to the left of the zero. These particles were assumed to have sizes spanning a $50 \mu\text{m}$ binwidth to correspond to this diagram.

seconds. The locations of these spectra on the flight track are indicated on Fig. 67.

From the spectra, it is evident that the majority of the contribution to the crystal concentration enhancement near the Park Range came from particles less than 250 μm in diameter. Between points 4 and 6, the concentration of particles with sizes less than 100 μm increased by a factor of 2-3. If one assumes a slow growth rate of 0.1 $\mu\text{m s}^{-1}$ for these particles, and assumes that the particles fell (or rose) through the cloud at 0.1 ms^{-1} during the growth, the nucleation point of these particles would be within 100 vertical meters ($< 1^\circ\text{C}$) of the observation point.

The most intriguing aspect of this data set was the absence of liquid water along the flight path. Virtually no liquid water was observed. If the small ice particles near the crest nucleated in the absence of measurable liquid water, the possible nucleation mechanisms are limited to deposition or sorption nucleation.

The increase in concentration was sufficiently close to the range (the peak concentration was east of the crest) that increases in concentration could have been associated with airflow compression in the primary mountain wave. Small particles could have developed due to fracturing of larger particles as collision rates increased in turbulence near the mountain crest. In short, other possibilities exist to explain the observations. However, the most likely explanation is nucleation by sorption or vapor deposition. If this is the case, the mechanism must require sufficient vapor supply rates since it was limited to the region near the mountain crest. Additional evidence must be obtained in future field work to determine if deposition or sorption

nucleation is important in Park Range cloud systems. Clearly, such mechanisms may be operating.

C. Surface measurements

In this section, measurements of precipitation rate, number flux (from shadow photographs), and echo top temperature are used to examine the relationship between echo top temperature and the flux of crystals to the surface.

Figure 69 shows the relationship between precipitation rate and number flux of particles arriving at the surface. In general, the number of particles arriving at the surface increases as the precipitation rate intensifies. Variations in particle densities due to various growth modes and disparity in the sample times necessary to take a shadow photograph (5-60 s) and make a precipitation measurement (15 min) contribute to the scatter.

Figure 70 shows the corresponding relationship between number flux and echo top temperature. With the exception of two points, all of the measurements with echo top temperatures warmer than -22°C produced precipitation with number fluxes no greater than $0.5 \text{ cm}^{-2} \text{ s}^{-1}$. In contrast, clouds with echo tops colder than -22°C produced precipitation with crystal number flux as high as $2.36 \text{ cm}^{-2} \text{ s}^{-1}$. 64% of the observations with echo tops colder than -22°C were greater than $0.5 \text{ cm}^{-2} \text{ s}^{-1}$. The data of Fig. 69 imply that these deep cold clouds can generally be associated with higher precipitation rates.

These data tend to confirm that nucleation processes are more effective in clouds which extend to temperatures colder than -22°C . However, it must be remembered that cloud depth is increased in these

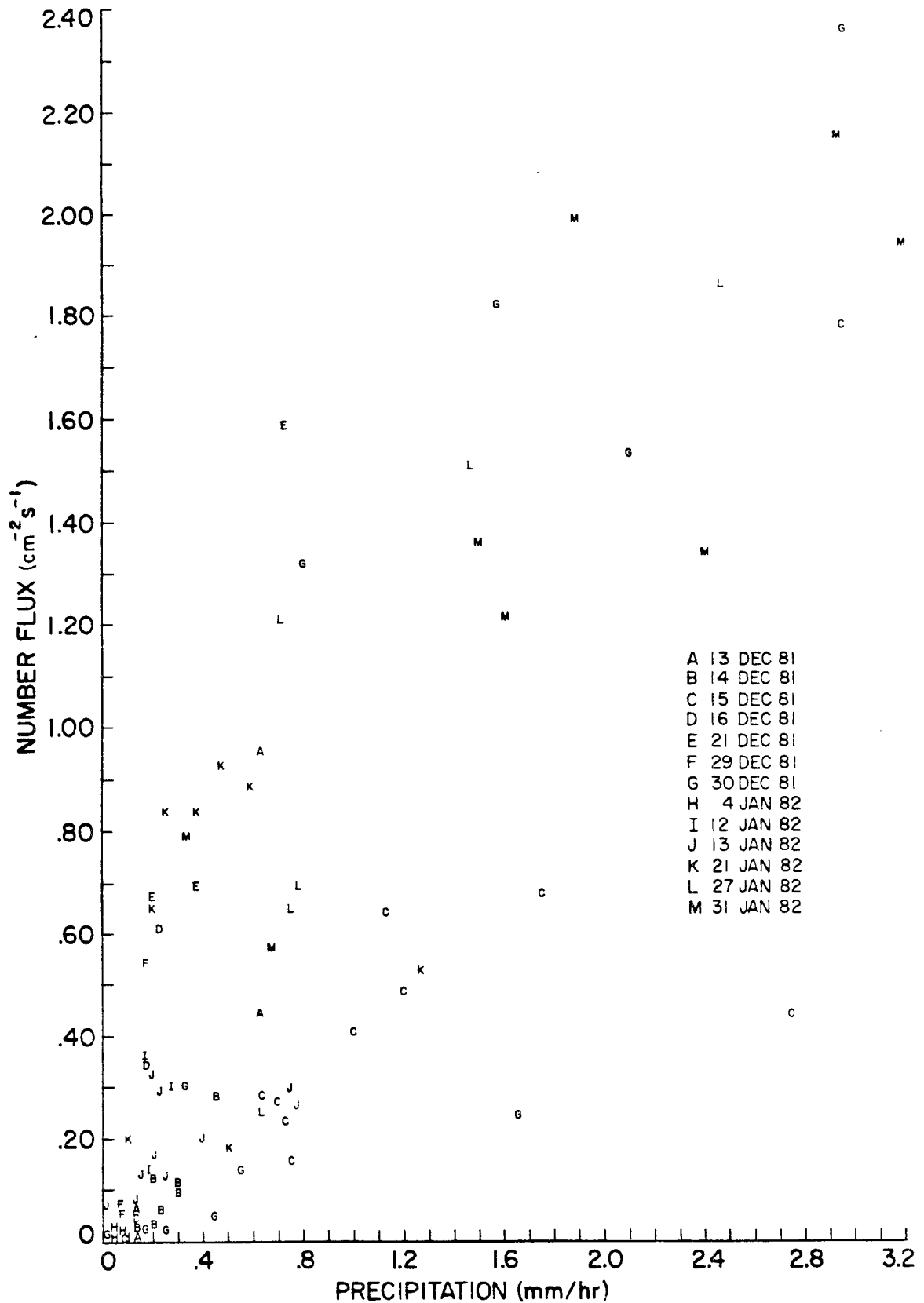


Fig. 69. Number flux vs. precipitation rate for the 1981-82 data set. Number flux was determined from individual shadow photographs.

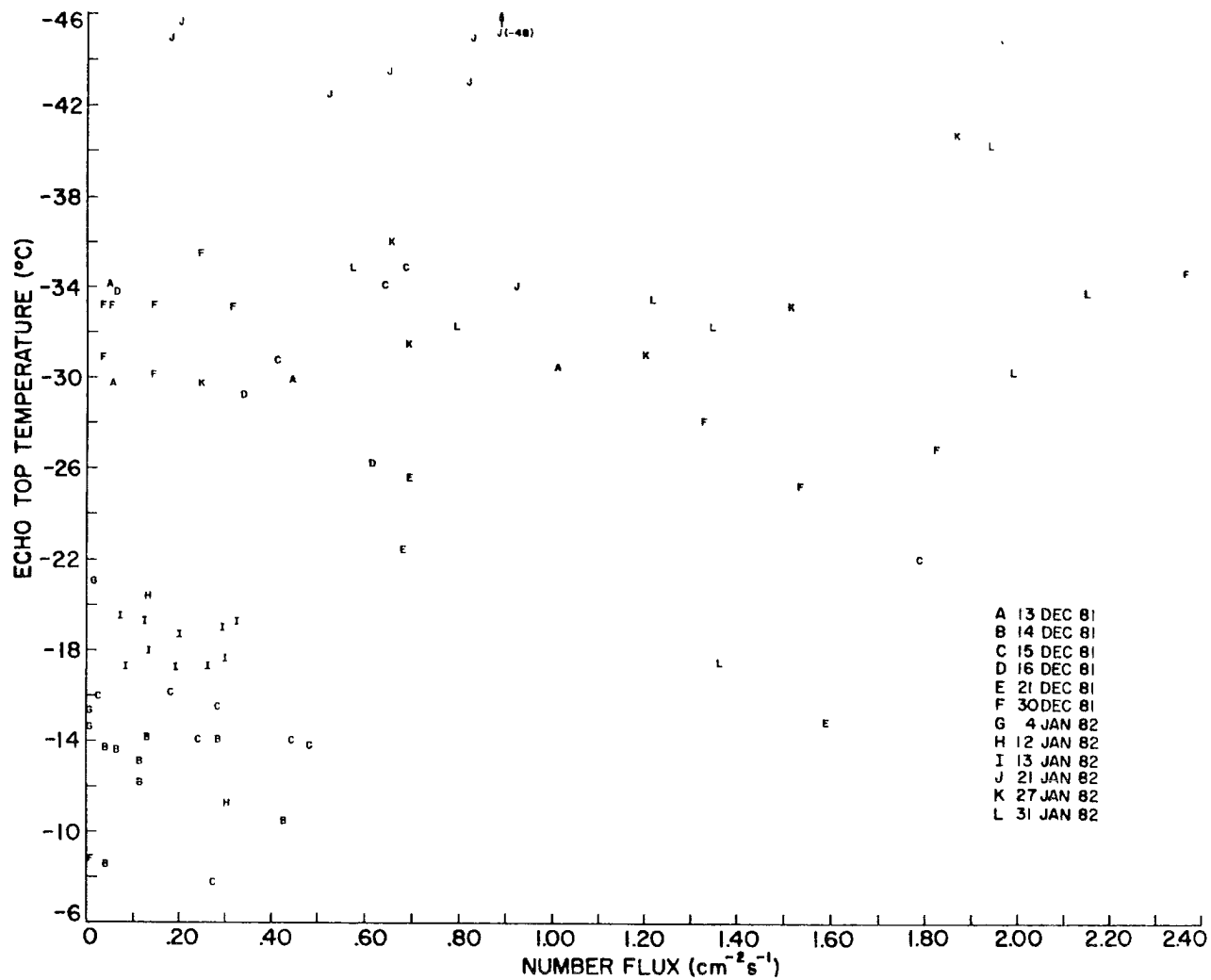


Fig. 70. Number flux vs echo top temperature for the 1981-82 data set. Number flux was determined from individual shadow photographs.

cases. The greater depth of cloud alone can contribute more crystals to the surface precipitation.

4. Ice multiplication

In this section, the physical evidence for secondary ice particle production in Park Range cloud systems is presented. Of the physical mechanisms suggested for ice crystal concentration enhancement, three have received considerable attention in the literature. These include (1) crystal fragmentation during collisions of ice particles; (2) ice splinter formation during riming and (3) droplet fragmentation during freezing. Based on criteria established in the literature and physical observations collected during the field programs, the potential of each of these mechanisms to modify crystal concentrations in Park Range cloud systems is assessed. A review of current research concerning these mechanisms precedes the analysis.

A. Review

(1) Crystal fragmentation: Field observations and modelling studies of crystal fragmentation in clouds have been reported by Hobbs and Farber (1972) and Vardiman (1972, 1978). Hobbs and Farber found that 50% of all stellar crystals collected at the ground in Washington's Cascade Mountains were fragments. The habits most frequently fragmented were P1b-f, P2a, P2f, P2g, P4b and CP1a. Using a simple model, they showed that fragmentation was probable when a 1 mm stellar crystal collides with droplets with diameters greater than 150 μm or graupel greater than 800 μm .

Vardiman (1972) investigated crystal fragmentation in four storms over the central Colorado mountains. He found an increase in the concentration of fragments during the passage of convective cells

embedded in orographic clouds. No habit discrimination was reported in his study. In his later paper, Vardiman (1978) observed collisions between natural particles and a fixed plate. By measuring the number of fragments produced and the fall velocity of the initial particle, he was able to parameterize fragmentation as a function of momentum of the initial particle, crystal habit (planar dendrites, spatial dendrites, and graupel) and degree of rime. He used this parameterization in a model of fragmentation which incorporated collision frequency and a "fragment generation function". His model results indicated that a broad distribution of ice particles promoted fragmentation, that unrimed particle collisions did not result in secondary ice particles, that fragmentation increases as particles become more heavily rimed, and that smooth orographic clouds are unlikely to produce fragments. The results of Hobbs and Farber suggest that Vardiman underestimated the fragmentation potential of dendritic crystals.

(2) Ice splinter production during riming: Prior to the classic experiments of Hallett and Mossop (1974), several studies of ice splinter production during riming failed to show any appreciable increase in the formation of secondary ice particles (Aufdermaur and Johnson, 1972; Mossop et al., 1974; Hemni, 1974). In 1974, Hallett and Mossop showed that copious numbers of ice splinters could be produced during riming under particular conditions not present in any of the previous experiments. Subsequent experiments by Mossop and Hallett (1974), Goldsmith et al. (1976), Mossop (1976) and Mossop (1978) defined conditions necessary for the ice splintering process to occur. These experiments showed that (1) ice splinter production was confined to a temperature range of -3°C to -8°C ; (2) the cloud must contain droplets >

25 μm diameter and $< 13 \mu\text{m}$ diameter; and (3) the cloud must contain ice particles large enough to initiate riming. They found that the production of splinters during riming reaches a maximum at -5°C . At this temperature, approximately one splinter is produced for every 250 droplets of $> 25 \mu\text{m}$ diameter accreted. Chisnell and Latham (1976) showed that this mechanism could account for the high concentration of ice particles observed in many marine cumuli with relatively warm ($> -10^{\circ}\text{C}$) tops (Mossop, 1970).

Subsequent experiments (Mossop and Wishart, 1978; Choularton et al., 1978; Mossop, 1980; Choularton et al., 1980; Griggs and Choularton, 1983) have studied the mechanism of ice splinter production and the physical explanation for the bounds specified by the previous experiments. Griggs and Choularton (1983) provided the most comprehensive explanation to date. Their study showed that internal freezing of a droplet occurred in one of three modes depending on temperature, if the heat loss to the droplet was fairly symmetrical. These three modes were related to protuberance production on the freezing droplets. Griggs and Choularton estimated that 1% of the protuberances fragment to form secondary ice particles although they were unable to document such fragmentation photographically. However, Mossop (1980) and Griggs and Choularton (1983) showed that introduction of ammonia into riming droplets suppressed both ice splinter production and protuberance formation. These experiments strongly imply that a relationship exists between protuberance production and ice splinter formation.

(3) Droplet shattering upon freezing: Studies of droplet shattering upon freezing which pertain to this study are those which examined the

process for small droplets. Hobbs and Alkezweeny (1968) found that only a small fraction of 50-100 μm diameter droplets shattered at temperatures between -20°C and -32°C and at -8°C when nucleated by AgI suspended in the drops. In a later study, Brownscombe and Goldsmith (1972) found no significant shatter between -10°C and -15°C for smaller droplets in the size range 20-50 μm diameter. Finally, Bader et al. (1974) measured the number of sub-micron ice particles produced during a droplet freezing event in freefall for two droplet sizes. They found that fewer than 10 sub-micron fragments were ejected when an 84 μm diameter droplet froze and less than 1 fragment per droplet when 30-42 μm droplets froze. Many other studies of droplet shattering have been conducted, but these all pertained to droplets much larger than those found in Park Range cloud systems.

B. Ice particle fragmentation

This section examines crystal fragmentation as a mechanism for enhancing ice crystal concentrations in Park Range cloud systems. Surface observations of ice particle structure are compiled for each habit class. These observations imply that dendritic crystals have a high potential for fragmentation. Aircraft measurements of ice particle spectra suggest that high ice crystal concentrations in the dendritic growth region may be associated with fragmentation during dendritic snowfall events.

(1) Surface observations: Eighty-nine shadow photographs containing 51,193 individual particles were collected during 13 separate storm events. These particles were classified and examined for fragmentation. 71% of the crystals were irregular. The amount of fragmentation, if any, could not be accurately assessed for these complex shapes. 4% of

the crystals were contained in aggregates and their detailed structure was obscured. 2.4% were heavily rimed. An additional 1.1% were complex spatial crystals. Fragmentation for these crystals was also difficult to assess. The remaining 21.5%, about 11,000 crystals, were examined for evidence of fragmentation. The results are summarized in Table 10.

Two groups of crystals emerge from this compilation. The first group, consisting of needles, columns, sheaths, bullets, capped columns, and plates, all showed little evidence of fragmentation. The vast majority of the crystals in this group, with the exception of needles, were < 1500 μm in their longest dimension. Needles were larger, often reaching 3000 μm . The tips of the needles and sheaths did not appear to suffer from fragmentation, such as that observed by Hobbs and Farber (1972). This difference may be due to different crystal concentrations and collision frequencies in the cloud systems studied. Hobbs et al. (1974) observed aggregates of needles, a feature not present in Park Range cloud systems. These aggregates imply higher collision rates for needles and a greater potential for fragmentation.

The second group of crystals, dendrites, underwent significant fragmentation. 7669 dendritic crystal forms were observed. 21.2% were large fragments and 51.7% were broken branches. Fragmentation was common whether or not riming was occurring. However, fragments appeared more frequent when rime was present on the branches. Examples of fragments are shown on Fig. 63,b,c,d.

It is important to note that fragmentation can occur as a result of impact with other crystals in the atmosphere or due to collisions with the collecting surface. In general, crystals which impacted and fragmented on the collector remaining in the vicinity of the impact and

TABLE 10
SURFACE OBSERVATIONS OF CRYSTAL FRAGMENTATION
1981-82 STORMS

<u>HABIT</u>	<u>CODE</u>	<u>SAMPLE SIZE</u>	<u>NUMBER FRAGMENTED</u>	<u>PERCENT FRAGMENTED</u>
Needles	N1a	699	0	0.0
	N2a	1	0	0.0
Sheaths	N1c	64	0	0.0
Columns	N1e	264	0	0.0
	N2c	71	1	1.4
	C1e	43	0	0.0
	C2b	12	0	0.0
	R1b	1	0	0.0
Bullets	C1c	19	0	0.0
	C2a	19	0	0.0
Capped Columns	CP1a	93	0	0.0
	CP1b	1	0	0.0
	CP1c	44	0	0.0
Plates	P1a	893	0	0.0
Stellar Dendrites	P1b	57	21	36.8
	P1c	292	35	11.9
	P1d	374	88	23.5
	P1f	2216	1211	54.6
Endplate Dend.	P2a	195	102	52.3
	P2c	3	0	0.0
	P2d	66	24	36.3
Centerplate Dend.	P2e	145	43	29.6
	P2f	154	59	38.3
	P2g	86	20	23.2
Other Dendrites	P3a	6	0	0.0
	P3b	2	0	0.0
	P3c	7	0	0.0
	P4a	6	0	0.0
	P4b	4	0	0.0
	P5	1	0	0.0
	R2b	25	9	36.0
Broken Branches	I3a,b	3969	3969	100.0

were easily identified as a single particle. Such fragments were not included in the fragment count. Only fragments with no clearly identifiable parent crystal or group were categorized as fragments.

These observations show that cloud ice crystal concentrations may be enhanced by fragmentation during crystal-crystal collisions in snowfall events which are characterized by a large dendrite population. Concentration enhancement should occur primarily in and below the dendritic growth zone (-17°C to -13°C) and should be accompanied by an increase in the population of aggregates, since aggregates are also a product of the collision of dendrites. Aircraft measurements which suggest that fragmentation may be important are discussed in the next section.

(2) Aircraft measurements: Aircraft soundings were carried out over RAD during four deep storm systems. Two of these systems had dendritic crystals present in the snowfall at RAD. Ice crystal concentrations and characteristics of the 2D-c spectra measured during these soundings are examined for evidence of ice crystal concentration enhancement by fragmentation. The other two cases are discussed in the following section on ice splinter production during riming. The data are presented in a case study format.

a. 5 January 82: Crystal concentrations and representative spectra from 2-Dc probe from a sounding over RAD between 1539 and 1546 are shown in Figs. 71 and 72. During this period, aggregated snowfall primarily consisting of planar and spatial dendrites fell at RAD and SPL. Figure 71 shows that a rapid increase in the concentration of crystals occurred through the depth of the dendritic growth region. Particle size spectra shown on Fig. 72 indicate that the majority of the increase in

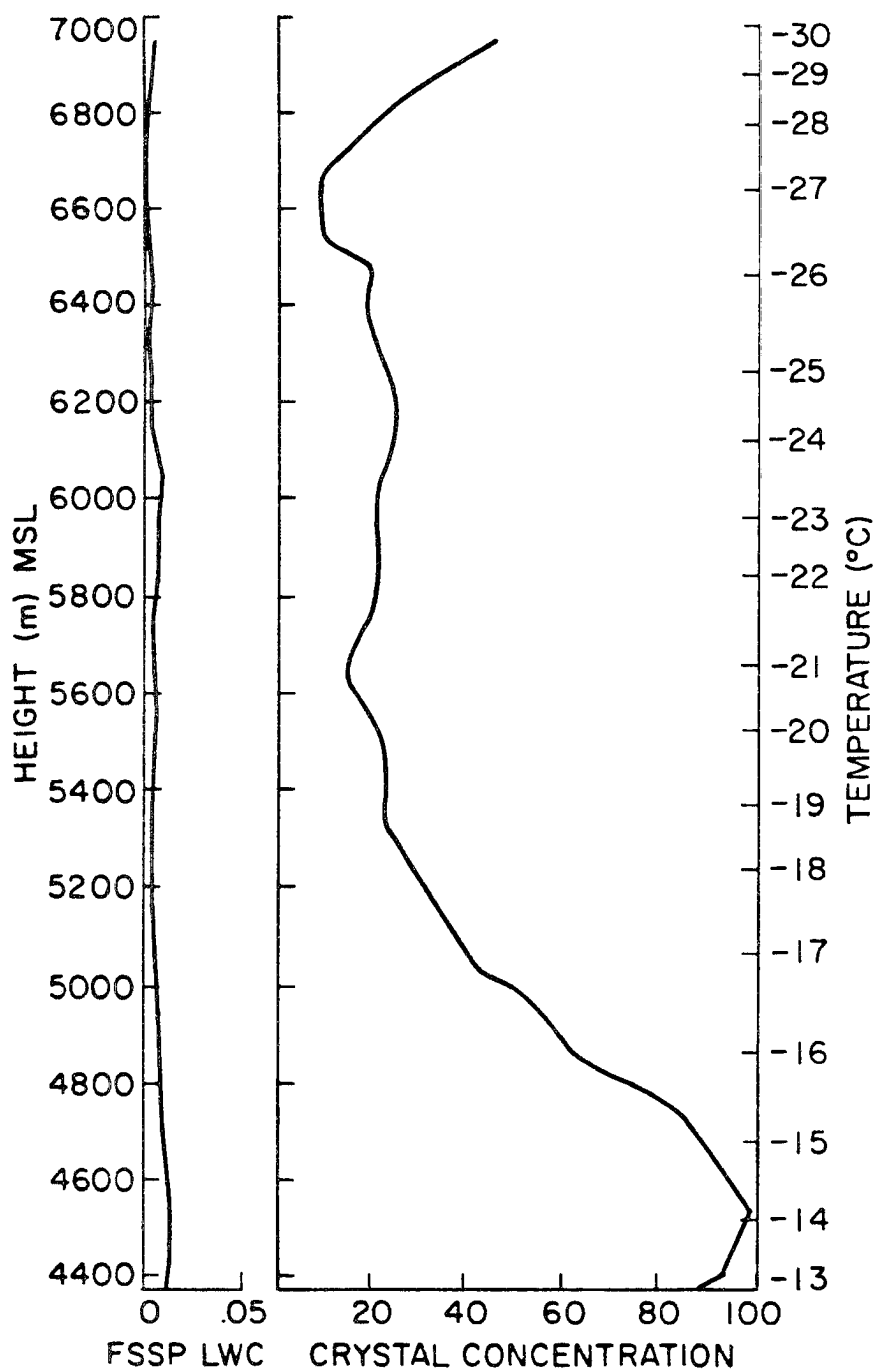


Fig. 71. Ice crystal concentrations (l^{-1}) as a function of height and temperature for the 1539-1546 GMT sounding over RAD on 5 Jan 82. FSSP liquid water contents are also shown.

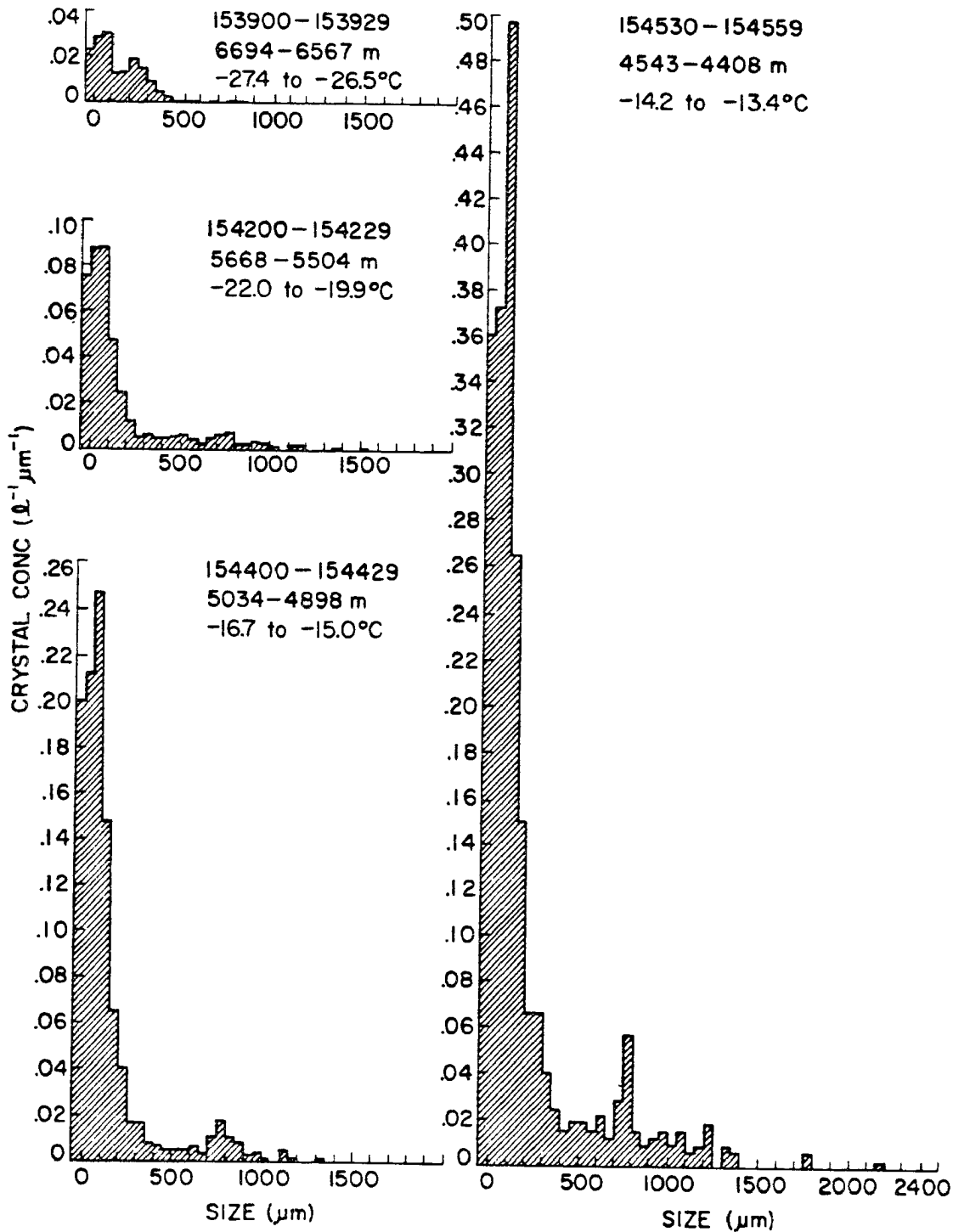


Fig. 72. Ice crystal size spectra for selected points on the 5 Jan 82 1539-1546 GMT sounding over RAD. Zero area images are displayed as a separate area category to the left of the zero. These particles were assumed to have sizes spanning a 50 μm binwidth to correspond to this diagram.

concentration was due to particles smaller than 300 μm . The cloud system was practically devoid of liquid water in this region. For this reason, nucleation processes were limited largely to vapor deposition or sorption. At such warm temperatures, it is unlikely that deposition nucleation could account for such a rapid increase in the small particle population. Because of their size, it is also unlikely that these particles originated much higher in the cloud. Secondary particle production by droplet freezing or ice splintering during riming was unlikely because of the absence of liquid water. The only plausible explanation for the observed increase is fragmentation. However, an instrumental question remains concerning the source of the fragmentation. Although it is clear from surface observations that fragments occur regularly in association with dendritic snowfall, it is likely that dendrites colliding with the 2D-c probe tips may also have fragmented and produced the increase in concentration. In this case, the contribution from each source is uncertain. However, ground observations of fragments clearly indicate that at least a portion of the increase was due to natural collisions. Clearly, all the appropriate conditions for fragmentation to occur were present in this case.

b. 31 January 82

The 31 Jan 82 case was the only case where the aircraft penetrated the low level cloud region near the mountain. In this case, the aircraft departed from Steamboat Springs Airport after the storm system moved into the area. The data extends from near ground level to 6100 m, still below cloud top.

Crystal concentrations and representative 2D-c spectra at points on the sounding are shown on Figs. 73, 74 and 75. During this period, snowfall consisted of cold temperature crystals, primarily irregulars, sideplanes (S1, S2, S3), plate assemblages (P7a) and cold temperature columns (C1f, C2a, CP1a). However, decelerator data collected during the ascent (see Fig. 57) indicated that dendritic crystals were also present in the snowfall. The slides also contained a very high density of unrecognizable particles.

From Fig. 73, it is evident that two distinct regions of enhanced ice crystal concentrations existed, the first at -24°C and the second over the temperature range -9°C to -12°C . Between the top of the sounding and -24°C crystal concentrations were nearly uniform at 20 l^{-1} . Spectra A in Fig. 74 was characteristic of this layer. Particles were distributed somewhat uniformly in the size ranges from 0-1000 μm . In the zone between -24°C and -23°C crystal concentrations increased to a maximum of 70 l^{-1} . Spectra B, characteristic of this region, shows a rapid increase in the small particle population, possibly associated with new nucleation and growth. Below this layer, crystal concentrations dropped to 30 l^{-1} . Spectra C, from this region, suggests that some of the large particles from the layer above may have precipitated into this layer. Beginning at -12.7°C , a significant enhancement in ice crystal concentrations occurred, reaching a high concentration of 87 l^{-1} at -9°C . Spectra D from Fig. 74 and E from Fig. 75 show the size distribution of crystals in this region. The greatest contribution to crystal concentration enhancement in this zone came from crystals in the small size ranges, particularly less than 350 μm . No liquid water was observed in this region or at lower altitudes.

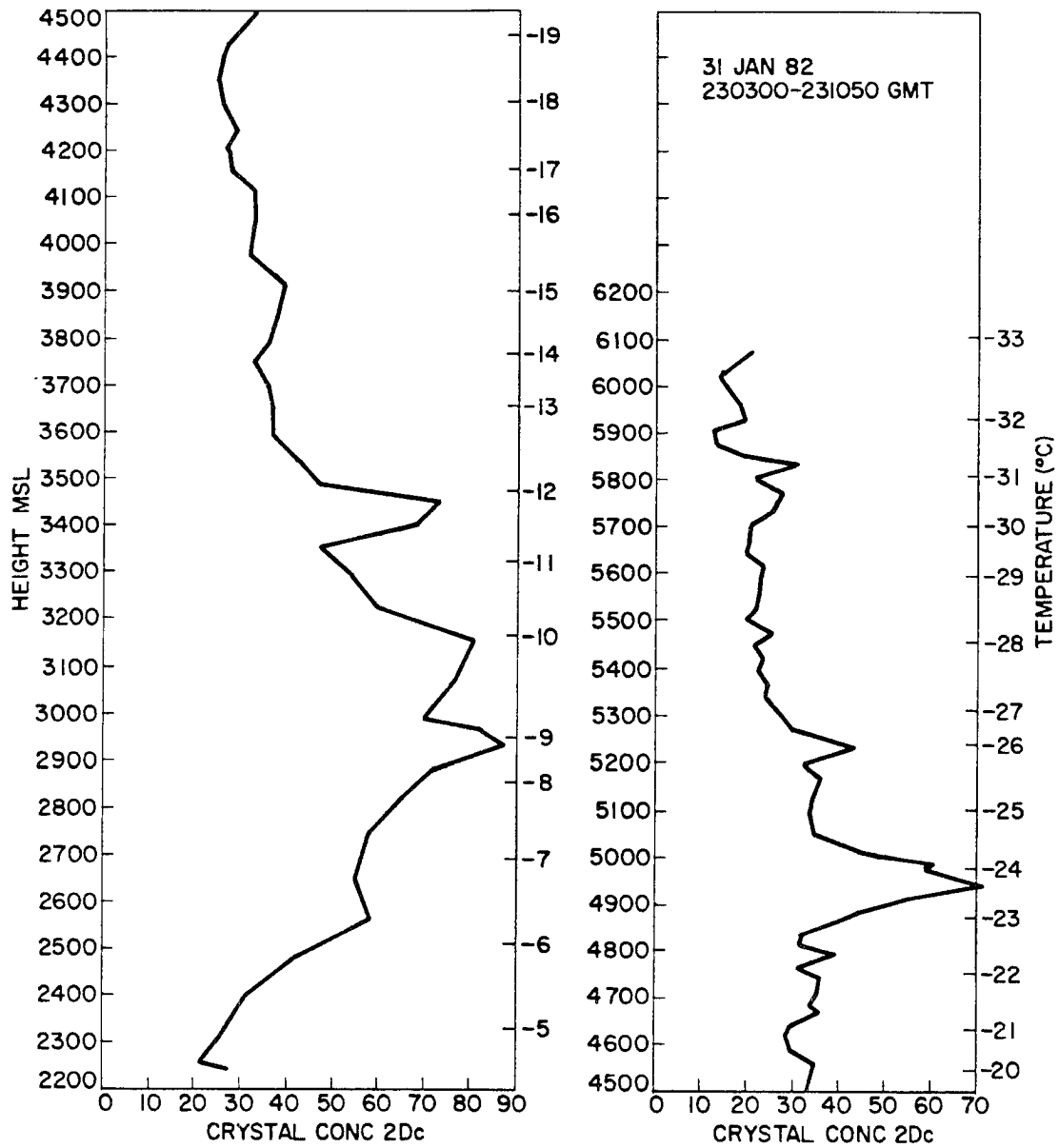


Fig. 73. Ice crystal concentrations as a function of height and temperature for the 2303-2310 GMT sounding 10 km west of RAD on 31 Jan 82.

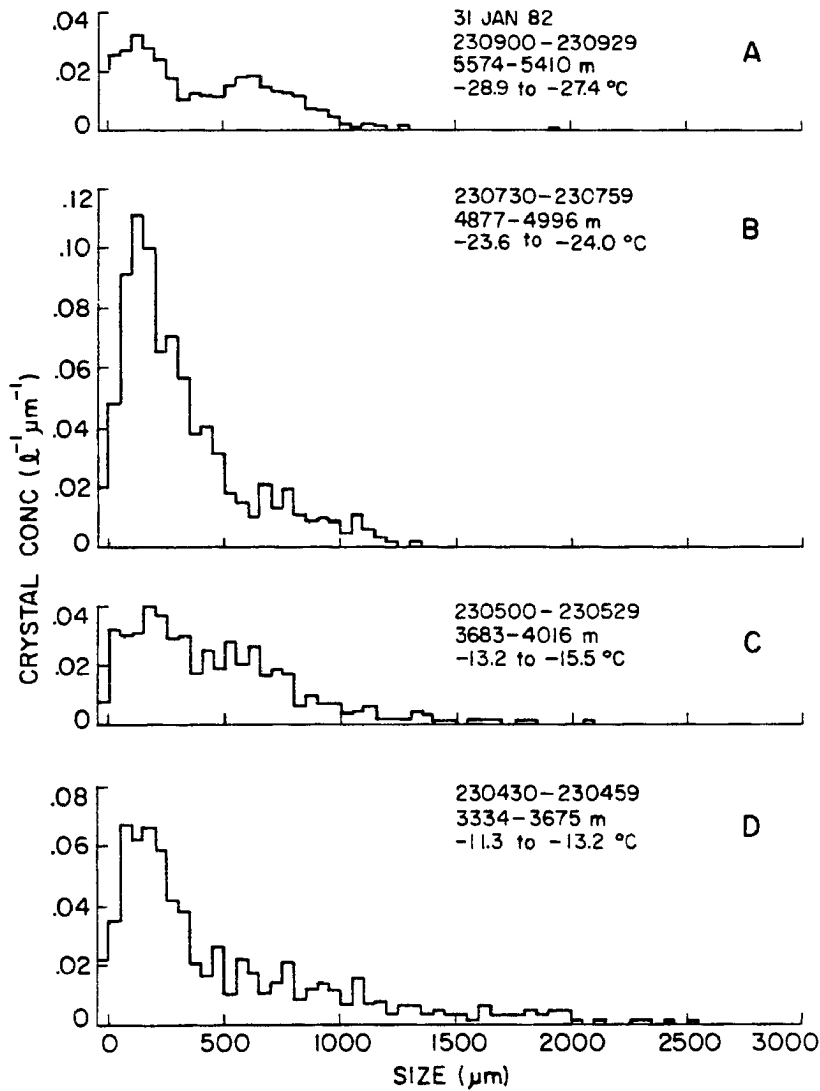


Fig. 74. Ice crystal size spectra for selected points (A-D) on the 31 Jan 82 2303-2310 GMT sounding. Zero area images are displayed as a separate category to the left of the zero.

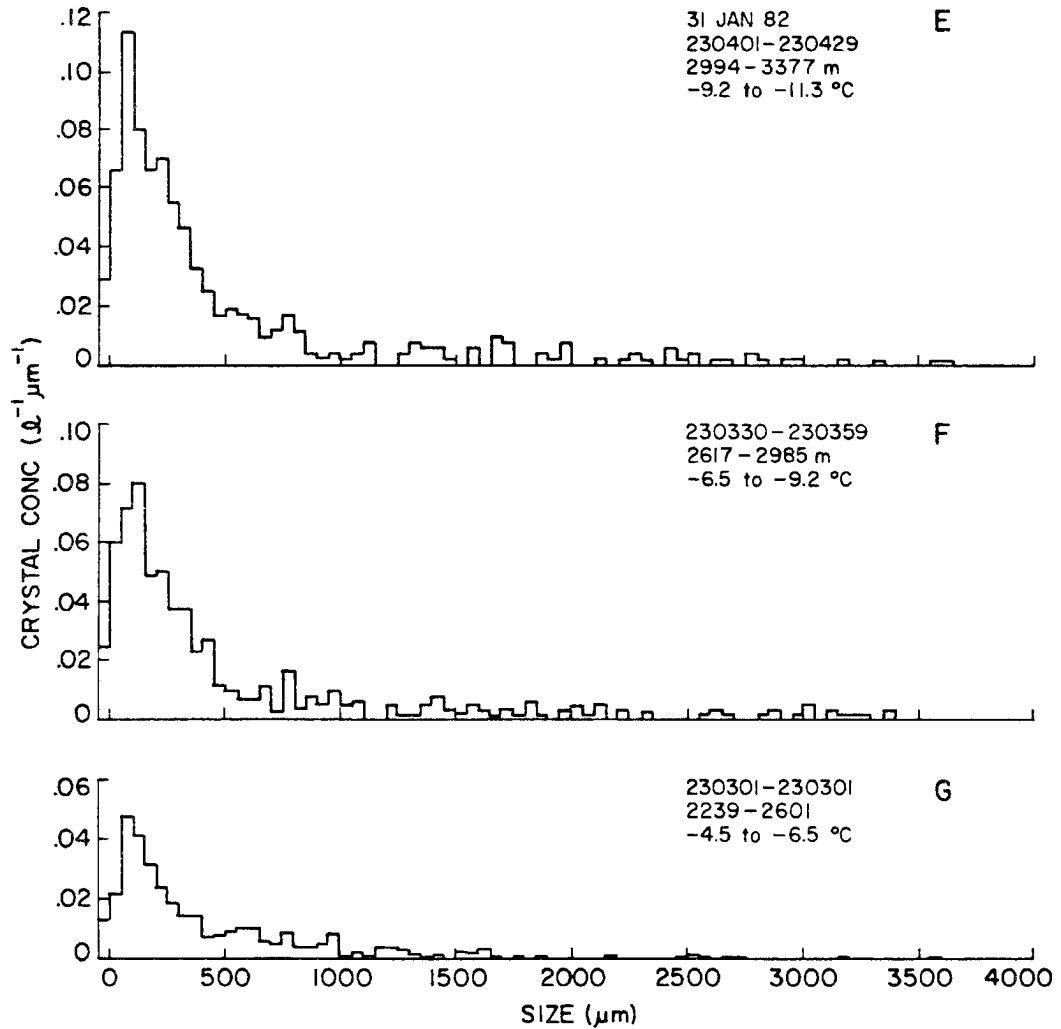


Fig. 75. Ice crystal size spectra for selected points (E-G) on the 31 Jan 82 2303-2310 GMT sounding. Zero area images are displayed as a separate category to the left of the zero.

Such increases in crystal concentration in the small size ranges must either be attributed to primary nucleation or a secondary ice crystal production mechanism. Nucleation in this case must be limited to deposition or sorption, neither efficient nor likely at such warm temperatures. Ice multiplication by riming or droplet freezing is impossible in the absence of liquid water. As with 5 Jan 82, the only reasonable mechanism for the observed ice crystal concentration enhancement is fragmentation. In this case, it appears that the large flux of cold crystals with high fall velocities collided with the smaller population of low fall velocity planar crystals promoting fragmentation. Such collisions would increase the population of crystals in the small size range. The magnitude of the enhancement in this case seems extreme considering the relatively small number of complete dendritic crystals observed. A second unknown is the source of the branched planar crystals, since the dendritic zone in the sampling area was not water supersaturated. These questions could not be addressed with the limited data set.

C. Ice splinter formation during riming

Laboratory studies discussed in the review have established three constraints for ice splinter production during riming:

- (1) The temperature must be between -3 and -8°C .
- (2) Droplets with diameters $\geq 25 \mu\text{m}$ and $\leq 13 \mu\text{m}$ must be present.
- (3) Ice particles with size and structure suitable for riming must be present.

In this section, each of these constraints are examined for Park Range cloud systems. The 1981-82 data set is reviewed for evidence of

the Hallett-Mossop (HM) mechanism. Two case studies are presented in which the HM process may have occurred.

(1) Physical constraints on the HM mechanism

a. Temperature: The narrow temperature limits which bound the HM ice splintering mechanism somewhat specify the altitude range where this process can occur in wintertime clouds over the Park Range. Figure 76 shows a 19 year climatology of the 70 KPa temperature for the months of November through March at Grand Junction, Co., approximately 200 km southwest of the Park Range. The 70 KPa level is approximately the same altitude as the crest of the mountain. During the mid-winter months of December to February, the mean 70 KPa temperature varies between -5 and -7°C . Nearly 40% of the time, the temperature at ridgetop is within the HM range. Most storm events occur at these temperatures, which correspond to the transition temperatures between a warm ridge and a cold trough. In the early and late winter months of November and March, the HM temperature range is generally within a few hundred meters of ridgetop.

During storm periods, liquid cloud base varies from 500 m below to 100 m above ridgetop. Therefore, if the HM process is to operate effectively in these wintertime cloud systems, it must occur within the lowest km of the cloud, and generally near the level of the ridgetop.

b. Presence of small ($< 13 \mu\text{m}$) and large ($> 25 \mu\text{m}$) droplets:

Climatologically, the HM temperature range is near cloud base in Park Range cloud systems. Measurements of droplet spectra at SPL in years subsequent to the 1981-82 experiment with a cloud gun have shown that droplets $< 13 \mu\text{m}$ diameter are common in these clouds. However, droplets with diameters $> 25 \mu\text{m}$ have seldom been observed. Droplets $> 30 \mu\text{m}$ have

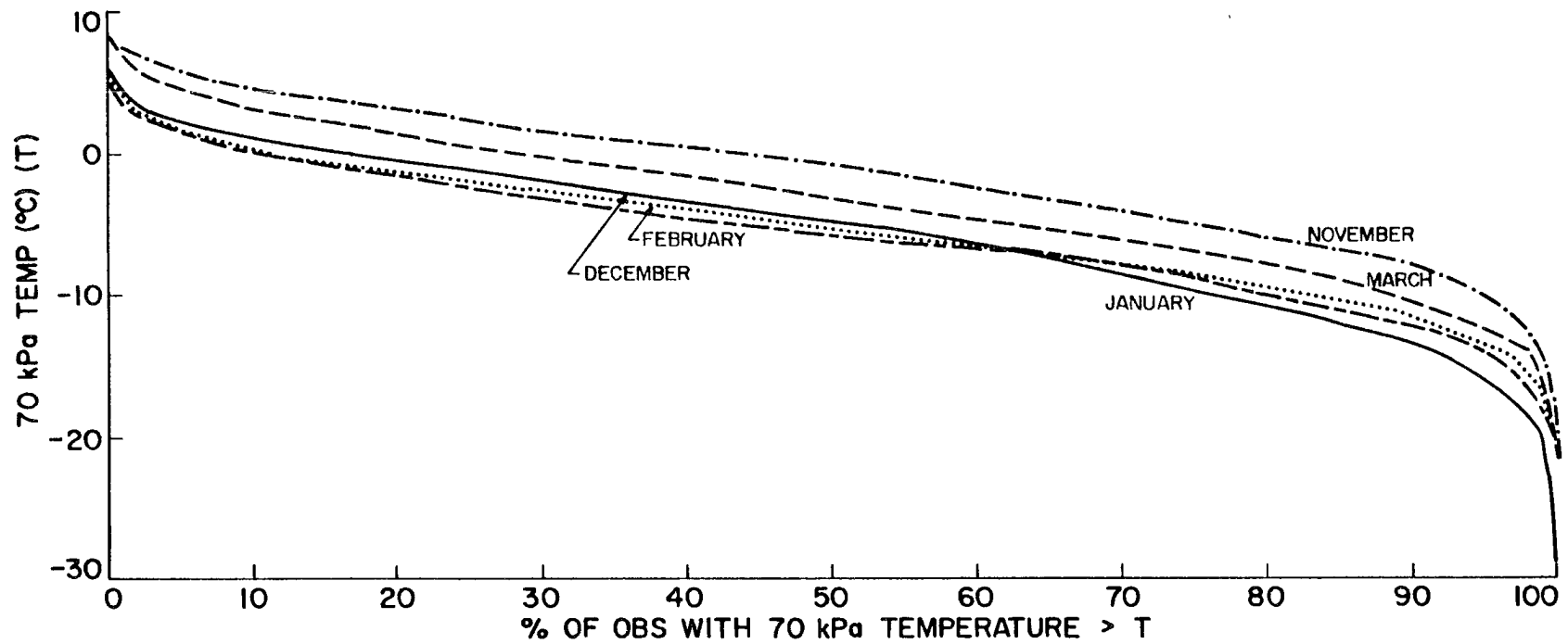


Fig. 76. 19 year climatology of the 70 KPa temperature for the months of November through March at Grand Junction, Co.

not been observed. Three possible reasons may explain the lack of large droplets: (1) Due to the proximity to cloud base, insufficient time is available for droplets to grow to the necessary sizes; (2) Cloud base is closer to the boundary layer and at least in some cases, may have CCN concentrations more characteristic of continental air. Droplet spectra in this region would therefore be more narrow; (3) Due to the large ice crystal flux through cloud base from the colder cloud regions, larger droplets will preferentially be removed by riming before they have a chance to grow to the necessary sizes. The major limitation of the HM multiplication mechanism in Park Range clouds is the requirement for large droplets in the appropriate temperature range near cloud base.

c. Presence of large ice particles: Large ice particles falling from levels colder than -10°C are nearly always present in Park Range cloud systems. Virtually all of these particles are large enough to be capable of accreting cloud droplets. Therefore, this constraint is not a limitation.

(2) Evidence for the HM process

Because of the temperature constraints associated with the HM mechanism, ice splinters ejected during riming have a high probability of developing into needles. If the HM mechanism had a positive impact on the precipitation, such needles should appear in the precipitation, particularly in Park Range clouds where they would form at altitudes near or below the mountain crest. During the 1981-82 program, needles were not present during most storms. However, significant numbers of needles were present during a two hour period of the 15 Dec 81 storm system. Needles were also present in smaller numbers during three hours

of the 21 Dec 81 storm. Shadow photographs taken during the 15 Dec 81 event are shown on Fig. 77.

Sixteen samples containing needles were collected at RAD at approximately 15 minute intervals during the two events. Of the 16 samples, 13 contained snow pellets and 15 contained rimed crystals. At SPL, 31 separate samples containing needles were collected at approximately 5-10 minute frequency. Of these, 20 contained snow pellets and 28 contained rimed crystals. These observations from the surface network indicate that liquid water was present in the cloud system, that riming did occur and that the crystal habits expected from an HM mechanism were present.

Figure 78 shows the vertical temperature structure of the atmosphere measured by the CG rawinsonde at 1500 and 1800 on 15 Dec 81. From this figure, one can see that the HM temperature range extended over a kilometer from 2800 to 3900 m. This temperature zone encompassed SPL. The temperature of maximum activity for the process was at 3100 m, about 100 m above the laboratory. Figure 79 shows the 2D-c crystal concentration measurements during a sounding over RAD. The upper levels of the cloud system contained several distinct layers. No crystal concentration enhancement occurred in association with the dendritic zone. This is consistent with the surface observations where planar particles were absent. More important to this section was the large enhancement in crystal concentration near -10°C . Such enhancement was almost entirely due to an increase in zero area images on the probe. Zero area images occur in association with particles of less than about 100 μm in diameter. Unfortunately, the aircraft could not descend further into the cloud. The spectra from the sounding are illustrated

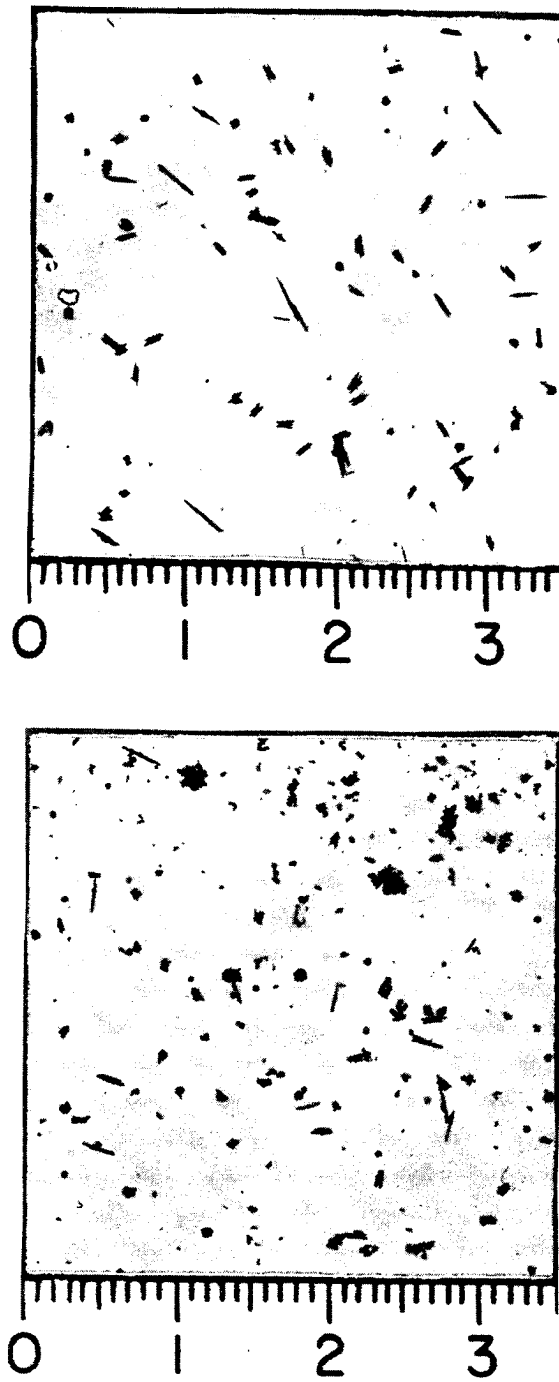


Fig. 77. Shadow photographs of the 15 Dec 81 storm showing a large number of needles.

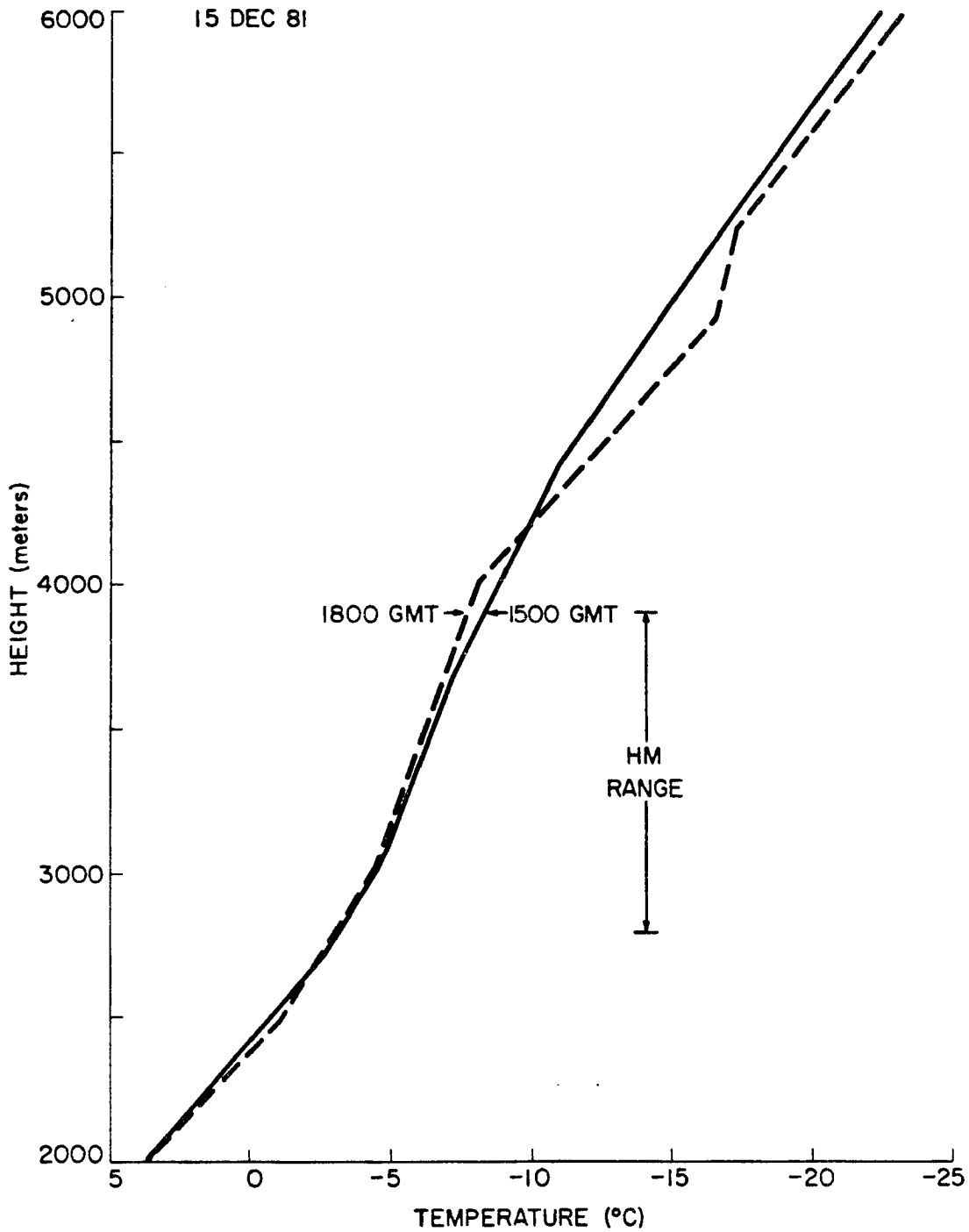


Fig. 78. Vertical temperature structure of the atmosphere at 1500 and 1800 GMT during the 15 Dec 81 storm system.

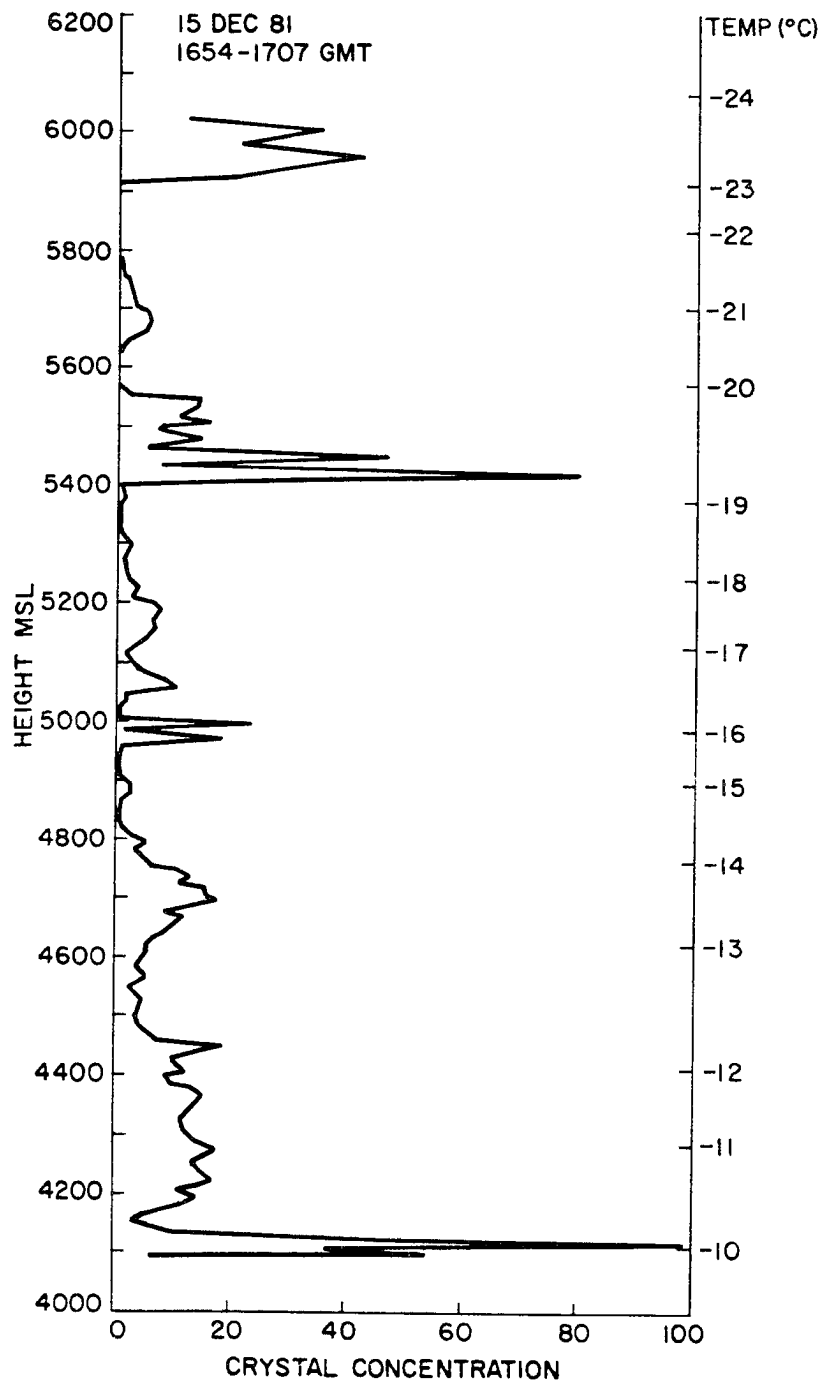


Fig. 79. Ice crystal concentrations (l^{-1}) as a function of height and temperature for the 1654-1707 GMT, 15 Dec 81 sounding over RAD.

in Fig. 80. At RAD and SPL during this period, precipitation consisted entirely of needles and snow pellets. Riming clearly was occurring during this event.

Droplet distributions were unavailable from aircraft or at the mountaintop on 15 Dec 81. Evidence of substantial liquid water concentrations in the cloud during this period were measured by the radiometer. Slant path values exceeded 2.0 mm to the north and south and exceeded 3.0 mm over the mountain. These were some of the higher values observed during the program. Based on this data, the existence of large droplets in the HM temperature range was clearly possible.

Figure 81 shows the vertical temperature structure of the atmosphere on 21 Dec 81 at 1500 and 1800 from rawinsondes launched at CG. These times nearly encompass the aircraft flight period and the needle/graupel precipitation event. From these soundings it is clear that the HM temperature range extended over 600 m in the vertical, lowered in elevation over the three hours and encompassed SPL during the entire period. The temperature of maximum activity of the splintering process (-5°C) was below the level of the laboratory.

Evidence for liquid water presence in the lower levels of the cloud below the aircraft measurements was available from the radiometric data. The magnitude of the liquid water contents measured by the radiometer during this period were too large to account for the water observed in the upper cloud layers. However, Rotorod measurements at SPL suggest a magnitude of liquid water content in the low levels of about 0.1 gm^{-3} . With such liquid water contents, the probability of a significant concentration of droplets $> 25 \mu\text{m}$ in the HM region was low. Despite the precipitation signature characteristic of the HM process at RAD and SPL,

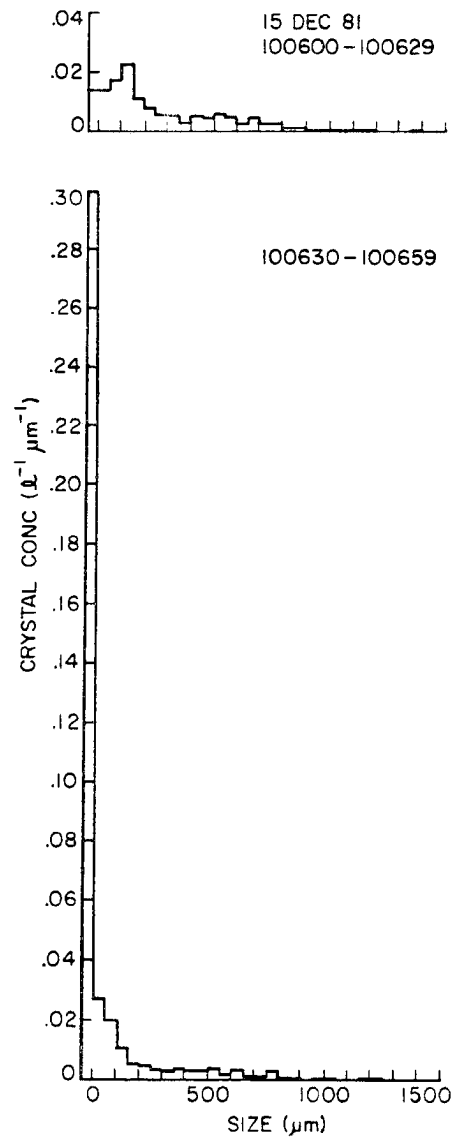


Fig. 80. Ice crystal size spectra in the -10°C region of the 1654-1707 GMT, 15 Dec 81 sounding over RAD. Zero area images are displayed as a separate category to the left of the zero.

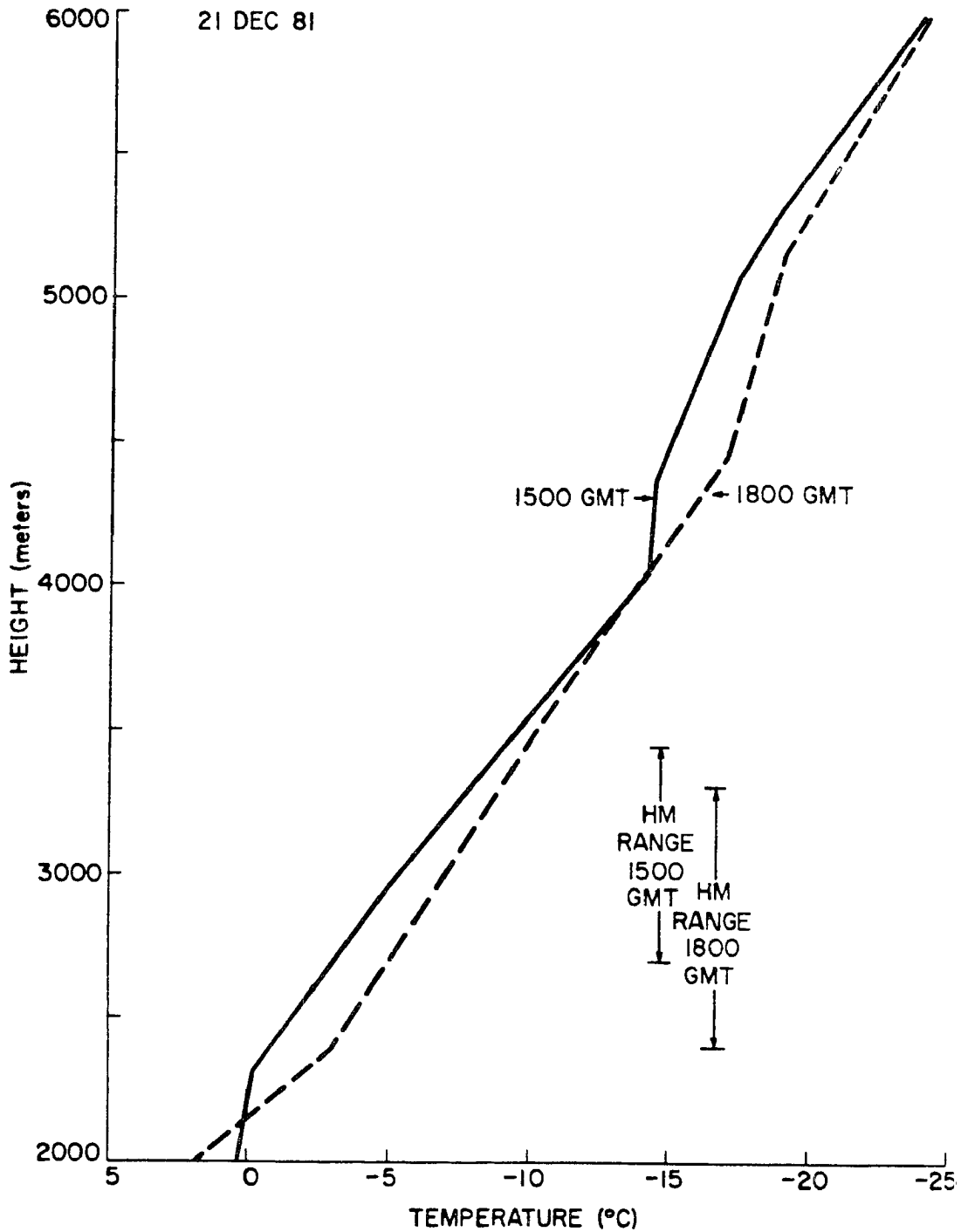


Fig. 81. Vertical temperature structure of the atmosphere at 1500 and 1800 GMT during the 21 Dec 81 storm system.

it is questionable whether the HM process did occur in the 21 Dec 81 cloud system.

In summary, circumstantial evidence exists that in a few cases, the HM process may be active. However, the general lack of needle-like precipitation and the absence of large droplets at mountaintop suggests that the process is probably not important in the majority of precipitation events.

D. Droplet shattering upon freezing

The characteristics of cloud droplet spectra observed in Park Range cloud systems were summarized in Table 6 of Chapter 3. These measurements showed that mean droplet diameters seldom exceed 20 μm . Droplet concentrations in the largest size bin of the FSSP were less than $1 \text{ cm}^{-3} \mu\text{m}^{-1}$ when large droplets were present. These measurements indicate that droplets with diameters greater than 50 μm are rare. The only laboratory studies which considered the freezing behavior of such small droplets were Hobbs and Alkezweeny (1968), Brownscombe and Goldsmith (1972) and Bader et al. (1974). These studies were all conducted using droplets in freefall. The former two studies reported no fragmentation of droplets with diameters less than 50 μm . Bader et al. determined that less than one sub-micron ice fragment was ejected for every three droplet freezing events when droplets with diameters between 30 and 42 μm froze.

These studies, together with the measurements of droplet spectra presented in Chapter 3, suggest that ice splinter production during droplet freezing is not an important source of ice crystals in Park Range cloud systems. Since virtually all of the droplets in these

clouds have diameters less than 30 μm , ice multiplication during droplet freezing is probably an extremely rare event.

5. Accretion

Accretion measurements can be used to infer the temporal evolution and physical distribution of liquid water in cloud systems. By necessity, the accretion process has already been discussed in some detail in the previous chapter. In Chapter 3, three regions of Park Range cloud systems have been identified where liquid water production may occur. Accretional growth is limited to these regions. In general, growth by accretion will contribute the most mass to particles in two of these regions, the low level region at temperatures warmer than -10°C , and the primary lift region near the mountain crest. Due to safety limitations, the accretion process in these regions could not be studied directly with aircraft. Information concerning accretion must be implied from surface and radiometric observations. Such analyses were completed in Chapter 3. The role of accretion in the upper cloud layer, particularly near cloud top, is limited by the small size of the ice crystals. Still, accretion may play an important role in crystal habit development and may indirectly effect the later growth of precipitation particles by aggregation. The purpose of this section is to supplement the analyses of liquid water structure in Chapter 3 with additional information concerning accretion in Park Range cloud systems. Two aspects of the accretion process are considered: (1) the role of accretion in upper cloud layers and near cloud top and (2) the frequency of occurrence of the accretion process and its effect on the distribution of precipitation. A brief review of literature pertinent to these discussions is presented in the following section.

A. Review

Studies of accretion in cloud systems have primarily focused on the microphysical aspects of the accretion process. Many research groups over the last two decades have attempted to determine the minimum crystal dimensions required for the onset of accretion. These studies have used direct measurements as well as theoretical models of accretion (Ono, 1969; Wilkins and Auer, 1970; Reinking, 1973; Iwai, 1973; Harimaya, 1975; D'Errico and Auer, 1978; Reinking, 1979; Hindman and Johnson, 1972; Pitter and Fruppacher, 1974; Schlamp et al., 1975; Pitter, 1977).

Such studies have established that the riming threshold diameter for plates is near 150 μm diameter and columns between 30–50 μm diameter. Branched planar crystals commenced riming after growing beyond about 250 μm diameter, radiating crystals at about 300 μm . Measured and theoretical collection efficiencies have also been determined (Kajikawa, 1974, Pitter and Fruppacher, 1974; Schlamp et al., 1975; Pitter, 1977).

A second emphasis of the microphysical studies has been to determine the orientation of fall of riming crystals, crystal cross-sectional area, and distribution of droplets on the crystal face (Ono, 1969; Sasyo, 1971; Zikmunda and Vali, 1972; Iwai, 1973; Reinking, 1973, 1974; Harimaya, 1975; D'Errico and Auer, 1978). These studies have generally concluded that crystals fall presenting the face of maximum resistance to the airflow. Rime accumulates on the prism face of columns and sheaths, and on the downward basal face of plates and branched planar crystals. The largest accumulations of droplets occur on the edges of the crystals except for sheaths, which appear to rime

uniformly. One goal of many studies has been to determine the size distribution of droplets which typically interact with ice crystals (Wilkins and Auer, 1970; Hariyama, 1975; D'Errico and Auer, 1978; Pitter, 1977; Schlamp et al., 1975). Such studies have generally concluded that droplets in the 10-15 μm diameter size range have a high efficiency for collection by plate-like ice crystals between 150 and 400 μm in diameter. The lower cutoff size was generally around 5 μm diameter.

Another emphasis of accretion research has been to determine the crystallographic structure and subsequent diffusional growth of accreted drops (Ono, 1969; Brownscombe and Hallett, 1967; Kikuchi and Uyeda, 1979a,b). The studies by Kikuchi and Uyeda attempted to explain the development of spatial dendritic crystals based on polycrystalline structure of accreted drops.

Unfortunately, very few studies have attempted to interpret cloud system structure in terms of accretion processes. Notable exceptions are the series of papers by Reinking (1973, 1975, 1979) and the work of Hobbs and collaborators in the Cascades (Hobbs et al., 1971; Hobbs, 1975a). Reinking found that many crystals in a given population did not begin to rime when the critical minimum size was reached. Rather, the onset of accretion was delayed or never occurred for large fractions of the crystals in a sample. Reinking attributed these variations to small scale variations in the liquid water content of the clouds. Hobbs used observations of riming on crystals collected at surface locations and with aircraft to specify the altitude and depth of liquid water layers in pre-frontal, frontal, post-frontal and orographic cloud conditions. It is interesting to note that many clouds in the Cascades frequently

have significant liquid water contents at temperatures warmer than -10°C , a feature found in many Park Range systems.

B. Accretion in upper cloud regions

(1) Cloud top region in warm clouds (tops $> -20^{\circ}\text{C}$)

Accretion near cloud top is limited by the size of the ice particles and water droplets as well as the residence time of the particles in the liquid water zone. Residence time is controlled by the size and fall velocity of the particle, the vertical velocity and condensation production rate in the cloud, and the ambient ice crystal concentration and size distribution. As a consequence, the residence time in the liquid water zone and subsequent riming potential of an individual crystal will vary from cloud to cloud.

In general, cloud systems with tops in the -10°C to -20°C range will produce crystals with plate-like habits during their earliest growth. Studies quoted in the previous section have found that the riming threshold of these crystals is near $150\ \mu\text{m}$ diameter. Using growth rates measured by Ryan et al. (1976) and fall velocities measured by Davis (1974), it is possible to calculate the fall distance of a F1a crystal prior to growing to the riming threshold. For the F1a habit, this fall distance is only a few meters. Based on this estimate, it is possible for riming to at least initiate in the liquid water regions near the tops of many cloud systems. In cases where the liquid water depth extends over a hundred meters, riming could become an important growth mechanism, particularly for particles originating near the very top of the cloud.

The droplet size distribution in the cloud top region can also strongly influence the effectiveness of the accretion process. Studies

described earlier have determined that droplets of 10-15 μm diameter have high collection efficiencies for small crystals. Comparing the spectra of 16 Jan 82 and 23 Jan 82 (Fig. 48), it is evident that cloud top riming can vary considerably due to droplet spectra variations. Both of these cloud systems were shallow with tops near -17°C and were very similar in many other respects.

Kikuchi and Uyeda (1979a,b) have established through direct observation that droplets often freeze in a polycrystalline structure. Such crystal structures serve as the framework for continued diffusional growth in many directions depending on the orientation of the crystalline axes in the frozen droplets. Riming near cloud top, particularly in cloud systems with tops in the vicinity of the dendritic growth region, promotes the development of spatial crystals. In cases of significant riming, these particles can develop the characteristics of the R3b spatial crystal. Crystals encountering few droplets potentially can develop such spatial habits as the P7a or P7b crystal. Unrimed particles would continue to develop as branched planar crystals. Particle combinations such as those described are often present during aggregation events. In Sec. 6, it is hypothesized that spatial dendritic particles promote aggregation particularly well due to their complex burr-like structures.

In summary, accretion near cloud top in warm ($> -20^{\circ}\text{C}$) clouds is highly dependent on many factors including CCN concentration and subsequent cloud droplet distribution, vertical velocity and condensate production rate near cloud top, ice particle concentrations and liquid water depth. When accretion occurs, it most likely will result in the production of spatial crystals. These crystals, because of their

complex shapes, frequently promote aggregation. Because these aggregates typically have higher fall velocities than the crystals which compose them, cloud top riming in these clouds may indirectly contribute to increased precipitation rates.

(2) Riming in upper regions of cold clouds (tops < -20°C)

Despite the cold temperatures associated with the upper levels of deep cloud systems, liquid water has been observed in these regions. Data collected on 21 Dec 81 has confirmed that liquid water contents of up to 0.15 gm^{-3} can occur at temperatures between -20°C and -32°C and that this liquid water interacts with ice particles in the riming process. The distribution of liquid water along the flight track is shown in Fig. 82. The conditions which must be present for such liquid water production are unclear because of the limited data set. However, this case had very low ice particle concentrations ($< 5 \text{ l}^{-1}$) throughout the region where liquid water was observed (Fig. 83). The liquid water in this region contributed to the production of rather large rimed particles. The rapid spread in the particle size distribution through the depth of the upper cloud layers (Fig. 84) and the shape of the 2D-c images (Fig. 85) strongly implies that snow pellet formation occurred in this region.

The frequency that high level supercooled water layers occur in Park Range cloud systems is unknown. The data available for other flights in deep cloud systems did not show any evidence of such large liquid water layers. Accurate assessment of the role of accretion in ice particle development in these cold cloud regions will require a much larger data set.

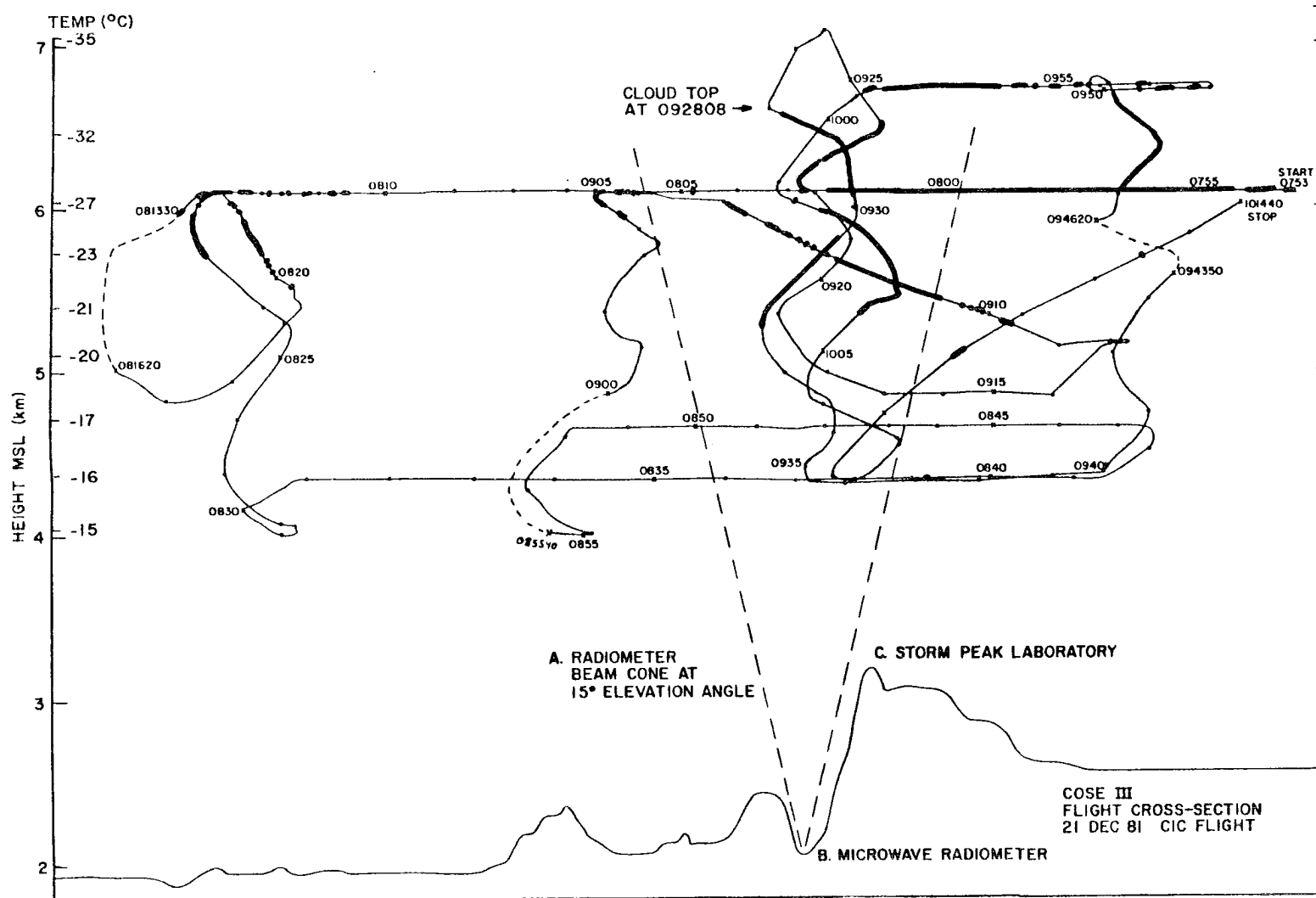


Fig. 82. Aircraft flight track for the 21 Dec 81 storm. Highlighted regions along the track denote region where measurable liquid water contents ($> 0.01 \text{ gm}^{-3}$) were present.

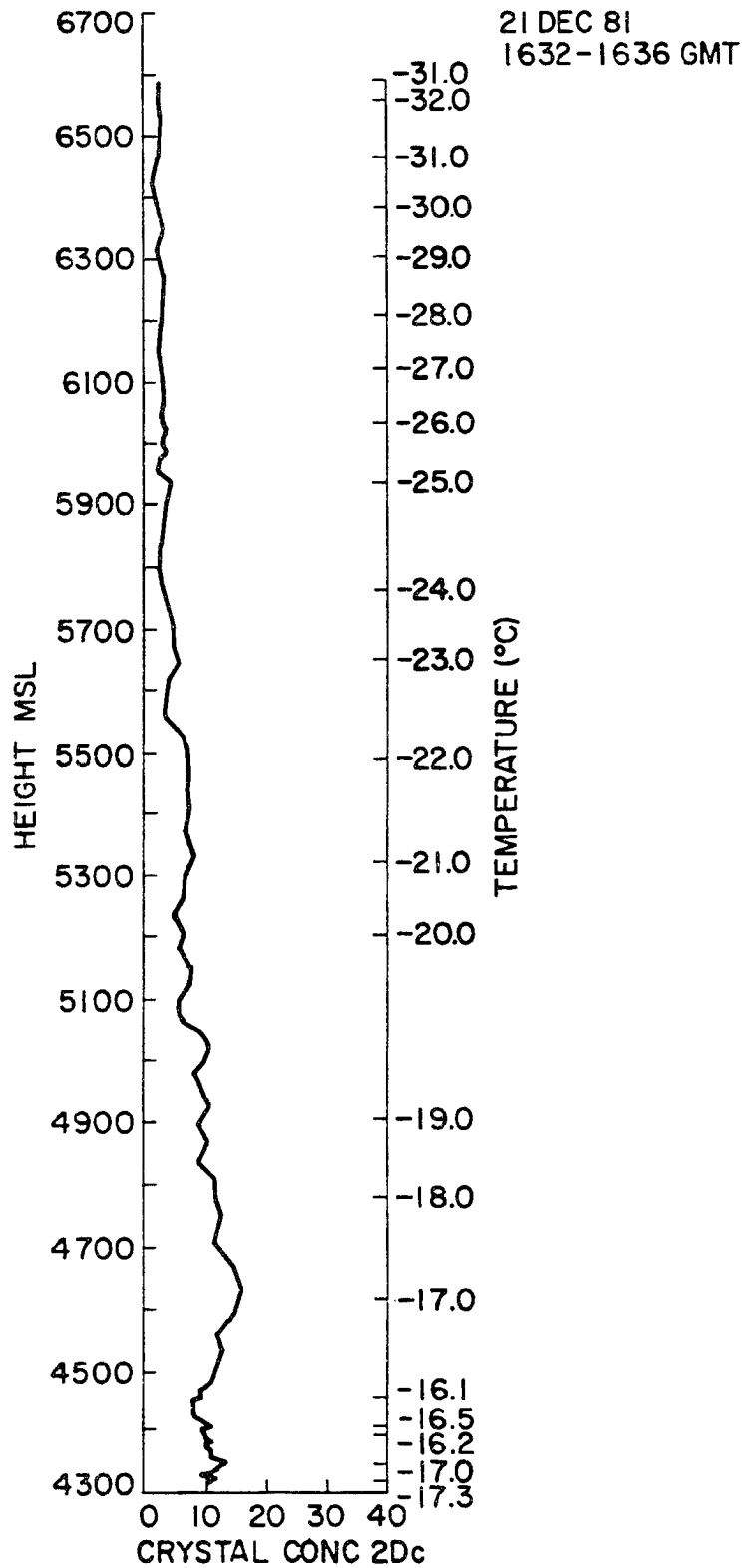


Fig. 83. Ice crystal concentration (l^{-1}) as a function of height and temperature for the 1632 to 1636 GMT, 21 Dec 81 sounding over RAD.

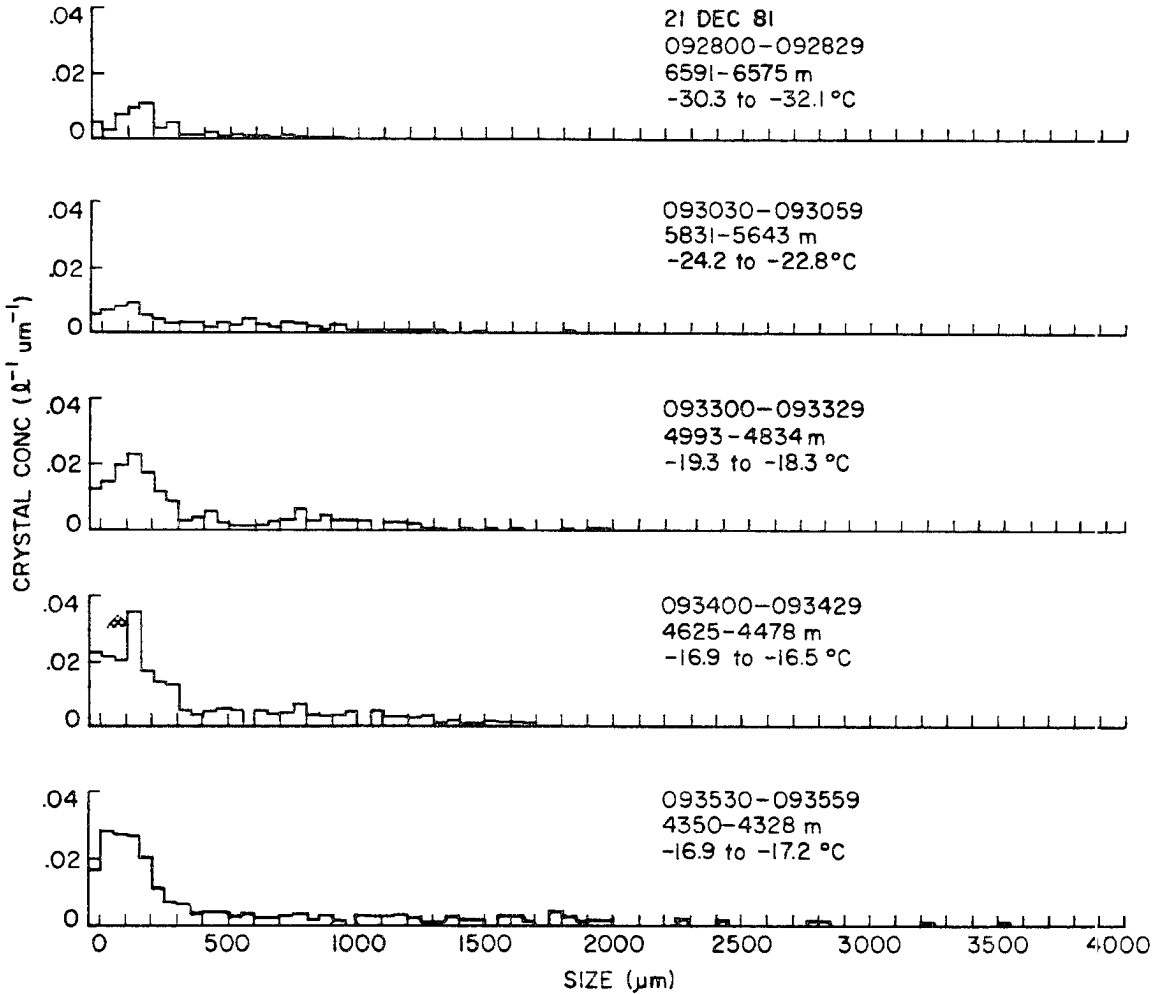


Fig. 84. Ice crystal size spectra at selected points on the 21 Dec 81 1632 to 1636 GMT sounding over RAD. Zero area images are displayed as a separate category to the left of the zero.

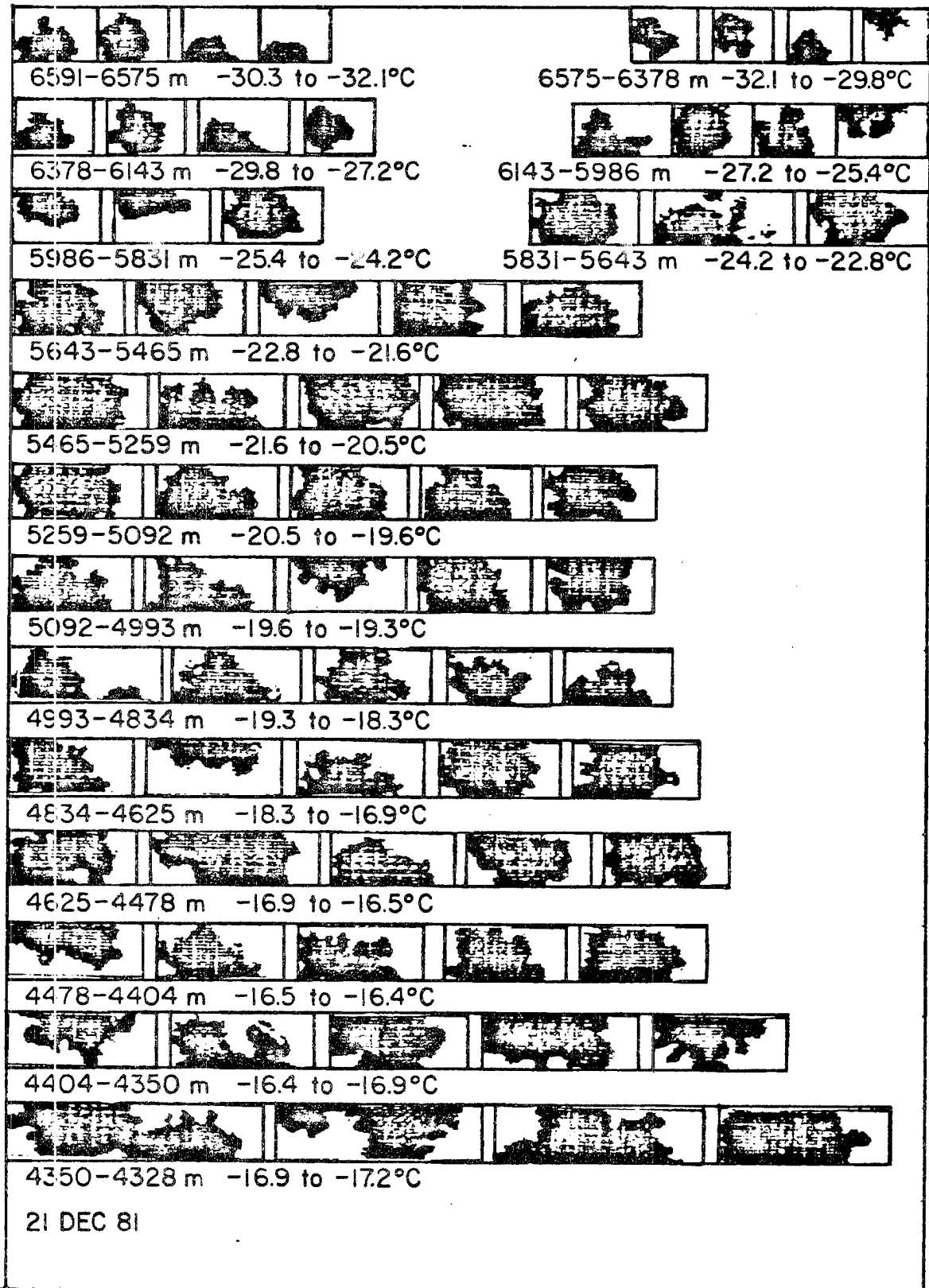


Fig. 85. Largest 2D-c images observed during 1032-1036 GMT, 21 Dec 81 sounding over RAD.

C. Frequency of accretion and effects on precipitation distribution

Surface measurements of rime intensity in Chapter 3 were used in coordination with other data sets to examine the temporal evolution of liquid water in Park Range cloud systems. From these analyses, it was clear that liquid water frequently occurs in sufficient quantities to initiate the accretion process. This section presents a more general summary of surface observations of accretion. This is followed by a qualitative discussion of accretion and its effect on ice particle trajectories.

The summary of ice particle habits presented in Table 9 differentiated rimed particles from unrimed particles only if the rimed particles were snow pellets or large graupel. Such graupel made up 2.36% of the total sample from the shadow photograph analysis. However, a much larger number of crystals in the shadow photograph samples were rimed to some degree.

To estimate the frequency that rimed particles occur in Park Range systems, the visual observations of particles on black felt were used. These were chosen over the shadow photographs because they were made at a much higher frequency, covered a wider range of storms, and were available from more than one site. The observations were divided into two classes, those where rimed particles were present and those where only unrimed particles were observed. The results of this classification are shown in Fig. 86.

During the storm events of 1981-82, 216 individual observations were made at SPL and 254 at RAD. These observations were collectively made during 23 separate storm events. During the storms, 77.7% of the samples at RAD and 72.2% of the samples at SPL contained rimed crystals.

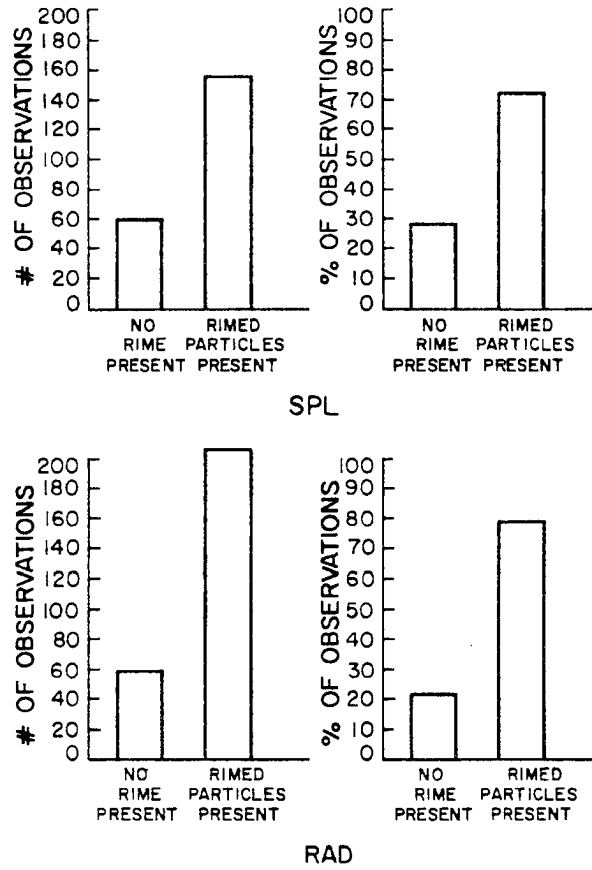


Fig. 86. Climatology of rime observations at RAD and SPL.

34.2% of the RAD samples and 36.1% of the SPL samples contained at least some heavily rimed crystals. It is important to note that in most samples, many crystals were present which were not rimed, or rimed very lightly. Often, these were in the majority. Examples of such a mixture of rimed and unrimed crystals are shown in Fig. 87. As in the Reinking studies, the degree of rime varied considerably in any one sample. The percentages quoted here represent the number of observations where rime was observed on at least part of the crystals in the sample. These observations imply that the accretion process is significant in production of both valley and mountaintop precipitation in Park Range systems.

The observations have some implications concerning trajectories of particles and the subsequent distribution of precipitation across the mountain. A general conclusion of many studies of ice crystal fall velocity is that rimed particles fall faster than their unrimed counterparts. Trajectories of rimed particles are naturally steeper. In general, the earlier diffusional growth of particles arriving rimed at RAD or SPL must have occurred much closer to the mountain than unrimed crystals of similar size and habit. In other words, riming selectively occurring on crystals falling within the zone of liquid water production near the mountain causes particles to fall at the same location as unrimed particles generated much further upwind.

A wide distribution of rime on a population of particles can be a consequence of the increase in liquid water production near the mountain in the orographic airflow. The dispersive nature of rime accumulation in a single sample can also be attributed to small scale variations in the liquid water structure. Such factors as small scale turbulence,

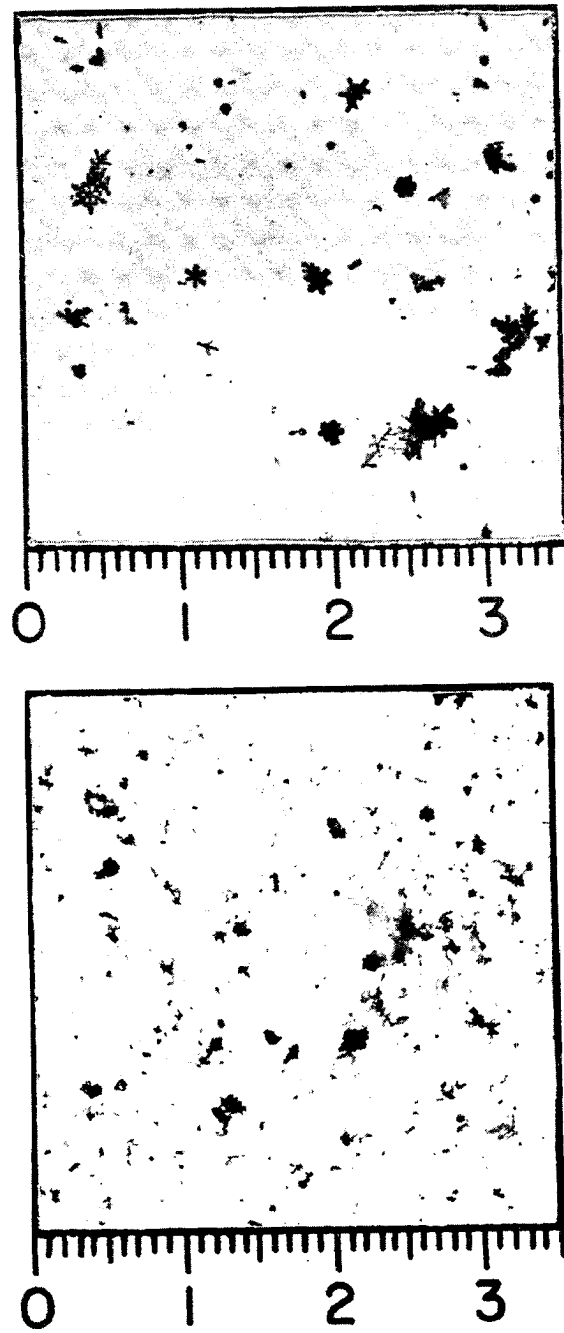


Fig. 87. Shadow photographs showing mixtures of rimed and unrimed particles.

convection, wave interactions, and variations in the ice crystal distribution all affect the actual distribution of liquid water in the cloud. Consequently, particles whose trajectories differ by only a few hundred meters may encounter quite different liquid water contents.

In any case, the effect of accretion is to cause particles to have steeper trajectories. The net result is to shift the distribution of precipitation windward of that which would have occurred had diffusional growth processes acted alone.

6. Aggregation

Aggregated ice particles comprise an important component of the total precipitation falling from Park Range cloud systems. The mechanisms by which aggregation occurs in these cloud systems are complex. Significant variations in the intensity and characteristics of the aggregates occur over time scales of less than an hour and often as short as five or ten minutes. The physical processes associated with the formation of aggregated snowfall in northwest Colorado wintertime cloud systems are discussed in the following sections. A review of previous work precedes the analysis.

A. Review

(1) Particle adhesion: Previous studies of the aggregation process have identified five mechanisms by which particles in contact adhere to each other. These mechanisms include (1) contact freezing of a liquid layer present on the crystals, (2) ice particle sintering, (3) electrical attraction, (4) mechanical interlocking of complex crystal shapes and (5) "cementing" of crystals during riming.

Early experiments concerning the force of adhesion of ice particles were done by Nakaya and Matsumoto (1954) and Hosler et al. (1957).

Nakaya and Matsumoto found that the force of adhesion decreased by a factor of five as the temperature during the experiment was lowered from -2°C to -15°C . Hosler et al. (1957) found the force of adhesion to vary from a few dynes at -25°C to 660 dynes at 0°C . Hosler and Hallgren (1960) measured the collection efficiency of very small ($<10\ \mu\text{m}$) crystals on discs with diameters of 127 and 360 μm in a wind tunnel. They found that aggregation occurred over a temperature range of -6 to -25°C , the limits of the experiment. Measured collection efficiencies were highest at -12°C . They associated this maximum with a transition in crystal habit.

Hosler and Hallgren speculated that their experiments could be explained by the existence of a liquid surface layer on the ice particles. This liquid surface was assumed to vary in thickness according to temperature and to freeze on contact with a colliding ice particle. They explained the maximum at -12°C by suggesting that the liquid layer was thicker on the basal plane than the prism face, enhancing the adhesive capability of platelike crystals. Theoretical support for the existence of a liquid layer was presented by Fletcher (1968).

An alternative mechanism for the adhesion of ice particles was studied experimentally and theoretically by Hobbs and Mason (1964). This process, called sintering, occurs because ice particles in point contact form a non-equilibrium system. In order to minimize the total free surface energy of the system, a requirement for equilibrium, a transport of water molecules toward the contact point must occur. Hobbs

(1965) showed that ice particles with radii of curvature of the order of 10 μm need to contact about 10 seconds to develop ice bonds of appreciable size.

A third mechanism that may enhance ice crystal aggregation is electrical attraction. Measurements of an excess positive charge on the basal plane of crystals by Smith-Johannsen (1965) have been used by Odencranz et al. (1968) and Magono and Tazawa (1972) to explain their observations of T-shaped aggregates of columns or plates. However, Smith-Johannsen (1969), in a later paper, calculated the charge separation induced by temperature gradients across growing crystals and found them insufficient to account for the large number of T's experimentally observed. The first quantitative measurements of the effects of electrical fields on crystal collection efficiency were reported by Latham and Saunders (1970). In their experiment, ice crystals of 1-10 μm diameter were carried past 0.2 cm ice spheres in a wind tunnel at temperatures ranging from -7°C to -27°C . They found that the growth rate of the collector in the presence of an induced electrical field exceeded the rate when no field was applied by 15% at 500 V cm^{-1} , 40% at 1000 V cm^{-1} and 80% at 1500 V cm^{-1} .

Observations of aggregation in natural snowfall have strongly implied that mechanical interlocking is responsible for the initial collection of ice crystals. Rogers (1974) found that aggregates of sizes greater than 1 cm were composed primarily of planar dendritic habits and spatial crystals with habits P7a, P7b and R3b. Ohtake (1969) concluded that large snowflake formation was due to mechanical interaction of crystals with fine branched structure. A similar conclusion was reached by Jiusto and Weickmann (1973) based on their

observations of snowflakes in Great Lake snowstorms and upslope storms near Denver, Colorado.

Hobbs et al. (1974) identified five types of aggregates in snowfall over the Cascade Mountains of Washington:

- (1) combinations of two or more bullets, side planes, columns, assemblages of plates, assemblages of sectors;
- (2) combinations of needles;
- (3) aggregates of planar dendrites;
- (4) aggregates of radiating assemblages of dendrites;
- (5) combinations of planar dendrites and radiating assemblages of dendrites.

The first two groups contained very small aggregates, seldom exceeding 2 mm. The latter three groups formed aggregates of size 2-6 mm, but often as large as 15 mm. The latter three categories have a high potential for interlocking.

The importance of supercooled water in enhancement of the aggregation process has received little attention in the literature. Rogers (1974) reported that many of the spatial crystals had a rimed core, but he did not observe rime on the branched region of the crystals. However, Jiusto and Weickmann (1973) reported that aggregates in Great Lake snowstorms were frequently rimed.

(2) Physical parameters controlling aggregation

a. Temperature: Studies of the relationship between the maximum diameter of aggregates and surface temperature (Magono (1953), Rogers (1974), Hobbs et al. (1974)) have all shown a distinct peak in the maximum dimension of aggregates when the surface temperature was near 0°C. Hobbs et al. (1974) showed a secondary maximum near -15°C with aircraft

observations. Magono (1953) attributed the enhanced aggregation to a better sticking efficiency. Hobbs et al. concluded that differences in the sizes of the various aggregates were due to differences in the crystals composing them rather than differences in the ground temperature or the precipitation rate. Rogers (1974) attributed the observations to three effects: 1) the depth of the "aggregation zone", between the dendritic zone and the surface, was larger allowing for more collisions; (2) warmer temperatures allow for more effective adhesion; and (3) the rate of vapor diffusion may be larger in the 0°C layer.

b. Crystal concentration: Modelling studies such as Jiusto (1971) have implied that aggregation is much more effective when cloud crystal concentrations are large. The only measurements of the effects of crystal concentration were provided by Hobbs et al. (1974). Hobbs et al. found from aircraft measurements with a continuous replicator and particle decelerator that the probability of aggregate occurrence increased as crystal concentration increased. Their data covered a range of 10-10000 l⁻¹, but had no size or habit discrimination.

c. Crystal size and habit: The size of individual crystals in aggregates varies considerably. Rogers (1974) noted that 75% of the aggregates in his sample contained an "origin" crystal of significantly larger size and of different habit. His observation, together with those of Hobbs et al. (1974) and Jiusto and Weickmann (1973) suggest that aggregation initiation may be due to ordered collisions of particles of different size and habit. This agrees qualitatively with the theoretical results of Passarelli and Srivastava (1979) who found that, at small dispersion of particle fallspeeds, the most effective collisions were between large and small particles.

(3) Collection efficiency and size spectra evolution

Airborne studies of precipitation evolution have generally shown that snow size spectra obey exponential relationships similar to those described by Marshall and Palmer in 1948 (Passarelli, 1978b; Houze et al., 1979; Lo and Passarelli, 1982). Passarelli (1978b) used his analytical model (1978a) and snow size spectra in one storm to deduce collection efficiencies of dendrites between -15°C and -12°C . Houze et al. (1979) found from studies of size spectra evolution that observed particles grow particularly well by collection. Lo and Passarelli (1982) implied from their measurements that aggregate breakup may also be important in the low cloud levels.

B. Surface observations of ice particle aggregation

Three aspects of the aggregation process were investigated using measurements collected at RAD and SPL. These include: (1) the role of surface temperature as a controlling parameter in the flux of aggregate precipitation, the number of crystals composing aggregates and aggregate formation; (2) the relationship between precipitation rate, the flux of aggregates to the surface and the number of crystals composing aggregates; and (3) the role of crystal habit in aggregate formation.

(1) Surface temperature: Several papers reviewed in the previous section presented evidence showing that the maximum diameter of aggregates increased as the surface temperature approached 0°C . One hypothesis suggested by several authors was that the 0°C layer is a region of enhanced collection efficiency due to the increased sticking efficiency of the ice crystals.

To examine this effect quantitatively for Park Range cloud systems, surface data on aggregation was stratified according to temperature

measured at RAD. During the 1981-82 experiment, precipitation samples were collected every 15 minutes on a 250 cm² felt board. The number of single crystals and crystals composing aggregates were counted under magnification for each sample. Simultaneous measurements of precipitation rate were made by weighing 15 minute samples of precipitation collected in a plastic container with a 160 cm² orifice. These measurements were used to determine aggregate flux defined as

$$F_a = R \left(\frac{n_a}{n_a + n_s} \right)$$

Here, F_a is the aggregate flux (mm/hr), R is the precipitation rate (mm/hr), n_a is the total number of crystals contained in aggregates collected in the sample and n_s is the total number of single crystals in the sample.

Figure 88 shows the aggregate flux as a function of surface temperature for all observations at RAD during the 1981-82 field season. No significant trend in the aggregate flux with surface temperature is evident from these data. During the experiment, the majority of the observations were made between -2.5 and +1.0°C. 55% of the samples in this temperature range contained no aggregates despite considerable variation in the precipitation rate (see next section). Values of aggregate flux greater than 1 mm/hr were observed over the temperature range of +2.2 to -7.2°C. Considerable variability was evident in all storms regardless of the surface temperature.

In Figure 89, the number of crystals composing aggregates is shown as a function of surface temperature. The vertical bars in the diagram represent the range of values observed in a single sample. Again, no significant trend is evident in the data. Aggregates with greater than 20 crystals were observed over a wide range of surface temperatures.

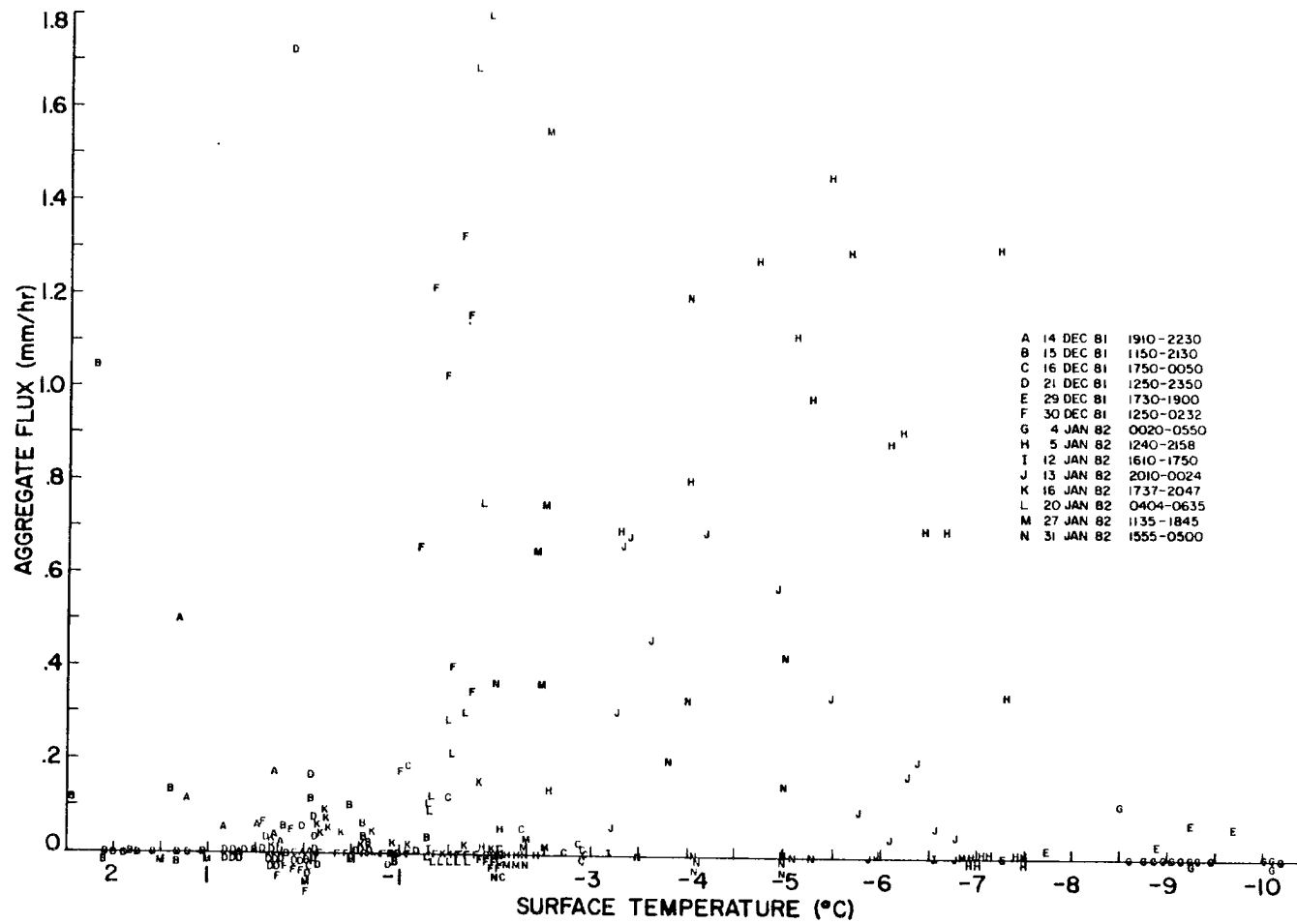


Fig. 88. Aggregate flux as a function of surface temperature at RAD.

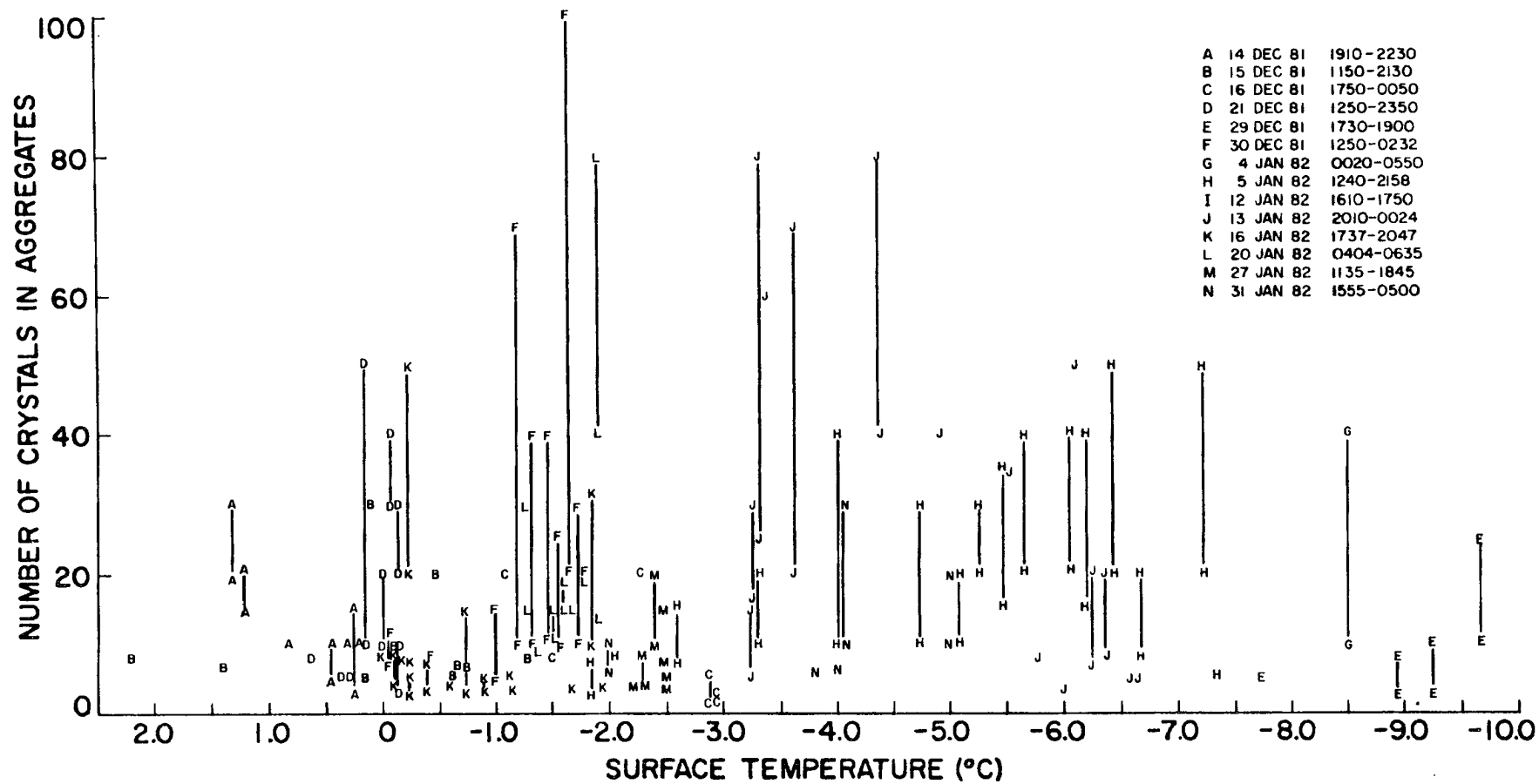


Fig. 89. Number of crystals in aggregates as a function of surface temperature.

However, observations of aggregates with over 50 crystals were limited to the range -1.2 to -4.4°C .

During most storm periods, simultaneous observations of crystal structure were available at RAD and SPL. SPL, approximately one kilometer above RAD, generally has a temperature $6-10^{\circ}\text{C}$ colder than RAD during storm periods. A comparison of observations at both sites provided an opportunity to assess the importance of the warm surface layer in promoting aggregation.

Figure 90 presents the complete climatology of observations of aggregation at both sites for all storms when simultaneous observations were available. On these figures, the boxes represent periods when routine observations were carried out at each site. Darkened areas indicate that aggregates were present in the collected samples. White areas indicate that only unaggregated particles were present. The surface temperatures at both sites are located directly below the boxes.

A summary of all simultaneous observations produced somewhat surprising results. Seventy-five percent of the observations were in agreement, that is, SPL and RAD both observed aggregates (30% of the observations), or neither observed aggregates (45% of the observations). However, 14% of the time, SPL observed aggregates and RAD observed only single particles. These observations occurred almost exclusively in shallow cloud systems. The precipitation mechanism which led to such observations will be discussed in a case study in Sec. C. Eleven percent of the time, only RAD observed aggregates. A third of these observations occurred in the 27 Jan 82 storm when the SPL temperature was -11°C and the surface temperature at RAD was between -2 and -3°C .

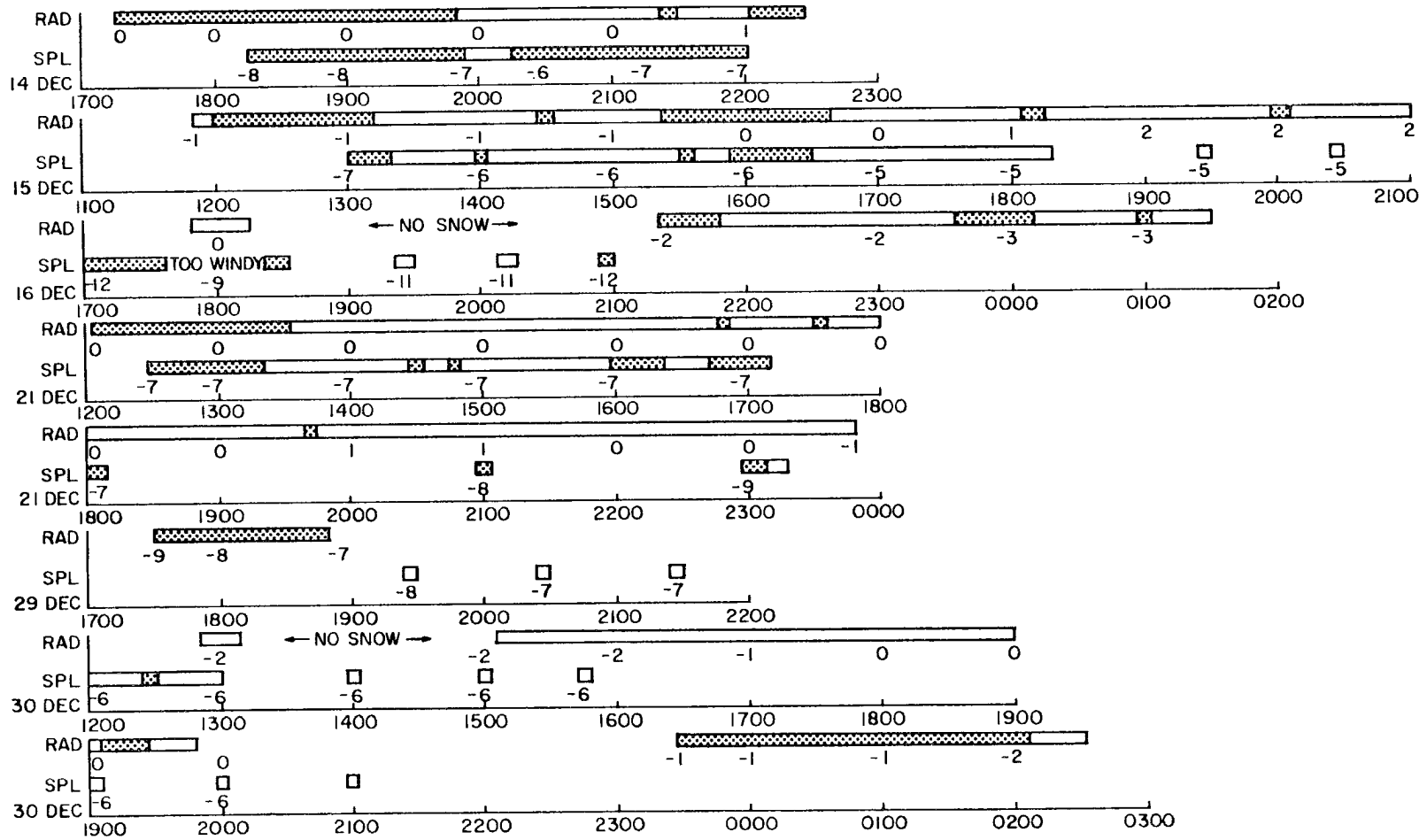


Fig. 90. Climatology of observations of aggregation at RAD and SPL when simultaneous measurements were available.

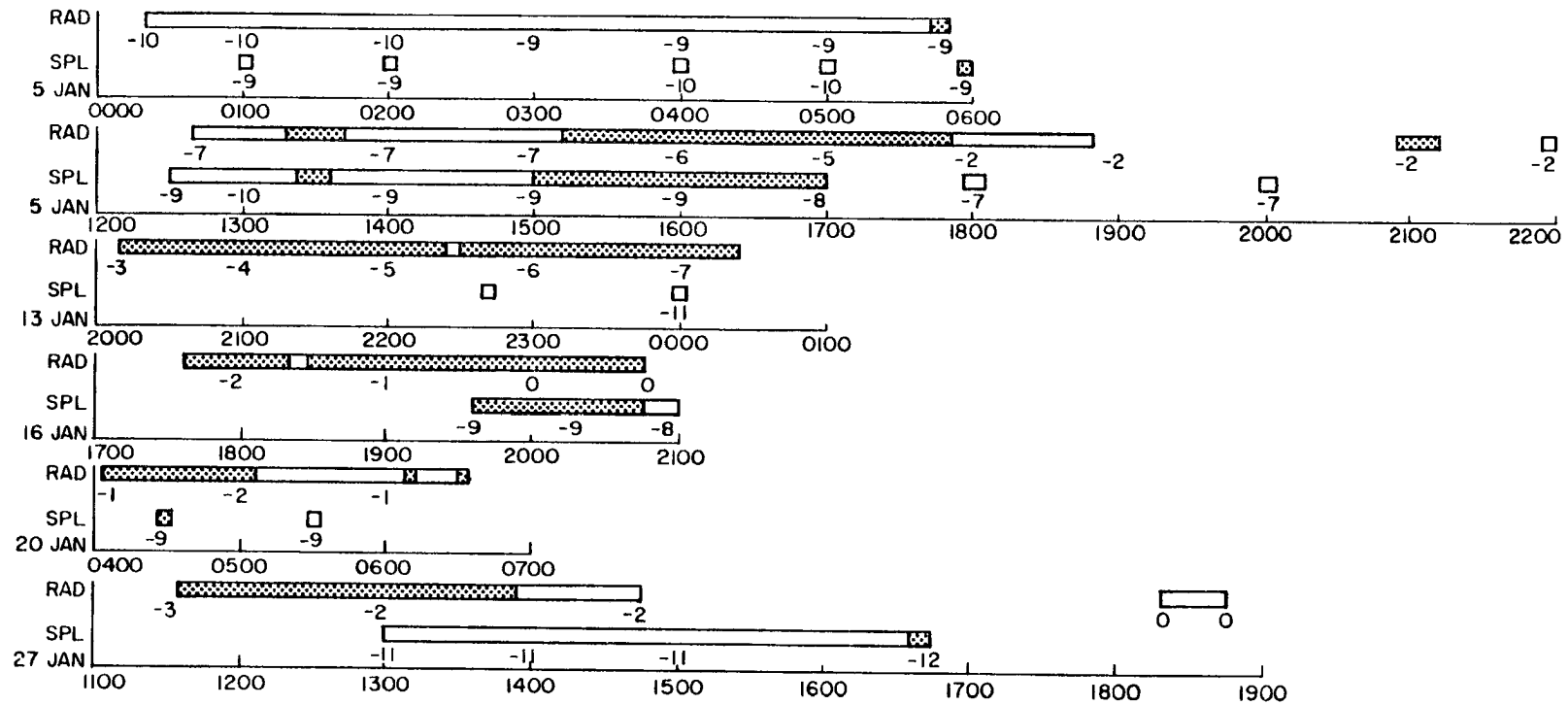


Fig. 90 (cont.). Climatology of observations of aggregation at RAD and SPL when simultaneous measurements were available.

These observations strongly suggest that the aggregation process initiates at temperatures well below 0°C in Park Range cloud systems and that a warm surface layer is not a general condition for the development of large aggregates. An important observation is the high degree of variability in the aggregation process in individual storms at the same temperature. Possible mechanisms for such variability will be discussed in Sec. D.

(2) Precipitation rate

Empirical assessment of observations of precipitation and liquid water structure presented in Chapter 3 suggested that higher precipitation rates were often associated with a higher degree of aggregated precipitation. This observation is examined more quantitatively in this section. Figure 91 shows the aggregate flux as a function of precipitation rate for each measurement at RAD during the 1981-82 experiment. Four sloping lines are placed on the diagram for visual interpretation. These are where 100%, 50%, 25% and 10% of the total precipitation was in aggregated form. Several important characteristics of aggregated precipitation are evident in this diagram.

In moderate to heavy precipitation (> 1 mm/hr), aggregates have a greater tendency to appear in the samples, but they often do not contribute substantially to the total precipitation flux. Aggregates appeared in 58% of the samples collected when precipitation rates were greater than 1 mm/hr. However, aggregates contributed over half the precipitation mass in only 28% of the samples. Many of the samples (42%) with precipitation rates > 1 mm/hr contained no aggregates. A general tendency toward increased riming was observed during heavy precipitation events where no aggregation occurred.

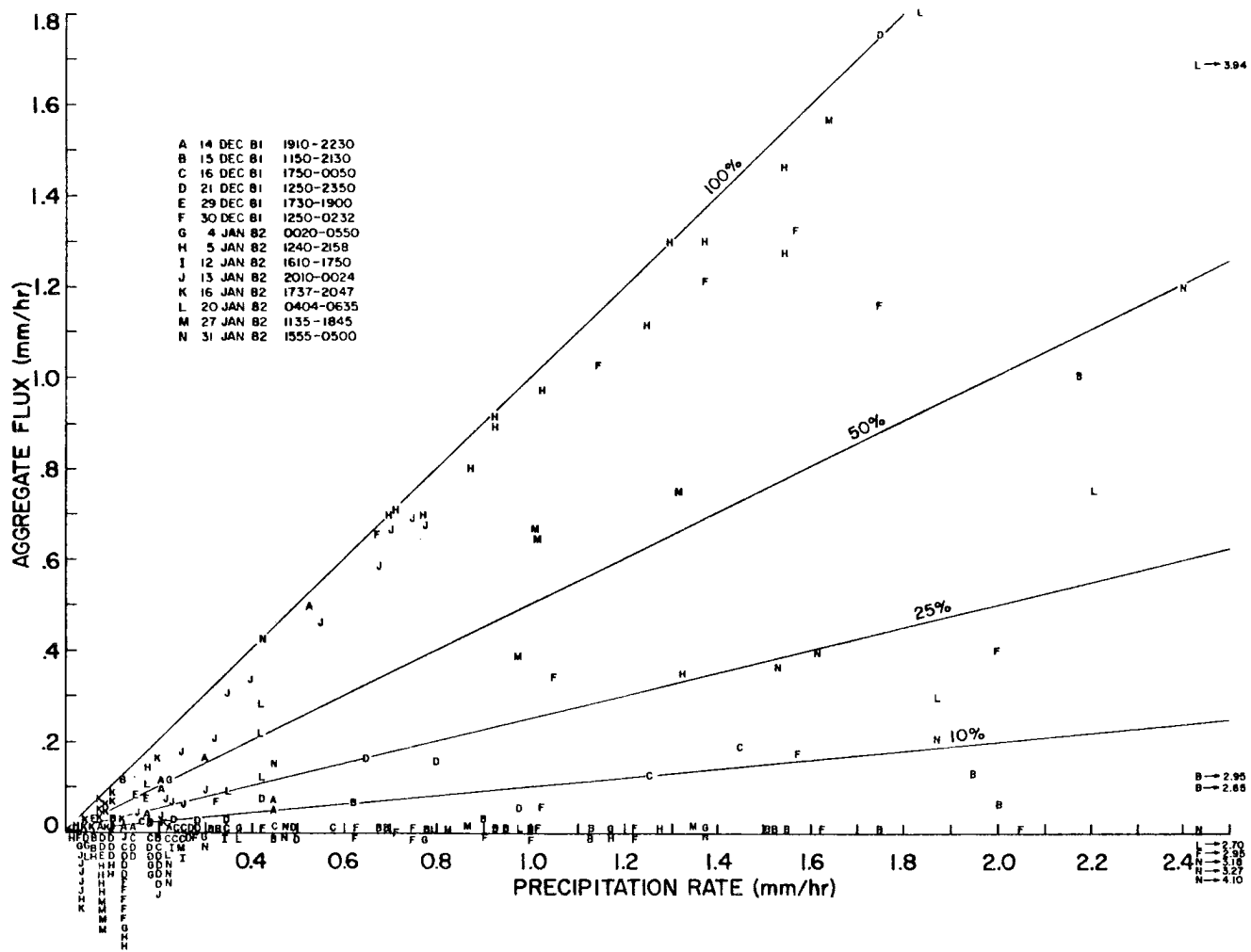


Fig. 91. Aggregate flux as a function of precipitation rate at RAD.

In light precipitation (< 1 mm/hr), 40% of the samples observed contained aggregates. In 20% of the samples, aggregates comprised over half the total precipitation mass. As indicated on Figure 92, aggregates were frequently observed at very low precipitation rates.

A high degree of variability in the aggregation potential of ice crystals occurred within short time periods in individual storms even when the precipitation rate did not change substantially. A good example is the data of 19 Jan 82 (see Fig. 91).

The relationship between precipitation rate and the number of crystals contained in aggregates is shown in Fig. 92. No significant trend is evident in this data. The most interesting aspect of the data is the occasional tendency for rather large aggregates of 20-40 crystals to form during periods with very low precipitation rates.

The general tendency for aggregates to form regardless of precipitation rate suggests that changing cloud ice crystal concentrations may play only a secondary role in the ice crystal aggregation process. Although high ice crystal concentrations in clouds will undoubtedly enhance the frequency of collision, the collection efficiency of these crystals is often low. However, particular habits exhibit high collection efficiencies due to their complex shapes. These particular crystals dominated all moderate to large sized aggregates. The effects of crystal habit are considered in the next section.

(3) Crystal habit

The characteristics of aggregates collected at RAD are examined in this section using shadow photography and visual observations on black velvet boards. The data are presented on a case study basis. Sixteen

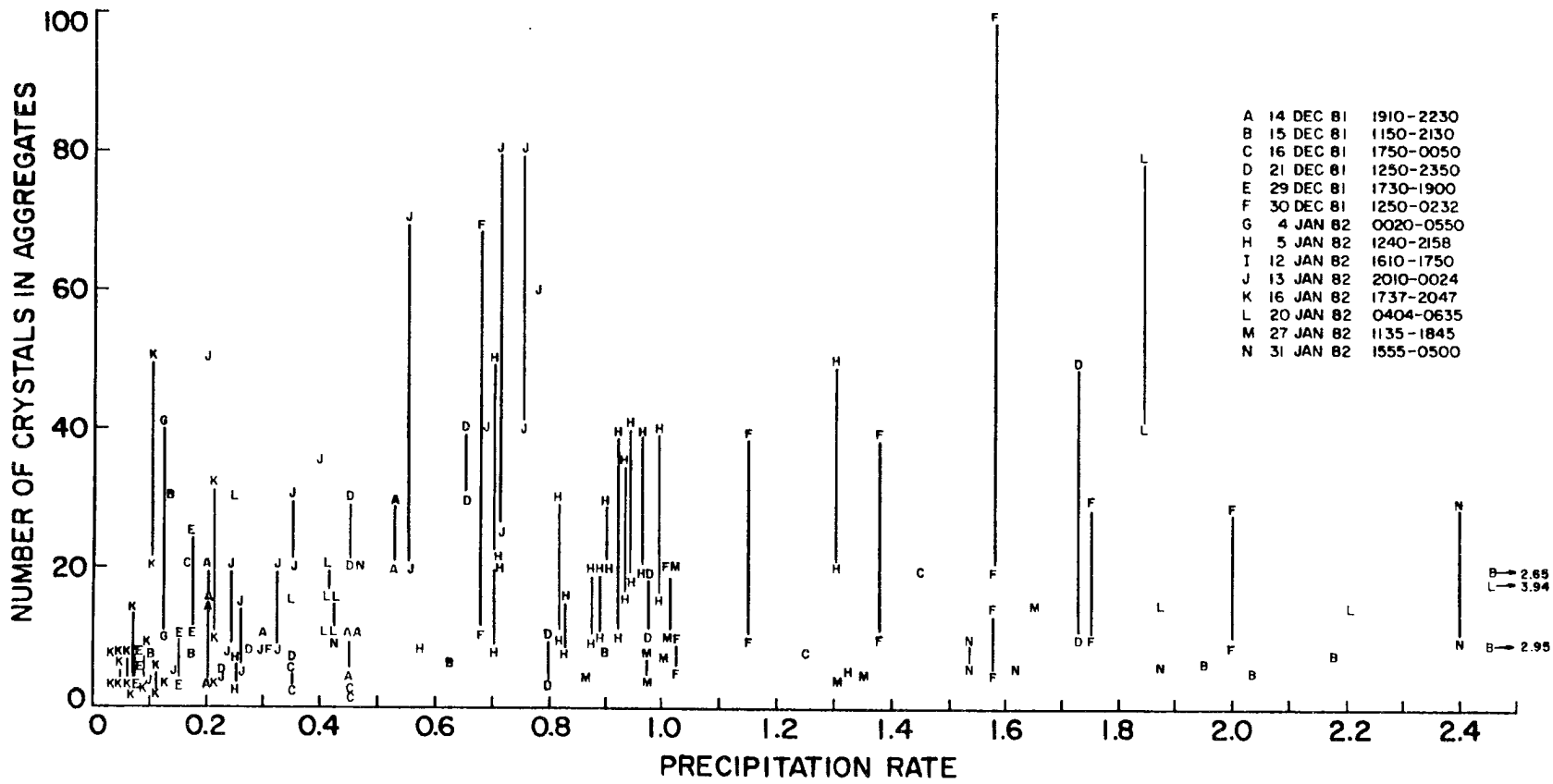


Fig. 92. Number of crystals in aggregates as a function of precipitation rate.

storms are examined. Shadow photographs for these storms are presented in Figs. 63, 93, 94, and 95.

a. 13 December 81: Two periods of aggregation occurred on 13 Dec 81. The first occurred between 1500 and 1800. The crystal habits were predominantly S1 and C2a. Based on the available photographs, these crystals were irregular, consisting of combinations of side planes. An example of these aggregates is shown on Fig. 63a. Aggregates were small, generally consisting of 2-3 crystals. Individual crystals were less than 1 mm. During the aggregation event, snowfall rates varied between 1.0 and 0.1 mm/hr.

The second aggregation event occurred during a 30 minute period beginning at 1940. Crystals in these aggregates were planar dendritic types with various degrees of rime (P1e, P1d, P1f, R2b, R1d). The snowfall rate was 0.1 mm/hr during this event. Shadow photographs were unavailable.

b. 14 December 81: Aggregates on 14 Dec 81 consisted almost entirely of planar dendritic forms, primarily P1e and P1f. Aggregates were observed over a six hour period. During this time, echo tops from the radar indicated that the cloud system was shallow, with tops near -16°C . Three shadow photographs from 14 Dec 81 are shown on Fig. 63. The aggregates on 14 Dec 81 were often composed of 10 crystals and frequently as many as 40. One characteristic evident on all the shadow photographs was that an unusually large (3-5 mm) well-branched planar dendrite was present in many of the aggregates. This was particularly true in large aggregates. Examples are clearly evident in Fig. 63c in the center and in all the large aggregates on Fig. 63d. Close examination of the large aggregate in Fig. 63b shows similar structure.

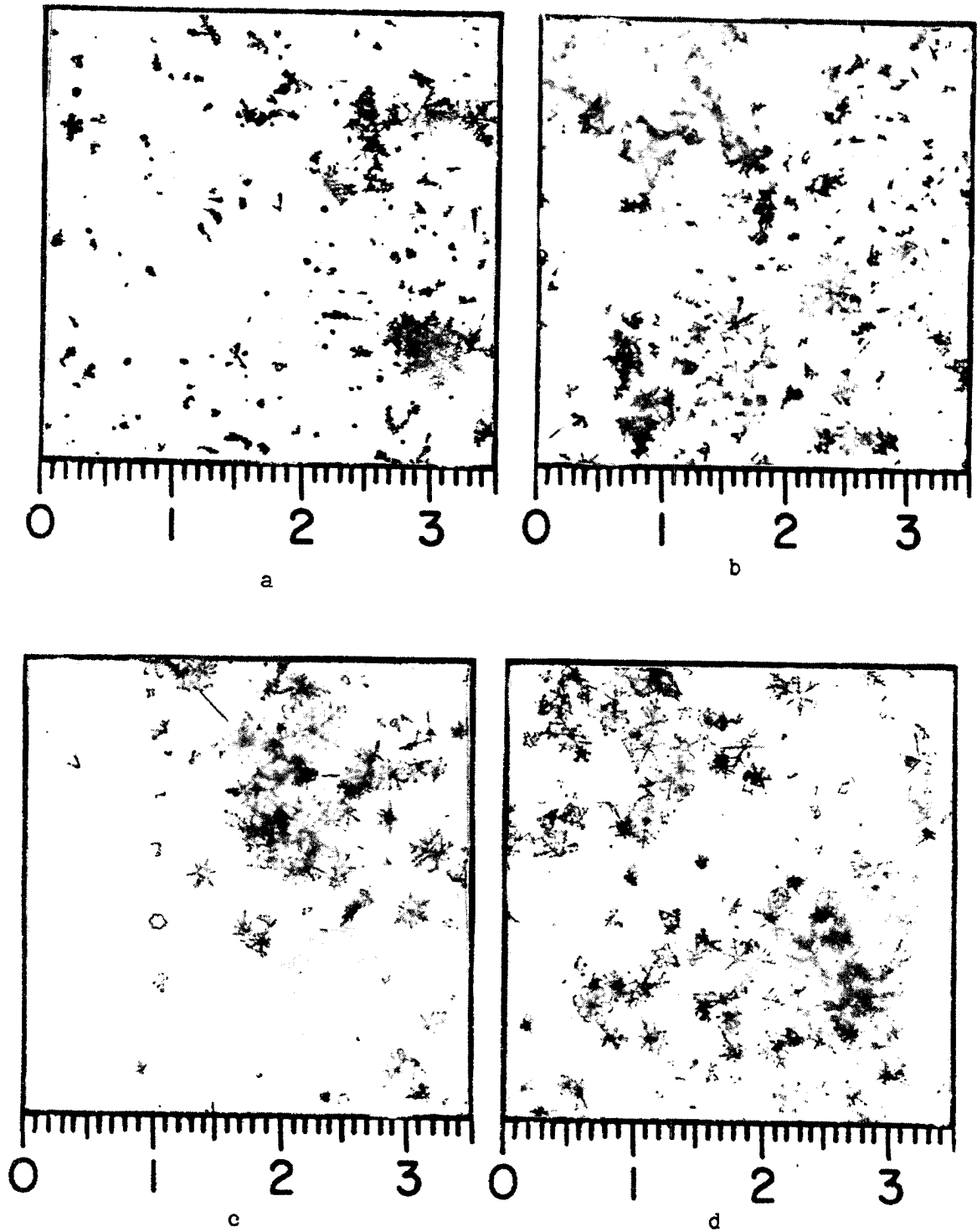


Fig. 93. Shadow photographs of aggregates in the 15 Dec 81 (a,b) and 29 Dec 81 (c,d) storms.

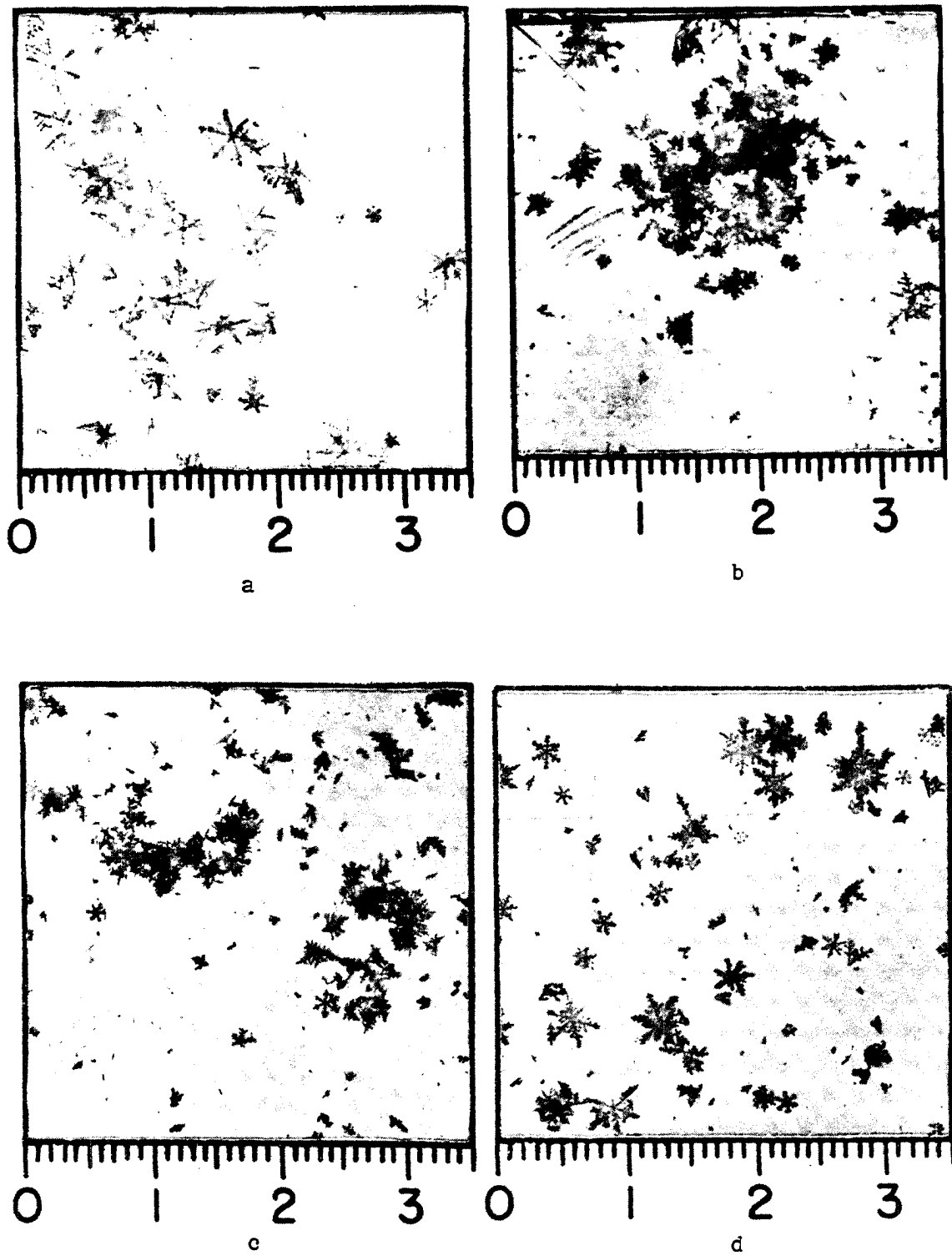


Fig. 94. Shadow photographs of aggregates in the 29 Dec 81 (a), the 30 Dec 81 (b,c) and the 4 Jan 82 (d) storms.

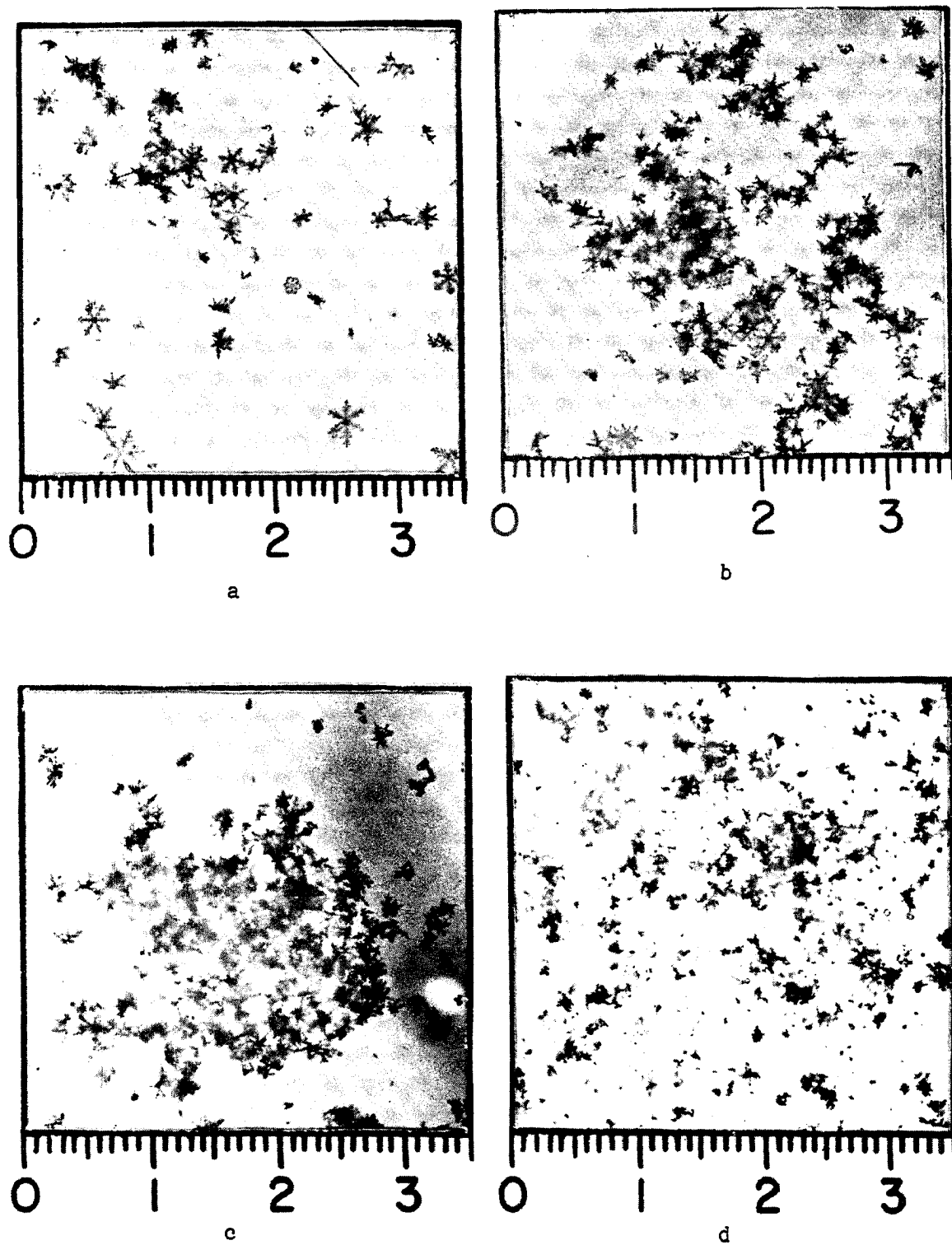


Fig. 95. Shadow photographs of aggregates in the 13 Jan 82 (a,b), the 21 Jan 82 (c), and the 27 Jan 82 storms.

It is evident from these photographs that the presence of large delicately branched crystals contributed substantially to the collection efficiency through mechanical interlocking. Light rime was also present on many of the aggregates. This rime appears to have accumulated after the aggregate formed. Aggregates of similar type were observed throughout the period at SPL (-7°C) indicating that the zone of aggregation formation extended well above the elevation of the -7°C isotherm. In fact, aggregates continued to be observed at SPL during several periods when only single crystals were observed at RAD.

c. 15 December 81: Aggregation occurred during five periods on 15 Dec 81, totalling about 3 hours of a ten hour storm event. Aggregation was generally light, despite a large precipitation rate at times. The two extended periods of aggregation were from 1200-1320 and 1520-1640. A shadow photograph from each of these periods is shown on Fig. 93a and 93b. The characteristics of aggregates in the samples were somewhat masked by rime accumulation and breakage. However, it is evident in the shadow photograph of Fig. 93a that large branched dendrites serve as collectors for many of the irregular crystal shapes. In the sample at 1530, the collection of rime on the aggregate is undoubtedly serving to consolidate the ice mass into a firmer structure. Although a large core crystal cannot always be identified in these photographs, many of the aggregates do contain the larger dendritic crystals. These may serve as the foundation of the aggregate structure. Only light aggregation was observed during these periods at SPL (-6°C). Aggregates at SPL were composed of planar dendritic forms.

d. 16 December 81: Crystals on this day were very small with irregular shapes characteristic of cold clouds. Nearly all crystals were

unaggregated. The few aggregates which did fall were primarily composed of 2-3 P7a crystals. An exception to this were occasional aggregates of up to 20 crystals. These only occurred during periods when planar dendritic forms were also observed. Unfortunately, shadow photographs were unavailable for periods with aggregated snowfall.

e. 21 December 81: One major aggregation event occurred during the 12 hour storm on 21 Dec 81. During this period, which lasted 1.5 hours, riming was significant. The component crystals of the aggregates were P1f, P7b, and P7a, but in most cases identification was difficult because of heavy rime. Only one poor quality shadow photograph was available. In this case, riming clearly aided in cementing crystals into a single ice mass. Very light aggregation occurred occasionally later in the day. These aggregates were also heavily rimed.

f. 29 December 81: Several excellent photographs of aggregates which fell during light snowfall (<0.2 mm/hr) were available for 29 Dec 81. These are shown on Figs. 93c,d and 94a. These aggregates are typical of the two types of large aggregates observed in Park Range snowfall. All of the aggregates contained rather large (4-5 mm) planar dendrites of P1f habit. The first type of aggregate (Fig. 93c,d) also contains numerous R3b and P7b crystals. These spatial crystals most frequently have a visibly rimed core upon which dendritic extensions grow. The rimed core present in these crystals indicates that riming occurred prior to the diffusional growth of the extensions. This is strong evidence that supercooled water was present within the dendritic growth regime. Evidence of such high level supercooled water was presented in Chapter 3. These crystals appear to collect on a "platform" provided by the larger planar crystals. Once the aggregate growth initiates, the

"platform" then continues the capture of smaller crystals as the fall velocity of the aggregates increases. A second type of large aggregate which occurs in the absence of R3b and P7b spatials is an assemblage of very large P1f planar dendrites. An example of such an aggregate is shown on Fig. 94a. These aggregates have been observed in very light snowfall at RAD.

g. 30 December 81: Three distinct periods of aggregation occurred on 30 Dec 81. The first period, which lasted 30 minutes, involved very light aggregation and extensive riming. The only photograph available had virtually all single particles except for one small aggregate with only one identifiable crystal. The second period, 2 hours long, was a heavy aggregation event. These aggregates were typical of large aggregates associated with moderate to heavy snowfall. Examples are shown on Fig. 94b and c. Again the core crystals were dendritic with few large crystals identifiable. The primary characteristic of these aggregates was the rime accumulation. It is this large mass accumulation that contributes substantially to the increase in precipitation rate. It appears that the rime accumulation occurred well after the initial formation stage of the aggregate indicating that the supercooled water occupied the lower cloud levels. From the photographs, it also appeared that fragmentation may have occurred along the aggregate edges. The third aggregation episode occurred late in the storm after a change in habit to colder crystals occurred. Unfortunately, no pictures were available to estimate the effectiveness of the aggregation during this period.

h. 4 January 82: This day was examined because aggregation did not occur despite the presence of many large planar dendritic crystals.

Figure 94d shows an example of such crystals. Aggregates were also not observed at SPL, despite light-moderate snowfall composed almost entirely of these crystals. Three factors contributed to the lack of aggregates on this day. Close examination of the majority of the crystals photographed indicated that these dendrites had a complex internal structure more similar to a P2d crystal, rather than the delicately branched P1f. A good example is the large dendrite in the upper right corner of Fig. 94d. These crystal forms do not have as great a capability to interlock with other crystals of similar type because few gaps exist in their structure. It is likely that collisions of these crystals result in few successful captures. The second factor which prevented aggregation was that the spatial dendritic forms (P7b, R3b) were not present. These crystals have arms perpendicular to the basal plane of a dendrite falling in hydrodynamic equilibrium and can interlock easier to provide a base for subsequent crystal capture. The last and possibly most important factor was that the precipitation rates were very low (0.025 mm/hr) during the dendritic snowfall period. Such low rates imply that collisions in the cloud were infrequent.

i. 5 January 82: This storm is presented as a major case study in section C.

j. 13 January 82: Aggregates fell throughout the day from this cloud system. Snowfall rates were light-moderate (0.2-0.8 mm/hr), despite the fact that the cloud was orographic and quite shallow, with echo tops at the -16°C level. Heavily aggregated snow fell much of the day at SPL (-10°C) indicating that the aggregation process operated very efficiently in the upper layers of the cloud. Aggregates during the early part of the storm were primarily composed of R3b and P7b crystals

although some planar dendritic crystals were evident. Figure 95a shows an example of a chain of seven spatials. As the storm progressed, both planar and spatial crystal types became more common. Figure 95b shows large aggregates composed of planar dendritic forms and primarily R3b spatials. Given the shallow nature of the cloud, the rapid formation of such aggregates requires specific conditions in the upper cloud region. These conditions will be described in the second major case study described in section C.

k. 16 January 82: This storm is presented as a major case study in section C.

l. 19 January 82: Aggregation was observed in association with strong convection on this day. Unfortunately, only limited observations were available. Spatial dendritic crystals dominated the aggregates but other crystal types, primarily S1, S2 and P7a were observed.

m. 21-22 January 82: This storm system was interesting because only one short period in the storm had aggregated precipitation. During most of the storm, the crystals were extremely small and unaggregated. Near the end of the storm, a rapid change occurred in the size and habit of the crystals, and large aggregates began to fall. An example of a 2.5 cm aggregate is shown on Figure 95c. The surface temperature at the time the sample was collected was -4.7°C . The primary crystal habits again were planar (P1f) and spatial (R3b) dendrites. Other crystals may be present in the aggregate, but its large size prevented a more detailed examination. This particular sample contained over 200 crystals. Aggregates were observed simultaneously at SPL (-13°C), although windy conditions prevented detailed observations.

n. 23 January 82: Data were not collected at RAD during this storm. However, measurements were made at SPL and with aircraft. The aircraft penetrations were during the shallow storm stage, late in the storm's evolution. During the entire period, the SPL temperature was -12 to -14°C. Heavy aggregation occurred. The primary crystal habits were P1f, R1b, and R2d. Some R4b snow pellets were observed. Aircraft measurements confirmed that the cloud was shallow and stable, with strong wave motion to the lee of the Range. Cloud top was 1.5 km above mountain top. A substantial quantity of supercooled liquid water was present at cloud top. This case study was very similar to the 16 Jan 82 storm described in section C. A detailed discussion of this type of cloud system will be given in that section.

o. 27 January 82: Aggregates on 27 Jan 82 were composed primarily of small highly rimed spatial crystals and fragmented dendritic forms. The habit of the majority of the crystals was masked by large rime accumulations. This storm was the only storm where aggregation occurred at RAD and not SPL for an extended period. During this period, however, aggregation was extremely light, with 96-98% of the crystals at RAD remaining unaggregated. Figure 95d shows an example of a rimed aggregate which fell during the early part of the storm. It appears in this case that rime accumulation was instrumental in solidifying the aggregate structure.

p. 31 January 82: Two types of aggregates appeared during this storm. The first type were very small aggregates of C2a, P7a, and R3c crystals. Aggregates were generally limited in size to 2-3 crystals. During a later phase of the storm, large planar dendritic forms appeared. Numerous spatial crystals (R3c, R3b) were also present. The switch in

crystal habit was accompanied by an increase in the size and number of aggregates.

C. Physical models of aggregation in cold cloud systems

(1) Aggregation in a deep cloud system

The storm selected for detailed study was the 5 Jan 82 system. This storm has also been discussed in Secs. 2 and 4. The 5 Jan 82 storm system evolved through several distinct stages during its passage through the study area. The storm developed in association with a rapidly moving trough system which passed over the Northern Colorado mountains. Warm advection occurred throughout the period.

Figure 96, three infra-red satellite images taken at 1315, 1415 and 1515, illustrate the stages of evolution of the storm. Two deep cloud regions are evident on Fig. 96a: the first, a narrow band extending southward into Colorado from Wyoming, and the second, a deep cloud region covering much of the state of Utah. Between the deep cloud regions a shallow orographically induced system was present. The deep cloud regions were characterized by heavier precipitation rates and aggregated precipitation. The orographic system produced light precipitation rates, with single rimed particles. The deep cloud region which covered the state of Utah (Fig. 96a) arrived in the Park Range region at 1450 (see Fig. 96b,c). Upon its arrival, a 2 hour quasi-steady period of heavy precipitation consisting primarily of unrimed aggregates commenced.

Figure 97 shows a sounding taken 60 km upwind of the crest of the Park Range at 1500, directly after the system moved over the region. Two important features are evident on this sounding: 1) the atmosphere was stable throughout the depth of the troposphere and 2) the winds aloft

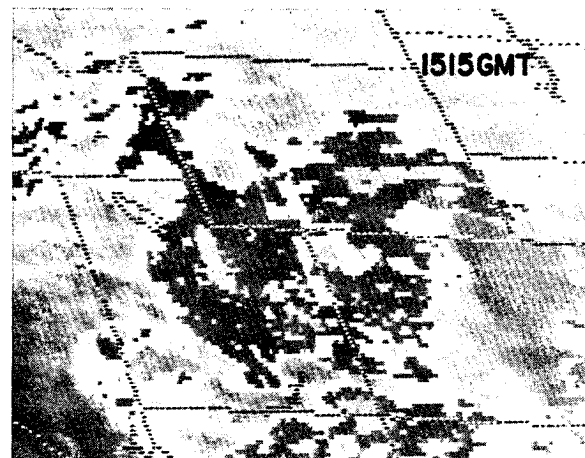
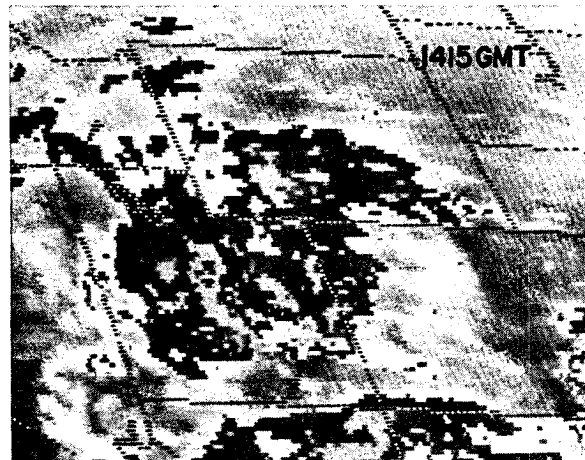
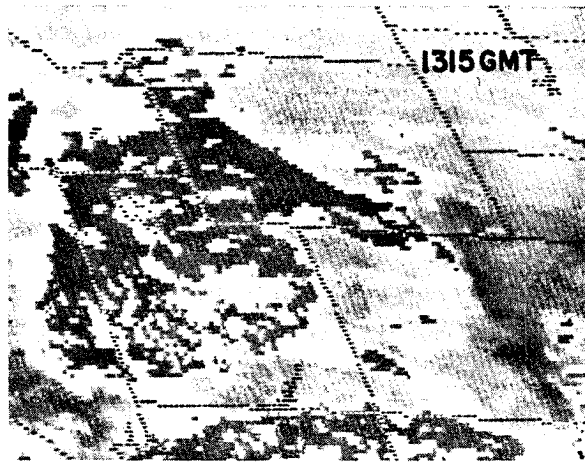


Fig. 96. Satellite images of the 5 Jan 82 storm at 1315, 1415, and 1515 GMT.

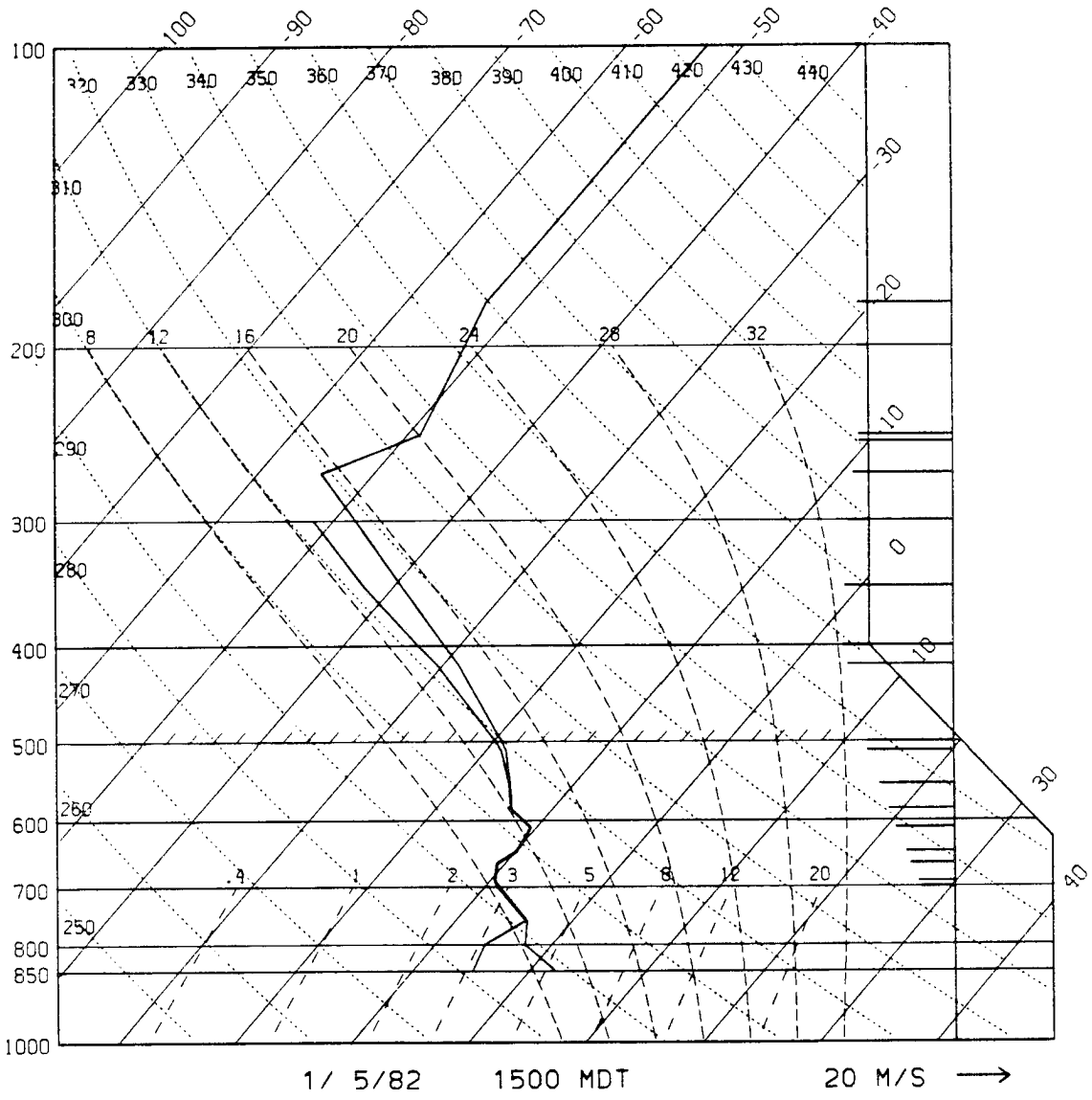


Fig. 97. 1500 GMT sounding at CG on 5 Jan 82.

were particularly strong. Winds veered with height from southwesterly at 18 ms^{-1} at 70 KPa to westerly at 34 ms^{-1} at 50 KPa. The sounding shows the magnitude of the westerly component of the wind velocity.

The ground based physical and remote sensing observations for the entire storm are shown on Fig. 98 and Fig. 99. The two hour quasi-steady period of heavy aggregated precipitation began at 1500. Crystal habits, degree of rime and aggregation were observed at SPL and RAD. These data are displayed in Figs. 98a,b and 99a,b. The data are segregated into rimed particles, unrimed particles and aggregates. Under aggregation, the symbols D and # for SPL indicate the degree of aggregation (0, no aggregation, M, moderate aggregation, A, virtually all particles aggregated) and the estimated number of crystals in the aggregate (#). On the figures, % is the percent of crystals in aggregates at RAD and #, the number of crystals in aggregates at RAD. Precipitation rate was estimated at SPL (Figs. 98c and 99c) and measured at RAD (Figs. 98d and 99d). The SPL estimate was visual and classified as 0 (none), L (light), M (moderate) or H (heavy). Figures 98e and 99e show the integrated liquid water content measured over the radiometer during the period. In the figure, 15° values are normalized by multiplying by the sine of 15° so that they can be compared to the vertical values. Figures 98f and 99f show the time-height display of reflectivity measured by the radar.

Throughout the 2 hour period, echo cloud tops ranged from 5.5 - 6.0 km. Radiometric measurements indicated that the cloud was devoid of supercooled liquid water. This was confirmed by crystal observations at SPL and RAD. Initially after the deep cloud system developed, rimed crystals were observed at both sites. Within a short time after the

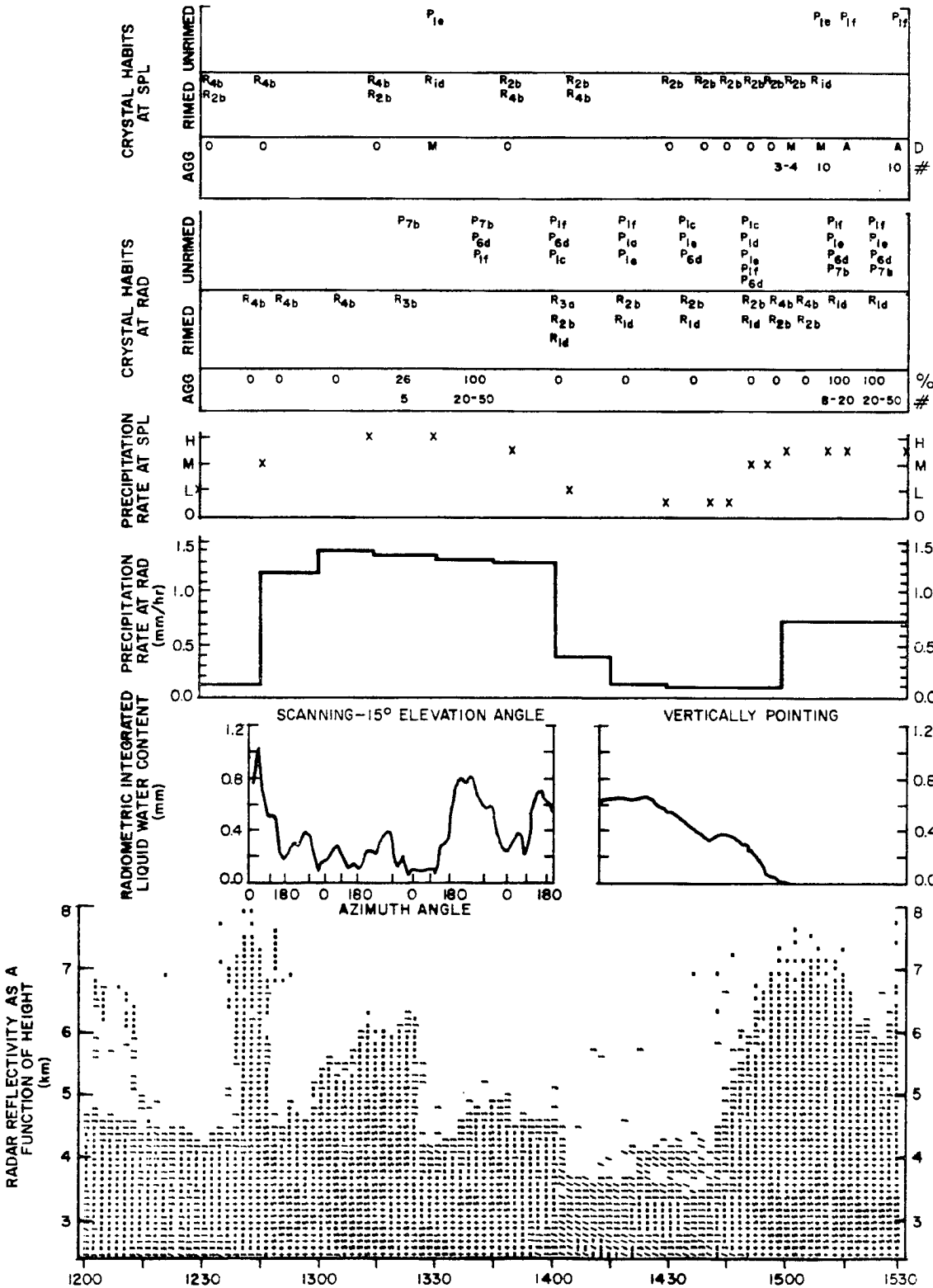


Fig. 98. Ground based and remote sensing measurements for the 5 Jan 82 storm from 1200-1530 GMT. Description of the data format is given in the text.

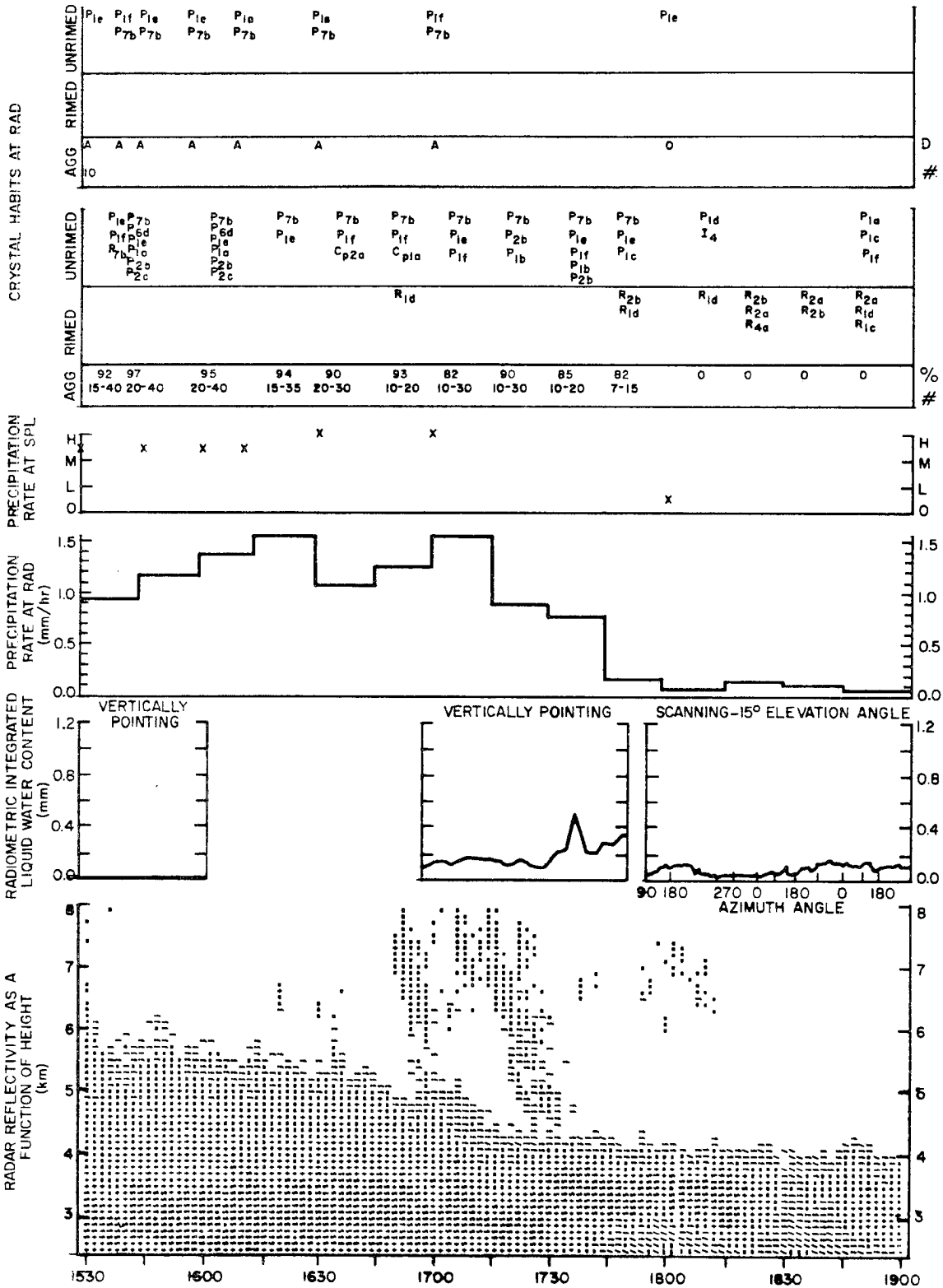


Fig. 99. Ground based and remote sensing measurements for the 5 Jan 82 storm from 1530-1800 GMT. Description of the data format is given in the text.

onset of the deep cloud, virtually all crystals collected at both sites were unrimed and highly aggregated. Precipitation with these characteristics continued to fall throughout the remainder of the two hour period. Crystal habits observed at both sites were all P1e, P1f, P6d and P7b. Based on these observations, the majority of the diffusional growth of precipitating crystals occurred within the dendritic temperature ranges. Precipitation rates at RAD varied from 0.70 to 1.55 mm/hr. Precipitation at SPL was moderate to heavy throughout the period.

The flight track for the Cheyenne II aircraft on 5 Jan 82 is shown on Fig. 100. Aircraft observations of the physical structure of this cloud between 6800 m and 4400 m from a sounding taken just upwind of the mountain between 1538 and 1546 were discussed in Sec. 4 and are shown on Figs. 71 and 72. Figure 71 shows the liquid water content measured by the FSSP and total ice crystal concentrations measured by the 2D-c probe. Throughout the sounding, liquid water contents were near zero. Ice particle concentrations ranged from 5 l^{-1} near cloud top to 100 l^{-1} at 4400 m. The size distribution of these ice particles at selected points on the sounding are shown in Fig. 72. Two important features concerning the evolution of the ice phase in this cloud system were evident from these spectra: 1) a large number of small ($<200 \text{ }\mu\text{m}$) crystals were present above and within the dendritic growth region, and 2) the upper cloud layers were dominated by diffusional growth processes. Aggregation growth began in the lower portion of the dendritic growth zone and accelerated rapidly between this region and the mountaintop level.

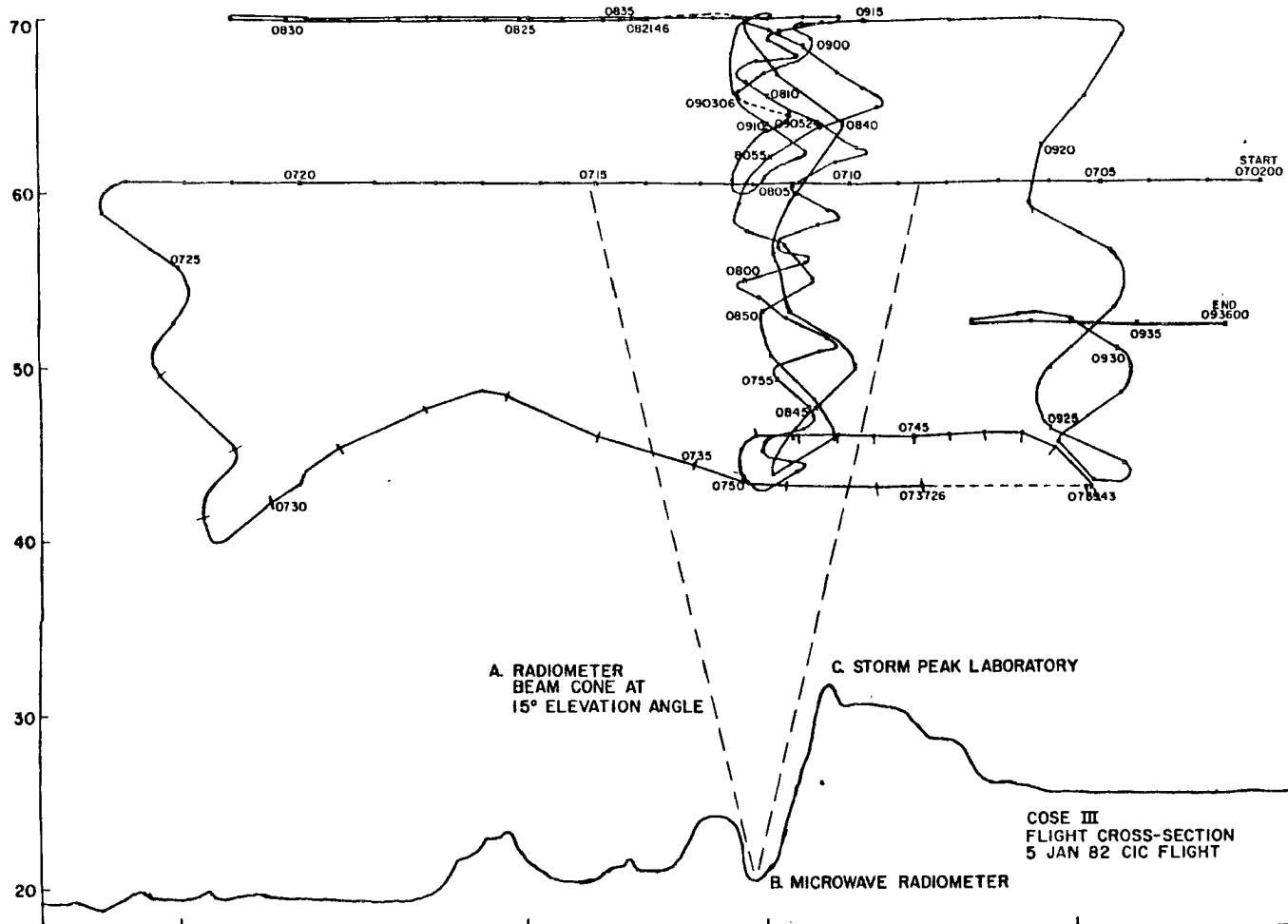


Fig. 100. 5 Jan 82 flight track of Cheyenne II.

An example of the rapid acceleration of the aggregation process in the lower region of the dendritic zone was available from the earlier sounding near Craig. On this sounding, the aircraft was able to descend to 4100 m, 300 m lower than the sounding over the radar. 2D-c images from this sounding were shown on Fig. 61. It is evident from these images that rapid growth of dendritic crystals occurred by vapor diffusion and then by aggregation in the region between -16°C and -13°C .

From ice crystal observations in the valley, at mountaintop and by the aircraft as well as radar reflectivity returns, a physical model of the aggregation process in this cloud system was developed. This is shown on Fig. 101. Four zones of particle growth were identified.

These were:

1) Colder than -17°C crystal growth was principally by diffusion. Crystal concentrations varied between 20 to 40 l^{-1} between -29 to -15°C . The majority of the crystals were $< 200\ \mu\text{m}$ in size. Examples of the largest 2D-c images observed on the sounding are shown on Fig. 102.

2) Between -15°C and -12°C aggregate embryos were identified (i.e., double crystal aggregates) and ice crystal concentrations were as high as 100 l^{-1} . The great majority of the crystals were small implying fragmentation (Sec. 4). Only the larger crystals interacted in the aggregation process.

3) Between -12°C and -10°C significant scavenging of the single crystal population by mature aggregates was prevalent. By the time precipitation particles reached the mountaintop observation site, virtually all crystals were significantly aggregated.

4) From -10°C to the valley floor (-5°C) aggregate-aggregate collection/breakup processes prevailed, although single crystal

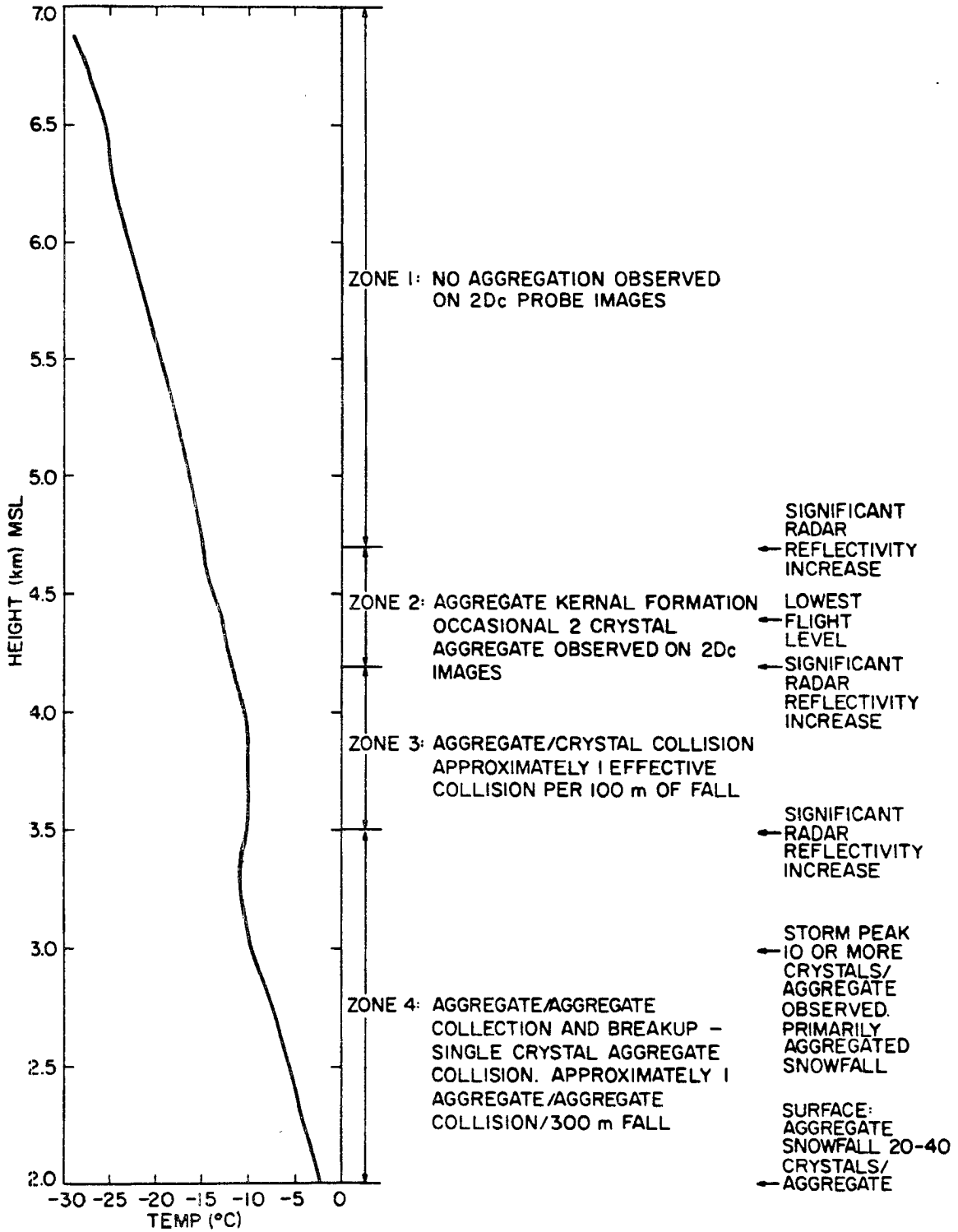


Fig. 101. Physical model of the aggregation process in the 5 Jan 82 cloud system.

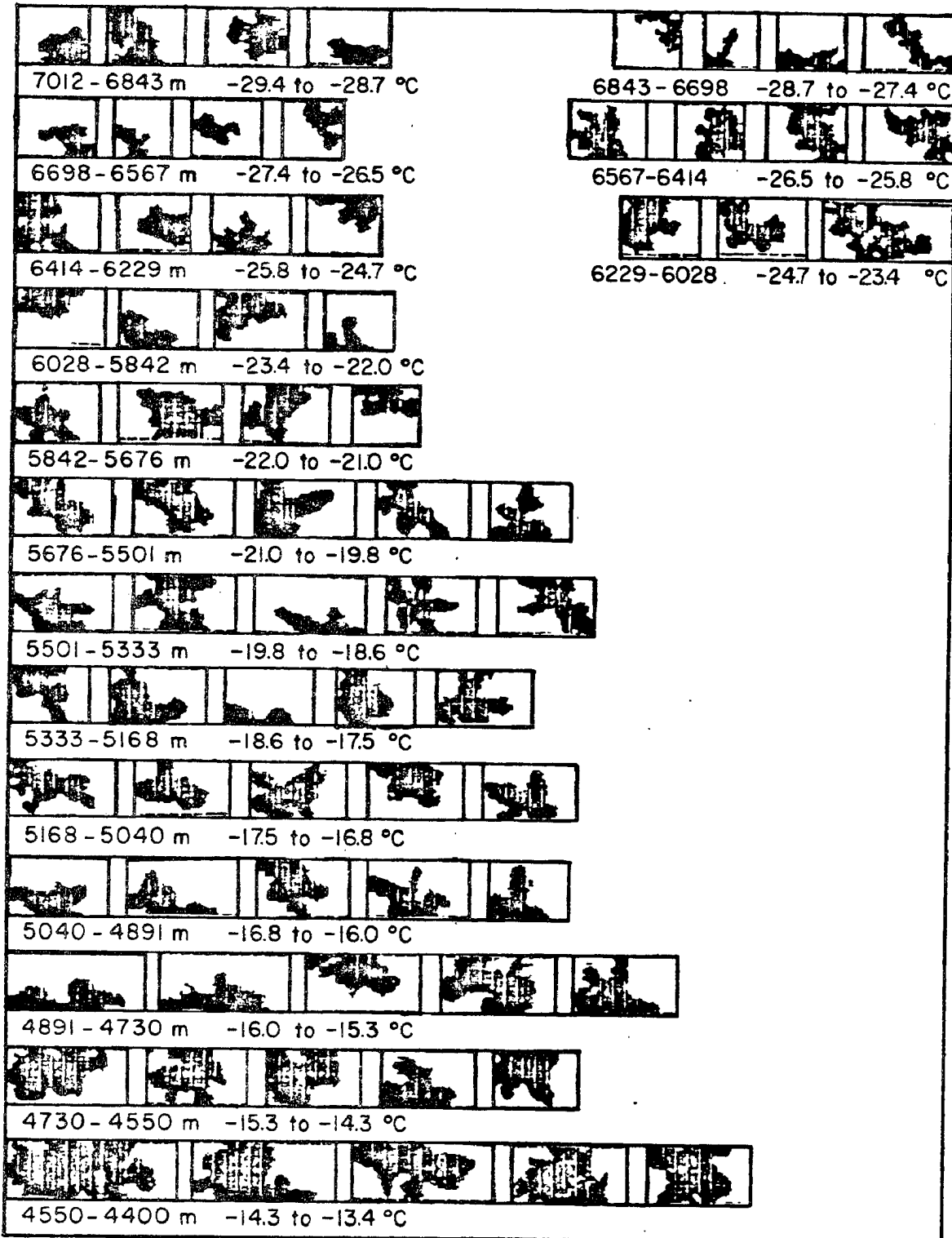


Fig. 102. Largest 2D-c images on the 5 Jan 82 sounding.

collection by aggregates continued. By the time precipitation particles reached the valley floor, they consisted of large aggregates.

This case study illustrates the aggregation process in a deep cloud system. In this case, the primary components of the aggregates were planar dendritic crystals. Although many variations are sure to occur in other deep cold cloud systems which produce heavily aggregated precipitation, the importance of the dendritic growth zone is evident. In the following section, aggregation in a shallow cloud system is examined. Again, the dendritic growth region was an important feature.

2. Aggregation in a shallow cloud system

Four shallow cloud systems, 14 Dec 81, 13 Jan 82, 16 Jan 82, and 23 Jan 82, produced significant aggregation events during the field program. These clouds all had tops between 4.0 and 4.5 km (1.0 to 1.5 km above the mountaintop) and cloud top temperatures between -15 and -20°C. The first two cloud systems, 14 Dec 81 and 13 Jan 82, were studied using surface and remote sensing measurements. Aircraft support was available for the 16 Jan 82 and 23 Jan 82 storms. In this section, the 16 Jan 82 case is used to illustrate the processes in shallow clouds which lead to the production of aggregates. This case was also discussed in Sec. 2 on dendritic crystal growth.

The 16 Jan 82 cloud system was shallow, stable, and had a well defined edge about 60 km upwind of the Park Range crest. Figure 103 shows a vertical profile of the cloud structure during the period when aircraft measurements were collected. The flight track is indicated on the figure.

Surface measurements of ice crystal structure at RAD during the flight period are compiled in Table 11. During the flight, snowfall was

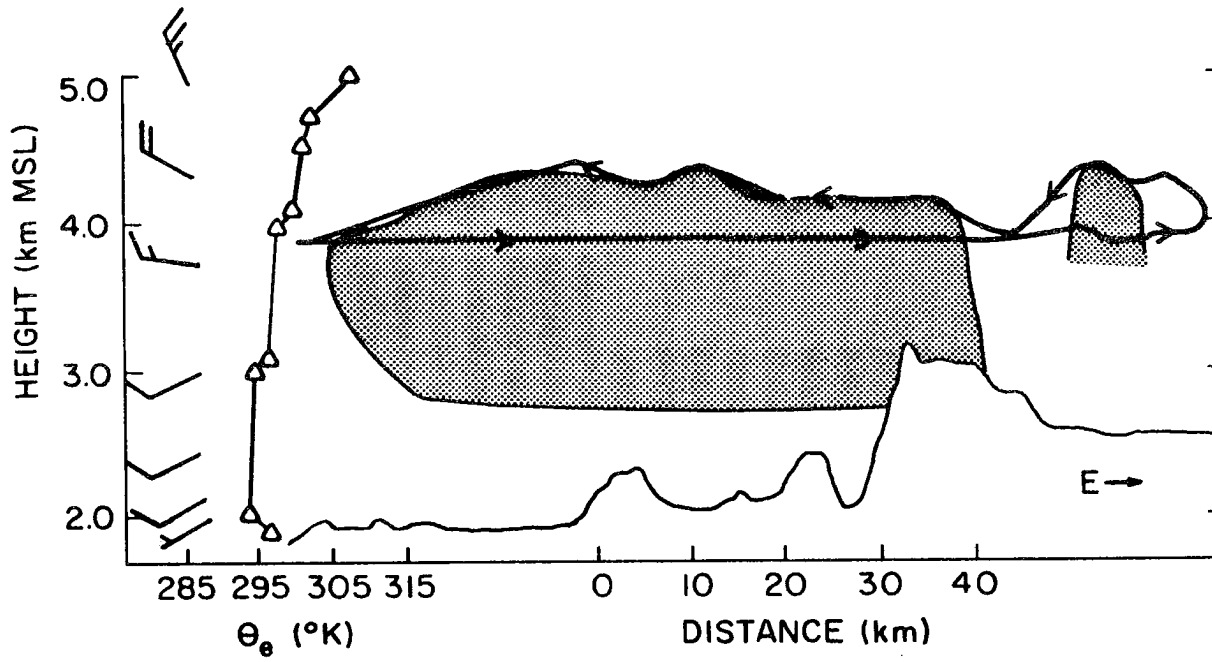


Fig. 103. Vertical profile of the 16 Jan 82 cloud system (from DeMott et al., 1985).

Table 11
SURFACE OBSERVATIONS AT RAD ON 16 JAN 82 DURING FLIGHT PERIOD

Time GMT	Sample time (s)	Number of single crystals and crystals in aggregates	Single crystal size (mm)	Habits	Precip rate (mm/h)
1910	10	single: 16 agg: 4,7,15	1.0-3.5	R3b, P1d, P7b	0.075
1920	10	single: 3 agg: 4	1.0-3.5	P1f, R3b	0.025
1937	10	single: 7 agg: 3,7	1.0-3.5	P1f, P1d, R3b	0.025
1950	20	single: 3 agg: 7	2.0-3.5	P1f, R4a	0.025
2008	30	single: 4 agg: 3,4,8	1.0-3.5	P1f,R3b	0.025
2020	10	single: 12 agg: 7,7,7,7,7	2.0-3.5	P1f, R3b, P1d	0.025
2035	10	single: 15 agg: 20,20,40,40,50	1.5-3.5	P1f, R3b	0.075
2047	10	single: 4 agg: 3,4,5	1.5-3.0	P1f, R3b	0.100

light, consisting primarily of aggregates of unrimed planar crystals and R3b spatials. At SPL (-9°C), snowfall was moderate and primarily composed of aggregates of planar dendrites. The sizes of these aggregates were not measured, but were estimated visually as large. Individual dendrites in the aggregates were 2-3 mm in diameter.

These particular habits, P1f and R3b, both require an environment at or above water saturation to grow. In addition, cloud droplets must be present within or above the dendritic growth region (-16 to -13°C) for the R3b crystal to develop a rimed core prior to growing dendritic extensions. Such conditions were found to exist near the top of the 16 Jan 82 cloud system.

Aircraft measurements of crystal concentrations, liquid water contents and state parameters from the horizontal transect near 3.9 km between 1932 and 1946 are shown on Figure 104. 2D-c images at two points along the track are shown on Figure 105.

Liquid water was observed at -16°C , 200 m below cloud top, throughout the transect. In addition, ice crystals were present in concentrations of $1-5 \text{ l}^{-1}$. Such an environment provides the necessary conditions for the production of the crystal habits observed in the snowfall on 16 Jan 82. The 2D-c images exhibit shapes characteristic of planar dendritic crystals as well as circular particles typical of the rime core. Spatial dendrites are difficult to separate from planar forms on the images because the projection often appears similar in two dimensions.

Typical droplet spectra from FSSP measurements during the transect are shown on Figure 106. Based on Pitter's (1977) calculations of ice particle/droplet collection efficiencies, particles of 200-400 μm

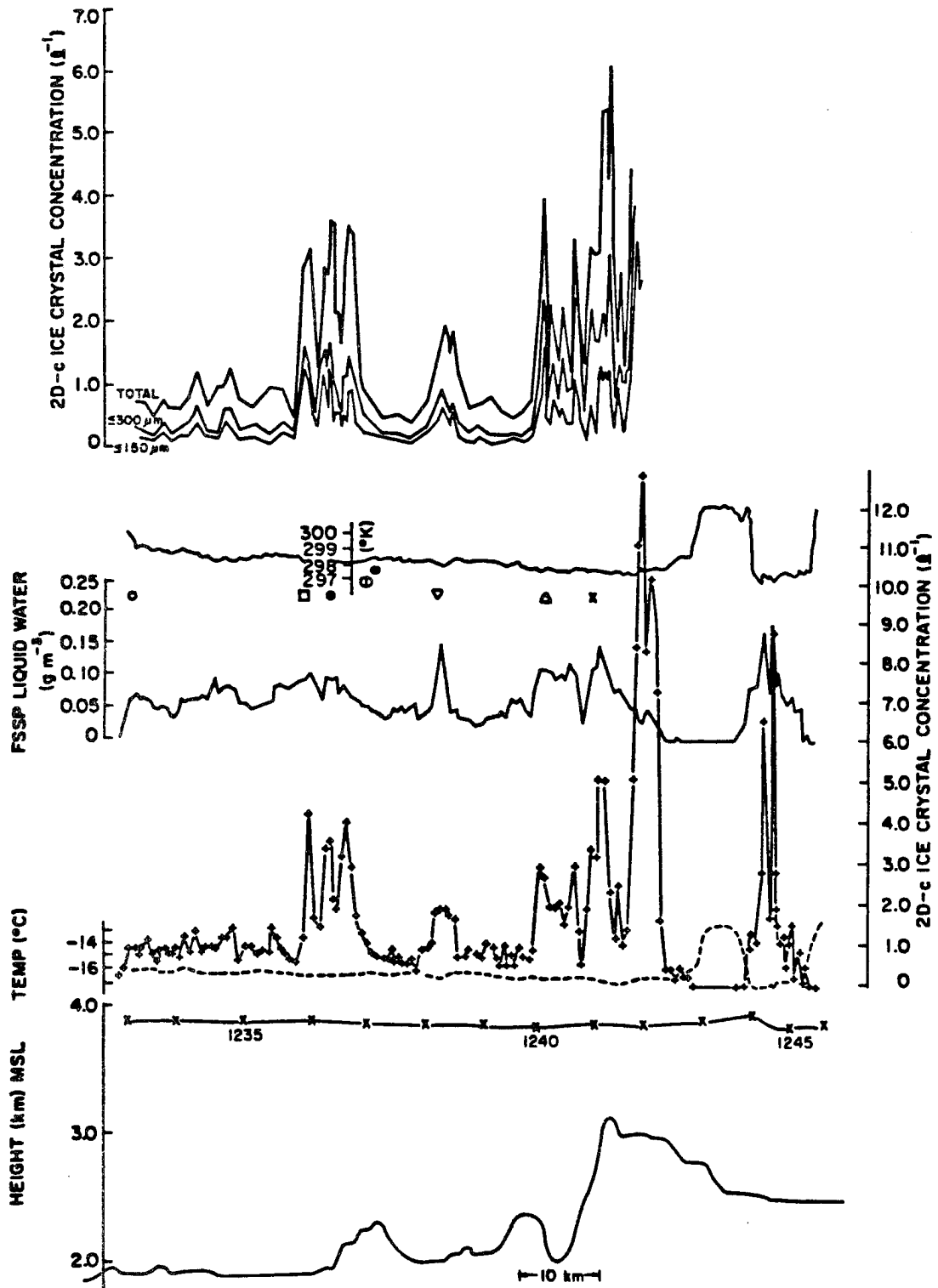


Fig. 104. Crystal concentrations, liquid water contents and state parameters from aircraft measurements near the top of the 16 Jan 82 cloud system. (from DeMott et al., 1985)

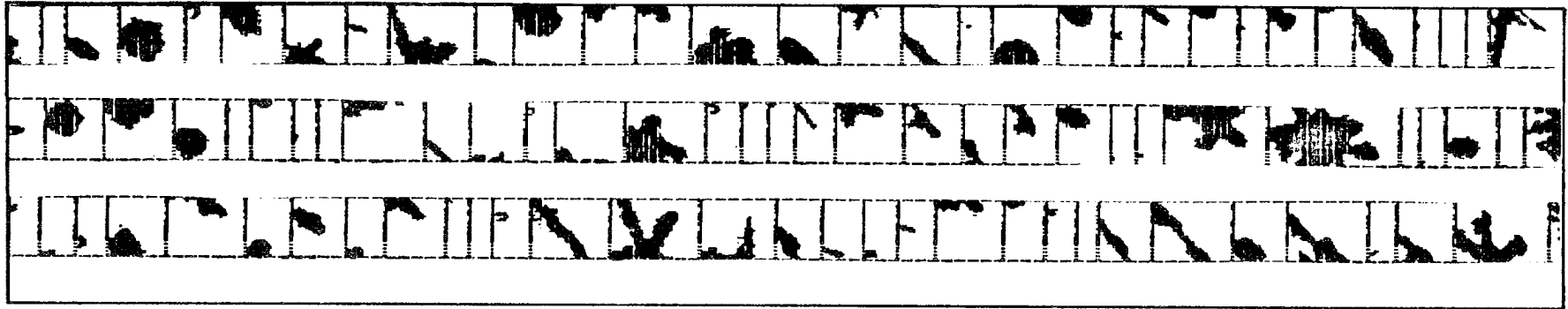


Fig. 105. 2D-c images from the 16 Jan 82 flight near cloud top.

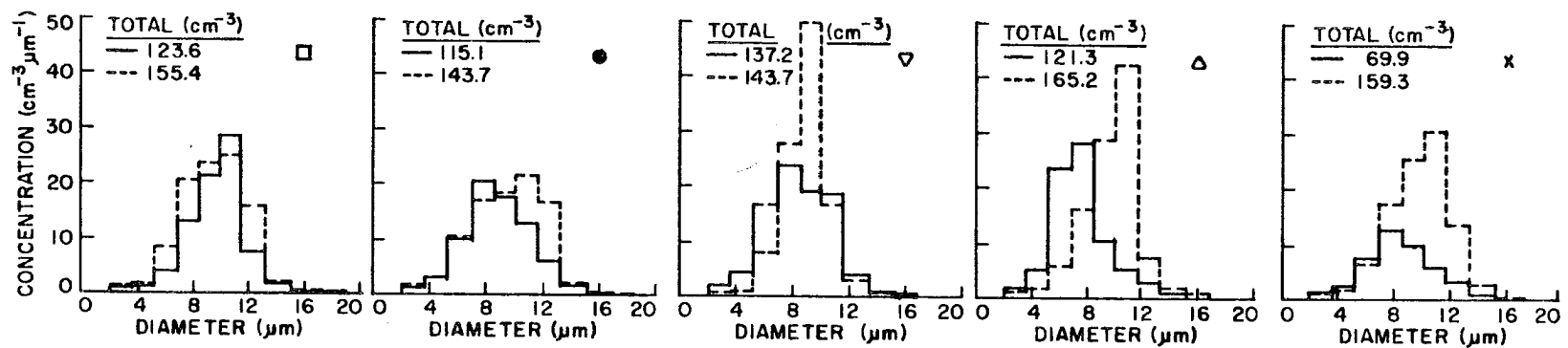


Fig. 106. Droplet spectra from the 16 Jan 82 flight near cloud top.
 (from DeMott et al., 1985)

(size of many images on the 2D-c record) and 10 μm diameter droplets have collection efficiencies of 0.6 to 0.8. Based on the 2D-c and FSSP observations, regions of high liquid water content in this cloud would support development of the rimed core of the R3b crystal. Other regions may be more effective in producing planar habits.

In such a shallow cloud system, time is an essential parameter for aggregation. Figure 62 shows a profile of a typical shallow cloud system such as the cloud of 16 Jan 82. Also shown are the trajectories of particles arriving at SPL and RAD for constant fall speeds of 10, 25, 50 and 100 cm/s. The dashed lines on the figure indicate the points in the cloud where the maximum diameter of individual dendritic particles would reach 500 μm and 1000 μm assuming an average growth rate of 1 $\mu\text{m}/\text{s}$. Typical crystals observed in aggregates at RAD had at least 1000 μm diameters. The 1000 μm boundary may be considered a somewhat arbitrary minimum threshold for aggregation initiation.

Individual planar dendritic particles have typical fallspeeds of 30-60 cm/s (Brown, 1970). Rimed spatial dendrites vary in fallspeed between 80 and 160 cm/s (Locatelli and Hobbs, 1974). These two crystal habits, because of their large differential fall velocity, have a high potential for ordered collisions. Aggregates of these crystals have the greatest potential to reach RAD in the short time available. From Fig. 62, it is clear that such aggregates can reach RAD, provided that aggregation proceeds quickly. The low snowfall rates at RAD (0.025 mm/h) and crystal habits (P1f and R3b aggregates) suggest that only a few of the cloud particles did aggregate in time to precipitate at the mountain base.

At SPL, the time requirement is relaxed considerably. 1000 μm particles have as long as 40 minutes to grow and collide in the upwind cloud and fall at SPL. In particular, aggregates of planar dendrites can easily form over the 35 km region within the 1000 μm threshold line and reach the mountain peak. The precipitation rate was much higher at SPL, individual crystals larger and aggregates much more common. These observations suggest that time and crystal habit are the most important parameters governing aggregation in cold cloud systems.

CHAPTER V SUMMARY AND CONCEPTUAL MODELS OF PRECIPITATION FORMATION

Data presented in the previous chapters were obtained during 22 separate storm periods. These storms occurred in a wide variety of environments, including convective bands, embedded cellular convection, widespread stratiform systems and shallow orographic clouds, and represent most major storms types affecting the region. In Chapter III, the temporal variation, physical distribution, and microphysical structure of supercooled liquid water were addressed. In Chapter IV, ice phase characteristics were analyzed. These included general characteristics such as ice crystal concentrations, crystal habits and precipitation climatology as well as detailed analyses of nucleation, secondary ice particle production, and growth by deposition, accretion and aggregation. In this chapter, the major results of the data analysis are summarized. This information is then assembled into conceptual models of microphysical processes in three generalized Park Range cloud systems.

1. Summary of data analysis

A. Supercooled water

(1) Temporal variations of the supercooled water field

The case studies of temporal variations in the supercooled liquid water field discussed in this paper represent various stages in the synoptic scale evolution of storms which affect the northern Colorado Rockies. Liquid water was found to occur in all stages of most of these

storms but the temporal variations in the magnitude of the liquid water contents were significant.

The cloud systems presented in Chapter III were divided into three general groups based on their relationship to the general synoptic features. These groups include pre-frontal and frontal storms, post-frontal storms and orographic storms.

a. Pre-frontal and frontal cloud systems

The analysis of the pre-frontal and frontal cloud systems was included in Chapter III. An additional case (5 Jan 82) was discussed in Chapter IV. The pre-frontal and frontal cloud systems exhibited the most variability in atmospheric structure of the three groups. Because of this variability, each of the four storms is summarized here.

On 22 Jan 82 and 30 Dec 81, the highest liquid water contents occurred prior to the onset of precipitation. In both cases, low level potential instability was present and deep convective motions occurred. In both cases, after the onset of precipitation, liquid water contents decreased substantially. However, later in the storm, after a reduction in precipitation rate, the magnitude of the liquid water content in the 22 Jan 82 storm stayed low, while the liquid water in the 30 Dec 81 storm increased again. The differences between the later evolution of the liquid water field during these cases were associated with differences in cloud depth, cloud top temperature and cross-barrier wind speed, all factors which favored liquid water production in the 30 Dec 81 storm.

The third pre-frontal cloud system occurred on 15 Dec 81. Regions of potential instability in this system were confined to temperature levels colder than -25°C . During this storm system both shallow (-18°C

tops) and deep (-30° to -35°C tops) cloud regions were observed. The deeper cloud regions most likely formed in association with weak convective motions in the upper troposphere. During this storm, no significant change in vertical temperature structure or cross-barrier wind speed occurred. The deep cloud regions were associated with high precipitation rates and low liquid water contents. The highest liquid water contents occurred during periods when the precipitation rates were low and the clouds were shallow.

The fourth pre-frontal system occurred on 5 Jan 82. The liquid water contents in this cloud system evolved in a similar way to 15 Dec 81. However, no potentially unstable layers were evident during this storm. The deep cloud periods of the 5 Jan 82 storm were associated with a wide area cloud region which advected into the area from the west. As with the 15 Dec 81 case, the highest liquid water values occurred when the cloud tops were warm and the precipitation rates were low.

Summarizing, three common features concerning the evolution of the liquid water field were observed in these cases: (1) an inverse relationship between precipitation rate and liquid water content was evident; (2) a direct relationship between cloud top temperature and liquid water content was observed; and (3) the amount of the liquid water content was consistently higher over the mountain slopes. The exception to the first relationship was the 22 Jan 82 storm, where a reduction in precipitation rate was not accompanied by an increase in liquid water content. However, in this case, the cloud top temperature remained very cold, between -30°C and -40°C .

b. Post-frontal cloud systems

The post-frontal cloud systems in this study exhibited more similarities. In all three cases, low level instability developed a few hours after frontal passage. The liquid water content in the three cases exhibited little variability upwind of RAD. However, in the vicinity of the mountain, liquid water contents varied considerably. As with the pre-frontal cases, the magnitude of the liquid water content over the ridge was inversely related to the precipitation rate at RAD.

Liquid water production near the ridgeline was associated with strong cross-barrier wind speeds and the release of low level potential instability. Fluctuations in the magnitude of liquid water and associated fluctuations in the precipitation rate upwind at RAD suggested that the liquid water was modulated by the ice crystal flux through the liquid water zone.

c. Orographic cloud systems

The three orographic cloud systems discussed in this paper formed in similar synoptic environments. The three systems were shallow, had tops warmer than -22°C , and had limited horizontal extent. In two cases, no significant changes in cloud top occurred. In the third, a deeper cloud layer advected into the region during the case study.

As in the previous cases, the changes in the liquid water field were inversely associated with changes in precipitation rate at RAD. In the case where the deeper cloud region advected into the area, a decrease in liquid water content was also associated with a decrease in cloud top temperature.

(2) Location of the liquid water in Park Range cloud systems

Supercooled liquid water will be produced locally in a cloud system when the condensate supply rate exceeds the diffusional growth rate of ice crystals present in the cloud volume. Three regions of stratified cloud systems over the Park Range satisfied these conditions. The first region, cloud top, was characterized by a local minimum in the crystal mass diffusional growth rate. This minimum resulted because the crystals near cloud top were quite small. The water balance near cloud top was examined quantitatively. Results of this theoretical study predicted that supercooled liquid water would be produced with minimum updraft velocities of a few cm/s, if the size distribution of the crystals was narrow and the crystal sizes were small. These calculations covered the range of crystal concentrations normally observed in Park Range clouds. Aircraft observations confirmed the theoretical predictions -- liquid water contents between 0.01 and 0.40 gm⁻³ were consistently observed near cloud top in several shallow storms with tops between -15°C and -20°C, as well as at the top of a deep storm with a top temperature of -31°C. Consideration of radiative processes strengthened the argument that liquid water would be produced at cloud top. Estimates of radiative cooling based on the work of Chen (1984) suggested that radiative cooling may often be as effective as adiabatic cooling in a narrow layer at cloud top.

The second region of liquid water production occurs near cloud base, particularly in shallow clouds with tops warmer than about -20°C and bases significantly warmer than -10°C. The presence of liquid water in this low level region was attributed to three factors: (1) Park Range cloud systems generally contain few ice particles nucleated and grown

within the warm temperature column/needle regime. Columnar crystals and needles have significant growth rates near -6°C . Their absence limits the rate at which diffusional growth can act to remove the available condensate; (2) Crystals with a-axis orientation falling through clouds at temperatures warmer than -10°C exhibit minimal diffusional growth rates; and (3) Condensate production rates are large near cloud base due to the warm temperatures present in this region. In shallow cloud systems, these three effects act synergistically. In clouds with tops colder than -20°C , the increased flux of ice particles and the larger flux of crystals with c-axis orientation from cold cloud levels limited liquid water production in the warmer low levels. For these reasons, liquid water occurs most often near cloud base when the tops of the clouds are warmer than -20°C .

The third region of liquid water production was observed in regions of strong orographic forcing near steep rises in topography. The most consistent and highest concentrations of supercooled water in most storms occurred over the windward slopes of the Park Range. Other topographic features had similar, but less pronounced effects. Liquid water production near steep topography is associated strong vertical motions induced by airflow deflection over the complex terrain.

Only weak evidence was available to determine the distribution of supercooled water in convective systems. Based on radiometric measurements and ground based observations of accretion, significant liquid water production was probably limited to the developing convective regions. In later stages of convective development, liquid water contents decreased and the cloud glaciated. Continued research is

necessary to specify the mechanisms of liquid water production and depletion in convective systems more precisely.

(3) Microphysical characteristics of the supercooled droplet population

Droplet concentrations in all cloud systems were very low compared to those expected for continental cloud systems. Mean droplet concentrations never exceeded 300 cm^{-3} and varied by as much as an order of magnitude at similar liquid water contents. In all cases, liquid water content was a function of droplet concentration. Four environmental factors were identified which contribute to the low droplet concentrations found in these systems: (1) during winter, inversions frequently limit the mixing which occurs between boundary layer air and the mid-level cloud layers inhibiting the rate at which cloud condensation nuclei (CCN) are resupplied to the cloud system; (2) a large fraction of the land surface in the area is frequently snow covered during winter inhibiting mechanical interaction with the surface and reducing the supply of CCN; (3) the northern Colorado region is relatively free of large anthropogenic sources of CCN and (4) scavenging of CCN may occur in cloud systems developing over upwind barriers such as the Wasatch and Uinta Ranges of Utah.

The functional relationship between droplet concentration and liquid water content indicates that peak supersaturations are achieved at a number of locations in the cloud at the leading edge of local liquid water production zones. These zones may be associated with gravity waves generated in the flow by topographic variations as well as vertical motions generated by convective or shear instability. In all observations, liquid water contents were found to vary significantly over short distances in the cloud systems.

The mean droplet diameter and standard deviation of the droplet spectra in Park Range cloud systems was strongly related to the ambient droplet concentration. A systematic broadening of the spectra was evident as the concentration of droplets available to the cloud system decreased. In cases where large droplet concentrations occurred, small mean diameter and narrow dispersion characteristics were observed.

B. The ice phase

(1) General characteristics

a. Ice particle concentrations

Variations in ice particle concentrations were significant in all Park Range cloud systems. A wide range of ice particle concentrations, spanning three orders of magnitude, were measured at all temperatures. The highest concentrations measured were 290 l^{-1} at -15°C to -16°C . 50% of the measured values were less than 20 l^{-1} except at the warmest temperatures. A general trend toward higher crystal concentrations was evident at temperatures warmer than the dendritic growth temperature range ($> -17^{\circ}\text{C}$). This trend was particularly pronounced in certain data sets where dendritic crystals were observed. The striking feature of the ice particle distribution was the extreme variability which can occur at all temperatures. Complexities associated with both nucleation and secondary ice particle production processes in these clouds give rise to such variability.

b. Crystal habits

Surface precipitation was dominated by irregular crystal habits and dendritic snowfall. The irregulars were made up of three crystal classes: (a) various combinations of side planes, plates, columns, bullets and randomly oriented crystal faces; (b) rimed particles and (c)

fragments too small to be clearly associated with any particular crystal habit. The dendrites were in four broad classes: (a) planar dendritic forms; (b) broken branches; (c) dendrites in aggregates and (d) spatial dendritic forms. Irregulars accounted for approximately 70% of the snowfall, dendrites about 20%. The remaining crystals were a mixture of plates, plate assemblies, columns, bullets, capped columns, needles and heavily rimed particles.

Aircraft decelerator measurements were limited to five flights. Two shallow orographic cloud systems, penetrated near cloud top, had high liquid water contents near cloud top and contained dendritic crystals. Surface observations confirmed that dendrites were the dominant crystal habit produced. All deep cloud systems were dominated at aircraft levels by columnar habits and, to a lesser extent, plates. Crystal habits observed at the ground in all but one system were substantially different suggesting at least some decoupling between the lower and upper levels of the cloud systems.

c. Precipitation rates

Low snowfall rates, measured at mountain base, were very common during Park Range storms. 40% of the time that measurements were conducted, the snowfall rate at the base of the mountain was between 0.0 and 0.2 mm/h. This snowfall accounted for only 6% of the total accumulation. Snowfall rates between 0.2 and 1.0 mm/h accounted for 35% of the total precipitation. Such snowfall rates also occurred during 40% of the observation period. Snowfall rates between 1.0 and 2.0 mm/h accounted for 37% of the precipitation. These events occurred during 15% of the observation period. Snowfall rates greater than 2.0 mm/h

accounted for 22% of the precipitation, although they only occurred 5% of the time.

(2) Growth by vapor deposition

Diffusional growth and habit characteristics of ice particles depend upon their temperature of formation and growth as well as the vapor density excess in their vicinity. Most of the precipitation from Park Range cloud systems was found to originate at temperatures colder than -20°C . Crystals arriving at the surface from such high levels of the cloud probably had trajectories which began well over a hundred kilometers upwind. During their fall, crystals generally encountered continuous changes in vapor density excess and temperature as well as variations in the concentration of liquid water droplets. As a result, most crystals arrived at the surface as irregular particles. The presence of a significant number of irregular cold temperature particles was seldom accompanied by a large flux of dendritic crystals. The mutually exclusive nature of these crystal habits suggests that the flux of cold temperature crystals through the dendritic zone reduces the vapor density excess in this region to below water saturation so that dendrites cannot form.

Crystals require a water supersaturated environment in a narrow temperature range (-13°C to -17°C) to form dendritic habits. Despite these restrictive limits, dendritic particles accounted for about 20% of the precipitation. A common feature of all but one dendritic snowfall event was the shallow nature of the clouds. In all of these cases, the top of the cloud system was in or near the dendritic growth temperature range. Aircraft flights near the top of several of these cloud systems confirmed that liquid water was present, indicative of possible water

supersaturated conditions. Estimates of dendritic growth rates based on 2D-c images through the dendritic region indicated that these crystals grow at rates near $1.0 \mu\text{m/s}$. Calculations of dendritic trajectories in shallow storms indicated that dendrites could reach the mountain base if nucleated in the dendritic growth region provided that the cloud has sufficient horizontal extent (about 60 km). In general, a much larger proportion of the crystals formed in the dendritic growth region precipitate on the mountain crest due to the proximity of the crest altitude to the dendritic growth regime. Dendritic crystals dominated the precipitation in only one deep storm. In this case, the dendritic zone was only penetrated at one location near the mountain crest. Water saturation in the dendritic zone was not observed. The characteristics of the cloud upstream were unknown.

Warm temperature crystals ($> -10^{\circ}\text{C}$) generally contributed little to the total crystal flux. The scarce population of these crystals was attributed to the inefficiency of nucleation at these temperatures and the lack of an active secondary ice multiplication mechanism.

(3) Ice nucleation

The study reported by DeMott et al. (1986) has shown that condensation freezing nucleation occurs rapidly in regions of orographic cloud systems where water droplets are present and water supersaturations exist. One such region is near cloud top, particularly in shallow stable clouds. A second possible region is the zone of rapid condensation near rapidly rising topography. DeMott et al. showed evidence of possible rapid nucleation in the descending currents to the lee of the mountain. In this region, contact nucleation through thermophoretic collection may be possible. The 21 Dec 81 study provided

limited evidence that deposition or sorption nucleation may also play a role in crystal formation. However, of these mechanisms, only condensation freezing nucleation has strong observational support. Surface observations of crystal flux and echo top temperature implied that clouds with echo tops colder than about -22°C produce substantially more ice particles at the surface than clouds with warmer echo tops. These data suggested that nucleation occurs more rapidly in the cold upper levels of deep clouds.

(4) Secondary ice particle production

Three mechanisms for secondary ice crystal production were reviewed and assessed for Park Range cloud systems. The first, crystal fragmentation, occurred during dendritic snowfall events. Shadow photograph analysis of over 11,000 crystals indicated that dendritic crystals have a large potential for fragmentation. Over 50% of all dendritic particles were fragmented. Enhanced crystal concentrations were measured in and below the dendritic growth temperature range by aircraft during two storms which contained dendritic crystals. Crystal concentrations in and below the dendritic growth range were factors of 2 to 5 higher than concentrations at colder temperatures during these storms. In one storm where no dendrites were observed in the precipitation, no increase in concentration was associated with the dendritic zone.

The second mechanism of secondary ice crystal production, ice splintering during riming, is constrained by temperature limits to the region around cloud base in Park Range systems. The limiting factor on the activity of the mechanism in this location is the presence of droplets with diameters greater than $25\ \mu\text{m}$. Under certain

circumstances, the proper conditions for the Hallett-Mossop (1974) mechanism may develop. One case during the experiment clearly had the potential for such ice multiplication. A second case may have had the proper conditions. In neither of these cases was the mechanism conclusively identified.

The third mechanism, droplet shattering during freezing, is probably rare in Park Range systems due to the very small number of droplets with diameters greater than 50 μm present in the clouds.

(5) Accretion

Liquid water was found in three cloud regions in stratified cloud systems: (1) near cloud top; (2) near cloud base at temperatures warmer than -10°C ; and (3) in regions of strong orographic forcing. Supercooled liquid water was also associated with the developing convection at the leading edge of a convective region. Significant riming generally occurred in all these liquid water regions. Based on individual case study analysis, the magnitude of the accretional growth in individual storms was closely related to the magnitude of the integrated liquid water content in the cloud system. When liquid water was present, accretion contributed significantly to the precipitation process.

In pre-frontal, shallow stratiform cloud systems, cloud particles arriving at RAD were often lightly rimed. At SPL, the concentration of rime on the particles was considerably greater. Precipitation rates were generally low at RAD and moderate at SPL. With the onset of deep cloud systems, the amount of rime observed on crystals sometimes increased initially, but rapidly reduced in intensity and often was completely eliminated. Precipitation observed during convective periods

was heavy at both sites and consisted initially of rimed and aggregated particles followed by a decrease in rime. In cases where a deep upper level stable cloud overruns the shallow stratiform system, the amount of riming decreased at both sites.

During post-frontal stratiform events, generally light rime, no rime or no precipitation was observed at RAD, while nearly all precipitation observed at SPL was moderately to heavily rimed.

One general characteristic of many precipitation samples was that rime selectively occurred on only a portion of the crystal population. These observations were attributed to two factors, the general increase in liquid water content due to orographic lift near the mountain and small scale variations in the liquid water field due to convection, turbulence or gravity wave structure. In general, over 70% of all samples contained lightly rimed particles at mountain and valley sites. Over 30% of all samples contained at least some heavily rimed particles.

Riming near cloud top was found to occur on certain days. The magnitude of riming near cloud top was related to many factors including the water droplet and ice crystal concentration and size distribution as well as the depth of the liquid water layer. Riming near cloud top may have been responsible for the development of spatial crystals, particularly when the cloud tops were near the dendritic growth region. Riming also was observed in the upper levels of a deep cold cloud system. Liquid water contents and ice particle size distributions in this cloud system were such that some snow pellets observed at the ground may have developed their rime structure at temperatures colder than -20°C .

(6) Aggregation

The primary component of aggregates in Park Range cloud systems are planar dendritic crystals and radiating assemblages of dendrites. In virtually all cases, the primary mechanism by which the crystals aggregated was mechanical entanglement. When the proper particles were present in the snowfall, aggregation occurred independent of surface temperature and precipitation rate. Significant aggregation failed to occur when these crystals were not present, even during heavy precipitation events. Substantial riming of the aggregates was observed on several occasions. Simultaneous riming and aggregation generally produced heavy precipitation rates. A feature of many aggregates was the presence of a large (4-5 mm) P1f planar dendrite within the aggregate. In aggregates composed entirely of planar dendrites, several of these crystals were contained in the aggregate structure. In cases where radiating and planar crystals were present, the radiating crystals attached to the basal face of the large planar crystal.

Many single and aggregated spatial crystals had a rimed core at the center of the dendritic arms. This rimed core is evidence of supercooled liquid water in the upper layers of the clouds. It was hypothesized that these crystals, because of their "burr" structure, were excellent collectors.

Aircraft and mountaintop measurements during the storms provided strong evidence that the aggregation process proceeds rapidly within and below the dendritic growth region. In the 5 Jan 82 study, an average effective collision rate of 1 crystal/100 m was deduced. On 23 Jan 82, large aggregates of dendrites were observed at mountaintop at -13°C , the base of the dendritic region.

The aggregation process underwent significant temporal variation. The intensity and characteristics of aggregates were observed to vary over time scales of an hour or less, and often as short as 5-10 minutes. These variations were attributed to mesoscale variations in storm system structure over the Park Range as well as to more subtle changes in the value of water supersaturation present in the dendritic growth temperature range.

2. Conceptual models of Park Range cloud systems

From the data presented in the previous sections, conceptual models of the liquid water distribution and ice phase processes in Park Range cloud systems have been developed. These are presented schematically in Fig. 107.

A. The shallow stratiform cloud system with cloud top temperature > -20°C

Figure 107A depicts a shallow stratiform cloud system with a warm cloud top (-15°C to -20°C). Based on a radar cloud top climatology of 412 hours of significant cloud cover over the Park Range (Fig. 108), these shallow clouds are present about 30-40% of the time that significant cloud cover existed. This type of cloud system generally had supercooled water in all three regions discussed in the text. The magnitude of the liquid water content varied significantly from one cloud system to another. A number of factors can contribute to these variations. These include temperature, humidity, ambient crystal concentrations, the magnitude of the cross-barrier wind speed, the cloud stability, and the ambient droplet concentrations and resulting droplet size spectra. However, it appears from data presented in previous sections that the primary control on the magnitude of the liquid water

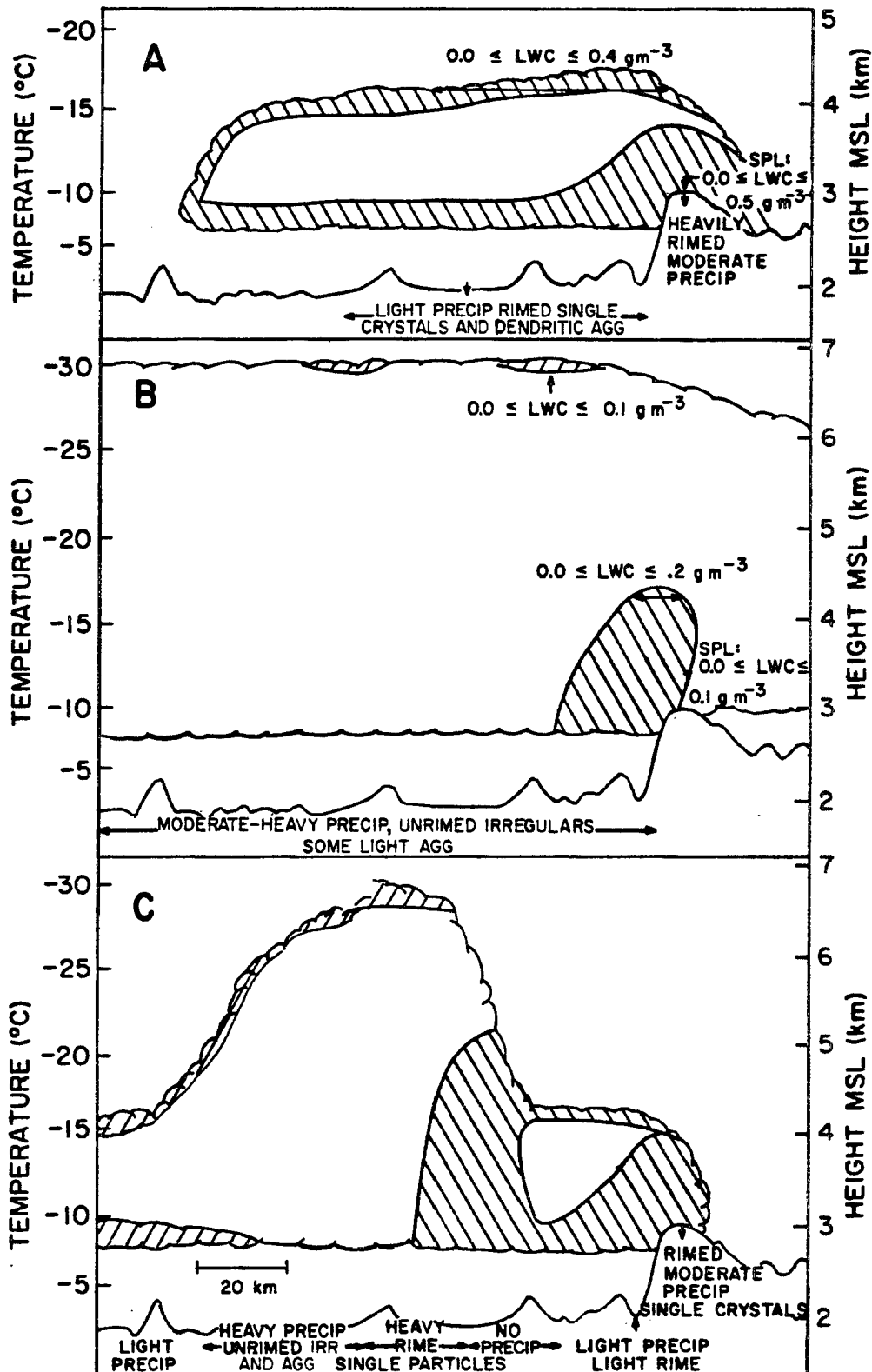


Fig. 107. Conceptual models of the supercooled liquid water distribution and ice phase interactions in Park Range cloud systems for (A) a shallow stratiform cloud system with a warm cloud top temperature (CTT) > -20°C; (B) a deep stratiform system with a cold cloud top temperature; and (C) a convective band embedded in a shallow stratiform system. The characteristic precipitation type is listed for each case along the bottom of the figure.

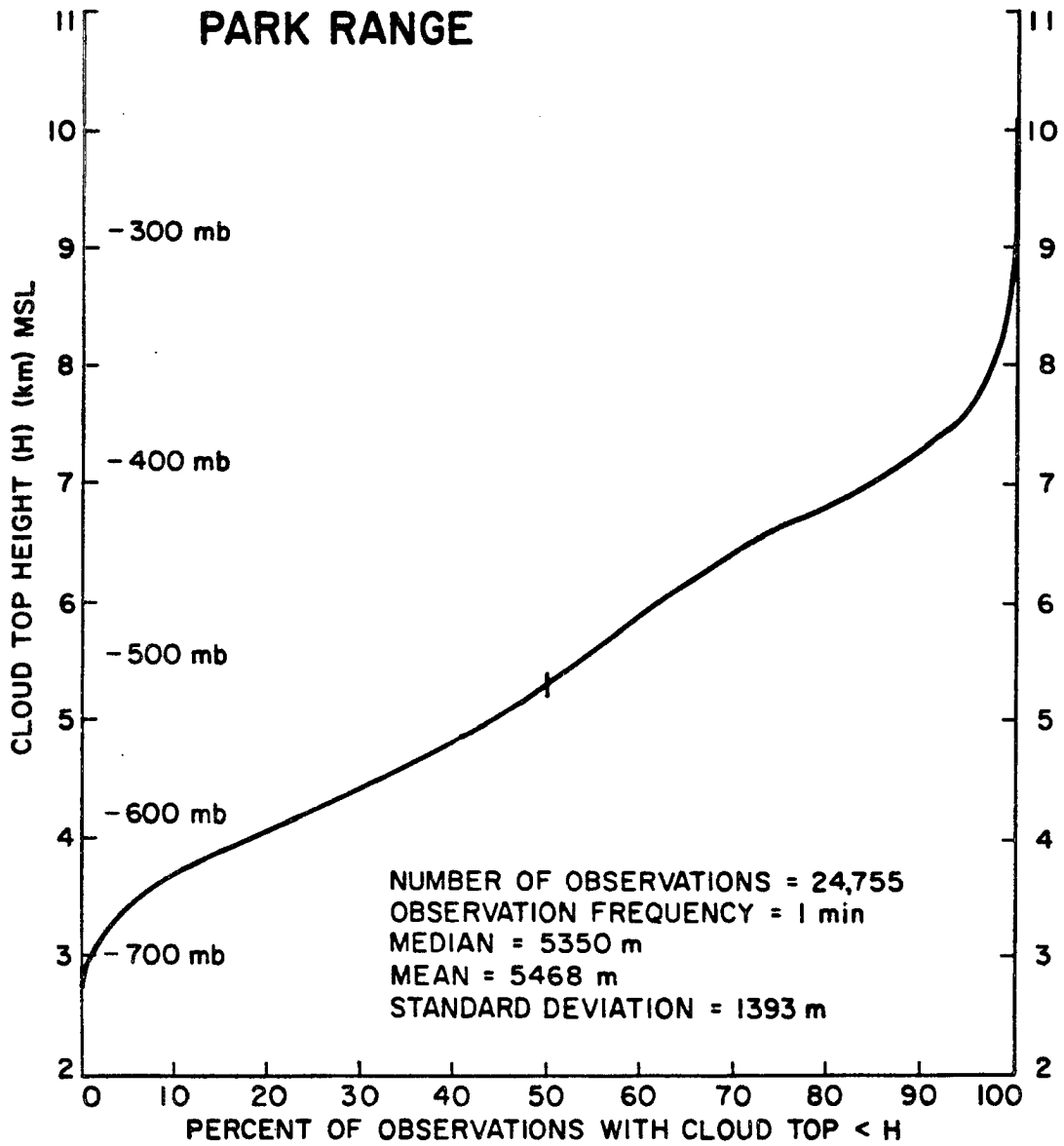


Fig. 108. Radar cloud top climatology for 412.6 hr of significant cloud cover over the Park Range.

content is the ice crystal concentration present in the cloud system. This conclusion is supported by the inverse relationship between liquid water concentrations and precipitation rate at RAD observed during many individual storm systems.

Data presented by DeMott et al. (1986), Rogers (1982), and Cooper and Vali (1981) all strongly support condensation freezing nucleation as a primary nucleation mechanism in these winter orographic cloud systems. By nature, this mechanism is limited to regions of the cloud where liquid water production occurs. In the shallow orographic cloud systems described in this work and in these three studies, cloud top and the upwind edge of the cloud were source regions for the newly nucleated ice particles. These regions met both requirements of liquid water production and a continuous source of ice nuclei.

Ice nucleation may not be limited to these regions. Condensation-freezing nucleation may occur interior to the cloud in regions of liquid water generation near steep topography. Data were not available to investigate this possibility. Evidence presented by DeMott et al. (1986) also suggested that contact nucleation may be important in the strong descending motion to the lee of the mountain due to thermophoretic capture. The size of crystals nucleated in these latter two locations would be limited by the short transit time to the lee side evaporation region.

In addition to promoting nucleation, the liquid water layer near cloud top strongly influences the subsequent diffusional growth of the ice particles. Evidence from many shallow storms confirm that the primary habits of crystals formed in these clouds are dendritic. Dendrites require a water supersaturated environment in a narrow

temperature range (-13°C to -17°C) to form, conditions satisfied at the top of many shallow Park Range cloud systems. Variations can be substantial. For example, a change in relative humidity of a few percent in the inflow air near cloud top or a change in the depth and temperature of cloud top by a few degrees can significantly alter the habits of the crystals produced in the cloud. The results of such changes near cloud top affect the later growth of particles by both aggregation and accretion and consequently affect the entire precipitation process.

In general, aggregation, fragmentation and accretion were all active processes in these shallow systems. As discussed in Chapter 3, riming occurred in three locations, at altitudes between cloud base and approximately the -10°C isotherm, in the vicinity of strong orographic lift near the mountain crest, and at cloud top. The formation of the liquid water in the lower regimes was attributed to three complementing factors: (1) the highest condensate production rates were generally in these cloud regions; (2) columnar crystals, which exhibit large diffusional growth rates at warm temperatures, were absent from these clouds; and (3) planar crystals exhibit minimal diffusional growth rates at temperatures warmer than -10°C . Near cloud top, riming may have contributed to the development of spatial dendritic crystals.

Aggregation and fragmentation occurred when dendritic crystals were present. As discussed in previous sections, these fragile habits have great potential to both fragment and interlock. On many occasions, aggregation was more frequent at the mountaintop than in the valley. In these clouds, a large fraction of dendrites nucleated near cloud top could not reach the valley floor in their short transit through the

cloud, even with the slightly enhanced fall velocities associated with aggregation. As discussed earlier, the majority of the particles in these systems impact on the mountain due to the shortened fall distance. Other mechanisms of ice crystal concentration enhancement were not found to be important in these clouds. The limiting factor inhibiting the Hallett-Mossop ice splintering process in these clouds was the lack of large droplets between -3°C and -8°C , a consequence of the proximity of this temperature range to cloud base.

In general, shallow orographic cloud systems seldom produced snowfall rates at mountain base greater than 0.7 mm/h. Snowfall from this type of cloud can occur for a short period of time or for many hours. The majority of the measurements were much less than that value. Snowfall rates were somewhat dependent on the horizontal extent of the cloud system. Crystals falling through cloud systems of large horizontal dimensions have sufficient time to grow and fall to the valley. In smaller systems, time simply was unavailable. Snowfall rates at mountaintop were generally heavier and not as critically dependent on the extent of the cloud system, due to the proximity of mountaintop to the dendritic growth temperature range and cloud top.

B. Deep stratiform cloud systems with tops colder than -20°C .

Figure 107B depicts the changes which occur in the liquid water distribution when a deep cloud system with cold tops ($< -25^{\circ}\text{C}$) is present over the Park Range. Based on Fig. 108, these deep cloud systems occur over the region about 30-40% of the time. Deep cloud systems have reduced liquid water both over the barrier and in the low level water zone. Crystal rime observations at RAD indicate that many times, the low level zone is completely eliminated. These storms are

often accompanied by higher precipitation rates. The higher ice crystal concentrations associated with the enhanced precipitation rates and large crystal flux to the surface most likely enhance removal of the water present in the system by accretion and suppress liquid water production by increasing the bulk diffusional growth. The cloud top region was sampled only once when deep cloud systems were present. Liquid water was observed at -31°C in this case. However, the data sample is too small to justify a strong conclusion concerning the presence of liquid water when the cloud tops are this cold.

Details of the nucleation processes in the upper levels of deep cold stratiform systems were not investigated. It is clear from surface measurements of crystal number flux that clouds colder than -20°C often produce higher precipitation rates and many more ice particles than their warmer counterparts. The lack of liquid water throughout a large depth of most deep cloud systems suggests that deposition or sorption nucleation may be important at low temperatures. However, liquid water observations at temperatures as cold as -31°C near cloud top indicate that cloud top may still be an important source of crystals in these systems. Limited evidence presented in Sec. 3 suggests that all nucleation mechanisms may be active. However, the nucleation mechanism responsible for the large number of ice particles present in these cloud systems has not been conclusively established.

The diffusional growth process in these cloud systems is complex. In general, the largest proportion of particles produced in these clouds were irregular. The source of most of these crystals was from temperatures below -20°C . The high percentage of irregular particles falling from these clouds was explained by considering typical particle

trajectories. In general, crystals arriving at the surface must have originated over a hundred kilometers upwind. During their fall, crystals formed at the colder temperatures encounter continuous changes in temperature, vapor density excess, and possible changes in cloud liquid water content. The net result of these many environmental changes is a complex crystal form.

In certain cases, a partial decoupling of upper and lower cloud levels was evident. In such cases, trajectories of many crystals in the upper cloud levels were quasi-horizontal -- the crystals fell slowly relative to the horizontal wind speed. In three cases studied, the crystal habits characteristic of the upper cloud levels (generally columnar) did not appear in significant quantities in the precipitation at the base of the mountain. Such decoupling is highly dependent upon the scale and lifetime of the cloud system, as well as the magnitude of the horizontal wind speed. Crystals from a large scale long-lifetime deep cloud system with low upper tropospheric wind speeds have a much higher probability of completing the transit from upper cloud levels to the surface. Such cloud systems frequently occur in association with the passage of a large scale trough system. Crystals falling from a cloud system with smaller scale features and higher upper tropospheric wind speeds will assume more horizontal trajectories, having less time to fall before their transit over the mountain. Such cloud systems are often associated with short waves embedded in the storm track of the polar jet stream.

Accretion in deep cloud systems was generally negligible, except in two cases where decoupling between the upper and lower levels of the cloud was evident. In these two cloud systems, precipitation was

dominated by rimed particles, snow pellets and needles. In one case (21 Dec 81), liquid water and snow pellet formation was observed at temperatures colder than -20°C . The needles may have been produced by a secondary ice splintering process, but liquid water contents measured in the Hallett-Mossop temperature range at mountaintop did not support such an argument. In the second case (15 Dec 81), high radiometric liquid water contents, a large needle flux and high crystal concentrations at temperatures warmer than -10°C did, circumstantially, satisfy the Hallett-Mossop requirements. These two cases, about 4.5 hours of precipitation, were the only documented times when ice splintering during riming may have occurred. Firm confirmation of the process was impossible because droplet spectra between -3°C and -8°C were unavailable.

With the exception of one cloud system, aggregation was generally limited to small combinations of cold temperature particles, such as aggregates of side planes (S1, S2, S3), bullet combinations (C2a), and irregular plate assemblages (P7a). These aggregates were generally small. In one cloud system (5 Jan 82), aggregates of dendrites occurred. This type of snowfall was characteristic of the shallow systems described in the previous section. In nearly all cloud systems, a large flux of dendrites was seldom accompanied by a large flux of cold type irregular crystals. The mutually exclusive nature of these habits suggests that the cold temperature crystals falling through the dendritic temperature range eliminate the potential for water supersaturation and effectively stop the production of dendrites. In the 5 Jan 82 case, where dendritic snowfall did occur from a deep cloud, decoupling of upper and lower levels was evident from crystal habit

observations at the surface and with aircraft. In this case, weak visual evidence from pilot records suggested that the cloud layer may have been split upwind of the mountain crest, allowing water supersaturation conditions to develop within the dendritic temperature range. With the data available, this explanation is no more than speculation. However, such an explanation does satisfy the physical and microphysical requirements necessary for the production of dendritic snowfall.

In summary, the general characteristics of deep wide-area stratiform systems are low liquid water contents, a large flux of irregular cold temperature crystals, minimal accretion and light aggregation. The aggregation is generally associated with these cold temperature crystals. In cases where the scale of the cloud system, the vertical moisture distribution and horizontal wind speeds at middle and upper levels promote decoupling, or layering within the cloud, many growth processes can occur. The structure, temperature, moisture content and depth of each cloud layer can effect the final means by which precipitation forms and reaches the surface.

C. Organized convection

Figure 107C depicts a period when a deep cloud region containing active convection moves through the Northern Colorado River Basin. Organized convection occurred on several occasions during the field program. Unfortunately, no aircraft data was available to study the internal structure of these bands. The lack of aircraft data reflects the difficulty in forecasting such convection in the northern Colorado mountains. General inferences can be made about such convective regions based on the surface and remote sensing data. Limited radiometric

evidence indicated a general increase in liquid water content in the cloud just prior to the onset of precipitation, followed by a period of reduced liquid water contents and heavy precipitation. Precipitation generally consisted of a mixture of particles from all temperatures colder than -10°C . These crystals were frequently rimed and often aggregated, particularly during the initial precipitation period.

These observations suggest that liquid water develops in the initial rising currents at the leading edge of the convective region. Such a water supersaturated environment supports all nucleation modes. Ice crystal formation probably occurs rapidly, as does diffusional growth. These high crystal concentrations promote aggregation and further water removal by accretion. Although such a scenario for precipitation development in these convective regions is supported by reasonable physical arguments, physical evidence must be amassed to determine if it is truly the case. Such questions remain the topic of future research.

CHAPTER VI PRECIPITATION AUGMENTATION

The primary purpose of weather modification operations in wintertime mountain cloud systems is to augment seasonal water supplies. The complete process of precipitation augmentation is complex. Research to determine the effects of weather modification efforts on single cloud systems and on total seasonal streamflow requires a multi-phase program of investigations conducted in a step-by-step logical sequence. The studies of the natural physical structure of the cloud systems presented in the previous chapters are the logical first step. From such studies, hypotheses concerning the evolution of precipitation in seeded cloud systems can be proposed. Testing such hypotheses in individual cloud systems is the second logical step in the overall research effort.

The purpose of this chapter is to propose physical hypotheses which can serve as the basis for future weather modification research efforts. These hypotheses are based on the physical results discussed in the previous chapters. The next phase of research in Northern Colorado River Basin cloud systems should focus on exploratory physical experiments to confirm or reject these hypotheses. Experiments within the current observational capabilities of cloud physics research programs are suggested to test the hypotheses. If such experiments are successful, a combined physical/statistical randomized approach should be undertaken. With such a careful approach, the ultimate goal of the research, evaluation of the use of weather modification technology as a tool to augment seasonal water supplies, can be achieved.

1. Requirements for modification of precipitation processes

Four basic requirements are necessary for effective modification of cloud systems: (1) supercooled water must be present; (2) sufficient time must be available for dispersion of the seeding agent, growth of the newly formed ice particles to precipitation size, and fallout to the surface; (3) artificial nucleants capable of glaciating the liquid at the appropriate temperatures must be available; and (4) an effective delivery system must be used. This thesis has primarily been concerned with the first of these requirements, supercooled water. The characteristics of ice nucleants used in weather modification operations have been recently studied by the Colorado State University Cloud Simulation and Aerosol Laboratory (CSAL). The technology of delivery has been refined, although no optimum solution exists at present. The least understood of all the requirements is time. Such information concerning the dispersion of seeding material, growth of particles, and changes in precipitation can only be understood by careful experimentation.

A. Supercooled liquid water

In Chapter III, physical arguments and supporting data were presented concerning the distribution of supercooled water in different cloud system types. Three regions of high liquid water contents were identified: near the top of the cloud, between cloud base and the -10°C isotherm, and in regions of strong orographic forcing near steep topography. The general hypothesis of weather modification is that introduction of additional ice nuclei into these liquid water zones will enhance nucleation, diffusional growth of additional particles, possible later growth by riming and aggregation, and finally additional

precipitation on the ground. For such a process to be effective, liquid water is required in three stages of growth of the additional particles.

Based on the CSAL results described in the next section, liquid water is necessary in most cases to initiate nucleation. The mechanism of all nucleants, with the possible exception of AgI-AgCl at cold temperatures, requires either the presence of droplets or water supersaturation (which will lead almost instantly to the presence of droplets). According to CSAL results, the introduction of additional ice nuclei into a glaciated cloud will have little effect of the ice crystal population. Any seeding strategy must be designed so that nuclei are targeted into one of these high water content zones to initiate the growth processes.

Once initiated, the diffusional growth process of the newly nucleated particles should proceed in the manner where cloud droplets evaporate at the expense of the growing ice particles. Although ice particles will grow most rapidly in a water droplet environment, the presence of liquid water is not a requirement for ice particle growth. However, maximum utilization of the available liquid is best accomplished by growth of the ice particles in an environment containing liquid water droplets.

The third growth mechanism which requires supercooled liquid water presence is accretion. Accretion acts rapidly to deflect particle trajectories downward by significantly enhancing fall velocities. In cloud systems with relatively short particle residence times, the process may often be critical to precipitation production.

Three generalized cloud system models were proposed in Chapters V. These included the shallow orographic cloud system with cloud tops

warmer than -20°C , the deep stratiform system with cloud tops colder than -20°C , and the convective band. In general, liquid water in the deep cloud systems was limited to the region near the mountain crest. Such cloud systems were generally efficient at precipitation production. Only one of the hypotheses discussed in the following section may apply to these clouds. However, in some deep cloud systems, such as the 15 Dec 81 and 21 Dec 81 cloud systems discussed in the previous chapters, a distinct decoupling of the upper and lower cloud regions occurred. Such decoupling was due in part to the quasi-horizontal nature of the particle trajectories associated with strong middle to upper tropospheric wind velocities. During such events, riming was observed on a portion of the crystal population collected at the surface. In these systems, the potential for liquid water production in the low-level cloud region may have been enhanced. These clouds may have a greater modification potential.

Convective bands observed during the program were generally very efficient precipitation producers. These clouds were observed to have liquid water production in their developing stages, but appeared extremely efficient at converting this liquid to the ice phase naturally. The processes within these cloud systems leading to the rapid utilization of the liquid water could not be studied because of sparse data. However, based on the high precipitation rates usually associated with these systems, it is clear that the processes were very efficient. In addition to the natural rapid utilization of liquid water in these systems, an even more difficult problem faces any effort at modification. With present data collection capabilities, the current sparse data network in the western United States, and the complexities

of western topography, the onset and duration of these systems is virtually unpredictable. Even satellite data is generally insufficient due to the frequent presence of high clouds. These bands are complex moving targets. Seeding strategies for such systems are difficult to develop and would be even more difficult to test. For these reasons, a seeding hypothesis for such systems will not be discussed.

The cloud system with the largest potential for precipitation augmentation is the shallow orographic cloud. This type of cloud system frequently has liquid water present in all three cloud regions, is quasi-stationary with respect to the mountain, can persist for several hours, frequently has rapid replacement of condensate by strong winds orthogonal to the barrier, and is the least efficient of all natural cloud system types. Because this cloud system has the highest potential for precipitation augmentation, all seeding hypotheses discussed in the following section can be applied to this cloud system.

B. Artificial ice nucleants

In recent years, the characteristics of materials commonly used in weather modification operations have been re-evaluated using the facilities of the CSAL. New, more efficient nucleating agents have also been developed. The results of the CSAL research have been reported by DeMott et al. (1983), Finnegan et al. (1984), Rilling et al. (1984), Morrison et al. (1984), and Blumenstein (1985). These studies have considered three aspects of the nucleation process: the yield or effectiveness of the various nucleants, the rate at which nucleation occurs, and the mechanism by which nucleation takes place. The major results of the CSAL investigations are important because of their direct

application to arguments concerning modification hypotheses. The major conclusions of the CSAL research are reviewed here.

Three aerosols have been characterized extensively by the CSAL. These include AgI-AgCl (DeMott et al., 1983), AgI-AgCl-NaCl (Finnegan et al., 1984), and AgI-NaI (Blumenstein, 1985). The AgI-NaI system was characterized under conditions of water saturation and three degrees of water supersaturation. The magnitude and duration of the supersaturations were unknown. The other systems were only characterized at water saturation.

The results of measurements of yield (effectiveness) from these studies are shown on Fig. 109. On this diagram, the degree of supersaturation associated with AgI-NaI is indicated by the values of $1/4 X$ (smallest supersaturation), $1/2 X$, and X (largest supersaturation), following the notation of Blumenstein. It is clear from these measurements that the AgI-AgCl and AgI-AgCl-NaCl systems are far superior at warm temperatures. At cold temperatures, all systems approach values of $2 \times 10^{15} \text{ g}^{-1}$, although the AgI-NaI system has a slight advantage at water supersaturation. Measurements of the effectiveness of AgI-NaI at cold temperatures and water saturation were not reported.

The rate at which nucleation occurred varied considerably in these studies. The time required for 90% of the crystals to be produced with AgI-AgCl aerosols after introduction into the cloud chamber varied from 25 min at -8°C to 12 min at -20°C . The AgI-AgCl-NaCl aerosol completed the reaction more quickly, producing 90% of the total crystal population in 18 min at -6°C and in 1 min at -20°C . Both of these aerosols react very quickly when introduced into the cloud chamber with transient

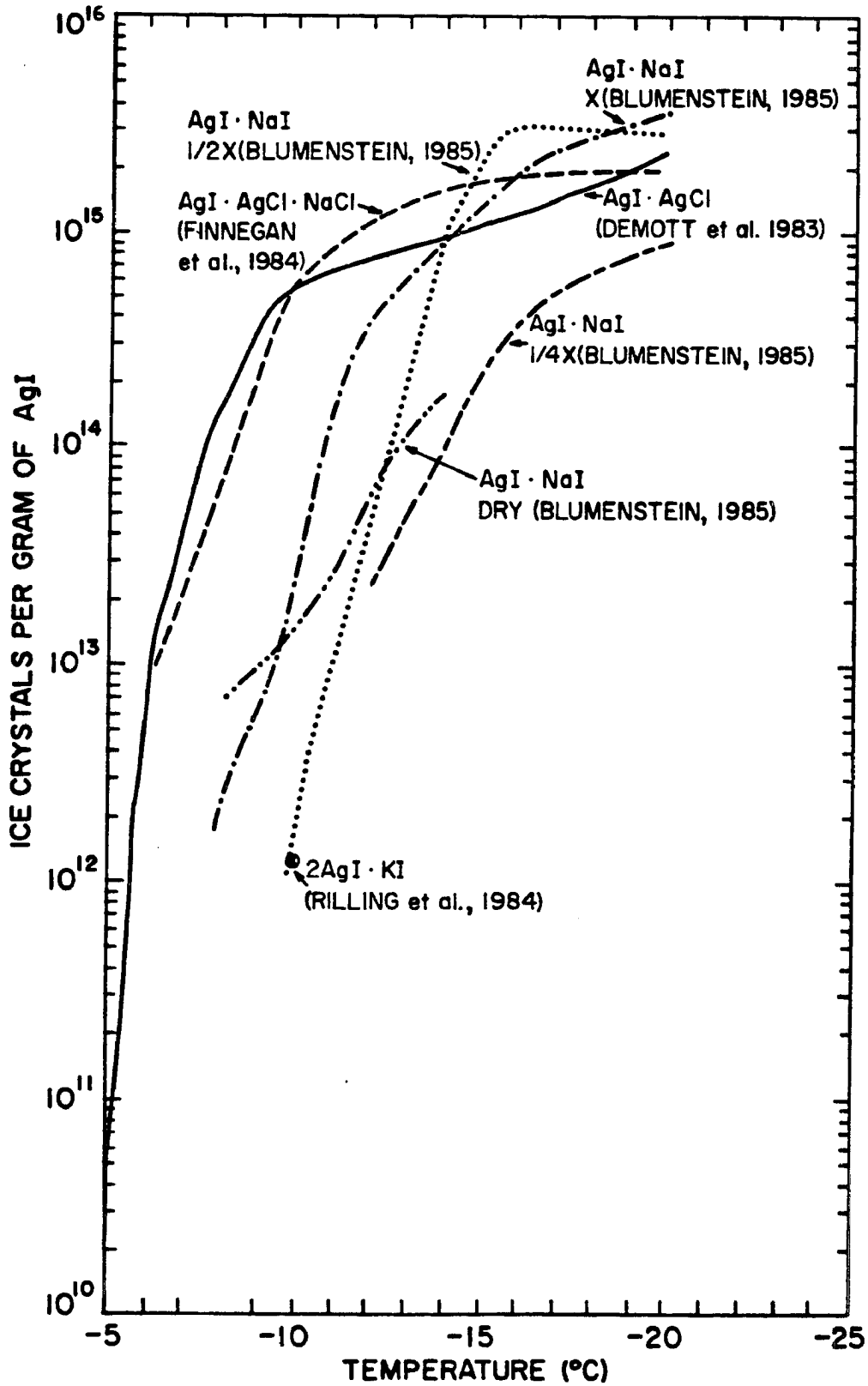


Fig. 109. Effectiveness of various nucleants measured at the Colorado State University Cloud Simulation and Aerosol Laboratory.

temperatures, the choice can be based on rates and mechanisms. The contact nucleation mechanism is limited by low droplet concentrations and inhibiting thermophoretic forces around the growing droplets. In contrast, the AgI-AgCl-NaCl aerosol serves initially as a cloud condensation nucleus. In a cloud region with developing liquid water contents, such nuclei have a distinct advantage. The rather rapid rate of ice crystal formation of this nucleus also provides an advantage in allowing the maximum potential growth time of the growing ice particles before encountering the barrier crestline. For these reasons, the best choice of nucleant to initiate cloud modification appears to be the AgI-AgCl-NaCl aerosol.

(2) Growth processes

Many investigators (e.g. Ryan et al., 1976) have shown that crystals growing at temperatures warmer than -10°C develop columnar or needle-like habits. A dramatic minimum in growth rates of both crystal axes occurs at -9°C , with a maximum in c-axis growth rate between -4°C and -6°C . The growth rates measured by Ryan et al. were near $0.3 \mu\text{m/s}$ at -9°C and $1.1 \mu\text{m/s}$ at -6°C . Typical maximum lengths of columns reported by many authors (e.g. Auer and Veal, 1970; Ono, 1969; Locatelli and Hobbs, 1974) seldom exceeded $2000 \mu\text{m}$. If a growth rate of $0.5 \mu\text{m/s}$ is assumed for the lifetime of a column growing by diffusion of water vapor, and the column grows to a size of $2000 \mu\text{m}$, its residence time within the cloud must be on the order of 4000 seconds or about one hour. Considering a mean wind speed in the growth layer of about 10 m/s , this time corresponds to an advection distance of about 40 km . Such particles in an unrimed state have fall speeds which increase from less than $.1 \text{ m/s}$ to over 1 m/s depending on size. Again, assuming a mean

fall velocity of about 0.5 m/s over the lifetime of the particle, this particle will fall about 2 km. Allowing for orographic lifting (which will decrease the net fall distance) and riming (which will increase the net fall distance), it is reasonable to expect that particles generated in the low-level liquid water zone, 30-40 km upwind of the mountain, have a high probability of arriving at the surface as precipitation. Such particles have an even greater probability of impacting the mountain crest.

These simple calculations were presented to illustrate the general feasibility of such a process. The magnitude of the effect on precipitation is much more difficult to assess because it depends critically on the particular cloud system microstructure and the actual activity of the generated nuclei in natural clouds. A detrimental effect will occur on trajectories of natural ice particles originating at colder cloud levels if there is a sufficient reduction of supercooled water. The partial or total elimination of the riming process on these natural crystals will result in a horizontal modification of the trajectories from those which would have occurred naturally. The timing of all of these processes is critical to the final effect on surface precipitation. The details of this complex redistribution of precipitation can only be assessed by direct testing.

(3) Hypothesis

Seeding the warm low-level water zone to increase precipitation should be done with the AgI-AgCl-NaCl aerosol because it functions by the condensation-freezing mechanism and has a high yield at warm temperatures. The best level for introduction of the nuclei should be between -8°C and -12°C . This temperature crosses the range where a

distinct minimum in both the c-axis and a-axis growth rates of crystals and is a probable location for sufficient water droplet production to initiate nucleation. Crystals produced in this region should fall into warmer cloud regions and grow primarily as columns. The crystals should grow initially by diffusion and possibly by accretion depending on liquid water availability and the distance between the nucleation point and cloud base. If introduced at least 30-40 km upwind, most of the particles should fall to the surface within the target area. The effect on natural cloud system particles falling from colder levels should be to decrease their rime accumulation and redistribute them further downwind. If seeding is conducted far enough upwind, these natural cloud particles should still fall in the target area. The net result should be increased precipitation within the target.

B. Precipitation modification by cloud top seeding

The tops of the shallow cloud systems discussed in previous chapters were consistently composed of supercooled liquid water. The presence of liquid water in this region presents an ideal opportunity for initiating nucleation because of the cold temperatures associated with cloud top. In addition, the distance of fall and temperatures of particle growth permit development of large particles. A physical hypothesis for nucleation and precipitation development resulting from cloud top seeding is presented in this section.

(1) Nucleation

Cloud tops of the shallow orographic cloud systems observed in the field study generally varied in temperature from about -15°C to -20°C . Within this temperature range, all nuclei function particularly well. However, the AgI-AgCl and AgI-AgCl-NaCl systems maintain high yields

over a wider range of temperatures at both water saturation and water supersaturation. Although a detailed discussion of delivery of seeding material is beyond the scope of this discussion, it is obvious that the most effective targeting would require direct delivery either by balloon releases, ridgetop generators or by aircraft releases. In such cases, dispersion of the material becomes a problem. In the case of AgI-AgCl-NaCl, the rapid rate of reaction would contribute to this problem rather than alleviate it. The slower rate of reaction of AgI-AgCl would provide a natural mechanism of dispersion and, as a consequence, affect more of the cloud volume.

(2) Growth processes

The evolution of ice particles introduced into the cloud top by seeding should closely parallel those of natural ice particles in the cloud systems. Particles exiting the cloud top region and falling through the -17°C to -13°C temperature range should grow as dendritic crystals. Based on growth rates of natural particles observed in the 5 Jan 82 storm, these particles should grow at rates near $1.0 \mu\text{m/s}$. Assuming dendritic habits, and higher crystal concentrations than occur in natural clouds, aggregation should occur below the -13°C level. If the particles pass through the low levels of the cloud in their transit to the surface, riming may also take place. The most critical factor in successful seeding of the cloud top region is proper targeting so that the crystals terminate within the target area. Large variations in wind speed and direction in storms, variations in cloud depth, and vertical wind shear will all significantly affect the transport of ice particles to the target. A few kilometers error in this case can be the difference between successful targeting and redistribution of

precipitation into the lee side evaporation region. A technique for assessing the proper seeding location is discussed in the following section on hypotheses testing. As with the case of seeding the low-level zone, a detrimental effect on the growth of natural ice particles may occur. Competition for available condensate between cloud ice particles will increase substantially after seeding. This may not only reduce the size of individual ice particles, but may also change their primary growth habits. An effective reduction in water supersaturation of less than a few percent to water saturation or below can substantially alter the growth habits of the crystals. Such changes may affect later growth by aggregation, decrease (or possibly increase) mean particle fall velocities, and, as a consequence, affect the entire cloud system microstructure. The effects on precipitation on the ground are unpredictable. Such effects can only be assessed by well designed physical tests. Possible strategies are discussed in a later section.

(3) Hypothesis

Seeding the cloud top region requires nuclei with high yield and sufficiently low rates of reaction to allow dispersion. Based on the CSAL results, the best choice is the AgI-AgCl system. Seeding cloud top utilizes an ideal environment for initiating nucleation because of persistent liquid water and cold temperatures. By proper selection of a targeting location at cloud top, the additional particles which develop will have sufficient time to grow, fall, and impact within the target area. Initial particle diffusional growth should occur at a rate of about $1.0 \mu\text{m/s}$ and result in the formation of branched planar crystals. Due to higher crystal concentrations, many of these particles will aggregate. The majority will impact on the mountain due to the

decreased fall distance between cloud top and the mountain crest. Those particles which do fall into the low-level liquid water content region will continue growth by accretion. Maximizing this effect requires that seeding be conducted further upwind so that particles can fall well upstream of the crest of the mountain.

C. Precipitation modification by seeding the region of strong orographic lift

Changes in cloud processes associated with seeding the region of strong orographic lift over the mountain slopes are restricted primarily by time. In general, flow acceleration due to airflow compression near the mountain crest complicates the time problem. Modification strategies to increase precipitation must deal critically with this time element. In this section, a hypothesis which incorporates this element is presented.

(1) Nucleation

Clearly, the nucleant with the most rapid rate of formation and highest effectiveness at warm temperatures is required. The most favorable choice is the AgI-AgCl-NaCl system.

(2) Growth processes

Limited physical evidence of effects of seeding the zone of strong orographic lift have been presented by Rhea et al. (1969). In their study, seeding this zone was associated with the appearance of very small (less than 100 μm) plates on crystal replica slides collected at mountaintop. Such particles contribute very little to the total precipitation. Based on low fall velocities of such particles, the majority of the particle population created by seeding probably advects to the lee side of the mountain. Production of a large number of these

particles probably decreases the total precipitation falling on the target ridge, since water utilized in the growth of these particles is no longer available for accretional growth of natural cloud particles. However, the downwind effects of such a redistribution of precipitation from the target ridge are unknown. In locations where several ridges are parallel to each other, and only short distances (10-20 km) exist between crestlines, the effect of a large flux of small particles into downwind liquid water zones could be substantial. Hypothetically, it could be possible to redistribute snowfall from one mountain ridge to another downwind, decreasing precipitation on the first ridge, increasing precipitation on the downwind ridge, and having a net effect of increasing the snowfall over the area encompassing both ridges. The most promising location for such an operation is the central mountain region of Colorado. In the Park Range region, the nearest downwind ridge is the Front Range, about 60 km to the east. The transport of particles such a long distance downwind at this location is not assured. However, the Park Range area does provide an excellent location to determine the lifetime of such particles. Possible methods to examine the lee side transport process are discussed later.

(3) Hypothesis

Seeding the zone of strong orographic lift requires a nucleus with a fast reaction rate and high yield at warm temperatures. The AgI-AgCl-NaCl nucleus meets these requirements. It is expected that direct seeding of the zone of strong orographic lift will result in a net decrease in precipitation on the primary target barrier. This will occur because (1) the newly formed particles have insufficient time to grow to appreciable sizes to acquire large fall velocities and (2) the

riming potential of natural ice particles entering the zone from higher levels will be decreased. The net effect will be an increase in small particles crossing to the lee side of the mountain. In regions where downwind ridges are present and the distance between the primary ridge and the downwind ridge is small, complete particle evaporation may not occur. The small particles entering the cloud and primary lift region associated with the second ridge will continue growth by diffusion and accretion and fall as precipitation. The overall impact on precipitation is a decrease on the upwind ridge, an increase on the downwind ridge, and an overall combined increase on both ridges.

3. Hypothesis testing

The hypotheses presented in the previous section require extensive physical testing to substantiate or refute their validity. In this section, a basic field experiment is discussed which can address many of the physical questions associated with these hypotheses. The design utilizes instrumentation currently available. The experiment is designed for the Park Range region, but can be adapted to other mountain locations with suitable modifications.

A. Instrumentation

Figure 110 shows a cross-section of the Park Range region with the instrumentation network required for the studies. Three north-south ridges transect the area. The primary ridge and target for precipitation enhancement is the Park Range. Directly upwind of the Park Range is a second ridge, Quarry Mountain. A third ridge, Mt. Harris, is located 30 km upwind of the Park Range crest. A network of generators should be placed along the crest of each of these smaller

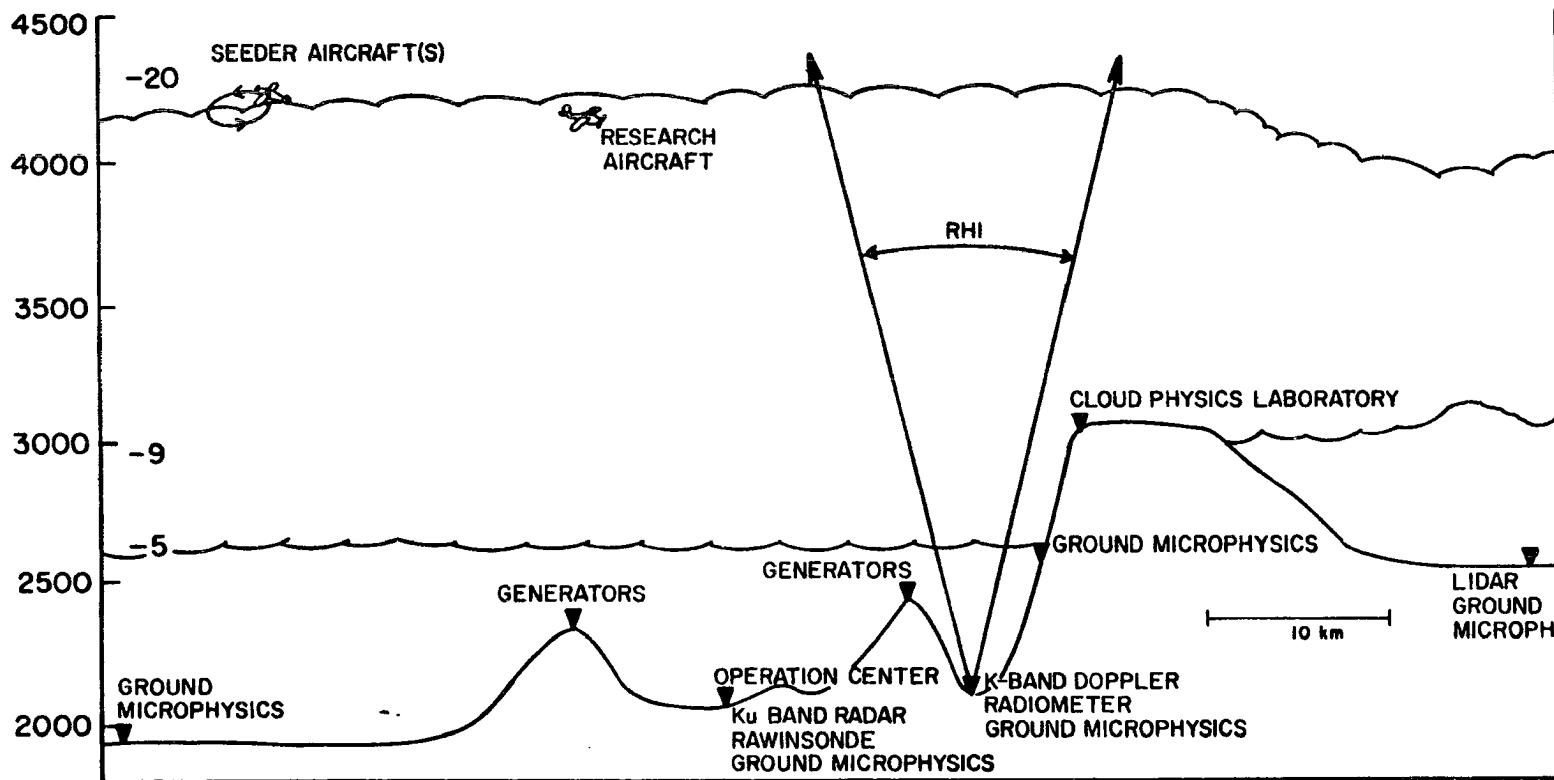


Fig. 110. Instrumentation network required for hypothesis testing experiments described in the text.

ridges. All generators should be equipped to burn $\text{AgI-NH}_4\text{I-NH}_4\text{ClO}_4\text{-NaClO}_4$ -acetone solutions to generate AgI-AgCl-NaCl aerosol.

Four major instrumentation locations are required. Approximately half way between the small ridges, a rawinsonde, Ku-band radar, ground microphysics station and operation center should be colocated. Colocation is important because information from this network will provide the primary information for seeding decisions. At mountain base, a K-band Doppler radar with RHI capability should be colocated with a dual-channel radiometer and a ground microphysics station. Both remote sensors should be used in an RHI mode during seeding experiments. At mountaintop, a complete cloud physics laboratory is required. To the lee of the mountain, a lidar should be colocated with a ground microphysics station. Two additional ground microphysics stations are required, one far upwind of the network to monitor cloud system extent and one half way up the Park Range to monitor seeding effects.

A minimum of two aircraft will be required for these experiments, a research aircraft and a seeding aircraft. Preferably, two or more seeder aircraft would enhance coverage and make it easier to detect an effect.

B. Physical experiments

Prior to a seeding experiment, the instrumentation should assume a climatological mode of scanning with the K-band doppler radar and radiometer performing azimuth scans. The Ku-band radar will monitor cloud top height. Rawinsondes should be launched every three hours. The experiment should commence when measured cloud tops are warmer than -20°C . Prior to the launch of the aircraft, the presence of supercooled water should be verified with the radiometer. If

appropriate conditions are present, aircraft launch should take place and a simple crystal trajectory model run on an operation center computer to determine the appropriate location to seed at cloud top. This model should start with developed precipitation particles at the target and determine their reverse trajectories using appropriate parameterizations for growth by riming, aggregation, and diffusion. A model such as the one described by Rauber (1981) can be easily adapted to such a task and used on a mini-computer. The results of this model guidance would be used to direct the aircraft to the appropriate location to seed at cloud top and establish the plane for RHI scans for the radiometer and radar.

(1) Seeding the low-level region

Delivery of seeding material to the -8°C to -12°C levels cannot be done with aircraft adequately in most mountainous environments in Colorado due to safety precautions associated with terrain restrictions. Two alternatives, ground-based seeding or balloonborne releases, can be used. It is imperative to release the material at the highest elevation possible to minimize transport time and avoid valley channelling flows. The material must be released far enough upwind so that a detectable effect can occur. The best approach for ground seeding, within the limitations of a physical experiment, is to release the aerosol from the upwind ridgeline of Mt. Harris. This experiment should only be done when the wind at low cloud levels will carry the material to the target in the vicinity of the radar/radiometer. The radar/radiometer should be operated in the RHI mode along the trajectory plane, established by the model. The expected responses should be the simultaneous increase in low-level reflectivity, a change in Doppler-derived fall velocities, a

reduction in integrated liquid water content, an increase in precipitation rate, an increase in the number of columns and needles in the precipitation sample, all timed with the model predicted time of the effect. Such a large number of variables could also be used as covariates in later statistical experiments if the results of the initial physical experiments are successful. Before such statistical experiments begin, repeatability should be established with the physical experiments.

(2) Seeding cloud top

The key to a successful cloud top seeding experiment is proper targeting. Prior to the start of a field experiment to test a cloud top seeding hypothesis, a simple three dimensional model of crystal trajectories should be developed and adapted to a small computer. The input parameters should be the rawinsonde-derived wind field, a simple parameterization of mountain generated vertical motions, and the crystal size and habit expected for the particles arriving at the target location. Growth equations and trajectories should be run in reverse, starting at the target and working backward to cloud top. The point of intersection of the trajectory with cloud top should give a reasonable idea of the seeding location to observe an effect at the ground. Care must be taken to account for the rate at which nucleation occurs, since the AgI-AgCl system should be used. This effect should also be incorporated into the model so that the real time output of the model is an x (latitude), y (longitude) and z (altitude) coordinate to seed. Seeding should actually be done along the y axis, parallel to the ridges, so that the center of the line corresponds to the point y. During the seeding experiment, the radiometer and radar should perform

RHI type scans along the plane connecting point (x,y,z) with the radiometer site and the cloud physics aircraft should fly along the same plane. The expected responses should be an increase in crystal concentrations along the seeding track at flight levels, a change in optical phenomena at cloud top from water droplet phenomena (glory) to ice particle phenomena (halos), the development of high reflectivity streaks emanating from cloud top within the seeding zones, a decrease in integrated cloud liquid water content, an increase in the precipitation rate, and an increase in the concentration of aggregates of branched planar crystals. Again, all of these effects should occur in a time window predicted by the model.

(3) Seeding the region of strong orographic lift

This seeding hypothesis is the most difficult to test. Initial tests of this hypothesis should be limited to the downwind transport of particles during seeding. The purpose of these tests is to determine the minimum and maximum distance necessary between mountain crests for a seeding effect to occur. These tests should be conducted with aircraft and lidar during storms where the visual cloud does not extend far downwind of the Park Range. Crystal concentrations in the downwind region should be measured continuously before, during and after the passage of the seeding effect. The lidar should be used to monitor continuously the presence of ice crystals and the level of transport. It is most important to measure the rate of evaporation of crystals with

aircraft. This is best accomplished by flying the aircraft along the wind vector and observing changes in the particle size spectra. These data can be incorporated into a more advanced hypothesis to determine the most appropriate separation distance required between mountain barriers to achieve a positive weather modification effect.

CHAPTER VII CONCLUSIONS

This paper describes the physical structure and temporal evolution of wintertime cloud systems over the Yampa River Basin, one of the eight major subbasins supplying water to the Colorado River. The primary purpose of this work was to provide a firm physical foundation for the evaluation of precipitation augmentation potential of these cloud systems. This work also extends the current understanding of the microphysical structure and evolution of the liquid and ice phases in cold cloud systems.

The information presented in this paper is based on data collected during two wintertime field programs conducted near Colorado's Park Range. A complement of remote sensing and airborne instrumentation were utilized, including the recently developed dual-channel radiometer, which allowed continuous monitoring of the evolving supercooled water field. Data were obtained during 22 separate storm periods. A wide variety of cloud systems occurred, including convective bands, embedded cellular convection, widespread stratiform systems and shallow orographic clouds. Data have been analyzed to determine the temporal variation, physical distribution, and microphysical structure of supercooled liquid water. Ice phase characteristics studied have included crystal concentrations and habits, nucleation, secondary ice particle production, and growth by deposition, accretion and aggregation. This information has been consolidated into conceptual models of precipitation development in three generalized cloud systems,

the shallow orographic cloud with cloud top temperature greater than -20°C , the deep cloud system with cloud top temperature colder than -20°C , and the convective band. A detailed summary of the results of this study is contained in Chapter V. The following are the most important conclusions of this work:

(1) The shallow orographic cloud system with cloud top temperature warmer than about -20°C has been identified as the system with the largest potential for precipitation augmentation. This type of cloud system was found to have persistent and significant liquid water contents in three regions: (1) near cloud top, (2) between cloud base and approximately the -12°C level, and (3) in regions of strong orographic forcing. Evidence is discussed which indicates that nucleation observed near cloud top in these clouds results from the condensation-freezing mechanism upwind of the mountain crest. The primary habits of crystals produced by these cloud systems were found to be dendritic. Aggregation, fragmentation and accretion were all active processes in these cloud systems. Riming occurred in all three liquid water zones. Aggregation and fragmentation were associated with dendritic habits. In general, these cloud systems seldom produced snowfall rates greater than 0.7 mm/hr at mountain base, but did produce greater snowfall rates at mountain top.

(2) Cloud and precipitation processes in deep cloud systems with tops colder than -20°C were identified. These cloud systems generally were found to have less potential for precipitation augmentation based on their reduced liquid water contents and frequent larger precipitation rates. Liquid water contents in deep stratiform cloud systems were generally limited to the region near the mountain crest. Exceptions

were cloud systems where considerable decoupling between the upper and lower cloud layers occurred. Such decoupling was attributed to quasi-horizontal crystal trajectories induced by strong middle and upper level tropospheric winds. In these cases, more widespread liquid water was observed. Large precipitation rates and the frequent lack of liquid water throughout a large depth of these clouds suggested that deposition or sorption nucleation may predominate at cold temperatures. In general, most particles arriving at the surface were observed to have irregular crystal habits. Accretion was found to be negligible, except in cases where decoupling occurred. Aggregation was generally limited to small combinations of cold temperature particles.

(3) The evolution of the supercooled water field in organized convective regions was studied. Radiometric data suggested that organized convective regions initially contained significant supercooled water, but in a short time convert to the ice phase naturally. Particles falling from such clouds were frequently rimed and aggregated. Many crystal habits were observed, suggesting complex growth processes. These cloud systems, because of their rapid evolution, large precipitation rates and short period of large liquid water presence, are the most difficult cloud system group for which a hypothesis for precipitation augmentation can be considered.

(4) New measurements were presented showing the rapid evolution of the liquid water field. Variations in the magnitude and distribution of liquid water in most of the cloud systems observed during the program were significant and occurred on short time scales (< 1 hr). Despite these variations, important trends were evident in the evolution of the liquid water were evident.

Three common features concerning the evolution of the liquid water field were observed in the pre-frontal cloud systems: (1) an inverse relationship between precipitation rate and liquid water content occurred; (2) a direct relationship between cloud top temperature and liquid water content was observed; and (3) the magnitude of the liquid water content was consistently higher over the mountain slopes.

In the post-frontal cloud systems studied, the supercooled water exhibited little variability upwind of the mountain base but varied considerably in the vicinity of the mountain. In these storms, the magnitude of the liquid water content over the ridge was inversely related to the precipitation rate at mountain base. Liquid water production near the ridgeline was associated with both orographic and convective forcing.

The orographic systems discussed in this paper were shallow, had tops warmer than -22°C , and had limited horizontal extent. In these systems, the changes in the liquid water field were inversely associated with changes in precipitation rate. In one case, a decrease in liquid water content was also associated with a decrease in cloud top temperature.

Based on these studies, it appears that in any particular cloud system, the highest liquid water contents are most likely to be associated with periods when (1) the precipitation rate at the base of the mountain is low and (2) the cloud top temperature is warm. (5) The importance of cloud top in precipitation processes was demonstrated. In this paper, the cloud top layer was shown to be composed primarily of liquid water using both theoretical arguments and direct observations. Because of liquid water presence, all nucleation

mechanisms are possible in this region. Consequently, cloud top serves as a source region for newly nucleated ice particles. In addition to promoting nucleation, the liquid water layer near cloud top strongly influences the subsequent diffusional growth of the ice particles. For example, evidence from many shallow storms indicated that the primary habits of crystals formed in these clouds are dendritic. Dendrites require a water supersaturated environment in a narrow temperature range (-13°C to -17°C) to form, conditions satisfied at the top of many shallow Park Range cloud systems.

(6) Three hypotheses for precipitation augmentation have been formulated based on the physical distribution of liquid water and evolution of precipitation processes observed in Park Range clouds. Field experiments which can be used to test each of the individual hypotheses were formulated. For each hypothesis, the physical processes which might occur in the seeded cloud system were specified and several observable parameters which should change during the seeding event are identified. Methodology and logistical procedures to conduct the observations are discussed.

In conclusion, the future of weather modification technology rides on our ability to integrate the knowledge gained from the physical studies of cloud systems into appropriate modification efforts. With a strong base of physical measurements of natural cloud system structure, changes in cloud systems resulting from modification efforts can be evaluated. The potential for seasonal precipitation augmentation by application of weather modification technology can then be assessed. Through these efforts, the final goal, effective water management, can be attained.

CHAPTER VIII FUTURE RESEARCH EFFORTS

Often in a study such as this, more questions are raised than answered. Much of the material presented here is based on data sets of limited scope. Confirmation of many of the conclusions of this work must be made with independent data sets.

More detailed case studies of the evolution of the liquid water field are required. A continuing effort must be made to compare radiometric liquid water measurements with an independent instrument. In this experiment, detailed measurements of CCN were unavailable. Such measurements would help to explain variations in the droplet spectra in these clouds. Detailed measurements with aircraft in the low-level liquid water region were lacking. In future experiments, it may be possible to investigate this region further upwind of the mountain where low-level flights may be possible. Much more detail is required concerning the liquid water region near cloud top, particularly in deep cloud systems where only limited measurements were presented.

The nucleation problem has only begun to be addressed. In particular, the mechanism of nucleation in deep cloud systems has received limited attention. Diffusional growth processes were found to be complex in deep cloud systems. Laboratory experiments are necessary to simulate the real growth of natural particles by exposing the particles to continuous variations in temperature, pressure, water vapor density excess, and liquid water content in a way characteristic of the fall of a natural ice particle. The details of the riming and

aggregation process below flight level were not directly observed in this study. Such data must be collected and analyzed if we wish to understand the details of these processes. The potential for the activation of the Hallett-Mossop (1974) ice splintering process was shown to depend crucially on the droplet spectra near cloud base in Park Range clouds. To assess the activity of the process in a climatological sense, measurements of the droplet spectra in this region must be analyzed from many storms. Such research can be done at the mountaintop laboratory.

Only limited research concerning convective bands was presented in this work. Much more detail is necessary to fully characterize the physical processes in the systems. Research using scanning surveillance radars is necessary to establish the extent of the banded structure of these cloud systems, and the relationship of these bands to the mesoscale and synoptic scale aspects of these storms.

This research emphasized natural cloud system structure. It has provided the basis for research of modified cloud system structure. Detailed experiments to test the hypotheses presented in this work are now required. A field experiment to accomplish such research has been suggested in Chapter V.

CHAPTER IX REFERENCES

Auer, A.H., Jr. and D.L. Veal, 1970: The dimensions of ice crystals in natural clouds. J. Atmos. Sci., 27, 919-926.

Aufdermaur, A.N. and D.A. Johnson, 1972: Charge separation due to riming in an electric field. Quart. J. Roy. Meteor. Soc., 98, pp 369-382.

aufm Kampe, H.J., H.K. Weickmann and J.J. Kelly, 1951: The influence of temperature on the shape of ice crystals growing at water saturation. J. Meteor., 8, 168-174.

Bader, M., J. Gloster, J.L. Brownscombe and P. Goldsmith, 1974: The production of submicron ice fragments by water droplets freezing in free fall or on accretion upon an ice surface. Quart. J. Roy. Meteor. Soc., 100, 420-426.

Baumgardner, D., 1983: An analysis and comparison of five water droplet measuring instruments. J. Climate Appl. Meteor., 22, 891-910.

Blumenstein, R.R., 1985: Characterization of silver iodide-sodium iodide ice nuclei using chemical kinetic methodology. Atmos. Sci. Paper #386, Dept. Atmos. Sci., Colorado State University, Ft. Collins, Colorado, 80523.

Bradford, M., J.D. Marwitz and B. Johnston, 1981: Hydrometeor spectra in a squall line and two rainbands in California. Proc. 8th Conf. Wea. Modif., Oct 5-7, Reno, Nev., Amer. Meteor. Soc.

Braham, R.R., Jr., J. McCarthy and J.A. Flueck, 1971: Project Whitetop - results and interpretation. Ppts. Intl. Conf. Wea. Modif., Canberra, Australia, Sept 6-11, pp 127-129.

Brown, S. R., 1970: Terminal Velocities of Ice Crystals. Atmos. Science Paper #170, Colorado State University, Fort Collins, Colorado. 80523

Brownscombe, J.L. and P. Goldsmith, 1972: On the possible production of submicron ice fragments during riming or freezing of drops in free fall. Int. Cloud Physics Conf., Roy. Meteor. Soc., London, England.

Brownscombe, J.L. and J. Hallett, 1967: Experimental and field studies of precipitation particles formed by the freezing of supercooled water. Quart. J. Roy. Meteor. Soc., 93, 455-473.

Cerni, T.A., 1983: Determination of the size and concentration of cloud drops with an FSSP. J. Climate Appl. Meteor., 22, 1346-1355.

Chappell, C.F., 1967: Cloud seeding opportunity recognition. Atmos. Sci. Paper #118, Dept. Atmos. Sci., Colo. State Univ., Ft. Collins, Co. 80523, 87 pp.

Chappell, C.F., 1970: Modification of cold orographic clouds. Ph.D. Dissertation, Dept. Atmos. Sci., Colo. State Univ., Ft. Collins, Co. 80523, 196 pp.

Chen, C., 1984: The physics of the marine stratocumulus-capped mixed layer. PhD thesis, Dept. of Atmospheric Science, Colorado State University, Ft. Collins, Co. 80521, 221 pp.

Chisnell, R.F. and J. Latham, 1976: Ice particle multiplication in cumulus clouds. Quart. J. Roy. Meteor. Soc., 102, 133-156.

Choullarton, T.W., D.J. Griggs, B.T. Humood, and J. Latham, 1980: Laboratory studies of riming and its relation to ice crystal production. Quart. J. Roy. Meteor. Soc., 106, 367-374.

Choullarton, T.W., J. Latham and B.J. Mason, 1978: A possible mechanism of ice spinter production during riming. Nature, 274, 791-792.

Cooper, W. A., 1977: Cloud Physics Investigations by the University of Wyoming in HIPLEX 1977, Dept. of Atmospheric Science, Univ. of Wyoming, Laramie, Wyoming. Report No. AS 119, 320 pp.

Cooper, W.A. and C.P.R. Saunders, 1980: Winter Storms over the San Juan Mountains Part II: Microphysical Processes. J. Appl. Meteor. 19, 925-941.

Cooper, W.A. and J.D. Marwitz, 1980: Winter Storms over the San Juan Mountains Part III: Seeding Potential. J. Appl. Meteor. 19, 942-949.

Cooper, W.A., and G. Vali, 1981: The origin of ice in mountain cap clouds. J. Atmos. Sci., 38, 1244-1259.

Davis, C.I., 1974: Ice nucleating characteristics of various AgI aerosols. Ph.D. Dissertation, Dept. of Atmospheric Resources and Mechanical Engineering, College of Engineering, University of Wyoming, Laramie, Wyoming, 259 pp.

DeMott, P.J., W.G. Finnegan and L.O. Grant, 1983: An application of chemical kinetic theory and methodology to characterize the ice nucleating properties of aerosols used in weather modification. J. Clim. Appl. Meteor., 22, 1190-1203.

DeMott, P.J., R.M. Rauber and L.O. Grant, 1986: Ice nucleation in wintertime orographic cloud systems. J. Atmos. Sci., accepted for publication.

D'Errico, R.E. and A.H. Auer, 1978: An observational study of the accretional properties of ice crystals of simple geometric shapes. Preprints Conf. Cloud Physics and Atmos. Electricity, Issaquah, Amer. Meteor. Soc., 114-121.

Dye, J.E. and D. Baumgardner, 1985: Evaluation of the Forward Scattering Spectrometer Probe. Part 1: Electronic and optical studies. J. Atmos. and Oceanic Tech., 1, 329-344

Elliott, R.D., W.W. Shaffer, A. Court, and J. F. Hannaford, 1978: Randomized Cloud Seeding in the San Juan Mountains, Colorado. J. Appl. Meteor., 17, 1298-1318.

Elliott, R.D., P. St. Amand and J. R. Thompson, 1971: Santa Barbara pyrotechnic cloud seeding test results, 1967-1970, J. Appl. Meteor., 10, 785-795.

Finnegan, W.G., F. DaXiong and L.O. Grant, 1984: Composite AgI-AgCl ice nuclei efficient, fast functioning aerosols for weather modification experimentation. 9th Conf. Wea. Modif., May 21-23, Park City, Utah, Amer. Meteor. Soc., pp 3-4.

Fletcher, N.H., 1968: Surface structure of water and ice, II - a revised model. Phil. Mag., 18 (156), 1287-1300.

Fraser, A. B., R. C. Easter and P. V. Hobbs, 1973: A Theoretical Study of the Flow of Air and Fallout of Solid Precipitation over Mountainous Terrain, Part I: Airflow model. J. Atmos. Sci., 30, 801-812.

Furman, W.R., 1967: Radar characteristics of wintertime storms in the Colorado Rockies. Atmos. Sci. Paper #112, Dept. Atmos. Sci., Colo. State Univ., Ft. Collins, Co. 80523, 40 pp.

Goldsmith, P., J. Gloster and C. Hume, 1976: The ice phase in clouds. Int. Conf. Cloud Physics, Boulder, Co., July 26-30, pp 163-167.

Gordon, G.L. and J. D. Marwitz, 1981: Secondary ice crystal production in stable orographic clouds over the Sierra Nevada. Proc. 8th Conf. Wea. Modif., Oct. 5-7, Reno, NV., Amer. Meteor. Soc.

Grant, L.O., 1965: Shapes and concentrations of snow crystals observed at 11,300 ft MSL near Climax, Colorado: Presented at the AMS National Meeting on Cloud Physics and Severe Local Storms. Oct 18-22, 1965, Reno NV. (Available from Colo. State Univ. Dept. Atmos. Sci., Ft. Collins, Colo. 80523.

Grant, L.O. and P.W. Mielke, 1967: A randomized cloud seeding program at Climax, Colorado, 1960-1965. Proceedings of the 5th Berkeley Symposium on Mathematical Statistics and Probability, Vol. 5, Weather Modification. Univ. California Press, Berkeley, Ca. Lib. Congress # 49-8189.

Grant, L.O. and R.D. Elliott, 1974: The cloud seeding temperature window. J. Appl. Meteor., 13, 355-363.

Griggs, D.J. and T.W. Choularton, 1983: Freezing modes of riming droplets with application to rime splinter production. Quar. J. Roy. Meteor. Soc., 109, 243-253.

Guiraud, F.O., J. Howard and D.C. Hogg, 1979: A dual-channel microwave radiometer for measurement of precipitable water vapor and liquid. IEEE Trans. Geosci. Electron., GE17, 129-136.

Hallett, J. and B.J. Mason, 1958: The influence of temperature and supersaturation on the habit of ice crystals grown from the vapor. Proc. Roy. Soc. London, A247, 440-453.

Hallett, J. and S.C. Mossop, 1974: The production of secondary ice particles during the riming process. Nature, 249, 26-28.

- Haraimaya, T., 1975: The riming properties of snow crystals. J. Meteor. Soc. Japan, 53, 384-392.
- Heggli, M.F., L. Vardiman, R.E. Stewart and A. Huggins, 1983: Supercooled liquid water and ice crystal distributions within Sierra Nevada winter storms. J. Clim. Appl. Meteor. 22, 1875-1886.
- Hemni, T., 1974: Secondary particle production from rimed ice. Ph.D. dissertation, Colorado State University, Ft. Collins, Co. 80523.
- Higuchi, K., 1956: A new method for the simultaneous observation of shape and size of a large number of falling snow particles. J. Meteor. 13, 274-278.
- Hill, G.E., 1979: Analysis of randomized winter orographic cloud seeding experiments in Utah. J. Appl. Meteor., 18, 413-448.
- Hill, G.E., 1980: Seeding opportunity recognition in winter orographic clouds. J. Appl. Meteor., 19, 1371-1381.
- Hill, G.E., 1982a: Analysis of precipitation augmentation potential in winter orographic clouds by use of aircraft icing reports. J. Appl. Meteor., 21, 165-170.
- Hill, G.E., 1982b: Evaluation of the Utah operational weather modification program. Final report to the National Oceanic and Atmos. Admin. under contract NA81RAC00023. Utah Water Research Laboratory, Utah State Univ., Logan, Utah. 291 pp.
- Hindman, E.E., 1967: Snow crystal and ice nuclei concentrations in orographic snowfall. Atmos Sci. Paper # 109, Dept. Atmos. Sci., Colo. State Univ., Ft. Collins, Colo. 80523, 83 pp.
- Hindman, E.E., R.D. Borys and P.J. Demott, 1983: Hydrometeorological significance of rime ice deposits in the Colorado Rockies. Water Res. Bull. 19, 619-624.
- Hindman, E.E., and D.B. Johnson, 1972: Numerical simulation of ice particle growth in a cloud of supercooled water droplets. J. Atmos. Sci., 29, 1313-1321.

Hobbs, P. V., 1965: The aggregation of ice particles in clouds and fogs at low temperatures. J. Atmos. Sci., 22, 296-300.

Hobbs, P. V., 1975a: The Nature of Winter Clouds and Precipitation in the Cascade Mountains and Their Modification by Artificial Seeding, Part I: Natural Conditions. J. Appl. Meteor., 14, 783-804.

Hobbs, P. V., 1975b: The Nature of Winter Clouds and Precipitation in the Cascade Mountains and Their Modification by Artificial Seeding, Part III: Case Studies of the Effects of Seeding. J. Appl. Meteor., 14, 819-858.

Hobbs, P.V. and A.J. Alkezweeny, 1968: The fragmentation of freezing water drops in free fall. J. Atmos. Sci., 25, 881-888.

Hobbs, P.V., S. Chang and J. D. Locatelli, 1974: The dimensions and aggregation of ice crystals in natural clouds. J. Geophys. Res., 79, 15, 2199-2206.

Hobbs, P. V., R. C. Easter, and A. B. Fraser, 1973: A Theoretical Study of the Flow of Air and Fallout of Solid Precipitation over Mountainous Terrain, Part II: Microphysics. J. Atmos. Sci., 30, 813-823.

Hobbs, P.V. and J. Farber, 1972: Fragmentation of ice particles in clouds. J. Rech. Atmos., 6, 245-258.

Hobbs, P. V. and B. J. Mason, 1964: The sintering and adhesion of ice. Phil. Mag., 9, 181-197.

Hobbs, P. V. and L. F. Radke, 1975: The Nature of Winter Clouds and Precipitation in the Cascade Mountains and Their Modification by Artificial Seeding, Part II: Techniques for the Physical Evaluation of Seeding. J. Appl. Meteor., 14, 805-818.

Hobbs, P. V., L. F. Radke, J. R. Fleming and D. G. Atkinson, 1975a: Airborne Ice Nucleus and Cloud Microstructure Measurements in Natural and Artificially Seeded Situations over the San Juan Mountains of Colorado. Research Report X, Contributions from the Cloud Physics Group, Dept. of Atmos. Sciences, University of Washington, Seattle, Washington.

Hobbs, P.V., L.F. Radke, A.B. Fraser, J.D. Locatelli, C.E. Robertson, D.G. Atkinson, R.J. Farber, R.R. Weiss and R. C. Easter, 1971: Studies of winter cyclonic storms over the Cascade Mountains (1970-1971), Contributions from the cloud physics group: Research Report VI, December, 1971.

Hobbs, P.V., L.F. Radke, A.B. Fraser, J.D. Locatelli, C.E. Robertson, D.G. Atkinson, R.J. Farber, R.R. Weiss and R. C. Easter, 1975b: The Cascade Atmospheric Water Resources Program. Final report to the U.S. Department of the Interior, Contract # 14-06-D-6999, Bureau of Reclamation, Denver, Colo.

Hobbs, P.V. and A.L. Rangno, 1979: Comments on the Climax and Wolf Creek Pass cloud seeding experiments. J. Appl. Meteor. 18, 1233-1237.

Hogg, D.C., F.O. Guiraud, J.B. Snider, M.T. Decker and E.R. Westwater, 1983: A steerable dual-channel microwave radiometer for measurement of water vapor and liquid in the troposphere. J. Climate Appl. Meteor., 22, 789-806.

Hogg, D.C., F.O. Guiraud, and E.B. Burton, 1980: Simultaneous observation of cool cloud liquid by ground based microwave radiometry and icing of aircraft. J. Appl. Meteor., 19, 893-895.

Hosler, C.L. and R.E. Hallgren, 1960: The aggregation of small ice crystals. Disc. Farad. Soc., 30, 200-208.

Hosler, C. L., D. C. Jensen and L. Goldshlak, 1957: On the aggregation of ice crystals to form snow. J. Meteor., 14, 415-420.

Houze, R.A., Jr., P.V. Hobbs, P.H. Herzegh and D.B. Parsons, 1979: Size distributions of precipitation particles in frontal clouds. J. Atmos. Sci., 36, 156-162.

Huggins, A.W., 1981: Classification and distribution of radar echos for the SCPP. Proc. 8th Conf. Wea. Modif., Oct 5-7, Reno NV., pp 36-37. Amer. Meteor. Soc.

Huggins, A.W., 1984: Development of radar echos in convective clouds in the Sierra Nevada after seeding with CO₂ pellets. Proc. 9th Conf Wea. Modif., May 21-23, Park City, Ut., pp 71-72, Amer. Meteor. Soc.

Humphries, J., 1984: Investigations of ground precipitation signatures in some Sierra Nevada aerial seeding experiments. Proc. 9th Conf. Wea. Modif., 21-23 May, Park City, Ut., pp. 79-80, Amer. Meteor. Soc.

Humphries, J. and J.A. Moore, 1981: Ground microphysics characteristics from a 3-year Sierra Nevada sample. Proc. 8th Conf. Wea. Modif., Oct 5-7, Reno, NV., pp 44-45., Amer. Meteor. Soc.

Iwai, K., 1973: On the characteristic features of snow crystals developed along the c-axis. J. Meteor. Soc. Japan, 51, 6, 458-465.

Jiusto, J.E., 1971: Crystal development and glaciation in a supercooled cloud. J. Rech. Atmos., 55, 69-85.

Jiusto, J.E. and H.K. Weickmann, 1973: Types of snowfall. Bull. Amer. Meteor. Soc., 54, 1148-1162.

Johnston, B., 1981: The kinematic structure of the rainbands on 15 February 1980 in California. Proc. 8th Conf. Wea. Modif., 5-7 Oct., Reno NV., pp 44-45, Amer. Meteor. Soc.

Kajikawa, M., 1972: Measurements of falling velocity of individual snow crystals. J. Meteor. Soc. Japan, 50, 577-584.

Kajikawa, M., 1974: On the collection efficiency of snow crystals for cloud droplets. J. Meteor. Soc. Japan, 52, 3, 328-335.

Keyes, C.G., F.D. Stover, J.V. Lunsford and M. Lentner, 1973: Jemez Atmospheric Water Resources Research Project. Final Report, Vol. 1 and 2, Bureau of Reclamation Contract 14-06-D-6803, Eng. Exp. Stat., New Mexico State Univ., 130 pp. (NTIS PB 234006/SGI).

Kikuchi, K. and H. Uyeda, 1979a: Cloud droplets and rain drops collected and frozen on natural snow crystals. J. Meteor. Soc. Japan, 57, 3, 273-280.

Kikuchi, K. and H. Uyeda, 1979b: On snow crystals of spatial dendritic type. J. Meteor. Soc. Japan, 57,3, 282-287.

Klazura, G.E., 1984: Description of winter precipitation characteristics at potential cloud seeding locations in the upper Colorado River basin. Proc. 9th Conf. Wea. Modif., 21-23 May, Park City, Ut., Amer. Meteor. Soc.

Knight, C.A., 1979: Observations of the morphology of melting snow. J. Atmos. Sci., 36, 1123-1129.

Kobayashi, T., 1961: The growth of snow crystals at low supersaturations. Phil. Mag., 6, 1363-1370.

Latham, J. and C.P.R. Saunders, 1971: Experimental measurements of the collection efficiencies of ice crystals in electric fields. Quar. J. Roy. Meteor. Soc., 96, 257-265.

Lo, K.K. and R.E. Passarelli, Jr., 1982: The growth of snow in winter storms: an airborne observational study. J. Atmos. Sci., 39, 697-706.

Locatelli, J. D. and P. V. Hobbs, 1974: Fallspeeds and Masses of Solid Precipitation Particles. J. Geophys. Res., 79, 15, 2185-2197.

Long, A.B., 1984: Physical investigations of winter orographic clouds in Utah. Final report of the Utah Department of Water Resources to the National Oceanic and Atmos. Admin., Coop. Agreement NA82 RAH 00001, Available from Utah Division of Water Resources, 1636 W. N. Temple, Salt Lake City, Utah. 84416

Magono, C., 1953: On the growth of snowflake and graupel. Sci Rep. Yokohama Nat. Univ., Sec. 1, #2, 18-40.

Magono, C. and C.W. Lee, 1966: Meteorological classification of natural snow crystals. J. Fac. Sci. Hokkaido Univ. Ser. 7, 2, 321-362.

Magono, C. and S. Tazawa, 1972: Aggregation phenomena of ice crystals. J. Meteor. Soc. Japan, Series II, 50(5), 489-493.

Marshall, J.S. and M.P. Langleben, 1954: A theory of snow crystal habit and growth. J. Meteor., 11, 104-120.

Marshall, J.S., and W. McK. Palmer, 1948: The distribution of raindrops with size. J. Meteor. 5, 165-166.

Martner, B.E., 1984: Seeding effects in non-convective clouds of the SCPP. Proc. 9th Conf. Wea. Modif., 21-23 May, Park City, Ut., pp 73-74. Amer. Meteor. Soc.

Marwitz, J.D., 1980: Winter storms over the San Juan Mountains, Part I: Dynamical processes. J. Appl. Meteor., 19, 913-924.

Marwitz, J.D. and R.E. Stewart, 1978: Cloud Physics studies in Utah during 1978. Report #AS 122, Department of Atmospheric Science, Univeristy of Wyoming, Laramie, Wy. 82071. Bureau of Reclamation Contract 7-07-93-V0001, Available from Bureau of Reclamation, P.O. Box 25007, Denver Federal Center, Denver, CO. 80225

Marwitz, J.D. and R.E. Stewart, 1979: Descriptions of cloud types in Sierra Nevada winter storms. Proc. 7th Conf. Planned and Inadv. Wea. Modif., Oct. 8-12, Banff, Alberta, pp 78-79, Amer. Meteor. Soc.

Marwitz, J.D., and R.E. Stewart, 1981: Some seeding signatures in Sierra storms. J. Appl. Meteor., 20, 1129-1144.

Marwitz, J.D., R.E. Stewart, T.S. Karacostas and B.E. Martner, 1978: Cloud Physics studies in SCPP during 1977-78. Report #AS 121, Department of Atmospheric Science, Univeristy of Wyoming, Laramie, Wy. 82071. Bureau of Reclamation Contract 7-07-93-V0001, Available from Bureau of Reclamation, P.O. Box 25007, Denver Federal Center, Denver, CO. 80225

Marwitz, J.D., R.E. Stewart, T.S. Karacostas and B.E. Martner, 1979: Cloud Physics studies in SCPP during 1978-79. Report #AS 123, Department of Atmospheric Science, Univeristy of Wyoming, Laramie, Wy. 82071. Bureau of Reclamation Contract 7-07-93-V0001, Available from Bureau of Reclamation, P.O. Box 25007, Denver Federal Center, Denver, CO. 80225

Mielke, P.W., Jr., L.O. Grant and C.F. Chappell, 1971: An independent replication of the Climax Wintertime Orographic Cloud Seeding Experiment. J. Appl. Meteor., 10, 1198-1212

Mielke, P.W., Jr., G.W. Brier, L.O. Grant, G.J. Mulvey and P.N. Rovensweig, 1981: A statistical reanalysis of the replicated Climax I and II wintertime orographic cloud seeding experiments. J. Appl. Meteor. 20, 643-660

Morrison, B.J., W.G. Finnegan and L.O. Grant, 1984: A laboratory characterization of dry ice as a glaciogenic seeding agent. 9th Conf. Wea. Modif., May 21-23, Park City, Utah, Amer. Meteor. Soc., pp 8-9.

Mossop, S.C., 1970: Concentrations of ice crystals in clouds. Bull. Amer. Meteor. Soc., 51, 474-479.

Mossop, S.C., 1976: Production of secondary ice particles during the growth of graupel by riming. Quart. J. Roy. Meteor. Soc., 102, 133-156.

Mossop, S.C., 1978: Some factors governing ice particle multiplication in cumulus clouds. J. Atmos. Sci. 35, 10, 2033-2037.

Mossop, S.C., 1980: The mechanism of ice splinter production during riming. Geophys. Res. Letters, 7, 167-169.

Mossop, S.C. and J. Hallett, 1974: Ice crystal concentrations in cumulus clouds: influence of the drop spectrum. Science, 186, 632-634.

Mossop, S.C. and E.R. Wishart, 1978: The mechanism of splintering during rime growth. Geophys. Res. Letters, 5, 1083-1086.

Mossop, S.C., J.L. Brownscombe and G.J. Collins, 1974: The production of secondary ice particles during riming. Quart. J. Roy. Meteor. Soc., 100, 427-436.

Nakaya, U., 1954: Snow Crystals: Natural and Artificial. Harvard University Press, 510 pp.

Nakaya, U. and A. Matsumoto, 1954: Simple experiment showing the existence of "liquid water" films on the ice surface. J. Colloid. Sci., 9, 41-49.

Neyman, J., E.L. Scott, and M. Vasilevskis, 1960: Statistical evaluation of the Santa Barbara randomized cloud seeding experiment. Bull. Amer. Meteor. Soc., 41, 531-547.

Odenkrantz, F.K., W.S. McEwan, P. St. Amand and W.G. Finnegan, 1968: Mechanism for multiplication of atmospheric ice crystals. Science, 160, 1345-1346.

Ohtake, T., 1969: Factors affecting the size distribution of raindrops and snowflakes. J. Atmos. Sci., 27, 804-813.

Ono, A., 1969: The shape and riming properties of ice crystals in natural clouds. J. Atmos. Sci., 26, 138-147.

Ono, A., 1970: Growth mode of ice crystals in natural clouds. J. Atmos. Sci., 27, 649-658.

Orgill, M., 1971: Laboratory simulation and field estimates of atmospheric transport-dispersion over mountainous terrain. PhD dissertation, Colorado State Univ., Ft. Collins, Co., 80523.

Passarelli, R.E., Jr., 1978a: An approximate analytical model of the vapor deposition and aggregation growth of snowflakes. J. Atmos. Sci., 35, 118-124.

Passarelli, R.E., Jr., 1978b: Theoretical and observational study of snow size spectra and snowflake aggregation efficiencies. J. Atmos. Sci., 35, 882-889.

Passarelli, R.E. and R.C. Srivastava, 1978: A new aspect of snowflake aggregation theory. J. Atmos. Sci., 36, 484-493.

Personne, P., J. L. Brenguier, J.P. Pinty and Y. Pointin, 1982: Comparative study and calibration of sensors for the measurement of liquid water content of clouds with small droplets. J. Appl. Meteor., 21, 189-196.

Pinnick, R.G., D.M. Garvey and L.D. Duncan, 1981: Calibration of Knollenberg FSSP light scattering counters for measurement of cloud droplets. J. Appl. Meteor., 20, 1049-1057.

Pitter, R.L., 1977: A reexamination of riming on thin ice plates. J. Atmos. Sci., 34, 684-685.

Pitter, R.L. and H.R. Pruppacher, 1974: A numerical investigation of collision efficiencies of simple ice plates colliding with supercooled water droplets. J. Atmos. Sci., 31, 551-559.

Plooster, M. N. and N. Fukuta, 1975: A Numerical Model of Precipitation from Seeded and Unseeded Cold Orographic Clouds. J. Appl. Meteor., 14, 859-867.

Politovich, M.K. and G. Vali, 1983: Observations of liquid water in orographic clouds over Elk Mountain. J. Atmos. Sci., 40, 1300-1312.

Pruppacher, H.R. and J.D. Klett, 1978: Microphysics of Clouds and Precipitation. D Reidel Publishing Co. Dordrecht, Holland. 714 pp.

Queney, P., 1947: Theory of perturbations in stratified currents with applications to airflow over mountain barriers. Dept. of Meteorology, Univ. of Chicago, Misc. Report No. 23.

Queney, P., G.A. Corby, N. Gerbier, H. Koschmieder, and J. Zierep, 1960: The airflow over mountains. World Meteor. Organ. Tech. Note No. 34.

Radke, L.F. and P.V. Hobbs, 1969: An automatic cloud condensation nuclei counter. J. Appl. Meteor., 8, 105-109.

Rangno, A.L. and P.V. Hobbs, 1980: Comments on "randomized cloud seeding in the San Juan Mountains, Colorado". J. Appl. Meteor., 19, 346-355.

Rasmussen, R., and H.R. Pruppacher, 1982: A wind tunnel and theoretical study of the melting behavior of atmospheric ice particles I: A wind tunnel study of frozen drops of radius $<500 \mu\text{m}$. J. Atmos. Sci., 39, 152-158.

Rauber, R.M., 1981: Microphysical processes in two stably stratified orographic cloud systems. Atmos Sci Paper #337, Dept. Atmos. Sci., Colo State Univ., Ft. Collins, Co. 80523

Rauber, R.M. and L.O. Grant, 1985: Precipitation augmentation potential of wintertime storms over the Tushar Mountains of Utah. Final report to the Utah Department of Water Resources. Available from Utah Division of Water Resources, 1636 W. N. Temple, Salt Lake City, Utah. 84416

Reid, J.D., 1976: Dispersion in a mountainous environment. Atmos. Sci. Paper #253, Dept. Atmos. Sci., Colorado State Univ., Ft. Collins, Co. 80523.

Reinking, R.F., 1973: Empirical assessment of accretion microphysics. Ph.D. dissertation., Colo. State Univ., Ft. Collins, Colo. 342 pp.

Reinking, R.F., 1974: Cross-sectional areas of snow crystals and the accretion process. Preprints Conf. Cloud Physics, Tuscon, Az. Amer. Meteor. Soc. 185-190.

Reinking, R.F., 1975: Formation of Graupel. J. Appl. Meteor., 14, 745-754.

Reinking, R.F., 1979: The onset and early growth of snow crystals by accretion of droplets. J. Atmos. Sci., 36, 870-881.

Reynolds, D.W., 1984: Progress and plans of the Sierra Cooperative Pilot Project. Proc. 9th Conf. Wea. Modif., 21-23 May, Park City, Ut. Amer. Meteor. Soc.

Rhea, J.O., 1967: A storm typing scheme for winter precipitation over and near the Park Range. 2nd Nat. Conf. Wea. Forecast., Nov., Ft. Worth, Tx.

Rhea, J. O., P. Willis and L. G. Davis, 1969: Park Range Atmospheric Water Resources Program. Final Report to the U.S. Dept. of Interior, Contract No. 14-06-D-5640, Bureau of Reclamation, Denver, CO.

Rilling, R.R., R.R. Blumenstein, W.G. Finnegan and L.O. Grant, 1984: Characterization of silver iodide-potassium iodide ice nuclei: rates and mechanisms, and comparison to the silver iodide-sodium iodide system. 9th Conf. Wea. Modif., May 21-23, Park City, Utah, Amer. Meteor. Soc., pp 16-17.

Rodi, A., 1984: Dry ice signatures in winter convective clouds over the Sierra Nevada. Proc. 9th Conf. Wea. Modif., 21-23 May, Park City, Ut., pp 69-70, Amer. Meteor. Soc.

Rogers, D.C., 1974: The aggregation of natural ice crystals. M.S. Thesis, Dept. of Atmospheric Research, University of Wyoming, Laramie, WY.

Rogers, D.C., 1982: Field and laboratory studies of ice nucleation in winter orographic clouds. Ph.D dissertation, Univ. of Wyoming, 161 pp.

Rogers, D.C., D. Baumgardner and G. Vali, 1983: Determination of supercooled liquid water content by measuring rime rate. J. Clim. Appl. Meteor., 22, 153-162

Rottner D. and G. Vali, 1974: Snow crystal habit at small excesses of vapor density over ice saturation. J. Atmos. Sci., 31, 560-569.

Rowland, W.F., G.L. Smith, D.A. Griffith, J.R. Vowell, D.L. Bailey, R.F. Reinking, R. Peace and D. Lehrman, 1973: Central Sierra Research Experiment. Final Report, Vol. 1-6, Bureau of Reclamation Contract 14-06-D-6592, California State University, Fresno Foundation Atmospheric Water Resources Research, 978 pp. (NTIS PB 225847, PB 225852).

Ryan, B.F., E.R. Wishart and D.E. Shaw, 1976: The growth rates and densities of ice crystals between -3°C and -21°C . J. Atmos. Sci., 33, 842-850.

Sasyo, Y., 1971: Study of the formation of precipitation by the aggregation of snow particles and the accretion of cloud droplets on snowflakes. Papers Meteor. Geophys., 22, 69-142.

Schlamp, R.J., H.R. Pruppacher and A.E. Hamilec, 1975: A numerical investigation of the efficiency with which simple columnar ice crystals collide with supercooled water droplets. J. Atmos. Sci., 32, 2330-2337.

Smith, R.B., 1979: The influence of mountains on the atmosphere. Advances in Geophysics, 21, Academic Press, 87-127.

Smith-Johanson, R.I., 1965: Resin Vapour replication technique for snow crystals and biological specimens. Nature, 205, 1204-5.

Smith-Johanson, R.I., 1969: Ice crystal agglomeration: T-Formation. J. Atmos. Sci., 26, 532-534.

Smith, P.L. and J.R. Miller, Jr., 1984: Comments on the Florida Area Cumulus Experiment's second phase (FACE-2) Part II, Replicated and Confirmatory Analysis. J. Clim. Appl. Meteor., 23, 1484-5.

Snider, J.B., 1983: Observations of liquid water in orographic clouds using a steerable microwave radiometer. 5th Symp. on Meteor. Observ. and Instrum., Toronto, Canada, Amer. Meteor. Soc., 196-198.

Snider, J.B., F.O. Guiraud and D.C. Hogg, 1980: Comparison of cloud liquid content measured by two independent ground based systems. J. Appl. Meteor., 19, 577-579.

Snider, J.B., and D.C. Hogg, 1981: Ground-based radiometric observations of cloud liquid in the Sierra Nevadas. NOAA Tech. Memo, ERL WPL-72, 46 pp, Available from NOAA/ERL/WPL, 325 Broadway, Boulder, Colo. 80307

Snider, J.B., and D. Rottner, 1982: The use of microwave radiometry to determine a cloud seeding opportunity. J. Appl. Meteor., 21, 1286-1291.

Squires, P., 1977: The Pyramid Lake Pilot Project, 1970-1975. Final Report, Vol. 1 and 2, Bureau of Reclamation contract 14-06-D-7000, Lab. Atmos. Phys., Desert Research Institute, Univ. Nevada System, Reno, NV., 476 pp, NTIS PB26695.

Stewart, R.E., 1979: Warm rain and ice crystal multiplication within Sierra Nevada storms. Proc. 7th Conf Planned and Inadv. Wea. Modif., 8-12 Oct, Banff, Alberta, pp 88-89.

Stewart R.E. and J.D. Marwitz, 1980: Cloud Physics studies in SCPP during 1979-80. Report #AS 125, Department of Atmospheric Science, Univeristy of Wyoming, Laramie, Wy. 82071. Bureau of Reclamation Contract 7-07-93-V0001, Available from Bureau of Reclamation, P.O. Box 25007, Denver Federal Center, Denver, CO. 80225

Stewart, R.E. and J.D. Marwitz, 1982a: Microphysical effects of seeding wintertime stratiform clouds near the Sierra Nevada Mountains. J. Appl. Meteor., 21, 874-880.

Stewart, R.E. and J.D. Marwitz, 1982b: The downwind spread of an initially vertical column of particles in a sheared environment. J. Appl. Meteor., 21, 1191-1193.

Strapp, J.W. and R.S. Schemenauer, 1982: Calibrations of Johnson-Williams Liquid water content meters in a high speed icing tunnel. J. Appl. Meteor., 21, 98-108.

Super, A.B., C.A. Grainger, J.T. McPartland, V.L. Mitchell and R.H. Yaw, 1972: Atmospheric Water resources Management Program, Final report, Part I, Bureau of Reclamation Contract 14-06-D-6798, Montana State University, 388 pp. (NTIS PB 218705).

Super, A.B. and J.A. Heimbach, 1983: Evaluation of the Bridger Range winter cloud seeding experiment using control gages. J. Climate Appl. Meteor., 22, 1989-2011.

Turner, F.M. and L.F. Radke, 1973: The design and evaluation of an airborne optical ice particle counter. J. Appl. Meteor., 12, 1309-1318.

Uttal, T., 1985: Distribution of liquid, vapor and ice in a phase budget of a Colorado orographic cloud system. Masters thesis, Colorado State University, Ft. Collins, Co. 80523

Vardiman, L., 1972: Ice crystal multiplication in convective elements of winter orographic clouds. Atmos. Sci. Paper #191. Dept. Atmos. Sci., Colorado State University, Ft. Collins, Co. 80523

Vardiman, L., 1978: The generation of secondary ice particles in clouds by crystal-crystal collisions. J. Atmos. Sci., 35, 2168-2180.

Vardiman, L. and J.H. Humphries, 1979: A case study of the Hallet-Mossop ice multiplication process in the Sierra Nevada. Proc. 7th AMS Conf. on Planned and Inadv. Wea. Modif. 8-12 Oct., Banff, Alberta, pp 98-99. Amer. Meteor. Soc.

Weiss, R.R. and P.V. Hobbs, 1975: The use of a vertically pointing pulsed Doppler radar in cloud physics and weather modification studies. J. Appl. Meteor., 14, 222-231.

Willis, P.T., 1970: A parameterized numerical model of orographic precipitation. Report to the Bureau of Reclamation, EGG Contract No. 14-06-D-5640. Available from Bureau of Reclamation, P.O. Box 25007, Denver Federal Center, Denver, CO. 80225

Wilkins, R.I. and A.H. Auer, 1970: Riming properties of hexagonal ice crystals. Preprints Conf. Cloud Physics, Ft. Collins, Co. Amer. Meteor. Soc., 81-82.

Young, K.C., 1974a: The role of contact nucleation in the ice phase initiation in clouds. J. Atmos. Sci., 31, 768-776.

Young, K.C., 1974b: A Numerical Simulation of Orographic Precipitation, Part I: Description of the Model Microphysics and Numerical Techniques. J. Atmos. Sci., 31, 1735-1748.

Young, K.C., 1974c: A Numerical Simulation of Orographic Precipitation, Part II: Comparison of Natural and AgI Seeded Conditions. J. Atmos. Sci., 31, 1749-1767.

Zikmunda, J. and G. Vali, 1972: Fall patterns and fall velocities of rimed ice crystals. J. Atmos. Sci., 29, 1334-1347.